IMPROVING QUALITY AND STABILITY OF BIOFUELS VIA FEEDSTOCK PRETREATMENT AND INLINE AND SECONDARY PROCESSING

by

ROGER NORRIS HILTEN

(Under the Direction of K.C. Das)

ABSTRACT

Renewable fuels will be required to meet the demand for transportation fuel in the near future. Deficiencies in biofuels including inadequate feedstock availability, low yield upon conversion, and poor fuel quality and stability have, as yet, limited widespread usage. The work described herein explores a variety of methods to improve the yield, quality, and stability of biomass-derived fuels. Bioconversion techniques attempted here included feedstock pretreatment by torrefaction, inline processing by catalytic esterification, and secondary processing by catalytic cracking in addition to primary processing by pyrolysis. Bioconversion techniques were undertaken in various combinations for both high free fatty acid and lignocellulosic material-derived feedstocks. Results have shown that vegetable oils can be treated effectively to generate gasoline, aromatic hydrocarbons (e.g. BTEX) in particular, at yields greater than 40 % (v/v). Also, results revealed that both gasoline and diesel hydrocarbons including aromatics and aliphatics were generated from the catalytic cracking of pyrolysis oils derived from lignocellulosic feedstocks including pine wood and peanut hulls. Catalytic esterification of bio-oil vapor resulted in the formation of esters and acetals. As a result of pretreatment and inline and secondary processing, significant improvements were seen in fuel quality and storage stability of biofuel products.

INDEX WORDS: biofuel, pyrolysis, catalytic cracking, torrefaction, bio-oil, HZSM-5

IMPROVING QUALITY AND STABILITY OF BIOFUELS VIA FEEDSTOCK PRETREATMENT AND INLINE AND SECONDARY PROCESSING

by

ROGER NORRIS HILTEN

B.S., The University of Georgia, 2002

M.S., The University of Georgia, 2005

A Dissertation Submitted to the Graduate Faculty of The University of Georgia in Partial Fulfillment of the Requirements for the Degree

DOCTOR OF PHILOSOPHY

ATHENS, GEORGIA

2012

IMPROVING QUALITY AND STABILITY OF BIOFUELS VIA FEEDSTOCK PRETREATMENT AND INLINE AND SECONDARY PROCESSING

by

ROGER NORRIS HILTEN

Major Professor: K.C. Das

Committee: Jim Kastner

Sudhagar Mani

Electronic Version Approved:

Maureen Grasso

Dean of the Graduate School

The University of Georgia

May 2012

ACKNOWLEDGEMENTS

This body of work would not have been possible without the efforts of many colleagues and the support of my family and friends.

TABLE OF CONTENTS

CHAPTER 1

INTRODUCTION AND LITERATURE REVIEW

Statement of Problem

According to data collected by the U.S. Energy Information Administration (EIA), total crude oil production is reaching a plateau (see Figure 1.1). As a consequence, for each of years 2006, 2007, 2008 and 2009, consumption has outpaced production (EIA, 2010a). Stored stockpiles have made up the difference thus far. However, since population and demand continue to grow, the oil production plateau means that per capita oil production is decreasing and the gap between supply and demand will continue to widen. Eventually, despite the world's ability and desire to consume more petroleum particularly in developing nations like China and India, stockpiles will diminish and the supply will not meet demand leading to shortages and skyrocketing prices. Renewable energy sources such as biomass could potentially meet the shortfall. However, renewable technologies have not yet matured enough to generate fuels on the scale and at the cost required to enter a broader national market. Of the total energy consumption of the U.S. in 2008, 105 EJ (99.44 quadrillion BTU), 84 % was fossil fuel-derived while only 7.4 % was derived from renewable sources, and of that, only 3.8 % was biomass-derived. For liquid transportation fuel, petroleum-only fossil fuel energy consumption for gasoline, jet fuel, diesel and residual fuel oil was 30 EJ (28 quad, 5.2 bil BOE) while biomass-derived biofuels contributed 1.48 EJ (1.4 quad, 0.26 bil BOE) (EIA, 2010b).

There is an opportunity for widespread usage of renewable biomass to produce electricity, heat and transportation fuels. Interest in biomass as a feedstock for renewable transportation fuel production has been increasing steadily over the last decade. The proliferation of first generation biofuels including biodiesel and ethanol, these predominantly generated from primary oils (e.g. palm, soybean, rapeseed) and corn, respectively, provides a positive outlook on the potential of biomass-derived fuels to become a dominant player in the transportation fuel market. However, public sentiment has not always been

positive for first generation biofuels, particularly due to the food-for-fuel dilemma and the potentially negative net energy ratio (i.e. output versus input) for corn ethanol. However, as second generation biofuels begin to emerge on the market, the use of other, non-food biomass sources for biofuels including waste material like crop residue (e.g. corn stover, sugar cane bagasse, nut shells), forestry residue (e.g. stumps, branches, treetops), landfill methane, mill wastewood, and food processing waste (e.g. waste oil, brewery waste) in addition to dedicated bioenergy crops (short rotation pine, switchgrass, energy cane, rapeseed) will effectively eliminate the food-for-fuel dilemma. As part of the work proposed here, we will focus on methods to generate liquid transportation fuels from a crop residue (peanut hulls), two food

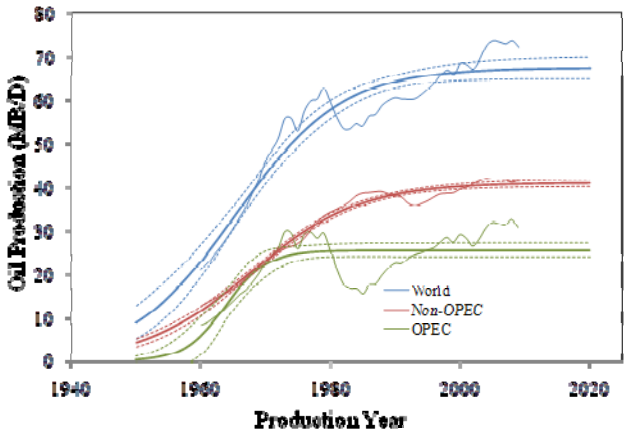

Figure 1.1. World oil production from 1960 to 2009.

processing wastes (poultry DAF skimmings and acidulated peanut oil) and a potential bioenergy crop (short rotation pine).

Production Potential

Using biomass for transportation fuel production is a practical choice due to the large yearly availability of biomass resources. An NREL study (Milbrandt, 2005) estimates that there are 423 mil dry tonnes yr^{-1} of biomass available for uses such as bioenergy. Currently, many biomass resources are underutilized, particularly waste materials such as crop and forestry residues. At an average energy density of 15 MJ kg^{-1}, the biomass available equates to 6.35 EJ (1.1 bil boe) of energy, enough to replace 20% of all transportation fuel if all the energy from the biomass could be transferred to fuel during

processing. In reality, 100% conversion is impossible. For fast pyrolysis, for example, the percentage of biomass energy converted to liquid is 65-77% (Singh et al., 2010). However, fast pyrolysis oil must be further processed to generate fuel suitable for transportation applications, a conversion often accomplished via hydrodeoxygenation (HDO). A study by the International Air Transportation Association (IATA, 2009) estimates the energy efficiency of pyrolysis combined with HDO to liquid fuel at 65.5 %. Given this conversion efficiency, pyrolysis-HDO-derived biofuels could supply 13.9% of all transportation fuel requirements if all available biomass was converted.

Conversion Pathways

Liquid fuels are derived from biomass via bioconversion, a generic term for converting biomass to value-added products. Bioconversion encompasses a variety of pathways for liquid fuel production including physicochemical (e.g. transesterification, esterification), biochemical (e.g. fermentation, anaerobic digestion), thermochemical (e.g. pyrolysis-HDO, gasification-Fischer-Tropsch synthesis). Bioconversion techniques can potentially generate high-quality "drop-in" fuels for transportation applications. For first generation biofuel production, the main bioconversion pathways have been biochemical (e.g. microbial fermentation for ethanol production) and physicochemical (e.g. transesterification or esterification for biodiesel production). Methods of bioconversion to be explored here are physicochemical (reactive condensation) and thermochemical (e.g. pyrolysis (fast and slow), fluid catalytic cracking (fixed- and fluidized-bed)).

Biofuel Limitations

Although thermochemical pathways can be used to generate liquid biofuels, several obstacles must be overcome before the biofuels can be used reliably as transportation fuels. The main issues are cost, quality, and compatibility relative to conventional fuels. For first generation biofuel, biodiesel, fuel property improvement, particularly viscosity reduction, was achieved via esterification of free fatty acids or transesterification of triglycerides. However, biodiesel production has been limited due to the cost and availability of high quality feedstock such as soybean or canola oil. Lower quality feedstocks can contain mixtures of triglycerides, free fatty acids and H_2O that make one-step transesterification impossible. For

low quality feedstocks such as waste fats and oils, one main quality issue is high viscosity, particularly at low temperatures, which leads to difficult cold weather starting and difficulty in vaporization with incomplete combustion in transportation fuel applications as a result. In addition, high viscosity and the resultant incomplete combustion lead to injector and piston coking, carbon deposition, excessive engine wear, and failure of engine lubricating oil (Harwood, 1984). Thus, methods must be utilized to reduce the viscosity of fats and oils and improve combustion. To avoid the difficulties in biodiesel production, another method to reduce the viscosity of fats and oils that can be used is catalytic pyrolysis (i.e. fluid catalytic cracking) whereby fatty acids and triglycerides are "cracked" into smaller chain length molecules. Of particular benefit is the fact that the cracking catalysts can be tailored to control the molecule size and influence the composition of the product.

When utilizing pyrolysis oils from lignocellulosic materials in liquid fuel applications, functional issues arise including filter blockage due to high ash content in the oils, pumping efficiency due to high viscosity, possible phase separation due to water, and corrosion due to low pH (Bridgwater, 1996; Adam et al., 2006). However, by upgrading pyrolysis oils, it is possible to produce liquid fuels from biomass that can more easily replace or supplement conventional hydrocarbon fuels (Sharma and Bakhshi, 1991; Bridgwater, 1996).

Another main limitation of lignocellulosic biofuels is poor storage stability. During prolonged storage, there is potential for bio-oils to undergo changes due to oxidative and thermal degradation. Oxidation can lead to polymerization resulting in viscosity increases. Thermal degradation causes partial decomposition of components and can lead to loss of volatiles. Bio-oil subjected to oxidative and elevated temperature storage conditions shows physical changes (e.g., viscosity increases and heating value decreases) and chemical composition changes (Boucher et al., 2000; Diebold and Czernik, 1997; Diebold, 2000; Oasmaa and Kuoppala, 2003). Most applications for bio-oils require that bio-oils retain favorable initial physical properties during storage, shipment and use (Diebold, 2000). Otherwise, filters, injectors, input lines, etc. may become obstructed and performance may suffer. In addition, the high level of reactive species and water content of bio-oil makes it unstable and corrosive under normal storage

conditions, which lead to physical and chemical changes and system degradation over time. In addition, high oxygen and water content (i.e. noncombustible components) also effectively lower the heating value of the fuel (Oasmaa and Kuoppala, 2003).

When subjected to prolonged or non-ideal storage conditions, bio-oil viscosity and chemical composition change dramatically mainly due to polymerization reactions (Adjaye et al., 1992). A higher degree of polymerization results in an increase in viscosity. Polymerization reactions that lead to viscosity increases are accelerated at higher storage temperatures where it has been shown that viscosity can increase from 0.009 cP day^{-1} when stored at -20 °C to more than 300 cP day^{-1} at 90 ˚C.

One goal of this study was to show whether standard methods for determining stability in hydrocarbon fuels are applicable for biomass-derived pyrolysis liquids. More specifically, we compared results from three accelerated aging stability ranking methods to determine consistency among rankings while at the same time observing the effects of aging and storage on pyrolysis oils. Stability of oils was determined by three accelerated aging procedures based on the change in viscosity, the formation of solids, and the onset of oxidation under heating. The first test assesses thermal stability while the other two are oxidation stability tests. The formation of insolubles (solids) and oxidation onset tests are based on ASTM D5304 (2006) and E2009 (2002), respectively. Measuring viscosity change with aging is not defined in a specific standard but has been recommended and used in several other studies of bio-oil stability (Diebold and Czernik, 1997; Oasmaa and Kuoppala, 2003; Boucher et al., 2000). The aging procedure for the test involves thermally treating the bio-oil at 80 ˚C for 24 hours. For a pine-derived bio-oil, viscosity change during this accelerated aging procedure correlated with storage of the bio-oil at room temperature for one year (Oasmaa and Kuoppala, 2003; Oasmaa and Peacocke, 2001).

Beyond measuring physical changes in bio-oil during storage, FT-IR will be used to examine compositional changes as well. FT-IR is an effective tool to evaluate functional group changes. Scholze and Meier (2001) showed that specific oxygenated groups that affect stability such as carbonyls express distinct changes in the intensity of absorption spectra after aging. The authors reported that with increasing carbon content in pyrolytic lignin (with a concurrent decrease in oxygen content), adsorption

bands representative of carbonyls at 1701, 1652, and 1600 cm^{-1} were significantly reduced. Thus, during aging, especially during oxidative aging, carbonyl bands should increase in intensity. Other oxygen-related bands, i.e. hydroxyl and methoxyl bands, were less affected by changes in oxygen content. For the current study, we will attempt to show changes in the intensity for bands that indicate oxygenated species.

Economic Considerations

One way to assess the viability of a biofuel production pathway is to compare energy output based on the energy density of the fuel and any co-products versus the energy input for producing the crop (i.e. energy to produce fertilizers, to pump water, to produce fuel for harvesting equipment and fuel for transporting biomass to a biorefinery) and for processing to finished fuel at the biorefinery. This ratio is often called net energy ratio (NER) or energy returned on energy invested (EROEI). EROEI estimates for conventional gasoline and diesel vary considerably depending on the petroleum source. Ou et al. (2008) reported EROEI values estimated at 0.74 and 0.77 for gasoline and diesel, respectively.

For biofuels, the range of EROEI is quite large – from significantly less than 1 to greater than 10. For corn ethanol, many studies have shown that EROEI is potentially unfavorable (< 1). From previous studies, estimates at 0.77 (Pimental, 2003; Pimental and Patzek, 2005), 0.886 (Ou et al., 2009), 0.969 (Yu and Tao, 2009), and 1.09 (Shapouri et al., 2002) are estimated without the energy credit of co-products. If the energy content of co-products (predominantly, animal feed) is included, Yu and Tao (2009) estimate that the EROEI for corn ethanol improves to 1.32, a positive energy balance. For ethanol from sweet sorghum, the value was found to be 0.68 (Ou et al., 2009). For biodiesel, EROEI varies depending on oil source and growing region. Using palm oil as a feedstock for biodiesel production, EROEI ranges from 3.4 (Pleanjai and Gheewala, 2009) to 7.78 (Yee et al., 2009). For *Jatropha* biomass, values range from 1.85 in India (Achten et al., 2010) to 2.0 in China (Ou et al., 2009). However, for waste materials, the energy invested for primary production of the main product is subtracted from the total production energy invested. Often, this energy investment is assumed to be zero for waste materials. However, wastes must still be collected and processed to fuels, processes that consume energy.

Improving Quality and Stability

In an early effort to improve bio-oil stability, Diebold and Czernik (1997) showed that additions of solvents could significantly improve stability by limiting viscosity changes during aging. Solvents used in the study included ethyl acetate, a mixture of methyl isobutyl ketone and methanol, acetone, methanol, a mixture of acetone and methanol, and ethanol. Their findings revealed that methanol at 10 wt. % enhanced bio-oil stability and reduced viscosity most effectively. The mechanism for stability improvement and viscosity reduction was attributed to four factors: 1) reduction in the concentration of reactive aldehydes through the conversion to hemiacetals and acetals, 2) transacetalizing larges hemiacetals and acetals to lower molecular weight acetals, 3) conversion of reactive organic acids to esters, and 4) transesterification of large esters to lower molecular weight esters.

The immediate effects of adding an alcohol to fast pyrolysis bio-oil are decreased viscosity and increased heating value (Moens et al., 2009; Oasmaa et al., 2004; Stamatov et al., 2006). These improvements make bio-oil more attractive for combustion applications in furnaces, boilers and gas turbines, or as an alternative to diesel where untreated bio-oils can require major changes to existing systems (Stamatov et al., 2006; Gust, 1997). The increase in heating value for bio-oils mixed with ethanol is due to the fact that ethanol has a higher heating value of 27 MJ kg^{-1}, which is higher than that of most fast pyrolysis bio-oils.

Most studies have directly added alcohols after pyrolysis (Diebold and Czernik, 1997; Moens et al., 2009; Oasmaa et al., 2004), a method which works well to increase stability and heating value of bio-oils. However, several recent studies (Junming et al., 2008; Lu et al., 2007; Mahfud et al., 2007; Tang et al., 2008; Zhang et al., 2006) showed that using reactive distillation of bio-oil coupled with an alcohol and an acid or base catalyst resulted in bio-oil esterification. Esterifying bio-oil can significantly improve the quality of bio-oil by lowering water content, viscosity, and the free-acid content. Additional improvements in bio-oil quality include an increase in heating value by as much as 50 % (Junming et al., 2008; Zhang et al., 2006) and an increase in stability due to the removal of acids that catalyze polymerization reactions. Junming et al. (2008) showed that after three months of aging, esterified bio-oil

exhibited very little viscosity increase. Ji-lu (2007) introduced well-sprayed ethanol into a bio-oil condenser as a precursor to spraying bio-oil once enough was produced. The intent was to quickly cool vapors to prevent polymerization reactions, though esterification was not observed.

Fischer esterification was proposed to be the reaction pathway in conversion to esters. The esterification reaction follows the equation, $RCOOH + C_nH_{2n}+1OH \Leftrightarrow RCOOC_nH_{2n+1} + H_2O$, leading to the formation of water and an ester. The simplest ester that can be produced is methyl formate, $HCOOCH_3$, when methanol (CH_3OH) is used as the alcohol and is reacted with formic acid, HCOOH. Industrially the reaction is always catalyzed by a strong acid. Several studies (Junming et al., 2008; Tang et al., 2008) have used solid acid catalysts to enhance the bio-oil esterification reaction which improved bio-oil quality by increasing HHV and pH and reducing specific gravity, viscosity and water content for esterified bio-oil.

Several studies (Chu et al., 1996; Kirumakki, 2006; Koster et al., 2001; Miao and Shanks, 2009) have shown the potential to use heterogeneous catalysts for esterifying model bio-oil compounds such as acetic acid. As an example, Miao and Shanks (2009) esterified acetic acid, a model bio-oil compound, using a mesoporous catalyst. Acetic acid conversion was close to 40 % at a 250 min reaction time at 50 °C using the catalyst. Zhang et al. (2006) esterified acetic acid in a reflux reactor and showed yields ranging from 15 % (no catalyst) to 100 % (solid acid catalyst). Koster et al. (2001) and Chu et al. (1996) performed vapor-phase esterification of acetic acid with ethanol. Koster et al. (2001) performed gas-phase esterification over several mesoporous catalysts, and showed moderate ester yields (< 25 %). Equilibrium for the reaction lies far to the right, especially in the vapor phase, for which the thermodynamic equilibrium constant is 367 for the reaction of ethanol and acetic acid to form ethyl acetate (Diebold, 2000).

In this study by utilizing a reactive condensation process, the intent is to increase the quality of bio-oil by effectively removing the undesired acidic compounds. In addition, it is proposed that adding an alcohol during condensation will better stabilize the bio-oil by quickly quenching bio-oil vapor to prevent secondary reactions and by simple dilution of reactive species before reactions can occur. In addition, we

theorized that carboxylic acids, including acetic and formic acid which occur in high concentration in bio-oil vapor (Gayubo et al., 2004a; Milne et al., 1997), would undergo Fischer esterification upon mixing with ethanol at elevated temperature to produce esters and water. Water formation should be evident in the overall water balance of pyrolysis. Due to the lower polarity of esters compared to carboxylic acids, the solubility of water in the oily phase of the bio-oil will be reduced. Thus, we expect that water produced during esterification will be concentrated in the aqueous phase of the bio-oil thereby reducing the water content of the oily phase. We also propose that acetalization is occurring following the general equation: $RCOH + C_2H_5OH \Leftrightarrow RCHC_2H_5O\text{-}C_2H_5O + H_2O$. Additionally, rapid condensation, esterification and acetalization will act to stabilize the bio-oil more effectively than simple condensation thereby increasing thermal and oxidative stability.

Since the reaction equilibrium constant in liquid phase is 42 (Diebold, 2000) compared to 367 in vapor phase (Diebold, 2000), we have made the assumption that once bio-oil leaves the heated reaction zone and condenses, esterification essentially ceases. Without a strong acid catalyst, Moens et al. (2009) showed very little reduction in acid number and carbonyl content for bio-oil/methanol mixtures even under heating and proposed that high water content prevents the esterification reaction from going to completion. Though esterification reactions have been proposed to proceed at room temperature without a catalyst (Diebold and Czernik, 1997), no quantification has been attempted. The eventual goal is to power a diesel engine with bio-oil that has been upgraded via esterification alone or in combination with other upgrading techniques to improve quality.

An additional method to improve biomass-derived oils is via catalytic cracking and reforming and hydrotreating as a means to produce high quality liquid fuels. Catalytic processes can either be integrated with pyrolysis systems to upgrade all vapors, or applied after pyrolysis on selected compounds extracted from pyrolysis products. Studies using in situ upgrading are abundant. Major work with catalytic pyrolysis began in the mid-eighties with the advent of zeolite catalysts – ZSM-5, in particular. ZSM-5 was developed by Mobil to convert methanol to gasoline (MTG) with a patent registered by Arguer and Landolt (1972). ZSM-5 is particularly effective in producing gasoline-range hydrocarbons due to shape-

selective pores in the surface (Renaud et al., 1987). Diebold and Scahill (1987) produced gasoline boiling range hydrocarbons by upgrading fast pyrolysis vapors from softwood sawdust in a vortex reactor using ZSM-5 catalyst. Renaud et al. (1987) converted vapor from pyrolysis of populus deltoids wood over ZSM-5. More recently, Williams and Nugranad (2000) pyrolyzed rice husks in a fluidized bed reactor with pyrolysis vapors being upgraded using a zeolite ZSM-5 catalyst. The study showed that in upgraded oils, molecular weight distribution decreased and the concentration of single ring and polycyclic aromatic hydrocarbons increased markedly compared to bio-oils produced during non-catalytic pyrolysis. Lu et al. (2007) used online FT-IR to show the formation of bio-gasoline from the catalytic pyrolysis of wheat straw using HUSY, REY, and HZSM-5 catalysts. Gasoline formation was indicated by the relative increase in the concentration of isoalkanes and aromatics. Adam et al. (2006) upgraded pyrolysis vapors from spruce (with organic liquid yields from 13-20 %) and Miscanthus biomass using several catalysts including several Al-MCM-41 catalysts and a commercial FCC catalyst. The quality of bio-oil was assessed for each catalyst by observing the yields of eight desirable and undesirable components in bio-oils produced including hydrocarbons, phenols, furans, acids, alcohols, carbonyls, PAHs, and heavy compounds. As much as 10 % (w/w of biomass) of the product liquid was identified as being comprised of desirable compounds.

Many studies have investigated upgrading of fast pyrolysis oil over catalysts in secondary processes (Baker and Elliott, 1988; Sharma and Bakhshi, 1993a; Sharma and Bakhshi, 1993b; Adjaye and Bakhshi, 1995; Valle et al., 2007). Other studies have attempted upgrading of selected bio-oil components separated after pyrolysis. Several studies have observed the effects of upgrading only the non-phenolic fraction (NPF) over HZSM-5 (Sharma and Bakhshi, 1993a; Sharma and Bakhshi, 1993b) to alleviate the coking effects caused by phenolic compounds. Several articles upgrade only the aqueous fraction or components making up the aqueous fraction of bio-oil. Gayubo et al. (2004b) transformed alcohols and phenol components over HZSM-5. Gayubo et al. (2004c) upgraded model compounds including aldehydes, ketones, and acids. Corma et al. (2007) used several catalysts including FCC, Al_2O_3,

USY, and ZSM-5-based FCC to upgrade representative biomass oxygenates including glycerol and sorbitol.

One way to minimize coke formation on zeolite catalysts is to remove coke precursors from the oil prior to upgrading. Compounds that are thought to promote coke formation include aldehydes, oxyphenols, furfural, and lignin-derived oligomers (Gayubo et al., 2005; Lu et al., 2010). Other studies (Gagnon and Kaliaguine, 1988; Laurent and Delmon, 1994a; Centeno et al., 1995; Wildschut et al., 2009) have indicated that the carbohydrate fraction is a major contributor to coke formation. In addition, water also acts to deactivate hydrogenation catalysts (Laurent and Delmon, 1994b). There is currently very little research that attempts to remove coke precursors from bio-oil prior to upgrading. We propose that pretreatment of biomass by torrefaction prior to pyrolysis could conceivably remove coke precursors and water from biomass and subsequently bio-oil prior to upgrading thereby reducing coke formation and improving bio-oil quality. Biomass torrefaction is a low temperature pyrolysis process, similar to coffee roasting, in which the biomass is heated in an inert environment (N_2) from ~200-275 °C. Torrefaction generates a hydrophobic solid, friable solid biomass with a reduced grinding energy requirement relative to untorrefied biomass (Phanphanich and Mani, 2010). Torrefied biomass has a lower oxygen content (CO, H_2O, and CO_2 are emitted during torrefaction) compared to untreated biomass, and torrefaction drives off a fraction of reactive and acidic intermediate components gases, such as acetic acid, furfural, and acetaldehyde (Phanphanich and Mani, 2010 ; Mani et al., 2009). Although some of these reactive gases generate coke on acid catalysts, leading to deactivation (Gayubo et al., 2004a; Gayubo et al., 2005), and that the NSF/DOE Roadmap (2007/2008, p 44) has indicated that the impact of torrefaction on thermochemical processing should be investigated, to date no research has been performed to determine the effect of torrefaction as a pretreatment for pyrolysis and catalytic cracking of biomass. Torrefaction, when coupled with pyrolysis and catalytic cracking, could provide synergistic effects not realized with drying and/or catalytic treatment alone.

Torrefaction effectively dries the biomass and decomposes hemicellulose. Several hemicellulose-derived compounds that are thought to produce coke in the subsequent upgrading step, such as acetyl

groups that form acetic acid, would be effectively removed via torrefaction. For example, hemicellulose-derived acetyl groups produced during pyrolysis can form acetic acid that condenses with bio-oil. Reactions of the acetic acid component during subsequent catalytic upgrading of the bio-oil can lead to severe catalyst coking. In addition after upgrading, some acetic acid is left unreacted, and thus, the acid ends up in the product causing high acidity (low pH). Thus, we propose that if hemicellulose is removed prior to pyrolysis, less acetic acid is formed during pyrolysis, and thus, less coke, should form upon catalytic upgrading. As an effect, we expect the pH and overall quality of the final product to be improved.

Research Objectives

For this study, we propose to improve processing and to generate higher quality liquid biofuels. Specific objectives are as follows:

1) Assess and optimize various accelerated aging procedures to assess biofuel storage stability,
2) Generate gasoline and diesel fractions from high free fatty acid waste oils using processing including pyrolysis and catalytic cracking over commercially-available catalyst,
3) Model FFA cracking reactions to optimize processing and product yield and quality,
4) Assess the effects of inline (with pyrolysis) esterification/acetalization using well-sprayed alcohol in bio-oil vapor,
5) Determine the effect of catalytic cracking on slow and fast pyrolysis bio-oils on the yield of fuel quality product,
6) Ascertain the effect of torrefaction pretreatment on the yield and quality of pyrolysis-derived bio-oil and on secondarily catalytically-cracked bio-oil,
7) Assess the effect of pyrolysis heating rate on catalytic cracking effectiveness including process and end product quality effects.

Table 1.1. Pyrolysis feedstock characterization[a].

Parameter	PP	PH	PC	PC T225	PC T250	PC T275
Moisture (w.b.)	7.06	8.6	9.58	5.78	5.11	2.89
Volatiles	80.2	71.7	80.6	76.1	76.1	72.0
Ash	0.36	4.2	0.63	0.23	0.17	0.30
Fixed Carbon	19.4	24.1	17.0	17.9	18.7	24.8
Lignin	26.5	29.2	38.6	N/A	N/A	N/A
Cellulose	47.2	43.1	42.8	N/A	N/A	N/A
Hemicellulose	20.2	4	12.4	N/A	N/A	N/A
C	52.6	55.4	50.3		54.6	58.4
H	5.7	5.1	5.92		5.99	6.05
N	0.2	1.4	0.18		0.27	0.25
S	0	0.1	0.05		0.05	0.05
O[b]	38.9	37.8	39.3		35.6	34.8
HHV (MJ kg^{-1})	20.6	20.3	20.0		21.3	23.7

[a]Values are in % (w/w) on a dry basis unless otherwise noted.
[b]By difference.

Experimental Plan

In an attempt to improve the quality and stability of biomass-derived oil in the current study, we propose to assess a variety of production aspects including biomass pretreatment, pyrolysis conditions, inline processing (reactive condensation), and secondary upgrading (fluid catalytic cracking).

Feedstock

Biomass materials will be in solid form as pine pellets ("PP", Southern Shaving Co., Cherryville, NC), peanut hull pellets ("PH", Birdsong Peanut Company, Blakely, GA), hammer-milled pine chips ("PC"), and in liquid form as pyrolyzed poultry DAF skimmings (i.e. DAF bio-oil) and acidulated peanut oil soap stock ("PSS", Golden Peanut Company, Alpharetta, GA). Liquid feedstock characteristics are given in Table 2. Additionally, thermally pre-treated (torrefied) biomass will be tested. The feedstock for the torrefaction and subsequent pyrolysis and catalytic cracking processes will be pine chips ("PC"). Torrefaction pretreatments were done previously in a large-scale (~1000 kg), batch rotating kiln reactor at temperatures 225, 250 and 275 °C. Torrefied feedstocks are henceforth referred to as PC T225, PC T250, and PC T275. Solid feedstock characteristics are provided in Table 1.

Table 1.2. Comparison of properties for LA, PSS, DAF feedstock and conventional fuels.

Parameter	LA	PSS	DAF bio-oil	Gasoline[a]	B100	No. 2 Diesel[b]
C	79.3	80.2	73.2	84.2	77.2	86.2
H	12.2	12.2	11.1	15.8	12.2	13.8
N	0.3	0.5	4.3	0	0	0
S	0	0	0.1	0	0	0
O[c]	8.1	7.0	8.1	0	10.6	0
H:C	1.85	1.83	1.80	2.3	1.9	1.9
O:C	0.02	0.02	0.10	0	0.1	0
HHV (MJ kg^{-1})[d]	39.6	39.8	36.1	48.5	35.9	45
d.b.[e]	39.6	39.9	37.8	48.5	36	45
HHV (MJ L^{-1})[d]	35.6	35.8	33.2	34.9	30.8	38.6
d.b.	35.7	35.9	34.8	34.9	30.9	38.6
% H_2O	0.1	0.2	4.7	0.0	0.18	0
pH	N/A	N/A	7	~7	7	~7
Viscosity (mm^2 s^{-1})[f]	22.9	59.7	37.8	< 1	2	1.9-4.1
Density (g mL^{-1})	0.9	0.9	0.9	0.72	0.86	0.85

[a]Assuming an average chemical formula, C_8H_{18}.
[b]Assuming an average chemical formula, $C_{12}H_{23}$.
[c]By difference.
[d]"As Received."
[e]"Dry Basis."
[f]Measured at 40 °C

Reactor Design

The first major aspect of the work involved generating slow pyrolysis bio-oil in UGA's existing batch slow pyrolysis unit ("BSPU") and continuous slow pyrolysis unit ("CSPU"). Secondly, the work involved the design and construction of three reactors – a fluidized-bed fast pyrolysis unit (FBPU), a fixed/fluidized-bed (depending on process conditions) fluid catalytic cracking unit (FCCU), and a reactive condensation unit (RCU).

BSPU – A schematic of the BSPU is given in Figure 1.2. Biomass was heated in the reactor at approximately 8 °C min^{-1} to the final operating temperature (400-600 °C) where it was held for 10-30 min. At the end of the holding period, the furnace was turned off, and the reactor was cooled in room air overnight with N_2 flowing before opening. In the BSPU reactor, solids remained in-situ while evolved gases/vapors were entrained in flowing N_2. Upon reaching the ice-cooled condensation unit, the majority

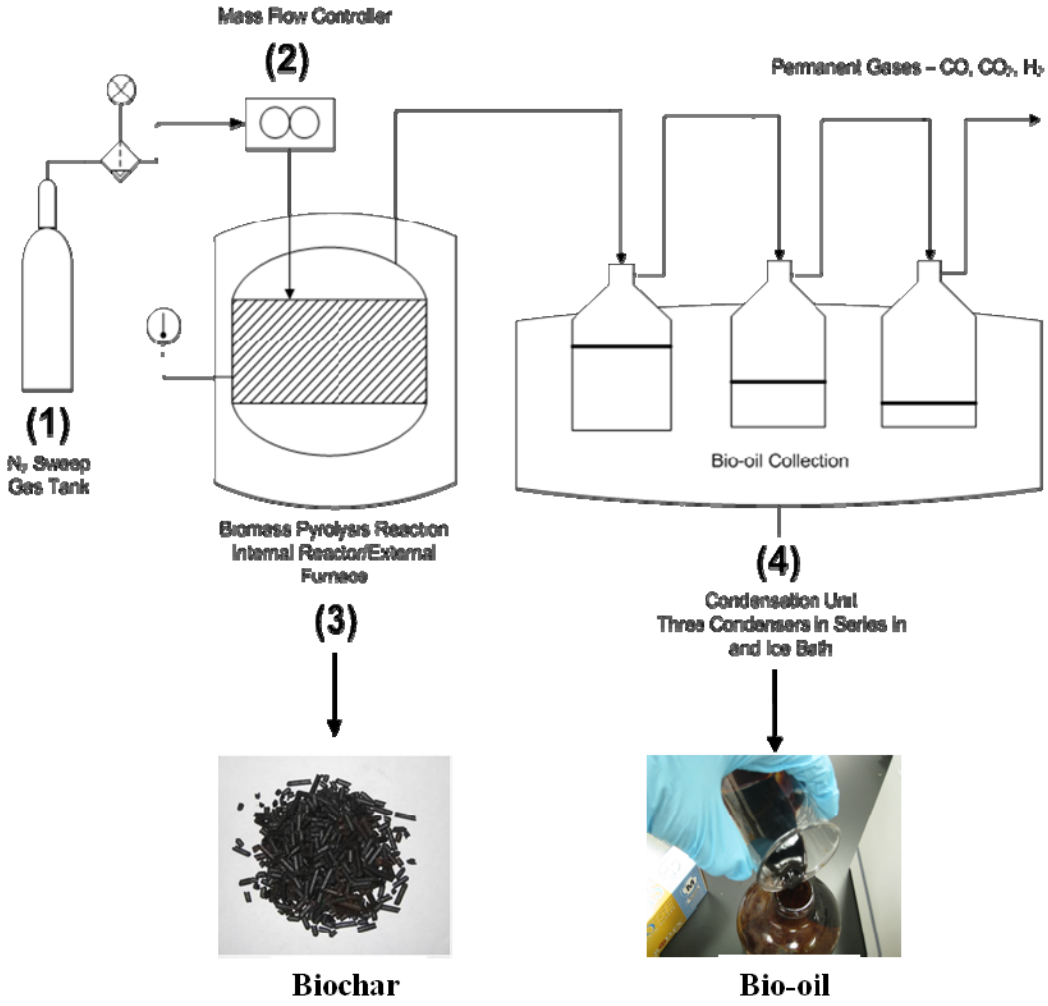

Figure 1.2. Batch pyrolysis unit used to generate biochar and bio-oil from peanut hulls – 1) Nitrogen sweep gas, 2) gas flow controller, 3) reactor holding biomass, and 4) condensation unit to collect bio-oil.

of condensable vapors were collected. A water trap (not shown) is used to collect the remaining vapor. Non-condensable gases were released to the atmosphere.

The first major aspect of the work involved generating slow pyrolysis bio-oil in UGA's existing batch slow pyrolysis unit ("BSPU") and continuous slow pyrolysis unit ("CSPU"). Secondly, the work involved the design and construction of three reactors – a fluidized-bed fast pyrolysis unit (FBPU), a fixed/fluidized-bed (depending on process conditions) fluid catalytic cracking unit (FCCU), and a reactive condensation unit (RCU).

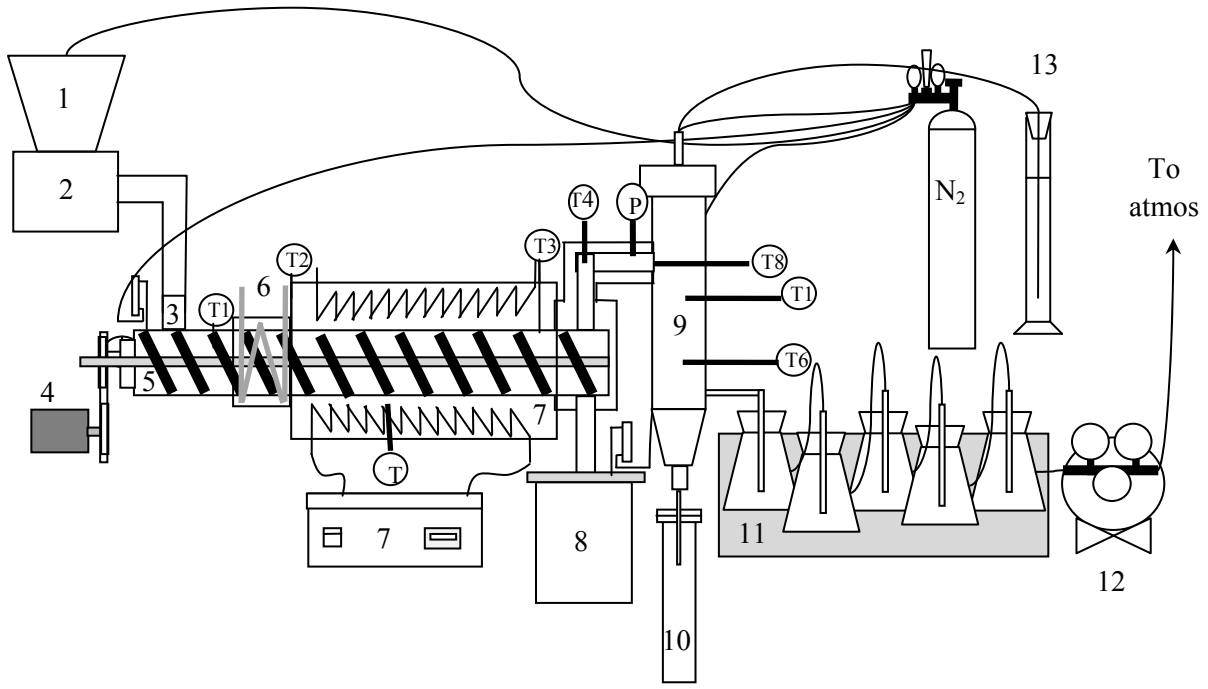

Figure 1.3. Schematic for the CSPU with attached reactive condensation unit. Components include: 1) biomass hopper, 2) vibratory feeder, 3) reactor inlet, 4) auger motor, 5) auger conveyer, 6) water cooler, 7) furnace and furnace control, 8) char collector, 9) reactive condensation unit, 10) bio-oil drip trap, 11) ice bath trap, 12) vacuum pump, 13) ethanol container.

BSPU – A schematic of the BSPU is given in Figure 1.2. Biomass was heated in the reactor at approximately 8 °C min^{-1} to the final operating temperature (400-600 °C) where it was held for 10-30 min. At the end of the holding period, the furnace was turned off, and the reactor was cooled in room air overnight with N_2 flowing before opening. In the BSPU reactor, solids remained in-situ while evolved gases/vapors were entrained in flowing N_2. Upon reaching the ice-cooled condensation unit, the majority of condensable vapors were collected. A water trap (not shown) is used to collect the remaining vapor. Non-condensable gases were released to the atmosphere.

CSPU – The CSPU shown in Figure 1.3 consists of a 100 mm O.D. stainless steel auger reactor. The auger is driven by a microprocessor-controlled ¼ hp electric motor. The auger continuously transports biomass feedstock through the reactor, which is externally-heated using a tube furnace (Lindberg/Blue M, model HTF55322A) The auger speed will be maintained at 1.5 rpm which translates to a solid residence time of 8.3 min in the reactor (residence time in the heated zone: 5.9 min).

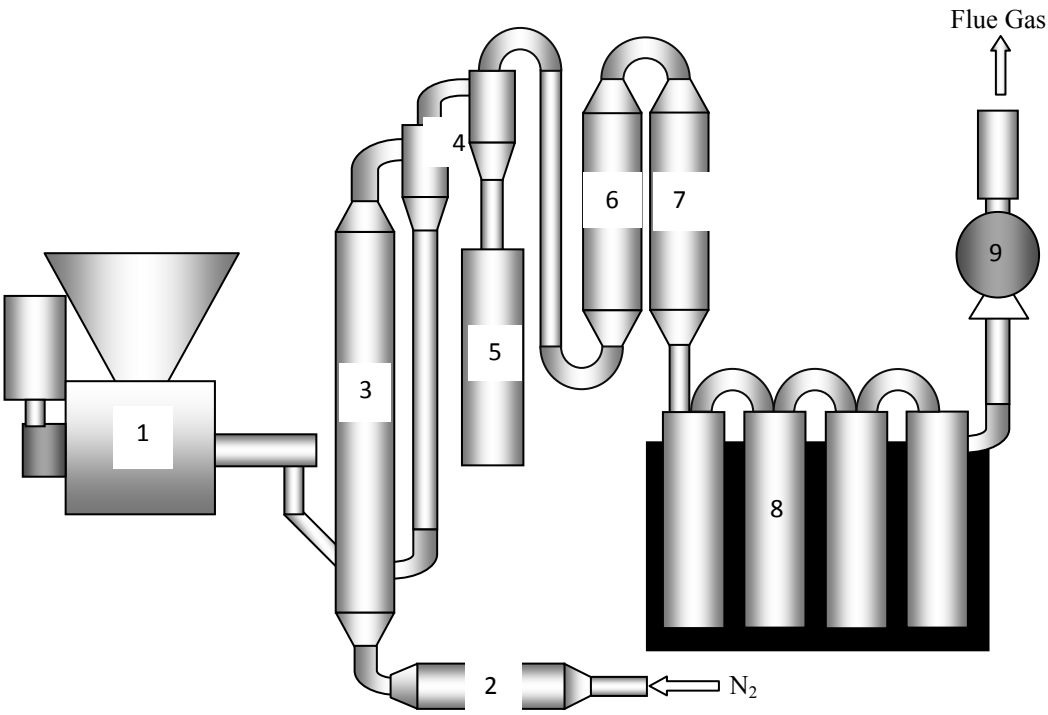

Figure 1.4. Fluidized-bed pyrolysis unit showing components: 1) biomass hopper/feeder, 2) gas pre-heater, 3) riser reactor, 4) cyclone separators, 5) char collector, 6) hot gas filter, 7) shell and tube condenser, 8) ice-bath condensers, and 9) exhaust fan.

FBPU – The FBPU design shown in Figure 1.4 consists of four main components – a biomass feeder (component #1), a reactor (#3), a solids separator (#'s 4 and 5), and a condenser (#'s 7 and 8).

FCCU – The FCCU (Figure 1.5) contains a catalyst bed with either H-ZSM-5 or FCC variety. The HZSM-5 catalyst was produced by calcining NH_4-ZSM-5 (Zeolyst International, CBV 5524 G). The catalyst has published values of 425 m^2 g^{-1} (measured 374), 0.46 mm, and 50 for surface area, particle size and SiO_2/Al_2O_3 ratio, respectively. The NH_4-ZSM-5 was calcined at 550 ˚C for 4 h to produce the hydrogen form, H-ZSM-5, resulting in stronger acid pore sites. The process reduced the overall pH from 4.98 to 3.06. The FCC catalyst was supplied by Grace Chemical – composition is proprietary.

RCU – The RCU (see Figure 1.6) is attached at the outlet of the CSPU. The RCU is expected to function as a means to condense and esterify acidic components. Ethanol was be used as the reactant (along with bio-oil vapor) in the unit. The RCU consisted of a 102 mm I.D. stainless steel tube with a reaction zone

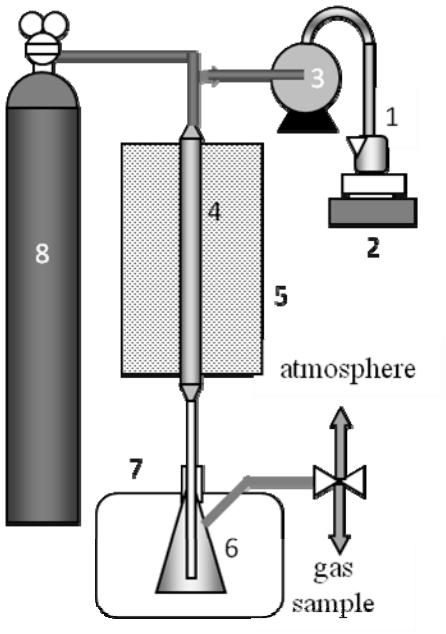

Figure 1.5. FCCU showing: 1) sample container, 2) sample preheater, 3) pump, 4) reactor, 5) furnace, 6) sample collector, 7) ice bath, and 8) inert gas source.

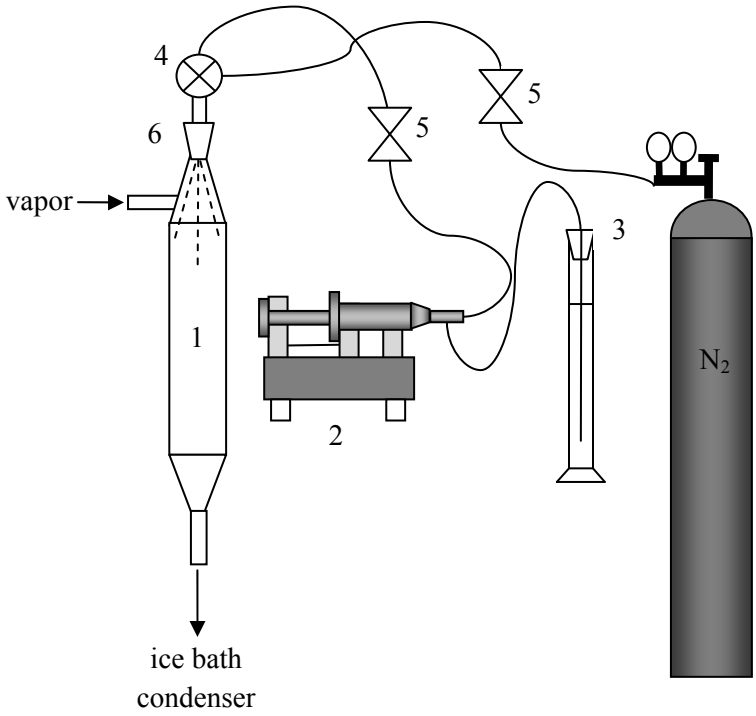

Figure 1.6. Reactive condensation system for FBP unit shown in Fig. 5. Items shown figure include; (1) wet scrubbing condenser, (2) peristaltic pump, (3) graduated cylinder containing ethyl alcohol, (4) junctions, (5) one-way valves, and (6) atomizing nozzle.

length, L=457 mm, meaning the

reaction zone volume was 3.8 L. In the reactor, vapors were contacted with atomized 100 % (200 proof) ethanol (C_2H_5OH, abbr. EtOH, supplied by Thermo Fisher Scientific) that was supplied using a peristaltic pump (Cole-Parmer L/S, model 7524-10) and input to the reactor by a small-bore (0.015 mm I.D.) cone-spray atomizer nozzle. In order to achieve adequate atomization of EtOH at low flow rates (1.5 – 2.0 mL min^{-1}), 0.1 L min^{-1} pressurized N_2 at 377 kPa (40 psig) was mixed with the EtOH prior to entering the atomizer nozzle. Temperature was measured at the inlet of the reactive condensing unit and at two points along the condenser's length. Heavier liquids condensed in a drip trap directly beneath the reactor. At a carrier gas flow rate of 3.6 L min^{-1}, the effective reactor volume (3.8 L) translated to a vapor residence time of 63.3 s in the reaction zone before entering the drip trap. Un-condensed vapor and non-condensable gases were routed through a series of five ice-bath traps that collected the remaining condensable vapor. Non-condensable gases exited to the atmosphere.

Experiment Summary

The proposed work consisted of five major experiments. Experiment 1 involved developing a method to determine the thermal and oxidative stability of bio-oil. Test materials included bio-oils derived from the pyrolysis of PP and PH in the BSPU. Experiment 2 involved the catalytic cracking of two high free acid liquid feedstocks: pyrolyzed (at 600 °C in the BSPU) poultry processing DAF waste ("DAF") and acidulated peanut oil soap stock ("PSS") in the FCCU in an effort to generate drop-in biofuels. An extension of Experiment 2, Experiment 3 will provide a detailed study of the mass transport and kinetics of PSS cracking on zeolite, HZSM-5. The next set of experiments will utilize lignocellulosic feedstocks processed under varied operating conditions. For Experiment 4, the CSPU will be used to generate bio-oil that will be processed inline using the RCU in an effort to improve fuel properties of the product, particularly the acidity, by chemically converting acids to esters. In experiment 5, bio-oils generated in the FBPU and the BSPU using feedstocks including PP, PH, PC, and torrefied PC were then processed in the FCCU in an attempt to improve fuel properties. The intent was to compare overall yield and quality of end products derived from the various treatment processes. Of particular are the effects of pyrolysis heating rate (slow or fast) and the effects of torrefaction pretreatment on the quality, stability, and yield of fuel components.

Dissertation Format

This dissertation is configured in "Manuscript Style" with experiments separated as chapters comprising accepted, submitted, or soon-to-be submitted manuscripts in addition to Introduction and Conclusion chapters. Experiments 1 through 3 are presented here as manuscripts in Chapters two through four. Each of these has been submitted, accepted and published. Experiment 3 (Chapter 5) has not yet been submitted, but submission is planned for summer 2012. The manuscript resulting from Experiment 4 (Chapter 6) has also been published. The work of Experiment 5 is part of a broader, ongoing research objective for the Biorefining and Carbon Cycling Program at the University of Georgia, and the work described here is less the culmination of project coming to a close but more of a snapshot of ongoing

activities. Three chapters (7, 8, and 9) comprising three manuscripts describe the results of Experiment 5. Experiments are further outlined below.

Permission to reprint has been granted for all published articles. For Elsevier journal publications (Chapters 2, 3, and 4), the right to publish an article in a thesis or dissertation is always allowed (see http://www.elsevier.com/wps/find/authorsview.authors/rights). Permission for reprinting the American Chemical Society article in Chapter 6 is provided in the Appendices section.

Summary of Manuscripts

Storage Stability Method Development for Bio-oil

As part of Experiment 1, the stability of PP and PH bio-oils generated in the BSPU and CSPU were assessed using three stability assessment methods. Bio-oils were phase-separated (removal of aqueous phase) generating an oily phase for each batch run that was split in two with one half receiving 10 % (w/w) methanol (MeOH) while the other half was left neat. This was done for bio-oils derived from both biomass sources from batch pyrolysis system thus creating four sample types. With the addition of the continuous system-produced bio-oil, the sample set thus consisted of 5 sample types including; PP bio-oil containing 3.9 % (w/w) EtOH (named PP-E), PP with 0 % MeOH (PP), PP with 10 % MeOH (PP-M), PH with 0 % MeOH (PH), and PH with 10 % MeOH (PH-M). Four replicates were produced for each sample type creating a total of 20 samples. All samples were stored at 4 ˚C until analyzed. Attempts were made to analyze samples within 24 h of production.

The stability of the bio-oils was assessed by measuring certain parameters before and after one of three accelerated aging methods. In the first method (Method 1), relative thermal stability of the bio-oil was measured by subjecting the oil to an aging procedure involving heating the oil to 80 °C and holding for 24 h. The variable of interest was viscosity and more specifically, the change in viscosity as a result of aging. For bio-oils, an increase in viscosity is expected due to polymerization reactions that occur during aging. For Methods 2 and 3, the oxidative stability of the oils was determined. Method 2 is based on ASTM D 5304, which was developed for determining the storage stability of middle distillate fuels such as No. 1D and No. 2D diesel, fuels that bio-oils are intended to replace or supplement. The test

parameter is the amount of insoluble material formed as a result of aging. Method 3 uses a programmed heating program in a differential scanning calorimeter (DSC) to determine the onset of oxidation (OOT) when heating the oil in an oxygen environment. After each aging procedure the chemical composition of the oils was assessed via GC-MS and FT-IR analysis to determine if any notable changes in oxygenated or higher molecular weight compounds were evident.

For stability Method 1, after aging, samples were cooled to room temperature and weighed to determine if any loss of volatiles has occurred. Afterwards, dynamic viscosity, μ, at 40 ˚C was measured at three shear rates. All other compositional parameters (pH, water content, CHNS-O, density) were also assessed, as well. From dynamic viscosity and density (μ/ρ), kinematic viscosity was calculated. Kinematic viscosity, v, versus shear rate was plotted to determine if a nonlinear (non-Newtonian) relationship was evident. The change in v was then determined on an absolute basis ($mm^2\ s^{-1}\ d^{-1}$) and on a relative basis using the viscosity index: $(v_{final} - v_{initial})/v_{initial}$ (Oasmaa and Kuoppala, 2003). A smaller increase (less change) in viscosity for a sample was assumed to indicate greater stability during prolonged storage.

For Method 2, stability is ranked based on the formation of insoluble material after an accelerated aging procedure. The test involved placing a known amount of pre-filtered (0.8 μm pore size filter) liquid into a pressure vessel that was then pressurized to 800 kPa (absolute) with oxygen. The vessel was heated to 90 ˚C in a forced air oven for 16 h. At the end of the heating period, the vessel was removed from the oven, depressurized, and allowed to cool to room temperature. The sample was then filtered under vacuum through a pre-weighed filter, washed with acetone solvent to ensure no bio-oil residue remains on the filter or glassware. Afterwards, filters were dried, and reweighed to determine the quantity of insoluble material formed.

According to ASTM D5304, insoluble material formation should be reported in mg of insoluble material per 100 mL of liquid. Since it is difficult to accurately measure volumes of bio-oil due to its adherence to glassware, in this study, we have reported the values by percent of total mass and in g of

insoluble material per g of liquid filtered. Approximately 100 g was filtered for each of three replicates for each bio-oil type.

Determining stability via Method 3 was an attempt to assess bio-oil oxidative stability more quickly than Method 2 using the OOT test described by ASTM E 2009. ASTM E2009 is typically used for edible oils and fats, lubricants, greases, and polyolefins, but was employed in this study. This test uses a DSC analysis to determine the temperature, known as oxidation onset temperature (OOT), at which oxidation (combustion) begins. As stated in the ASTM method, samples with higher OOT are more stable. The method entailed placing approximately 3 mg of sample into the measuring cell of the DSC and heating the sample from 25 to 250 ˚C at 10 ˚C min^{-1} in an oxygen atmosphere (50 mL min^{-1}). At a sample-specific temperature, oxidation initiated generating an exothermic peak on the DSC curve. OOT was determined by extrapolating the point of intersection between the baseline and the slope of the exothermic peak at the onset of oxidation. Stability of the oils was ranked based on OOT where a higher OOT value indicates a more stabile the oil. No studies have been found that attempt to use this method for bio-oil stability determination. Since performing the method requires only 30 minutes, it provided a quick alternative to other stability assessment methods.

FFA Conversion to Fuel Over HZSM-5

Three chapters (Chapter 3, 4, and 5) comprise the effort to determine the effects of catalytic cracking on high free fatty acid feedstocks including poultry-derived DAF waste ("DAF") and acidulated peanut oil soap stock ("PSS") will be determined. For DAF, multiple processing steps were required including drying (24 h at 105 °C) in a forced air oven, pyrolysis (8 °C min^{-1} ramp to 600 °C followed by 30 min holding period) in the BSPU, and finally, catalytic cracking (at 400, 450, and 500 °C) in the FCCU. For PSS, the feedstock required no preprocessing steps, and could be directly processed in the FCCU. Multiple catalysts were used in the fixed-bed catalytic reactor including HZSM-5 and a commercially-available (W.R. Grace and Co.) fluid catalytic cracking (FCC) catalyst.

Process related parameters that were varied during the experiment outlined in Chapter 4 included catalyst type (HZSM-5 or FCC), catalyst to oil ratio (C/O), and weight hourly space velocity (WHSV, h^{-}

[1]). We observed the effect of process parameters on product yield (solid, liquid, and gas). Solid material was generated in the form of reactor char and catalyst coke. Catalyst coke was determined by subjecting spent catalyst to combustion in a thermogravimetric analyzer (TGA) while measuring the weight change.

Product oil properties of interest were, generally, quality and stability. Quality was determined in terms of fuel properties (HHV, water content, viscosity, cloud point) and stability in terms of oxidation onset temperature. In addition, chemical composition of the oils was ascertained via GC-MS and GC-FID analysis. Of particular interest was the formation of aromatic hydrocarbons, compounds often formed as a result of processing liquids with HZSM-5. Of these hydrocarbons, benzene, toluene, ethylbenzene, and xylene (including ortho- (o-), meta- (m-), and para- (p-) isomers), collectively known as BTEX, were quantified.

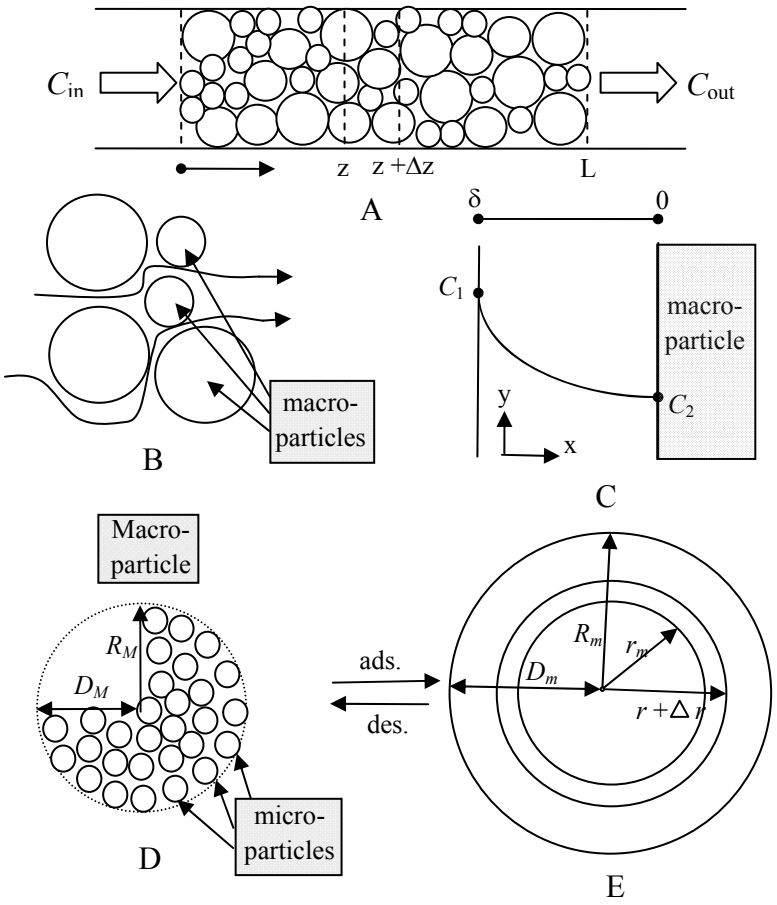

Figure 1.7. Fixed-bed reactor model showing modes of transport in bulk phase between macroparticles (A and B), through the stagnant layer on the macroparticle surface (C), through the macroparticle void spaces (D), and within the spherical macroparticle or microparticle (E). Based on Haynes (1975).

The experiment outlined in Chapter 5 involved a detailed study of the reaction kinetics and mass transport effects in play during catalytic cracking of PSS. A model was developed and validation was attempted for the conversion of oleic and linoleic acid over HZSM-5 catalyst. The overall system was modeled as a reaction in porous solid media. Figure 1.7 indicates the modes of transport to be modeled as part of Experiment 3.

Using the FCCU, varied concentrations of feedstock (varied by carrier gas flow rate) were passed across multiple height beds of HZSM-5. The main intent was to determine the reaction rate and indicate whether the reaction was mass transfer- or intrinsic reaction rate-limited. Of interest during the experiments were the conversion of free fatty acids including oleic and linoleic acid which were chosen as model compounds in PSS and the yield product compounds including BTEX.

An attempt was made to determine the intrinsic reaction rate using DSC analysis as described in ASTM E698 wherein a non-isothermal heating program is used at multiple heating rates to determine the change in the reaction peak temperature. From this data, activation energy (E), pre-exponential factor (k_0), rate constant, and half-life ($t_{1/2}$) could be determined for the reaction. Thusly, the reaction rate at a given temperature was determined using the Arrhenius equation.

Upgrading Lignocellulosic Bio-oils

A variety of methods were attempted as a means to improve the quality and stability of bio-oil. Methods included a biomass pretreatment process (i.e. torrefaction, Chapters 9 and 10), an inline vapor phase upgrading process (i.e. reactive condensation, Chapter 6), and secondary vapor phase upgrading process (i.e. catalytic cracking, Chapters 7, 8, 9, and 10).

Outlined in Chapter 6, reactive condensation was incorporated into a pyrolysis bio-oil upgrading scheme. In an attempt to improve the oil quality, alcohol was atomized into a stream of uncondensed bio-oil vapor in the RCU at ratios up to 50:50 ratio (v/v) in order to rapidly and simultaneously cool, condense, and esterify carboxylic acids in the vapor phase. The reactor is shown in Figure 1.6, and its placement is after the solids separation system in the continuous slow pyrolysis unit (CSPU) but prior to the ice bath condensing units. Variables of interest included carboxylic acid conversion (i.e. extent of ester formation as verified by GC-MS and quantified by GC-FID) and fuel properties (e.g. heating value, viscosity, water content, stability).

Biomass feed was supplied to the reactor by a vibratory feeder (Eriez, model H036C). For pyrolysis experiments, the biomass and carrier gas feed rates were held constant to ensure consistent pyrolysis conditions. Pyrolysis vapors leaving the reactor were then directed passed through the reactive

condensation unit where ethanol was injected and then through a series of five ice-bath traps to condense any remaining bio-oil. In order to prevent high-boiling vapor (tar) from clogging the pyrolysis reactor and reactive condensation unit, the pyrolysis reactor's exhaust line was heated to maintain vapor temperature above 450 °C. Slow pyrolysis conditions were assumed based on the solid phase residence time, the two-phase nature of the bio-oil end-product, and the yield of char and gases. Non-condensable gases were purged from the system via a vacuum pump attached to the last ice-bath trap in the series and vented to atmosphere. Solids were collected in a stainless steel char collector at the outlet of the reactor where the material was cooled at room temperature under in an inert environment. An inert atmosphere was maintained in the reactor and char collector by supplying nitrogen to various inlets in the system. The nitrogen flow rate was 3.6 L min^{-1} distributed as follows: 2 L min^{-1} into the main reactor, 0.5 L min^{-1} into the hopper, 1 L min^{-1} into the char container, and 0.1 L min^{-1} into the reactive condensing unit. Thermocouples were installed at various locations to monitor temperatures (see Figure 1.6).

The quantity of biomass in the vibratory feeder hopper was weighed before and after each pyrolysis run to determine the total amount supplied to the reactor. Biomass feed rate was assumed to be steady throughout each run. Solid material, namely char, was collected and weighed as was condensed liquid in the drip and ice-bath traps to determine product yield. A simple mass balance was used to calculate the quantity of non-condensable gases.

For the experimental runs, the biomass feed rate was kept constant to ensure equivalent characteristics for the vapor feed entering the reactive condensing unit, while the EtOH atomization rate was varied from 0 to 6 mL min^{-1}. Total yield of bio-oil was determined by weighing the whole product then subtracting the weight of EtOH added during the run.

As part of our effort to improve the quality of biomass-derived fuels via fluid catalytic cracking, we expanded upon previous work by including lignocellulosic feedstocks. In particular, we assessed the effectiveness of catalytic upgrading of PP- and PH- and torrefied PC-derived liquids based on the formation of desirable end-products including aromatic and aliphatic hydrocarbons. We utilized a GC-FID method to quantitatively assess the concentration of several products and reactants. In addition, the

time-on-stream of FCCU runs was varied to note the effect on conversion resulting from catalyst deactivation.

The catalytic cracking experiment consisted of three distinct objectives: 1) determine the effectiveness of slow pyrolysis followed by catalytic cracking as a means to generate liquid biofuels, 2) compare the effects of pyrolysis heating rate (i.e. slow or fast pyrolysis) on the catalytic cracking process and on the end-product quality, and 3) determine the effect of torrefaction pretreatment on both the pyrolysis process (slow and fast) and the catalytic cracking process and on end-product quality.

Objective 1

The assessment of catalytic cracking effectiveness for slow pyrolysis oils derived from lignocellulosic feedstock involved determining the yield of liquid product and byproducts (e.g. catalyst coke, reactor char) and indicating the presence of desirable end products (e.g. BTEX, linear alkanes, PAHs) in the product liquid in addition to determining the effect of upgrading on macro fuel properties of the liquids, higher heating value (HHV) in particular. Feedstocks for this experiment included PP and PH bio-oil generated from slow pyrolysis at 500 °C. Table 1.3 provides characteristics for the bio-oil feedstocks.

Objective 2

As part of Objective 2, two distinct experiments were undertaken. Both experiments used pine chips as the feedstock for bio-oil production. The work involved two conversion steps: a pyrolysis step and a catalytic cracking step. The difference between Experiment 1 and Experiment 2 was the method of bio-oil production, the heating rate of the production method, in particular. The first experiment involved subjecting pine chip biomass, PC, to slow pyrolysis at 500 °C with a heating rate at approximately 8 °C min^{-1} in the BSPU. Lower heating rates generally cause secondary reactions that result in the formation of secondary pyrolysis products (i.e. char, non-condensable gases). The oil from slow pyrolysis consisted of two phases with a clear separation between phases. The lower, heavier phase exhibited some desirable fuel qualities including low viscosity (<50 $mm^2 s^{-1}$), good energy density (~ 30 MJ kg^{-1}), and low water

content (~5 %) relative to fast pyrolysis oil. The tradeoff was that the yield is lower than that of fast pyrolysis.

The second experiment will use fast pyrolysis processing using the FBPU for bio-oil generation at a heating rate at approximately 1000 °C s^{-1}. Although the yield of fast pyrolysis oil is high (65-80 %), the water content is also very high (~25 %) meaning that the heating value is quite low (~16 MJ kg^{-1}).

Table 1.3. Characteristics of bio-oils produced by batch pyrolysis.

Parameter	Bio-oil characteristics			
	PP	PP-M	PH	PH-M
	None	Methanol	None	Methanol
Solvent (%,w/w)	0	10	0	10
C	74.0 ± 3.5	70.8 ± 5.5	72.0 ± 0.8	67.9 ± 0.3
H	8.0 ± 0.7	8.7 ± 1	8.6 ± 0.3	9.0 ± 0.3
N	0 ± 0	0.3 ± 0.2	2.2 ± 0.1	2.0 ± 0
S	0 ± 0	0 ± 0	0.1 ± 0	0.1 ± 0
O[a]	18.0 ± 4.1	20.3 ± 6.5	17.2 ± 1.2	21.0 ± 0.4
HHV(MJ kg^{-1})	30.1 ± 0.9	28.2 ± 0.5	29.9 ± 2.9	29.7 ± 1.1
H_2O (%)	3.3 ± 0.8	5.0 ± 1.3	6.5 ± 3.0	5.8 ± 0.8
υ (mm^2 s^{-1}) at 40 °C	21.9 ± 3.1	8.8 ± 0.4	60.0 ± 18.1	16.9 ± 0.9
ρ (g mL^{-1})	1.11 ± 0.2	1.07 ± 0.1	1.07 ± 0.1	1.05 ± 0.2

[a] By difference.

In the second processing step, catalytic cracking, experimental parameters common to both experiments that were manipulated included catalyst type, C/O (a function of time-on-stream, feed rate, and catalyst bed height) and catalyst temperature. A three-way ANOVA test along with a multiple comparisons test (using either the Holm-Sidak or Tukey method) were used to determine how experimental parameters affected yield of product and byproduct and end product quality.

Objective 3

For this objective of the catalytic cracking experiment, PC and torrefied PC was used as the fast pyrolysis feedstock. Characteristics for biomass feedstock are given in Table 1.4. Production parameters including liquid, solid and gaseous yield were determined. In addition, conversion of bio-oil components

including guaiacol, creosol, acetic acid and yield of desirable chemical species (e.g. BTEX) were determined. We hypothesized that torrefaction would remove undesirable coke precursors (acetaldehyde, acetic and formic acid) from the feedstock prior to pyrolysis with the result being higher quality intermediate (pyrolysis oil) containing fewer carboxylic acids, an effect which would improve the final product after the catalytic cracking step. Measures of quality included heating value, CHNS-O, and stability (via OOT assessment).

Table 1.4. Torrefied biomass feedstock characteristics.

Parameter	Feedstock Characteristics (%, w/w d.b)											
	PC T100			PC T225			PC T250			PC T275		
	AVE	±	95% CI	AVE	±	95% CI	AVE	±	95% CI	AVE	±	95% CI
Moisture[a]	0.03	±	0.02	0.48	±	0.28	0.35	±	0.10	0.01	±	0.02
Volatiles	81.4	±	0.02	80.0	±	0.22	77.9	±	1.20	72.3	±	0.47
Ash	0.30	±	0.04	0.36	±	0.03	0.39	±	0.05	0.20	±	0.16
Fixed Carbon	18.3	±	0.02	19.6	±	0.24	21.7	±	1.15	27.5	±	0.31
C	46.9	±	0.2	48.3	±	0.5	48.4	±	0.1	53.3	±	0.6
H	5.98	±	0.1	5.88	±	0.1	5.83	±	0.1	5.60	±	0.0
N	0.45	±	0.1	0.88	±	0.2	0.82	±	0.1	1.00	±	0.3
S	0.00	±	0.0	0.00	±	0.0	0.00	±	0.0	0.00	±	0.0
O[b]	46.3	±	0.2	44.6	±	0.2	44.6	±	0.1	39.9	±	0.5
HHV[c] ($MJ\ kg^{-1}$)	18.6	±	0.1	19.1	±	0.1	19.1	±	0.1	21.1	±	0.3

[a]Wet basis

[b]By difference

[c]Calculated following Channiwala and Parikh (2002)

For the catalytic cracking objective, oils were preheated (unstirred) and injected using a peristaltic pump (Cole-Parmer, Model L/S Digital) at 1.5 mL min^{-1} into a 2.2 cm I.D. tubular reactor and passed across a fixed bed of HZSM-5 catalyst (FCCU from Figure 1.5). An inert gas flow (N_2) was maintained at 50 mL min^{-1} for most experiments. Reactions were undertaken in the FCCU wherein catalyst zone temperature was held between 400-550 °C. For these experiments, we have assumed plug flow reaction

conditions, which implies that temperature is isothermal radially, although the temperature may vary somewhat longitudinally due to heat of reaction.

Effectiveness of upgrading was determined using a variety of measures. Firstly, process parameters including yield of product and byproduct (gas, char, tar, and coke) were measured. The intent was to determine which combination of process parameters (pretreatment method, catalyst type, C/O, catalyst temperature) produced the highest yield of product for each bio-oil generated for each biomass type. In order to maximize product yield, byproduct formation must be minimized.

Analytical Methods.

Beyond process parameters, products and byproducts were thoroughly characterized to assess upgrading effectiveness. The product liquids were analyzed to determine CHNS-O, water content, pH, density, higher heating value, viscosity, and chemical composition. Measurement of CHNS-O shows the effectiveness of upgrading in the various experiments by indicating oxygen content reduction and an improvement in the H:C and O:C ratios implying hydrocarbon formation. We expected that in all experiments, water content in the product would be reduced due to formation of hydrocarbons in which the solubility of water is low. Both density and viscosity should be reduced due the cracking of large molecules and the formation of aromatic and short to mid-range length hydrocarbons. Higher heating value should increase due the decrease in oxygen and water content and increase in carbon content. We expected the analysis of chemical composition for the upgraded products as measured via GC-MS to indicate the formation of aromatic (e.g. benzene, toluene, ethylbenzene, and xylene) and aliphatic hydrocarbons (e.g. C_5-C_{18} alkanes). We also expected to see a reduction in the concentration of oxygen-containing species including phenols, aldehydes, ketones, and organic acids for the lignocellulosic biofuels generated. A calibrated GC-MS method (see Figure 1.8 for calibration factors) was used to determine concentrations of reactants (guaiacol, creosol, and acetic acid) and BTEX products based on 6-point calibrations with pure compound mixtures with internal standard, heptane.

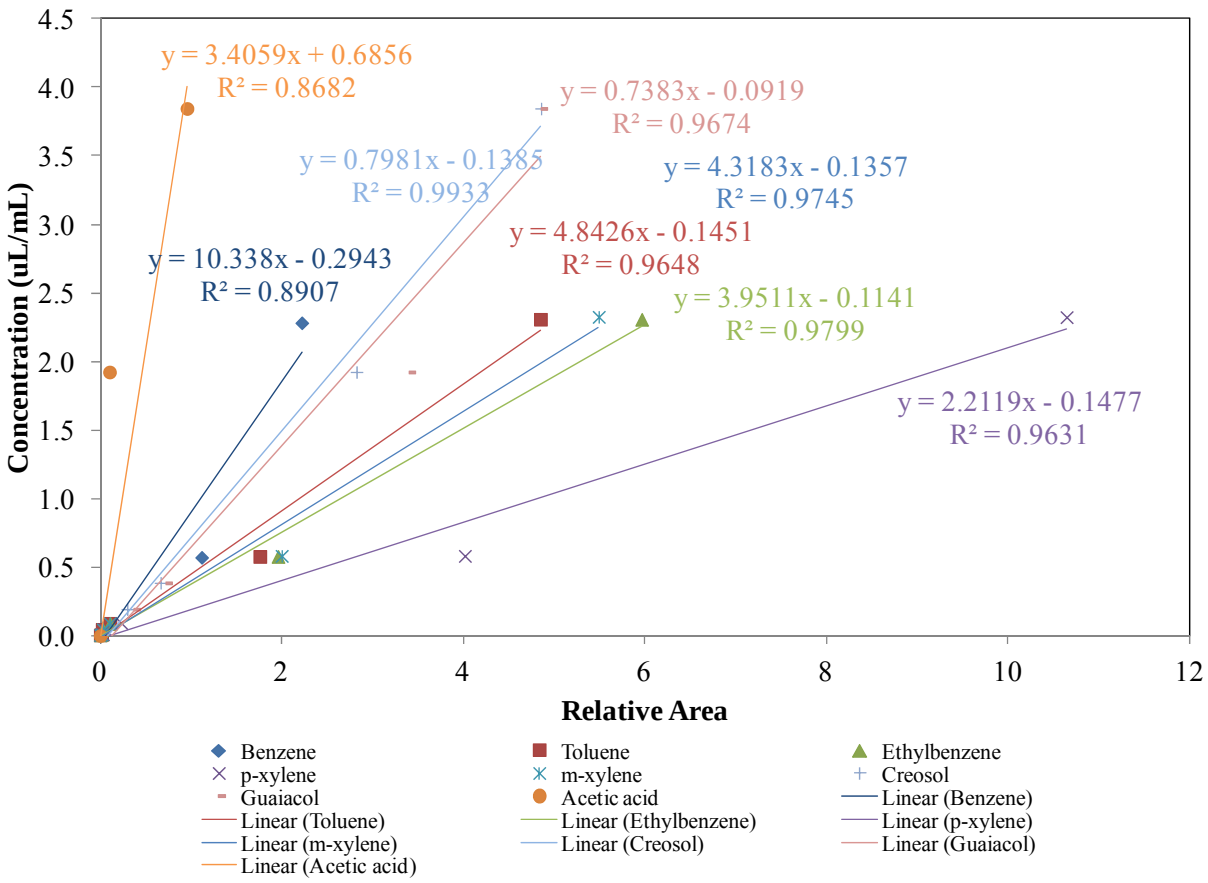

Figure 1.8. Calibration factors for BTEX, acetic acid, guaiacol, and creosol.

Byproducts were characterized, as well. Byproduct gases were sampled periodically at the catalytic reactor outlets and analyzed using a GC-TCD. Char, which was considered to be the solid, non-coke material formed during pyrolysis and catalytic cracking, was quantified. Tar, the acetone-soluble material forming on the catalyst, was also quantified. Coke formed on spent catalyst during catalytic cracking was quantified by subjecting the spent catalyst to temperature-programmed desorption (oxidation) in a thermogravimetric analyzer (TGA). Evolved gases were characterized qualitatively using a TG-attached mass spectrometer.

CHAPTER 2

COMPARISON OF THREE ACCELERATED AGING PROCEDURES TO ASSESS BIO-OIL STABILITY[1]

[1] Hilten, R., Das, K.C. 2010, *Fuel*, 89: 2741-2749. Reprinted here with permission of the publisher.

Abstract

The current study utilizes three stability ranking methods to compare oxidative and thermal stability of alcohol-stabilized and un-stabilized slow pyrolysis bio-oil. Procedures were based on standard methods established by ASTM (D5304 and E2009) for hydrocarbon fuels and on a widely used method that assesses viscosity change over time. Each method involves an accelerated aging procedure ranging from several minutes to 24 hours. Average stability rankings for bio-oils produced from two biomass feedstock (pine and peanut hull) in two pyrolysis units were compared. Bio-oils in order from most to least stable included; methanol-stabilized pine pellet oil, un-stabilized pine pellet oil, ethanol spray-condensed pine pellet oil, methanol-stabilized peanut hull oil, and un-stabilized peanut hull pellet oil. FT-IR spectra from pre- and post-aging showed an increase in the relative concentration of C-O (phenols, carboxylic acids, esters, and ethers) and C=O (carbonyl) functional groups for aged samples.
Keywords: bio-oil, stability, thermal, oxidative, accelerated aging, pyrolysis

Introduction

Bio-oil is a potential renewable energy source for electricity and heat generation as well as being an alternative transportation fuel. However, several hurdles must be crossed before bio-oil can be used reliably. One of the main hurdles is poor storage stability of the oils. During storage, there is potential for bio-oils to undergo changes due to oxidative and thermal degradation. Oxidation can lead to polymerization resulting in viscosity increases (Oasmaa et al., 1997; Diebold and Czernik, 1997) and gumming of tanks and fuel lines. Thermal degradation causes partial decomposition of components and can lead to loss of volatiles which also leads to increased viscosity (Oasmaa et al., 1997; Diebold and Czernik, 1997). Both storage conditions lead to viscosity and compositional changes (Oasmaa et al., 1997; Diebold and Czernik, 1997; Diebold, 2000; Oasmaa and Kuoppala, 2003; Boucher et al., 2000). Most applications for bio-oils require that bio-oils retain favorable initial physical properties during storage, shipment and use (Diebold, 2000). Otherwise, filters, injectors, input lines, etc. can become obstructed.

In an effort to increase stability, Diebold and Czernik (1997) showed that additions of solvents could significantly decrease viscosity changes during aging. Solvents used in the study included ethyl acetate, a mixture of methyl isobutyl ketone and methanol, acetone, methanol, a mixture of acetone and methanol, and ethanol. Their findings revealed that methanol at 10 wt. % enhanced bio-oil stability and reduced viscosity most effectively. The mechanisms of the increase in stability and reduction in viscosity was attributed to four factors: 1) reduction in the concentration of reactive aldehydes through the conversion to hemiacetals and acetals, 2) transacetalizing larges hemiacetals and acetals to lower molecular weight acetals, 3) conversion of reactive organic acids to esters, and 4) transesterification of large esters to lower molecular weight esters.

Another method of stabilizing bio-oil is through conversion to ethyl esters using ethanol along with a catalyst. Junming et al. (2008) showed that bio-oils reacted with ethanol over a solid acid catalyst exhibited increased stability (less viscosity change during storage), increased higher heating value, and lower water content and acidity than non-esterified bio-oil.

Beyond measuring physical changes in bio-oil during storage, several methods can be used to examine compositional changes as well. Fourier transform infrared spectroscopy (FT-IR) is one tool to evaluate functional group changes. Scholze and Meier (2001) showed that specific oxygenated groups that affect stability such as carbonyls express distinct changes in the intensity of absorption spectra after aging. The authors reported that with increasing carbon content in pyrolytic lignin (with a concurrent decrease in oxygen content), adsorption bands representative of carbonyls at 1701, 1652, and 1600 cm^{-1} were significantly reduced. Thus, during aging, especially during oxidative aging, carbonyl bands should increase in intensity. Other oxygen-related bands, i.e. hydroxyl and methoxyl bands, were less affected by changes in oxygen content.

The goal of this study is to show whether standard methods for determining stability in hydrocarbon fuels are applicable for biomass-derived pyrolysis liquids. More specifically, we will compare results from three accelerated aging stability ranking methods while observing the effects of aging and storage on pyrolysis oils. Stability of oils will be determined by three methods based on

viscosity increases, the formation of solids, and the onset of oxidation under heat. The first test is a thermal stability test while the other two are oxidation stability tests. FTIR will be used to show changes in several oxygen-containing functional groups in the oils before and after aging to determine relative changes in function groups due to oxidation and polymerization. The formation of insolubles (solids) and oxidation onset tests are based on ASTM D5304 (2006) and E2009 (2002), respectively. Measuring viscosity change with aging is not defined in a specific standard but has been recommended and used in several other studies of bio-oil stability (Diebold and Czernik, 1997; Oasmaa and Kuoppala, 2003, Boucher et al., 2000). The aging procedure for the test involves thermally treating the bio-oil at 80 ˚C for 24 hours. For a pine-derived bio-oil, viscosity change during this accelerated aging procedure correlated with storage of the bio-oil at room temperature for one year (Oasmaa and Kuoppala, 2003; Oasmaa and Peacocke, 2001).

Materials and Methods

Bio-oil production

Pelletized feedstock came from either pine or peanut hull biomass. Pyrolysis liquid was produced in two slow pyrolysis systems – one continuous feed system and one batch system. The two pelletized biomass, pine (PP) and peanut hull (PH), were used to produce three sample types; an ethanol spray-condensed pine pellet oil from continuous pyrolysis, a pine pellet batch bio-oil, and a peanut hull pellet batch bio-oil. The aqueous fraction was removed by decantation prior to analyses.

During the experiments, two pyrolysis systems were used. The continuous system was composed of an auger-driven, transported bed reactor contained in a tube furnace maintained at 500 ˚C. Pyrolysis vapors were quenched using atomized ethanol to quickly condense the liquid and to esterify acids following Hilten et al. (2010). For the experiment, a bio-oil quenched and reacted with ethanol at a bio-oil to ethanol ratio of 24:1 was analyzed to observe the effects of ethanol-esterification on stability. Only pine pellet biomass was used in the continuous reactor. The reactor for the batch system was cubical in shape with internal dimensions, 20 H x 20 W x 20 D cm, with two 1.3 cm ports for the introduction of inert gas and the removal of evolved gases and vapors. For pyrolysis experiments, the reactor was filled

with 2 – 3 kg of biomass (pine or peanut hull pellets) and was placed in a muffle furnace that increased the temperature from 25 to 500 ˚C at ~ 8 °C min^{-1}. A thermocouple measured the internal temperature of the biomass. Upon reaching an internal biomass temperature of 500 ˚C, a holding period of 30 min was sustained. Then, the furnace was turned off, and the reactor was allowed to cool to room temperature. Both pyrolysis systems used nitrogen, N_2, as the inert carrier gas. Heavier bio-oil fractions produced by the continuous system were collected in a drip trap directly beneath the spray-condensing tower, while lighter fractions were condensed and collected in a series of glass flasks in an ice bath. Only oil collected in the drip trap was analyzed in the current experiment. For the batch system, a series of stainless steel traps in an ice bath were used to condense and collect all the bio-oil. Thus, spray-condensed bio-oil from the continuous system was a heavier fraction than from the batch system.

Bio-oils produced during batch runs exhibited two clearly-defined phases. The bio-oils were phase-separated using a separatory funnel to produce an oily and an aqueous phase bio-oil. The aqueous phase was stored for future analysis, while the oily phase for each batch run was split in two with one half receiving 10 % (w/w) methanol (MeOH) while the other half was left neat. This was done for bio-oils derived from both biomass sources from batch pyrolysis system thus creating four sample types. With the addition of the continuous system-produced bio-oil, the sample set thus consisted of 5 sample types including; PP bio-oil containing 3.9 % (w/w) EtOH (named PP-E), PP with 0 % MeOH (PP), PP with 10 % MeOH (PP-M), PH with 0 % MeOH (PH), and PH with 10 % MeOH (PH-M). Four replicates were produced for each sample type creating a total of 20 samples. All samples were stored at 4 ˚C until analyzed. Attempts were made to analyze samples within 24 h of production.

Bio-oil compositional analysis

Water content

Liquid samples were analyzed for water content using a volumetric Karl Fischer titrator (Mettler-Toledo model DL31) following ASTM D1744 (1992) and ASTM E203 (2001). The titrant (AquaStar Composite 5K) used is intended for materials containing aldehydes and ketones. The solvent (Aquastar Solvent KC) contains dichloromethane for enhanced solubility with oils and fats.

Ultimate analysis

Samples were analyzed for elemental carbon, hydrogen, nitrogen, sulfur, and oxygen (ultimate analysis) using a LECO brand (Model CHNS-932) with optional pyrolysis furnace (Model VTF-900) following protocols outlined in ASTM D5291 (2007) and D 3176 (2002). The analyzer was calibrated using sulfamethazine (C – 51.78 %, H – 5.07 %, N – 20.13 %, and S – 11.52 %) as the reference material. C, H, N, S, and O were determined on a dry basis according to ASTM D 3176 (2002) using water content values determined by Karl Fischer titration.

Gross calorific value

Gross calorific value, or higher heating value (HHV), was accomplished using an isoperibol bomb calorimeter (Parr, Model 1351) following ASTM D5865 (2007) and D4809 (2006). The bomb calorimeter was calibrated using benzoic acid as the standard material.

Density

Density (ρ) in g mL^{-1} was determined gravimetrically using 2 mL Gay-Lussac pycnometers. This parameter is required in order to calculate kinematic viscosity from measurements of dynamic viscosity.

Viscosity

Bio-oil samples were analyzed for dynamic viscosity, μ, at three sheer rates using a Brookfield DV-I+ Viscometer with a UL/YZ spindle adapter. The method used is a modified version of ASTM D2983 (2004) using higher temperatures than the standard due to the very high viscosity of bio-oil at low temperature. Kinematic viscosity, v, was determined by dividing dynamic viscosity by specific gravity as determined using a pycnometer. Most samples were analyzed for viscosity at 25 and 45 ˚C. However, one stability analysis method involved measuring viscosity at 40 ˚C before and after an accelerated aging procedure.

Chemical composition

GC-MS and FT-IR were used to determine the composition of the bio-oils. FT-IR of the liquid samples was performed in attenuated total reflectance (ATR) mode using a Varian Scimitar (model 2000) analyzer. GC-MS analyses were accomplished using a Hewlett-Packard (model HP-6890) gas

chromatograph in conjunction with a Hewlett-Packard mass spectrometer (model HP-5973) with a mass selective detector. The GC contains an HP-5 MS column at 30 m length, 0.25 mm i.d., and 0.25 μm film thickness. The method used was as follows: inlet temperature, 230 ˚C, detector temperature, 280 ˚C (mass spectrometer interface temperature), flow at 1 mL min^{-1} He, and oven at 40 ˚C for 2.5 min followed by a ramp at 8 ˚C min^{-1} to 250˚ C (held for 5 min). The mass spectrometer scan range was from 15-500 mass units. Sample size was 1 μL and samples were prepared for analysis by diluting to 2.5 % (v/v) with acetone and adding 0.0625 % (v/v) heptane as an internal standard.

Chromatograms and spectra were viewed and compounds were identified using Agilent Technologies software (MSD ChemStation D.03.00.611) which uses a probability-based matching (PBM) algorithm to match unknown spectra to those found in a library. The mass spectral library used was the National Institute of Standards and Technology's 1998 version (NIST 98). The quality of a match determined by ChemStation is defined as the probability that the unknown is correctly identified as the reference. The quality can be between 1 and 100 with values above 90 considered very good matches.

Bio-oil stability analysis

Thermal stability

The first method used to determine the stability of bio-oil involved measuring viscosity prior to and after an accelerated aging procedure to determine the change. Similar methods have been used in several studies (Diebold and Czernik, 1997; Oasmaa and Kuoppala, 2003; Lede et al., 2007; Czernik et al., 1994). Using this procedure, pre-weighed and analyzed bio-oil samples were heated at 80 ˚C for 24 h in a forced air oven. The main variable of interest was viscosity which was measured at 40 ˚C using Brookfield DV-I+ viscometer. An increase in viscosity indicates that polymerization reactions have occurred that have formed larger molecules. Bio-oils that show less relative change during aging are expected to demonstrate greater stability during long-term storage.

After aging, samples were then allowed to cool to room temperature and were reweighed to determine if any loss of volatiles occurred. Afterwards, dynamic viscosity at 40 ˚C was measured at three shear rates. All other compositional parameters were then assessed. Dynamic viscosity and kinematic

viscosity were determined as stated in the previously in the "Viscosity" section. Kinematic viscosity values versus shear rates were then plotted to determine first if a nonlinear relationship was evident which would indicate non-Newtonian behavior. The change in kinematic viscosity, v, was determined on an absolute basis ($mm^2\ s^{-1}\ d^{-1}$) and on a relative basis using the viscosity index: $(v_{final} - v_{initial})/v_{initial}$ (Oasmaa and Kuoppala, 2003). A smaller increase (less change) in viscosity for a sample indicates a more stable material during prolonged storage.

Oxidative stability

Method 1 - Solids formation

The second stability assessment method was based on ASTM D 5304 (2006), which was developed for determining the storage stability of middle distillate fuels such as No. 1D and No. 2D diesel, fuels that bio-oils are intended to replace or supplement. Stability by this method is ranked based on the formation of insoluble material after an accelerated aging procedure. Following the standard procedure, a known amount of pre-filtered (0.8 μm pore size filter) liquid was placed into a pressure vessel that was then pressurized to 800 kPa (absolute) with oxygen. The vessel was then heated to 90 ˚C in a forced air oven for 16 h. At the end of the heating period, the vessel was removed from the oven, depressurized, and allowed to cool to room temperature. The sample was then filtered under vacuum through a pre-weighed filter and washed with acetone solvent to ensure no bio-oil residue remained on the filter or glassware. Afterwards, filters were dried, and reweighed to determine the quantity of insoluble material formed during the aging period.

According to ASTM D5304, insoluble material formation should be reported in mg of insoluble material per 100 mL of liquid. Since it is difficult to accurately measure volumes of bio-oil due to its adherence to glassware, in this study, we chose to report the values by percent of total mass and in g of insoluble material per g of liquid filtered. Approximately 100 g were filtered for each of three replicates for each bio-oil type.

Method 2 - Oxidation onset temperature

In an attempt assess bio-oil oxidative stability more quickly, an oxidation onset test following ASTM E 2009, typically used for edible oils and fats, lubricants, greases, and polyolefins, has been employed in this study. This test uses differential scanning calorimetry (DSC) analysis to determine the temperature, known as oxidation onset temperature (OOT), at which oxidation (combustion) begins under heating in oxygen environment. As stated in the ASTM method, samples with higher OOT are more stable. The method entails placing approximately 3 mg of sample into the measuring cell of the DSC and heating the sample from 25 to 250 ˚C at 10 ˚C min^{-1} in flowing oxygen (50 mL min^{-1}). At a sample-specific temperature, oxidation initiates. The OOT was determined by extrapolating the point of intersection between the baseline and the slope of the peak at the onset of oxidation. Stability of the oils was then ranked based on OOT where a higher OOT value indicates a more stable the oil. No studies have been found that attempt to use this method for bio-oil stability determination. Since performing the method requires less than 30 minutes, it was proposed to be a quick alternative to other stability assessment methods.

Chemical changes during accelerated aging

Changes were observed between un-aged bio-oil and bio-oil subjected to accelerated aging (heating) processes that were either oxidative thermal or solely thermal using GC-MS and FT-IR analyses. The attempt to identify and quantify compounds was by no means exhaustive. The intent was merely to show which, if any, groups of compounds had changed concentration. GC-MS analysis was expected to show that for aged bio-oil, there would be a shift to higher molecular weight compounds compared to un-aged bio-oil. This phenomenon would have been evident as a shift to compounds with longer retention times in GC and larger mass to charge ratios in the MS assuming compounds generated were still within the capacity of the GC to volatilize. Sample size was 1 µL, and samples were prepared for analysis by diluting to 2.5 % (v/v) with acetone and adding 0.0625 % (v/v) heptane as an internal standard.

FT-IR spectroscopy was used to show the formation and relative concentration of oxygenated groups that had formed to due to the oxidation of the bio-oil components during storage. An FT-IR analyzer (Varian model Scimitar 2000) was used in attenuated total reflectance (ATR) mode. Three replicates of sixteen scans were taken in the range from 4000-600 cm^{-1} and averaged for each bio-oil.

Results and Discussion

Biomass characterization

Table 2.1 shows the characteristics of the two biomass feedstock used in the experiment. Pine pellet and peanut hull pellet biomass were similar in most respects except that the peanut hull pellets had a greater fraction of ash and lesser fraction of hemicellulose.

Bio-oil characterization

Table 2.2 gives the results for compositional analyses performed on the bio-oil samples. The theoretical values for C, H, N, S and O for ethanol are 52.1, 13.1, 0, 0, and 34.7 %, respectively. For methanol, these values are 37.5, 12.6, 0, 0, and 49.9. Thus, addition of solvent to bio-oil simultaneously decreased carbon content while increasing oxygen content assuming no reactions are occurring between the alcohols and bio-oil constituents. Water content in the bio-oil decreased with the addition of a solvent, though only slightly. Viscosity was substantially reduced by the addition of methanol; 56.9 to 20.5 $mm^2 s^{-1}$ for PP and 435.4 to80.0 $mm^2 s^{-1}$ for PH bio-oil. These reductions are greater than what would be expected if the alcohols were simply mixing with bio-oil. Thus, it is expected that reactions such as esterification, transesterification, acetalization, and transacetalizations are occurring as observed previously (Diebold and Czernik, 1997).

Stability assessment

Thermal stability

Table 2.3 shows the results of viscosity measurements (assessed at 40 °C) for the five sample types after aging for 24 h at 80 °C. All samples were weighed before and after thermal aging to ensure that there was no substantial loss of volatiles. No samples lost more than 0.1 % (w/w) of volatiles. Sample PP-M, pine pellet-derived oil stabilized with 10 % (w/w) MeOH, showed the most favorable

thermal aging characteristics with a 1.1 $mm^2 s^{-1} d^{-1}$ increase in viscosity. PH, a peanut hull-derived bio-oil containing no MeOH, showed the worst thermal stability with a viscosity increase of 11.2 $mm^2 s^{-1} d^{-1}$ due to the accelerated aging procedure. The stabilizing effect of methanol addition was consistent with results observed in Diebold and Czernik (1997). Particularly, the addition of methanol to bio-oil increased the stability by decreasing the change in viscosity over time relative to un-stabilized bio-oil. An interesting point to note is that when viscosity index is used as the ranking measure as opposed to the absolute change in viscosity, the order for the PH and PH-M are reversed. This ranking discrepancy occurred due to the fact that the initial viscosity of PH as measured at 40 °C was much higher at 60 $mm^2 s^{-1}$ versus 17 $mm^2 s^{-1}$ for PH-M so the relative change was smaller.

Oxidative stability

Method 1 - Solids formation

Table 2.4 shows the percent of insoluble material collected upon filtering relative to the weight of oil filtered (minus the weight of methanol) after bio-oils were stored at 90 ˚C for 16 h while pressurized to 800 kPa with pure O_2. Again, PP-M showed the best aging stability, but this time for oxidative stability. PH-M was once again ranked lowest for stability. Greater oxidative stability as determined by this method indicates greater resistance to gum formation in tanks. No studies were found that attempt to use solid formation as a measure of stability for bio-oil. However, solids formation determination as used in this study was determined to be comparable to the standard stability measure (viscosity change, above) and repeatable.

Method 2 - Oxidation onset temperature

Figure 2.1 shows a typical DSC curve during an OOT determination. Bio-oils were heated from 25 to 350 ˚C at 10 ˚C min^{-1}. Table 2.4 shows the values for the OOT for the five sample types assessed in the study. Values were obtained by taking the average of two instrumental replicates for four samples of each type. Thus, the values are an average of OOT of eight measurements. As shown by this analysis, PP (shown in Figure 2.1) exhibited the highest oxidation stability at 144.5±3.8 ˚C while un-stabilized PH showed the poorest stability at 128.5±4.8 ˚C. The onset of oxidation could not be determined for PP-E,

an ethanol-containing pine pellet-derived bio-oil. For this sample type, the majority of the sample evaporated during heating and did not measurably oxidize within the temperature range. It was assumed that some components evaporated from the bio-oil, as well, as such components would also evaporate under normal aging for both hydrocarbon fuels and bio-oils. As with solids formation, no studies were found that attempted to use the OOT method for bio-oil stability determination. However, the corroboration with viscosity and solids formation methods show that at the very least, OOT has potential to be used for quick stability determination.

Table 2.5 summarizes the rankings from each of the accelerated aging stability assessment methods. An average ranking was calculated to rate the oxidative and thermal stability of the bio-oils as determined by the three analytical methods. Overall, PP, pine pellet bio-oil stabilized with MeOH, was most stable, followed by PP-E and then PP. PH-M and PH ranked 4th and 5th, respectively. We expected that the high hemicellulose content of pine pellet biomass would lead to the generation of a bio-oil containing more organic acids that would conceivably drive acid-catalyzed aging reactions. Even though the acidity as measured by pH of PP bio-oil was between 1.5-1.9 and considerably lower than that of PH oil at 2.5-3.5, increased acidity appeared to have less affect on the stability of the oils than expected.

Chemical changes during accelerated aging

Figure 2.2 shows the GC spectra for PH bio-oil that was un-aged (A) and aged by a solely thermal process (B). The major peaks after aging match those of un-aged bio-oil qualitatively. However, peak size varies somewhat. By normalizing the spectrum based on the area of the internal standard, heptane, comparisons could be made regarding the relative concentration of compounds before and after aging. Many compounds are evident in the chromatogram that are in very low concentration and that were poorly identified by the spectra matching program (MSD ChemStation). Figures 2.3 and 2.4 compare the normalized area for the major peaks in the GC spectra for PH and PP bio-oil, respectively, and list corresponding compounds identified by their mass spectra. For the thermally aged PH bio-oil, concentrations of many compounds appear to have increased. There are several notable exceptions, however, including a phenolic compound, eugenol (17.86 min) that decreased concentration. Conversely,

tetradecane (16.75 min) among others has a relatively higher concentration. The thermally aged bio-oil showed an increase in the concentration of essentially all phenolic compounds identified with the exception of eugenol. Several methyl esters with retention time greater than 24 min showed very little change in concentration with aging.

GC-MS results for PP bio-oil after aging showed that there were few major changes in the concentration of compounds relative to un-aged bio-oil. Figure 2.4 shows the normalized peak area for compounds in the range from 1.95 – 34 min retention times. Peak areas for most compounds identified were reduced somewhat after aging. Most notably, all phenol compounds, accept for 4-methylphenol (11.23 min) which appeared after aging, were reduced in concentration after aging. However, several new compounds were evident. Specifically, acetic acid, a product of esterification, a proposed aging reaction, was identified in the aged oil. In addition, 3-hexanone (a ketone at 4.5 min), α-pinene (a bicyclic terpene at 7.84 min), methyl cycloheptene (a cycloalkene at 7.98 min), and camphene (a bicyclic monoterpene at 8.17 min) were present in after aging. The lack of evidence for major compositional changes in PP bio-oil after thermal aging despite the physical changes that occurred, e.g. an increase in viscosity, indicated that the range for which GC-MS analysis was able to sense was likely not broad enough to observe compositional changes due to polymerization.

In addition to a shift to higher molecular weight compounds in both PP and PH bio-oil, we also expected to observe a change in specific functional groups, especially those representing oxygenated groups in oxidatively-aged bio-oils. In order to observe these functional group changes, FT-IR analysis was utilized. Figure 2.5 shows FT-IR spectra in the fingerprint range from 2000-700 cm^{-1} for un-stabilized PP and MeOH-stabilized PP-M prior to and after oxidative aging (a) and thermal aging (b). Figure 6 similarly shows FT-IR spectra for PH and PH-M. All major bands are present in each of the bio-oil-aging process combinations' spectra. Absorbance intensity, however, varies somewhat with bio-oil type and aging method. Absorbance was normalized to the highest peak in the fingerprint range. Absorbance was assumed to be representative of the relative concentration of proposed functional groups. For PP-M bio-oil, the largest absorbance value to which to the spectrum was normalized was 1025 cm^{-1}

while for un-stabilized PP, the value was 1706 cm^{-1}. The large peak at 1025 cm^{-1} for PP-M is representative of C-O stretching vibrations resulting from a primary alcohol, in this case methanol which had been added to the bio-oil. The methanol band for PH-M was around 1035 cm^{-1}. For PH and PH-M, the band with the highest absorbance in the fingerprint range was 1742 cm^{-1} which indicates C=O stretching vibrations that are consistent with the presence of saturated aliphatic esters shown in Figure 2.3.

Scholze and Meier (2001) found that for pyrolytic lignin, increases in bands at 1701 (C=O stretch in unconjugated ketones, carbonyl and ester groups), 1652 (C=O stretch in conjugated π-substituted aryl ketones), and 1600 (aromatic skeletal vibrations) cm^{-1} generally correspond to decreases in carbon content relative to oxygen content and were attributed to the formation of carbonyls including aldehydes, esters, and ketones. An increased concentration of carbonyl, ester, and ether groups is characteristic of bio-oils during aging as an effect of oxidation (Diebold, 2000; Czernik et al., 1994).

For PP bio-oils, changes in functional group band intensities were also seen. From Figure 2.5a, it can be seen that the band at 1600 cm^{-1} (aromatic skeletal vibrations) increases for PP after aging but not for PP-M, indicating the benefit of methanol stabilization. For PP and PP-M that underwent oxidative aging, a noticeable change in peak height was evident at both 1600 and 1515 cm^{-1}, another band representing aromatic skeletal vibrations. Aromatic skeletal vibrations can be attributed to benzene ring vibration (Mohebby, 2005). These bands indicated a reduction in the ratio of carbon to oxygen, meaning that oxidation had occurred. Other changes evident in oxidatively-aged bio-oil included increased band intensity for ketones (1670 cm^{-1}), ethers (1120 cm^{-1}), and esters (1265 and 1155 cm^{-1}). It is expected that ethers and esters formed due to acetalization and esterification reactions, respectively, reactions common in bio-oil during storage (Diebold, 2000). An increase at 1265 and 1155 cm^{-1} indicating C-O stretch in esters was also evident in thermally aged PP bio-oil (Figure 2.5b), with the un-stabilized bio-oil, PP, showing greater change than stabilized PP-M. Ether formation (1120 cm^{-1}) was not seen in thermally-aged PP bio-oil.

For PH bio-oils stabilized with methanol, changes in the concentration of oxygenated compounds with C-O groups were noticeably reduced relative to un-stabilized bio-oils. In Figure 2.6a for example, the band at 1232 cm^{-1} in PH and PH-M indicates C-O stretching in esters that have formed as a result of esterification. The intensity of this band increases upon oxidative aging (Figure 2.6a), and specifically increases somewhat more for un-stabilized PH. The band at 1200 cm^{-1} representing phenols increased in intensity for PH after aging, particularly for oxidatively-aged bio-oil. This result supports GC-MS results that showed an increase in the concentration of phenols. There was no indication of the formation of ethers. After thermal aging, PP and PH bio-oils generally indicated fewer changes in functional group absorbance intensity (Figures 2.5b and 2.6b) relative to oxidatively-aged materials. Particularly, there was little evidence of the formation of oxygenated species that were clearly increased in concentration in oxidatively-aged bio-oils (Figures 2.5a and 2.6a).

Conclusions

The results of three stability assessment methods were compared for oily fraction of bio-oils derived from slow pyrolysis of either pine or peanut hull pellet biomass. The effects of methanol addition on bio-oil stability were also observed. The stability assessment methods ranked the bio-oils similarly. Assessment of thermal stability by the change in viscosity after aging at 80 °C for 16 h indicated that PP-M ranked highest at +1.1 $mm^2 s^{-1} d^{-1}$, followed by PP-E at +3.2, then PH-M at +6.8, followed by PP at +7.5, and finally PH at +11.2 $mm^2 s^{-1} d^{-1}$. Oxidative stability was determined by solid formation and oxidation onset temperature (OOT). Ranking by lowest % change in solid formation indicated that PP-M was most stable (0.035±0.04 %) followed by PP (0.071±0.01 %), PH-M (0.944±0.25 %), PP-E (0.118±0.06 %), and then finally PH (1.193±0.58 %). OOT ranked the bio-oils as follows from most to least stable: PP (144.5±3.8 °C) > PP-M (134.3±6.92 °C) > PH (129.3±3.13 °C) > PH-M (128.5±4.77 °C). Although no two methods ranked the oils in exactly the same order, it was concluded that each method shows merit and could be used to assess bio-oil stability.

The average of rankings was as expected from most to least stable: PP-M, PP, PP-E, PH-M, PH. The method using solid formation ranked the oils as expected. This method is the most difficult,

however, requiring pressure vessels and filtering equipment. With the ease and speed at which OOT can be assessed using DSC makes it most favorable for determining stability. However, since sample size for this test is small (~ 3 mg), standard deviation can be high meaning that a large number of replicates may be required to reduce standard deviation enough to show statistical significance.

Compositional analysis by GC-MS indicated distinct changes in the composition of the bio-oil as a result of aging. For PH bio-oils aged by the thermal-only process, phenolic compounds appeared to increase in concentration. Few other GC-MS-identified compositional changes were abundantly clear for PH bio-oils. For PP bio-oils, the concentration of phenols as measured by semi-quantitative GC-MS appeared to decrease somewhat after aging. However, several new compounds appeared including 3-hexanone, α-pinene, methyl cycloheptene, and camphene appeared after aging. A further indication of aging reactions, acetic acid was formed, which is a product of esterification. However, there was no clear shift to higher molecular weight compounds within the range of volatility for which the GC-MS was capable of observing.

FT-IR analysis revealed several major changes in the bio-oils upon aging. Changes in PH and PH-M included an increase in the intensity of the band at 1232 cm^{-1} indicating C-O stretching in esters, more so in un-stabilized PH. For PP bio-oil, it can be seen that the band at 1600 representing aromatic ring vibration increases for PP after aging but not for PP-M, indicating the benefit of methanol stabilization. Additional aromatic skeletal vibrations were clearly increased at 1515 cm^{-1} for PP and PP-M after oxidative aging. FT-IR spectra showed increases in bands representing C-O stretch in esters (1265 and 1155 cm^{-1}) and ethers (1120 cm^{-1}) were also formed particularly after oxidative aging in the PP bio-oils. After thermal aging, PP and PH bio-oils generally indicated fewer changes in functional group absorbance intensity relative to oxidatively-aged materials. In addition, methanol addition showed clear benefits by reducing changes in functional group intensity in methanol-stabilized bio-oils.

Acknowledgements

This research was conducted using financial support from the U.S. Department of Energy Biorefinery Research Project grants, the State of Georgia Biorefinery grant, and the University of Georgia

Experiment Station. We thank Richard Speir for carrying out pyrolysis runs and bio-oil separations. We also thank Joby Miller, Damion Martel, Jenille Tulloch, Kate Lee, and Elizabeth Fortner for assistance in analyzing materials.

References

ASTM D 1744 – 92 (1992). Standard Test Method for Determination of Water in Liquid Petroleum Products by Karl Fischer Reagent. Easton, MD: American Society for Testing and Materials, 1992.

ASTM D 2983-04a (2004). Standard Test Method for Low-Temperature Viscosity of Lubricants Measured by Brookfield Viscometer. Easton, MD: American Society for Testing and Materials, 2004.

ASTM D 3176-89 (2002). Standard Practice for Ultimate Analysis of Coal and Coke. Easton, MD: American Society for Testing and Materials, 2002.

ASTM D 5291-02 (2007). Standard Test Methods for Instrumental Determination of Carbon, Hydrogen, and Nitrogen in Petroleum Products and Lubricants. Easton, MD: American Society for Testing and Materials, 2007.

ASTM D 5304-06 (2006). Standard Test Method for Assessing Middle Distillate Fuel Storage Stability by Oxygen Overpressure. Easton, MD: American Society for Testing and Materials, 2006.

ASTM D 5865-07a (2007). Standard Test Method for Gross Calorific Value of Coal and Coke. Easton, MD: American Society for Testing and Materials, 2007.

ASTM D4809-06 (2006). Standard Test Method for Heat of Combustion of Liquid Hydrocarbon Fuels by Bomb Calorimeter (Precision Method). Easton, MD: American Society for Testing and Materials, 2006.

ASTM E 2009-02 (2002). Standard Test Method for Oxidation Onset Temperature of Hydrocarbons by Differential Scanning Calorimetry. Easton, MD: American Society for Testing and Materials, 2002.

ASTM E 203-01 (2001). Standard Test Method for Water Using Volumetric Karl Fischer Titration. Easton, MD: American Society for Testing and Materials, 2001.

Boucher M, Chaala A, Pakdel H, Roy C. (2000). Bio-oils obtained by vacuum pyrolysis of softwood bark as a liquid fuel for gas turbines. Part II: Stability and ageing of bio-oil and its blends with methanol and a pyrolytic aqueous phase. Biomass Bioenergy 2000; 19: 351-361.

Czernik, S., Johnson, D., Black, S. (1994). Stability of wood fast pyrolysis oil. Biomass Bioenergy 7(1-6): 187-192.

Diebold, J. P., Czernik, S. (1997). Additives to Lower and Stabilize the Viscosity of Pyrolysis Oils during Storage. Energy Fuels 11: 1081-1091.

Diebold, J.P. (2000). A Review of the chemical and physical mechanisms of the storage stability of fast pyrolysis bio-oils. Subcontractor Report for the National Renewable Energy Laboratory: Golden, CO, January 2000. NREL/SR-570-27613.

Hilten, R., Bibens, B., Kastner, J., Das, K.C. (2010). In-line esterification of pyrolysis vapor with ethanol improves bio-oil quality. Energy Fuels 24: 673-682.

Junming, X., Jianchun, J., Yunjuan, S., Yanju, L. (2008) Bio-oil upgrading by means of ethyl ester production in reactive distillation to remove water and to improve storage and fuel characteristics. Biomass Bioenergy 32(11): 1056-1061.

Lédé, J., Broust, F., Ndiaye, F., Ferrer, M. (2007). Properties of bio-oils produced by biomass fast pyrolysis in a cyclone reactor. Fuel 86: 1800-1810.

Mohebby, B. (2005). Attenuated total reflection infrared spectroscopy of white-rot decayed beech wood. International Biodeterioration and Biodegradation 55: 247–251.

Oasmaa, A., Kuoppala, E. (2003). Fast pyrolysis of forestry residue. 3. Storage stability of liquid fuel. Energy Fuels 17: 1075-1085.

Oasmaa, A., Leppämäki, E., Koponen, P., Levander, J., Tapola, E. (1997). Physical characterization of biomass-based pyrolysis liquids – Application of standard fuel oil analyses. VTT, Technical Research Centre of Finland, ESPOO.

Oasmaa, A., Peacocke, C. (2001). A guide to the physical property characterization of biomass-derived fast pyrolysis liquids. VTT Research Publications. VTT Technical Research Center of Finland.

Scholze, B., Meier, D. (2001). Characterization of the water-insoluble fraction from pyrolysis oil (pyrolytic lignin). Part I. PY-GC/MS, FTIR, and functional groups. J. Anal. Appl. Pyrolysis 60: 41-54.

Figure Captions

Figure 2.1. DSC plot showing oxidation onset temperature for PP-M bio-oil.

Figure 2.2. GC-MS spectra for PH bio-oil A) before and B) after thermal aging at 80 °C for 24 h.

Figure 2.3. Peak areas normalized to internal standard, heptane, and retention times for major compounds evident in PH bio-oil before (solid bars, "Pre") and after (open bars, "Post") thermal aging as identified by GC-MS analysis.

Figure 2.4. Peak areas normalized to internal standard, heptane, and retention times for major compounds evident in PP bio-oil before (solid bars, "Pre") and after (open bars, "Post") thermal aging as identified by GC-MS analysis.

Figure 2.5. FT-IR spectra for PP and PP-M bio-oil before ("Pre") and after ("Post") a) aging in O_2 (790 kPa) at 90 °C for 16 h and b) aging in at 80 °C for 24 h in sealed bottles. Spectra are normalized to the highest peak in the range 2000-700 cm^{-1}.

Tables

Table 2.1. Pyrolysis feedstock characterization.

Parameter	Feedstock Characteristics[a]	
	pine	peanut hull
Moisture (w.b.)	7.4	8.6
Volatiles	80.9	71.7
Ash	0.1	4.2
Lignin	26.5	29.2
Cellulose	47.2	43.1
Hemicellulose	20.2	4.0
C	52.6	55.4
H	5.7	5.1
N	0.2	1.4
S	0.0	0.1
O[b]	38.9	37.8
HHV (MJ kg^{-1})	20.6	20.3

[a]Values are in % (w/w) on a dry basis unless otherwise noted.

[b]By difference.

Table 2.2. Characteristics of bio-oils produced by continuous (PP-E) and batch pyrolysis (all others).

Parameter	Bio-oil Characteristics									
	PP-E		PP		PP-M		PH		PH-M	
Solvent	ethanol[b]		none		methanol		none		methanol	
(%, w/w)	3.9		0		10		0		10	
C	54 ± 0.8		74 ± 3.5		70.8 ± 5.5		72 ± 0.8		67.9 ± 0.3	
H	6.3 ± 0.1		8 ± 0.7		8.7 ± 1		8.6 ± 0.3		9 ± 0.3	
N	0.2 ± 0		0 ± 0		0.3 ± 0.2		2.2 ± 0.1		2 ± 0	
S	0.1 ± 0		0 ± 0		0 ± 0		0.1 ± 0		0.1 ± 0	
O[a]	39.5 ± 0		18 ± 4.1		20.3 ± 6.5		17.2 ± 1.2		21 ± 0.4	
HHV ($MJ\ kg^{-1}$)	18.4 ± 0.9		30.1 ± 0.9		28.2 ± 0.5		29.9 ± 2.9		29.7 ± 1.1	
H_2O (%)	9.1 ± 0.4		3.3 ± 0.8		5 ± 1.3		6.5 ± 3		5.8 ± 0.8	
ν ($mm^2\ s^{-1}$) at 40 °C	22.7 ± N/A		21.9 ± 3.1		8.8 ± 0.4		60 ± 18.1		16.9 ± 0.9	
ρ ($g\ mL^{-1}$)	1.23 ± 0.3		1.11 ± 0.2		1.07 ± 0.1		1.07 ± 0.1		1.05 ± 0.2	

[a]By difference.
[b]Ethanol was added in a reactive environment and therefore the sample is not a mixture.

Table 2.3. Viscosity change in bio-oil due to accelerated aging.

Bio-oil	Viscosity Increase			Viscosity Index[a]			
	% d^{-1}	$mm^2\ s^{-1}\ d^{-1}$	Rank	Value		S.D.	Rank
PP-E	14.3	3.2	2	0.14	±	N/A	2
PP	34.1	7.5	4	0.34	±	0.13	4
PP-M	12.9	1.1	1	0.13	±	0.04	1
PH	15.4	11.2	5	0.15	±	N/A	3
PH-M	40.2	6.8	3	0.4	±	0.37	5

[a]Viscosity index: $(v_{final}-v_{initial})/\ v_{initial}$.

Table 2.4. Insoluble material formation and oxidation onset temperature for bio-oil as a result of accelerated aging.

Bio-oil	Solid Formation[a]				Oxidation Onset			
	(%)		S.D.	Rank	(°C)		S.D	Rank
PP-E	0.118	±	0.06	3	N/A[b]	±	N/A	N/A
PP	0.071	±	0.01	2	144.5	±	3.8	1
PP-M	0.035	±	0.04	1	134.3	±	6.92	2
PH	1.193	±	0.58	5	128.5	±	4.77	4
PH-M	0.944	±	0.25	4	129.3	±	3.13	3

[a]Solid formation relative to g of oil filtered minus MeOH.

[b]Complete evaporation prior to oxidation onset.

Table 2.5. Stability rankings for bio-oils assessed by three stability determination techniques.

Bio-oil	Stability Ranking			
	Viscosity[a]	Solids[b]	OOT	Ave Rank
PP-E	2	3	N/A[c]	2.5
PP	4	2	1	2.3
PP-M	1	1	2	1.3
PH	5	5	4	4.7
PH-M	3	4	3	3.3

[a]Ranked by absolute viscosity increase ($mm^2\ s^{-1}\ d^{-1}$).

[b]Ranked by % of insolubles (w/w) formed during 16 h aging.

[c]Complete evaporation prior to oxidation.

Figures

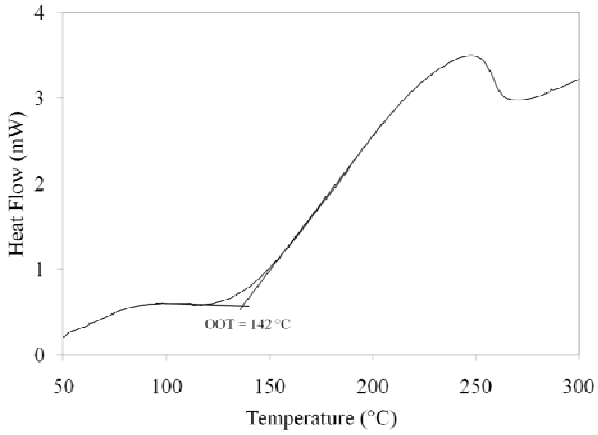

Figure 2.1. DSC plot showing oxidation onset temperature for PP-M bio-oil.

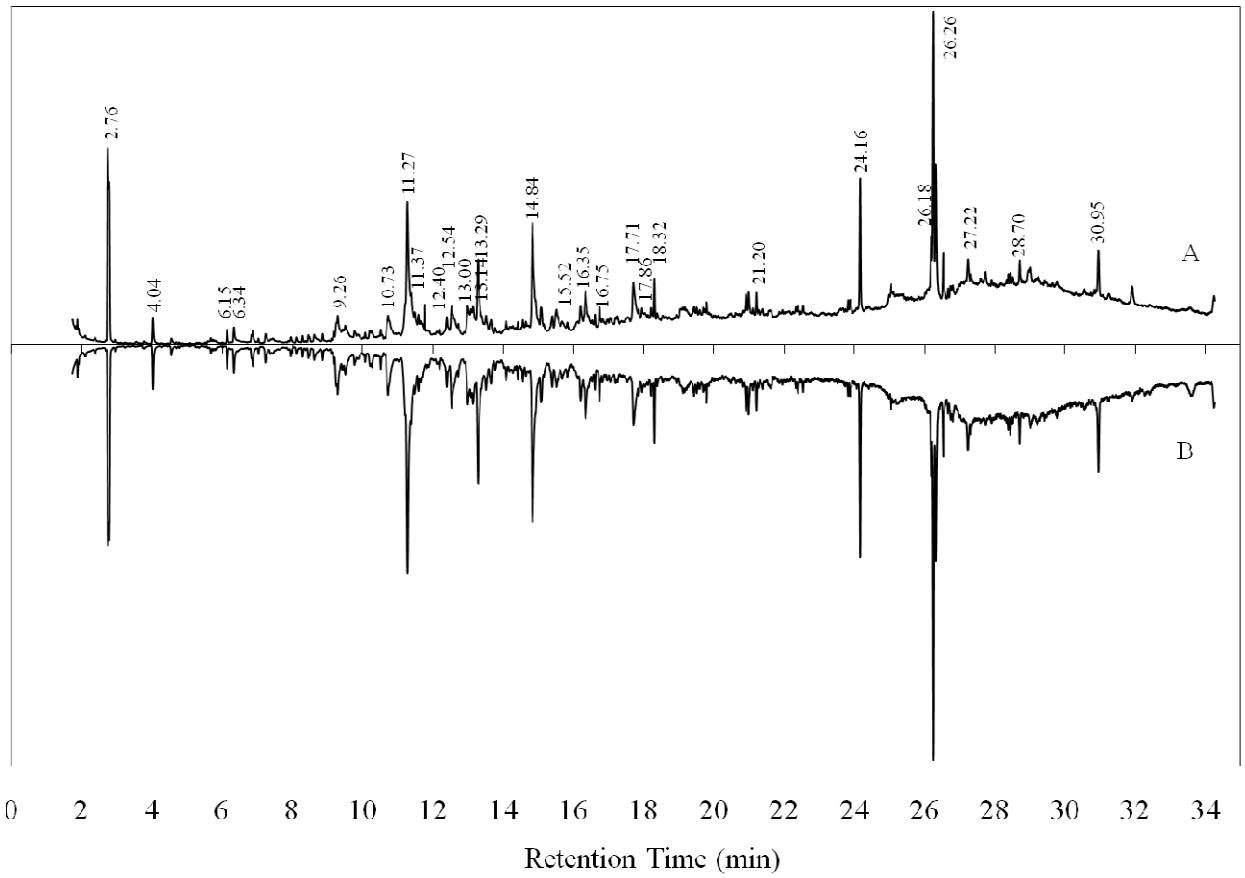

Figure 2.2. GC-MS spectra for PH bio-oil A) before and B) after thermal aging at 80 °C for 24 h.

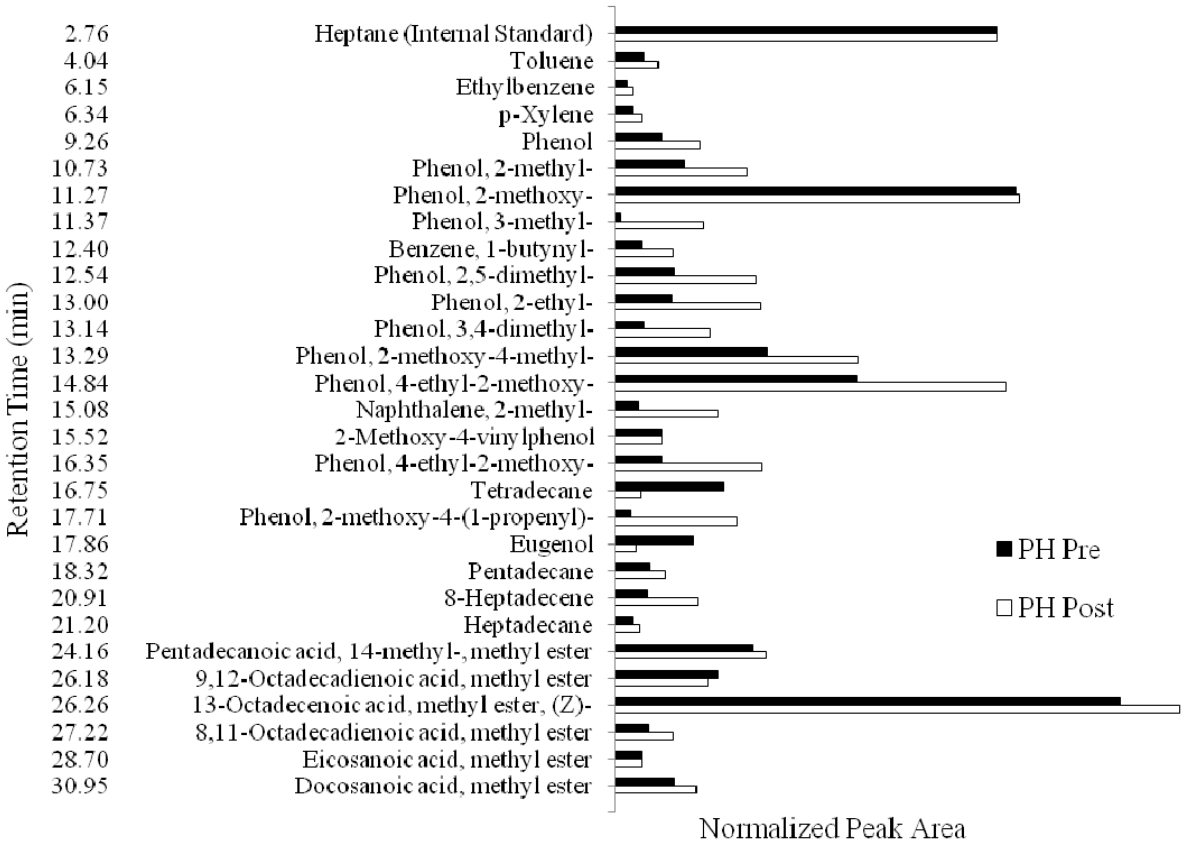

Figure 2.3. Peak areas normalized to internal standard, heptane, and retention times for major compounds evident in PH bio-oil before (solid bars, "Pre") and after (open bars, "Post") thermal aging as identified by GC-MS analysis.

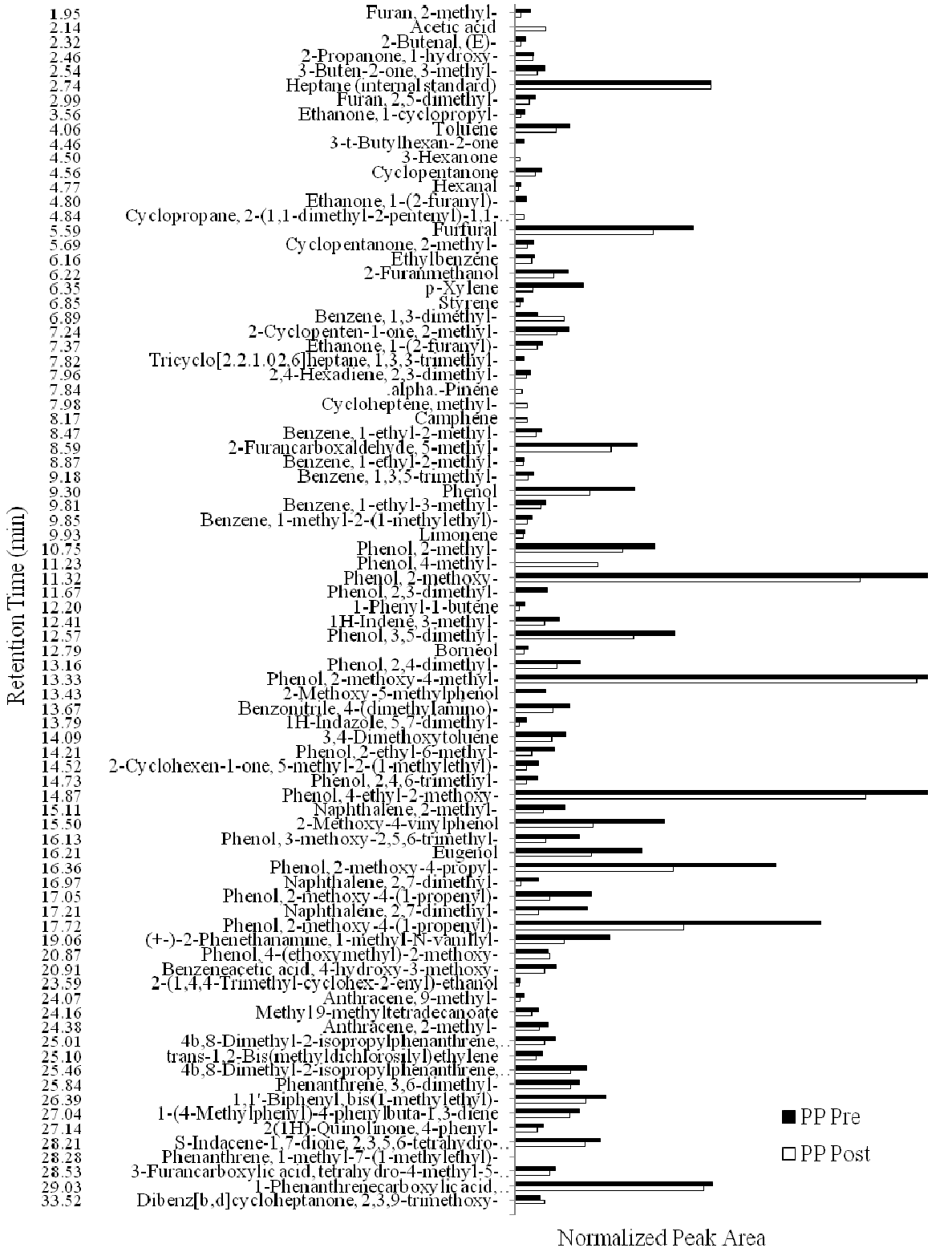

Figure 2.4. Peak areas normalized to internal standard, heptane, and retention times for major compounds evident in PP bio-oil before (solid bars, "Pre") and after (open bars, "Post") thermal aging as identified by GC-MS analysis.

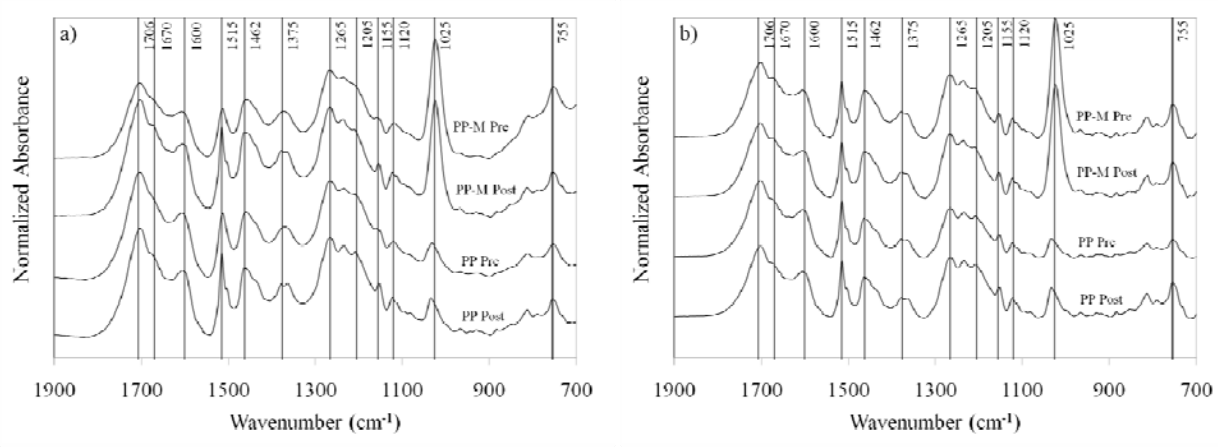

Figure 2.5. FT-IR spectra for PP and PP-M bio-oil before ("Pre") and after ("Post") a) aging in O_2 (790 kPa) at 90 °C for 16 h and b) aging in at 80 °C for 24 h in sealed bottles. Spectra are normalized to the highest peak in the range 2000-700 cm^{-1}.

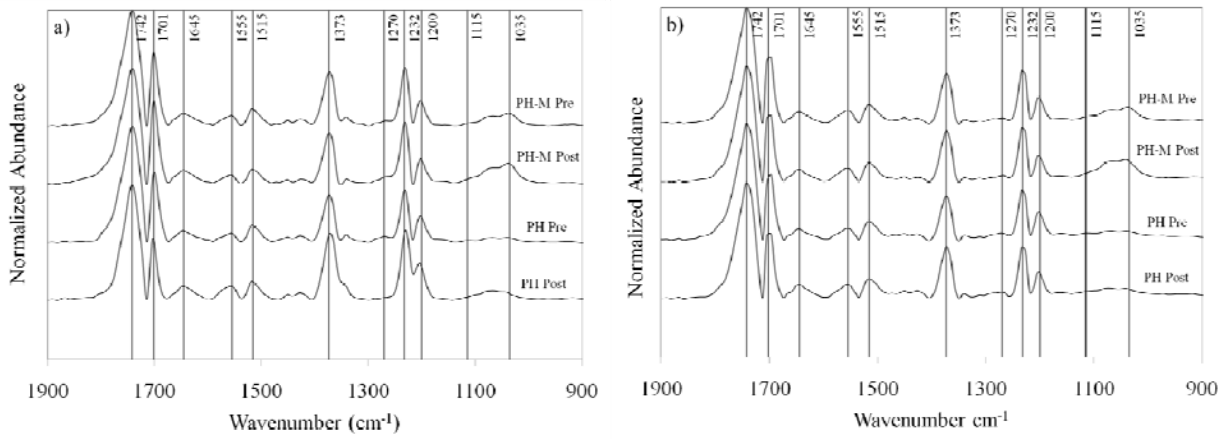

Figure 2.6. FT-IR spectra for PH and PH-M bio-oil before ("Pre") and after ("Post") a) aging in O_2 (790 kPa) at 90 °C for 16 h and b) aging in at 80 °C for 24 h in sealed bottles. Spectra are normalized to the highest peak (1742 cm^{-1}) in the range 2000-700 cm^{-1}.

CHAPTER 3

PRODUCTION OF FUEL FROM THE CATALYTIC CRACKING OF PYROLYZED POULTRY DAF SKIMMINGS[2]

[2] Hilten, R., Speir, R., Kastner, J., Das, K.C. 2010, *Journal of Analytical and Applied Pyrolysis*, 88: 30-38. Reprinted here with permission of the publisher.

Abstract

A two-step thermochemical process, pyrolysis followed by catalytic cracking, was used to produce liquid fuels from poultry dissolved air flotation (DAF) skimmings, a waste material generated during poultry processing. Raw DAF-derived solids were dried and subjected to pyrolysis at 400, 500, 600 or 700 °C to thermally crack the material into three physical phases; a gas, solid, and liquid. The liquid phase, DAF bio-oil, was further processed in an attempt to produce a liquid fuel capable of powering a diesel engine. After catalytic processing and collection, the DAF bio-oil exhibited a higher heating value (HHV) of 36 MJ kg^{-1}, which is less than the reported HHV of diesel (45.7 MJ kg^{-1}), similar to biodiesel (36-40 MJ kg^{-1}), but much higher than the HHV of bio-oil produced from the bioconversion of woody biomass (20 MJ kg^{-1}). DAF bio-oil analysis generated measurements of HHV (MJ kg^{-1}), cloud point (°C), viscosity (mm^2 s^{-1} at 40 °C), and water content (%) revealed values of 36, 61.7, 37.8, and 4.72, respectively. After catalytic cracking, HHV increased to 40.2 MJ kg^{-1}, cloud point decreased to -2.7 °C, viscosity decreased to 1.6 mm^2 s^{-1}, and water content decreased to 1.9 % making it comparable to conventional fuels. The upgraded DAF bio-oil could be utilized as a fuel for direct combustion in industrial boilers for steam generating, blended with petroleum fuels as an additive, or used directly as diesel transportation fuel.

KEYWORDS: dissolved air flotation; DAF; catalytic cracking; biofuel; pyrolysis; green diesel.

Introduction

Dissolved Air Flotation (DAF) is often used in the meat processing industry (poultry, swine, and bovine) to clarify wastewater by suspending and removing solids and oils. The byproduct of this process is a sludge with high moisture content (~ 70 %) that consists primarily of fats and proteins. After the removal of organic material using DAF, wastewater can then be treated in conventional wastewater treatment systems. As an alternative, Sena et al. (2009) showed that DAF processing followed by an advanced oxidation process could effectively generate an effluent with organic loads acceptable for discharge. However, the issue of what to do with DAF solid waste still remains. Much of the DAF waste is land-filled, land-applied as fertilizer or rendered for animal feed. All of these disposal methods present

their own problems such as transportation and materials handling costs. In addition, high water content in DAF also poses a problem in rendering applications where additional fees for dewatering can be incurred. According to Render Magazine's 2006 Market Report, 4.3 mil tonnes of fat and grease were generated in the U.S. from the animal slaughter industry in 2006 (Swisher, 2007). The USDA publication, "Poultry – Production and Value 2008 Summary" (USDA, 2009), states that 8.9 bil broiler birds were produced in the U.S. in 2008. Based on an estimate of 34 g of DAF skimmings generated per bird (Payne, pers. comm.), 303,000 tonnes of wet DAF was generated in 2008 from broiler production. As an alternative to disposal or rendering, this material could be converted into a liquid transportation fuel to help eliminate any disposal problems and would also serve as a value-added, marketable product derived from a waste stream.

Thermochemical approaches are often used to generate value-added products including liquid and gaseous fuels and activated carbons from a wide range of waste materials including fats and grease (Adebanjo et al., 2005; Lima et al., 2004; Twaiq and Mohamed, 2003; Anjos et al., 1983), wood (Li et al., 2009; Peacocke et al., 1994; Chen et al., 2003), seed/nut waste (Baquero et al., 2003; Domínguez et al., 2007; Das et al., 2004; Lua and Guo, 2002), and agricultural residues (Pütün, 2002; Demirbas et al., 2004). Pyrolysis and catalytic cracking are two commonly utilized thermochemical conversion techniques. Each process generates products in three physical phases; a solid, liquid and gas. The solid phase remaining after pyrolysis contains most of the minerals, or ash, that if left in the material could pose problems in fuel applications. The removal of ash is particularly important in DAF upgrading due to relatively high levels (2 %) that are present as a result of the use of polymers of acrylamide and ferric chloride which are used as flocculating agents (Smith et al., 2009). The liquid phase evolved during pyrolysis and catalytic cracking can, when condensed, be used as a liquid fuel. Also evolved during thermal process, permanent gases may include CO, CO_2, H_2, and CH_4 along with many others including C_2-C_6 gases in small concentrations.

Adebanjo et al. (2005) explored animal fat (lard) pyrolysis for which the oil produced exhibited a very similar cetane number (46) and higher heating value (40 MJ kg^{-1}) to those specified by ASTM D975,

"Standard specification for diesel fuel oil." Smith et al. (2009) showed that pyrolysis of poultry processing DAF followed by solvent extraction could be used to improve the quality of DAF such that it resembles diesel. Lima et al. (2004) produced diesel-like fuels from pyrolysis of vegetable oils. Many studies have used fixed-bed catalytic upgrading to produce fuels from plant-derived oils (Twaiq and Mohamed, 2003; Anjos et al., 1983). In Twaig and Mohamed (2003), a mesoporous acid catalyst was used to crack palm oil achieving an 80-90 % yield of liquid hydrocarbons. Additionally, several studies have used zeolites to upgrade vegetable oils to liquid fuels via fluid catalytic cracking (Li et al., 2009; Ooi et al., 2004). The prospect of producing liquid fuels from waste fats and oils has prompted commercial interest, as well. For example, Tyson Foods and ConocoPhillips placed a target of producing 175 million gallons of diesel from animal fats using conventional hydrotreatment processes in existing refineries in 2008. Using hydrotreatment, Conoco states that it is able to produce high-quality liquid fuels from fats. However, hydrotreatment technology cannot be scaled down to distributed small units because of the difficulties to produce and handle hydrogen in small systems (Kanellos, 2007).

The overall goal of this project is to develop a thermochemical technology to convert Dissolved Air Flotation (DAF) skimmings from poultry processing into a fuel using pyrolysis followed by catalytic cracking to produce renewable diesel and gasoline. Very little research has been devoted to the thermochemical transformation of DAF, and none found has attempted to generate "green" liquid fuels from the material. The main advantage of thermochemical conversion over widely used chemical conversion (transesterification) to produce biodiesel is that reaction time for thermochemical conversion is much shorter (seconds versus hours) such that a continuous flow system can be designed and integrated into poultry processing operations. In addition, the size and structure of resulting molecules can be better controlled in a thermochemical process to produce a bio-oil with desirable physical properties. Furthermore, catalytic cracking does not produce a liquid waste such as glycerol that is generated during transesterification.

Materials and Methods

Pyrolysis of poultry DAF skimmings

Pyrolysis of raw DAF was performed in previous research, and detailed results are given elsewhere (Smith et al., 2009). A brief description of the process will be described here. Using a batch reactor system, pyrolysis was performed at various temperatures with yields of solids, liquids, and gases determined by weighing the empty reactor vessel before the DAF was added so that both the weight of the sample used and the weight of char produced could be measured. The furnace was designed with two ports so that inlet and outlet lines could be connected to the reactor body for carrier gas and exhaust. A thermocouple was inserted into the reactor vessel so that the internal temperature of the sample could be measured during pyrolysis.

Pyrolysis was conducted at four different final internal temperatures ranging from 400 to 700 °C. The vapors were routed through a set of four condensers arranged with the first two in parallel and the subsequent two in series. The condensers were weighed before and after pyrolysis to determine the weight of bio-oil generated. The yield of the oil was then calculated using the weight of the oil produced relative to the initial weight of the DAF sample. The non-condensable gases that left the condensers were vented to the atmosphere. Liquid samples generated from the highest-yielding pyrolysis temperature runs were used in all subsequent

Catalytic Cracking

The catalytic upgrading experiment consisted of 6 treatments (performed in triplicate or 18 runs) in which three reaction temperatures (400, 450, and 500 °C) and two catalysts (H-ZSM-5 and FCC) were assessed. Cracking generated a solid, liquid and gas.

The main components of the upgrading system consisted of a 450 mm length, 23.8 mm i.d. reactor, a peristaltic pump, and an ice bath condensing system. The system, shown in Figure 1, was packed with a 20-30 g fixed bed of catalyst, either pure zeolite (H-ZSM-5) or commercially-available fluid catalytic cracking (FCC) variety. The H-ZSM-5 catalyst was produced by calcining NH_4-ZSM-5 (Zeolyst International, CBV 5524 G) at 550 ˚C for 4 h to produce the hydrogen form, H-ZSM-5, resulting

in stronger acid pore sites. The calcining process reduced the measured pH from 4.98 to 3.06. The catalyst has published values of 425 m^2 g^{-1}, 0.46 mm, and 50 for surface area, particle size and SiO_2/Al_2O_3 ratio, respectively. The NH_4-ZSM-5 catalyst was received from the manufacturer as a fine powder. In order to avoid clogging in the reactor, the catalyst was granulated by mixing with water, drying, crumbling, and sieving to the desired size, ~ 1-2 mm. The FCC catalyst was supplied by Grace Chemical – composition is proprietary. FCC catalyst was also supplied as a powder. Granulation was achieved in the same manner as H-ZSM-5.

Bio-oil, generated via pyrolysis of the DAF, was cracked using a reactor and process similar to that prescribed by ASTM D5154, "Standard test method for determining activity and selectivity of fluid catalytic cracking (FCC) catalysts by microactivity testing." As advised, preheated oil, DAF bio-oil (DAF BO) in this case, was pumped into the reactor where it was vaporized and then passed over the catalyst bed maintained at 400, 450, or 500 °C. For H-ZSM-5 and FCC catalyst packing, 20 and 30 g of catalyst were used, respectively. Initially, a 20 g fixed bed was attempted using the FCC catalyst, but the higher density of the FCC catalyst resulted in shorter bed height relative to H-ZSM-5 and thus, shorter residence times for the bio-oil vapor. The product from the 20 g catalyst loading runs exhibited poor cold flow properties and no water formation indicating that very little cracking had been achieved. Thus, 30 g of FCC was used such that the catalyst bed height was similar to that of the lower density H-ZSM-5. Bed height and volume for both catalysts was approximately 10 cm and 38 cm^3, respectively.

Catalyst to bio-oil ratios (cat:oil) for FCC and H-ZSM-5, as defined by ASTM D5154 as the mass of catalyst in the bed divided by the mass of feed fed to the reactor, were 0.4 (20 g) and 0.6 (30 g), respectively. The weight hourly space velocity (WHSV, units are hr^{-1}), defined as the oil feed rate (g h^{-1}) divided by the mass of catalyst (g), ranged from 4.3 to 6.5 hr^{-1}. Catalyst contact time, 3600/(WHSV · cat:oil), thus ranged from 1395 to 2093 s. Reaction time was approximately 23 s.

Upgraded bio-oil vapor was condensed in a series of glass flasks in an ice bath. Non-condensable vapors were sampled periodically during catalytic cracking and analyzed by micro-GC (Agilent model 3000A) while the balance of gas was emitted to outside air.

Product yield

Reactor and catalyst were weighed before and after each run to determine the extent of solid formation. Solid material was categorized and quantified as coke, char, or tar. Coke was considered the amount of material adhered to the catalyst after washing with acetone. Char was the material that formed in the reactor but not on the catalyst itself. Finally, tar was considered the acetone-soluble material that was removed from the catalyst by washing. Liquid yield was categorized as either oily or aqueous phase. The percent yield of oily and aqueous phase was determined relative to the total amount of bio-oil introduced to the reactor. During upgrading, gases were also produced and samples of evolved gases were taken and assessed determine the extent of catalyst deactivation. The catalytic cracking of DAF was expected to produce CO_2 as a product which would decrease in concentration relative to N_2, the carrier gas, as the catalyst was deactivated. Thus, deactivation was estimated by observing the CO_2 relative to N_2 over the course of the run.

Characterization of products

Product parameters assessed included chemical composition of liquid (GC-MS) and gas (GC), elemental content (C, H, N, S and O), H:C and O:C ratio, oxidative stability (OOT), cloud point (CP), higher heating value (HHV), H_2O content, viscosity and density (ρ), and pH.

Compositional analysis

The formation of desired compounds including gasoline- and diesel-range hydrocarbons was verified using a Hewlett-Packard (Model HP-6890) gas chromatograph containing an HP-5 MS column, 30 m in length, with a 0.25 mm I.D. and 0.25 μm film thickness in conjunction with a Hewlett-Packard mass spectrometer (Model HP-5973) with a mass selective detector. The method used was as follows: inlet temperature of 230 ˚C, interface temperature at 280 °C, a flow of 1 mL min^{-1} He, the oven initially at 40 °C for 2.5 min followed by a ramp at 8 °C min^{-1} to 250 °C (held for 5 min). Masses were scanned from 15-500 mass units. Sample size was 1 μL and was prepared for analysis by diluting to 2.5 % with acetone.

Chromatograms and spectra were viewed and compounds were identified using Agilent Technologies software (MSD ChemStation D.03.00.611) which uses a probability-based matching (PBM) algorithm to match unknown spectra to those found in a library. The mass spectral library used was the National Institute of Standards and Technology's 1998 version (NIST 98).

The methods and details for analysis of gases evolved during pyrolysis are given elsewhere (18). During catalytic cracking, gases were sampled at 15 min intervals and analyzed by GC (Agilent 3000A micro-GC) to determine the concentration of gases (H_2, CO, CO_2, CH_4, and other C_2-C_6) as a means to assess catalyst deactivation. Columns on the GC included an MS 5A PLOT (10 m length x 32 mm diameter), a PLOT U (8 m x 0.32 mm), an alumina PLOT (10 m x 0.32), and an OV-1 (10 m x 0.15 mm x 2.0 μm). After column separation, compounds were detected and quantified with thermal conductivity detectors that were calibrated using a refinery gas calibration mix (Agilent, part #5184-3543).

CHNS-O, H:C, and O:C

Measurement of CHNS was accomplished by instrumental means using a Leco analyzer (model CHNS932) following a modified version of ASTM D5291. Using CHNS results, oxygen was calculated by difference. Based on CHNS-O results, H:C and O:C ratios were obtained. The molar ratio of hydrogen to carbon gives a good indication of the nature of hydrocarbons in bio-oil. Given an average chemical formula, $C_{12}H_{23}$, diesel fuel has an H:C ratio of 1.92. This is expected since compounds comprising diesel are mostly long-chain hydrocarbons where each "link" in the chain is composed of two hydrogen atoms attached to one carbon. Thus, the ratio should be about 2. For biodiesel, H:C is about 1.9 but varies with the level of saturation in the C-C bonds of the feedstock used to produce the material.

The ratio of oxygen to carbon, O:C, indicates the level of oxygenation in a material. For diesel fuel, O:C is essentially zero. Biodiesel FAMEs have oxygen content around 10 % so O:C is about 0.1. For gasoline, the ratio varies depending on the amount of oxygenates added which can include methyl tert-butyl ether (MTBE), ethyl tert-butyl ether (ETBE), and ethanol. Although oxygen increases the efficiency of combustion, the heating value is decreased so fuel economy is reduced with higher oxygen content.

Reducing oxygen content in biofuels is currently a primary goal for many researchers. Pyrolysis-derived bio-oils are no exception with bio-oils commonly containing > 20 % oxygen by weight. Catalytic upgrading using solid acid zeolite catalysts is one proposed method to decrease oxygen.

Higher heating value

HHV was determined by combusting a 0.5 g sample in a bomb calorimeter (Parr model 1351) following ASTM D240. One intent aim of the project was to upgrade DAF-derived waste such that the HHV was similar to that of bio-diesel and diesel. HHV for diesel is about 45 MJ kg^{-1} or 38.6 MJ L^{-1}. Biodiesel's HHV is usually between 36-40 MJ kg^{-1} and 31-34 MJ L^{-1}. For gasoline, the value is 48.5 MJ kg^{-1} or 34.9 MJ L^{-1}.

OOT and CP

As a measure of stability and cold flow properties, OOT (oxidation onset temperature) and CP (cloud point) were determined via differential scanning calorimetry (DSC) analysis. The OOT was determined as outlined by ASTM E 2009. OOT is a measure of a material's oxidation stability. The DSC curves were attained using a Mettler Toledo (model DSC823e) with a heating rated of 10 °C min^{-1} to 350 °C and a gas flow rate of 50 mL min^{-1} of O_2. The OOT was determined graphically from the DSC curve of heat flow (W) versus temperature. The CP temperature was determined from DSC curves obtained at a heating rate of 10 °C min^{-1} and a nitrogen carrier gas flow rate of 50 mL min^{-1} in accordance to ASTM D4419. The test was conducted by increasing temperature from -40°C to 200 °C and then back to -40 °C.

Water content

Water content in the oils was determined by Karl Fischer titration using a Mettler-Toledo titrator (model DL31), following ASTM E203 guidelines. H_2O content in diesel and gasoline is essentially 0 %, while in biodiesel, H_2O content is substantially less than 1 %.

Kinematic viscosity

Dynamic viscosity was measured using a Brookfield (model DV-I+) rotational viscometer with a ULA-ZY low-volume adapter. Kinematic viscosity was calculated by dividing dynamic viscosity by density as measured by 2 mL Gay-Lussac pycnometers. Viscosity is important since engine components

are sized based on fuel properties such as viscosity. Higher viscosity fuels require larger fuel lines, more robust fuel filters, and larger injectors. According to ASTM D975, the range of acceptable kinematic viscosity for diesel is 1.9 – 4.1 $mm^2 s^{-1}$ as measured at 40 °C. For biodiesel, viscosity can be as high as 6.0 $mm^2 s^{-1}$. For gasoline, kinematic viscosity is less than 1 $mm^2 s^{-1}$. Density for diesel and gasoline is 0.85 and 0.72 g mL^{-1}, respectively. For direct usage of DAF-derived biofuel in these applications, viscosity must be similar.

pH

The pH of liquid product was measured directly using a Mettler-Toledo pH meter and probe. For diesel, biodiesel, and gasoline, pH values are near-neutral.

Results and Discussion

Pyrolysis of poultry DAF skimmings

Figure 3.2 shows the yields of products at different final pyrolysis temperatures. The pyrolysis of DAF skimmings yielded a very high yield of oil. The highest yield of oil was at the 600 °C where the average oil yield was 78.5%. A yield of 79 % is considerably higher than that of bio-oil from fast pyrolysis of wood (~ 60 %) (Bridgwater et al., 1999). The lowest average yield of oil was 66.9 % at an operating temperature of 400 °C. At this temperature, there was evidence of incomplete volatilization of bio-oil as shown by the tarry material left in the reactor vessel at 400 °C. Since pyrolysis at 600 °C generated the highest yield of liquid, DAF BO from this temperature was used for catalytic upgrading.

Table 3.1 shows the physical properties of raw DAF and DAF BO. It is clear from Table 3.1 that the quality of DAF BO is improved over raw DAF as shown by improvements in HHV, H:C ratio, viscosity, and cloud point. Although HHV was not as high as Adebanjo et al. (5) observed after lard pyrolysis at 40 MJ kg^{-1}, the improvement from 32 to 36 MJ kg^{-1}, the removal of ash, and the production of a lower viscosity liquid make pyrolysis an attractive processing option for DAF.

Catalytic Cracking

Product yield

DAF bio-oil (DAF BO) from the highest-yielding pyrolysis temperature (600 °C) was chosen for subsequent catalytic cracking. DAF BO was used as control for remainder of experiments in addition to DAF BO treated at catalytic cracking temperature with no catalyst bed. Catalytic cracking was performed at three temperatures; 400, 450, and 500 °C using H-ZSM-5 and commercial FCC catalysts. Cracking yielded a liquid, solid, and gas. Figure 3.3 (a and b) shows the yield for oily liquid (non-aqueous) and non-condensable gas. As seen in Figure 3.3a, oil yield significantly decreased (at $\alpha = 0.01$) with increasing temperature while slightly increasing with increasing catalyst to oil ratio (cat:oil, not significant at $\alpha = 0.05$). A decrease in liquid yield with temperature was expected as more DAF feed was converted to water and non-condensable gas as shown in Figure 3.3a as an increase in gas yield. Ideally, catalytic cracking would deoxygenate the liquid by converting all oxygen in the feed to water, CO, or CO_2 leaving only hydrocarbons in the oily liquid. However, carbon and hydrogen are lost during deoxygenation, as well, and liquid yield decreases.

Figure 3.4 shows the yield of solid byproducts including coke, char, and tar. Generally, cracking experiments with no catalyst yielded no solid material. The exception was the 400 °C run during which char formed in the reactor. In fact, experiments performed at 400 °C produced the most solid material. FCC produced less coke than H-ZSM-5 when comparing data from oils catalytically cracked at 450 °C. In future experiments, we plan to explore a wider range of catalyst to feed ratios to maximize yield and quality while minimizing coke.

Characterization of products

Table 3.1 gives physical properties of the liquid product from the most successful catalytic cracking run (FCC catalyst at 500 °C) based on HHV, viscosity, and water content along with the raw DAF, DAF BO, and B100 biodiesel (obtained from U.S. Biofuels, Inc., Rome, GA). Compositional analysis indicated the formation of many gasoline- and diesel-range hydrocarbons. Both the pyrolyzed DAF and the

catalytically cracked DAF BO showed much improvement relative to the raw DAF. Main improvements include increases in HHV and H:C ratio and reductions in O:C ratio, viscosity, and cloud point.

Compositional analysis

Using GC-MS analysis to determine the chemical composition, it was found that catalytically upgraded DAF BO qualitatively contained higher levels of aromatic and aliphatic hydrocarbons than DAF BO. Figure 3.5 shows the GC results from catalytically upgraded DAF BO at 400, 450, and 500 °C, DAF BO, and biodiesel. The main components that appeared to crack (decrease in concentration) during processing of DAF BO were fatty (alkyl) acids, fatty (alkyl) amines, and at least one amide. We expect that long chain fatty acids including hexadecanoic acid (peak S) and octadecanoic acid (peak U) in DAF BO (#2 in Figure 3.5) have cracked to form CO_2 and medium-chain hydrocarbons (octane to heptadecane, peaks H-Q) some of which have cyclized and aromatized to form aromatic hydrocarbons such as benzene (W), toluene (G) and xylene (Y), compounds collectively known as BTX and common in gasoline. Fatty (alkyl) amides such as peak V in chromatogram #2 could have conceivably cracked to form additional nitriles and alkane and aromatic hydrocarbons. Diesel fuel specifications from ASTM D975 require an aromatic content less than 35 %. Further testing is required to determine if that specification has been met. The presence of fatty nitriles (R and T) caused the nitrogen content of the DAF BOs, both before and after upgrading, to be high which will likely lead to high NO_x emission during combustion. Before engine testing, nitriles will need to be removed using some physical separation such as distillation or chemically by some thermocatalytic means to avoid excess NO_x emission during combustion.

Several studies have shown that the concentration of carbon-containing gases (and liquid products) evolved during catalytic cracking over zeolite catalysts decreases relative to the time on stream (Gayubo et al., 2004; Valle et al., 2007). Such a reduction in the concentration of liquid and gaseous products indicates a reduction in catalyst activity. It was desired to determine the extent of catalyst deactivation during cracking experiments. We attempted to observe the phenomenon by measuring the concentration of evolved gases over time. Table 3.2 provides a list of evolved gases observed and the gases' minimum and maximum concentration during a 75 min run. The evolved gas was dominated by

lower molecular weight gases (< 44 g mol^{-1}). We expected that the concentration of carbon-containing gases would decrease over the run as the catalyst was deactivated. However, this was not evident during the relatively short runs performed during this study (~ 60 min). Figure 3.6 shows the concentration of the main evolved gases relative to N_2 over the course of a 75 min catalytic upgrading run at 450 °C using H-ZSM-5. It is clear that as runtime increased the relative amount of H_2 increased indicating deeper cracking. The increase in H_2 is likely the result of tarring and coking of the catalyst that partially blocks the product pathway slowing the flow of DAF vapor and increasing the residence time. Such a hindering of vapor flow over a catalyst has been observed in other studies (Gayubo et al., 2004; Vitolo et al., 1999).

CHNS-O, H:C and O:C

It appears as though steady state was reached around 30 min, at which point, most evolved gas concentrations leveled off. Based on off-gas composition during the run, no evidence of catalyst deactivation was observed during the time tested (60 min). Since longer runs were not attempted, additional work is required to determine if and when catalyst deactivation begins. Results from CHNS analysis shown in Table 3.1 indicate that DAF BO that has not undergone catalytic cracking is quite similar to biodiesel. Carbon content was reduced and oxygen content increased after catalytic cracking relative to both biodiesel and DAF BO. The H:C and O:C ratios for DAF BO prior to cracking were most similar to diesel and biodiesel. However, upon cracking the H:C decreases and O:C increases. The decrease in H:C was likely due the formation of aromatic hydrocarbons that have lower H:C relative to longer, straight chain compounds and due to the evolution of hydrogen as H_2 and other hydrocarbon gases shown in Table 3.2. The increase in O:C provided evidence that deoxygenation was not particularly successful. Many oxygenated compounds remained in the product. O:C likely increased as a result of the creation of hydrocarbon gases that formed during catalytic cracking as seen in Figure 3.6.

Higher heating value

The HHV was improved by pyrolysis and further improved by catalytic cracking. The HHV value for FCC-cracked DAF BO exceeded 40 MJ kg^{-1}. The increase was due to the existence of shorter chain hydrocarbons and aromatic hydrocarbons in the cracked liquid that have higher energy density than

longer aliphatic hydrocarbons. However, the energy density per unit volume (in MJ L^{-1}) increased to a lesser degree, since the cracking of long chains to shorter chain hydrocarbons also decreased the density.

OOT and CP

The effect of catalytic cracking on the OOT was unclear. It was expected that OOT would increase for the cracked oils indicating an increase in oxidative stability, but was not the case. However, the CP was reduced after cracking as predicted due to the formation of shorter hydrocarbon chains with lower melting point temperatures. The CP for the FCC-cracked sample (~ -3 °C) was much improved over that of biodiesel (~ 12 °C) meaning that the cold flow properties, such as the pour point, should be improved. ASTM D975 advises that the CP be below the 10^{th} percentile minimum ambient temperature for diesel fuel. In the southeastern U.S. where this study was undertaken, the coldest month is January during which the 10^{th} percentile temperature is -7 °C. Thus, either deeper cracking of DAF BO or blending with diesel may be required if catalytically cracked DAF BO is to be used in winter months as a fuel for diesel engines.

Water content

Water content was improved in catalytically cracked samples as evident in Table 3.1. Although many cracking reactions generate water as a product, the solubility of H_2O in the upgraded liquid decreased and an aqueous layer formed that was easily removed by decanting. The decreased water solubility was due to the formation of hydrocarbons. Although water content did not meet the requirement of less than 0.05 % water and sediment as prescribed by ASTM D6751 (biodiesel) and D975 (diesel), improved cracking should generate a product with even lower water solubility. Meeting the water and sediment requirement indicated by ASTM standards is the object of future study.

Kinematic viscosity

The viscosity of raw DAF was greatly reduced as a result of pyrolysis. Even at room temperature, the DAF BO (after pyrolysis at 600 °C) was still a semi-solid at room temperature, but was free flowing at 40 °C. Cracking was expected to reduce the viscosity by decreasing the chain length of components in the oil and was indeed the case as shown in Figure 3.7. Thermal processing at 400, 500

and 600 °C without a catalyst slightly reduced viscosity, while the addition of catalyst greatly reduced viscosity. The kinematic viscosity of FCC-cracked DAF BO at 1.6 $mm^2 s^{-1}$ was actually lower than ASTM-specified viscosity for diesel fuel (1.9 – 4.1 $mm^2 s^{-1}$). For catalytically cracked DAF BO to be used as diesel, distillation to remove low boiling aromatics may be required to adjust the viscosity to reach the specified diesel fuel range.

pH

The pH was measured as an indication of acidity and corrosion potential relative to biodiesel. While the DAF BO pH was close to neutral, the pH for cat-cracked samples indicated that the oils were generally basic ranging in pH from 7.7 to 9.3. Further testing to determine corrosion potential is needed to determine if catalytically cracked DAF BO meets ASTM diesel specifications.

Conclusions

Results clearly showed the potential to generate a diesel-like renewable fuel from poultry DAF skimmings. After pyrolytic processing and collection, the DAF BO exhibited a higher heating value (HHV) of 36 MJ kg^{-1}, which is somewhat less than the published energy density of diesel (45.7 MJ kg^{-1}) and bio-diesel (40 MJ kg^{-1}), but is much improved over the energy density of bio-oil produced from the bioconversion of woody biomass (20 MJ kg^{-1}). These results indicate the potential for use of this high free fatty acid feedstock for production of renewable fuel. Subsequent catalytic cracking of DAF BO was successful at generating fuel with physical and chemical properties similar to diesel. For the best performing catalyst-temperature combination (FCC, 500 °C, cat:oil=0.6), the major improvements to DAF BO quality after catalytic cracking included:

- an increase in higher heating value from 36.1 to 40.2 MJ kg^{-1}
- a decrease in cloud point from 62 to -2.7 °C
- a decrease in viscosity from 37.8 to 1.6 $mm^2 s^{-1}$
- a decrease in water content from 4.7 to 1.9 %

Although it has been shown that biodiesel FAMEs can be produced from DAF using pyrolysis followed by solvent extraction and esterification (Smith et al., 2009), pyrolysis and catalytic cracking procedure is

a two-step process that could easily be integrated into a poultry processing facility as a continuous flow system. In addition, catalytic cracking can be tailored to produce a range of compounds with range of boiling points and volatility. Thus, upgraded DAF can be produced that can be used in diesel, gasoline, or jet turbine engines. A fractional distillation column could easily be integrated into the catalytic cracking system to separate these various fractions.

Given the compounds identified in catalytically upgraded DAF BOs using GC-MS analysis, such as aromatic and alkyl hydrocarbons, the liquid should be soluble in both biodiesel and diesel meaning that DAF BO could be used as a fuel additive or extender. Alternately, we expect that catalytically cracked DAF BO can be directly burned in a diesel engine. However, due to the high nitrogen content remaining after catalytic cracking due to the existence of fatty nitriles, NO_x emissions may be high.

We expect that the technology developed in the current study can be integrated into poultry processing facilities. Not only will this help poultry processors reduce the cost to dispose of DAF skimmings, but it will also provide process and transportation fuel which could be used internally or sold. Alternately, the process could conceivably be integrated into biodiesel manufacturing facilities to broaden the range of feedstock that biodiesel producers can use to produce renewable fuel. In this case, the DAF feedstock would become more valuable, and could be sold "as is" to biodiesel producers with no prior upgrading.

Acknowledgements

We thank our industry collaborators on this project; Tyson Foods, Inc. and Pilgrim's Pride, Inc. Also, we appreciate the work of lab assistants Joby Miller, Kate Lee, Damion Martel, and Jenille Tulloch. Support for this work was provided by Georgia Traditional Industries Program's as a Food Processing Advisory Council (FoodPAC FY 2009) project.

References

Adebanjo, A., Dalai, A., Bakhshi, N. (2005). Production of diesel-like fuel and other value-added chemicals from pyrolysis of animal fat. Energy and Fuels 19(4): 1735-1741.

Anjos, J., Gonzalez, W., Lam, Y., Frety, R. (1983). Catalytic decomposition of vegetable oil. Applied Catalysis 5: 299-308.

Baquero, M., Giraldo, L., Moreno, J., Suárez-García, F., Martínez-Alonso, A., Tascón, J. (2003). Activated carbons by pyrolysis of coffee bean husks in presence of phosphoric acid. J. Anal. Appl. Pyrolysis 70: 779-784.

Bridgwater, A., Meier, D., Radlein, D. (1999). An overview of fast pyrolysis of biomass. Organic Geochemistry 30(12): 1479-1493.

Chen, G., Andries, J., Luo, Z., Spliethoff, H. (2003). Biomass pyrolysis/gasification for product gas production: the overall investigation of parametric effects. Energy Conversion and Management 44: 1875-1884.

Das, P., Sreelatha, T., Ganesh, A. (2004). Bio-oil form pyrolysis of cashew nut shell – characterization and related properties. Biomass and Bioenergy 27: 265-275.

Demirbas, A., Sahin-Demirbas, A., Demirbas, A. (2004). Liquid fuels from agricultural residues via conventional pyrolysis. Energy Sources 26(9): 821-827.

Domínguez, A., Menéndez, J., Fernández, Y., Pis, J., Valente Nabais, J., Carrott, P., Ribeiro Carrott, M. (2007). Conventional and microwave induced pyrolysis of coffee hulls for the production of a hydrogen rich fuel gas. J. Anal. Appl. Pyrolysis 79: 128-135.

Gayubo, A., Aguayo, A., Atutxa, A., Prieto, R., Bilbao, J. (2004). Deactivation of a HZSM-5 Zeolite Catalyst in the Transformation of the Aqueous Fraction of Biomass Pyrolysis Oil into Hydrocarbons. Energy and Fuels 18: 1640-1647.

Kanellos, M. (2007). "Tyson, ConocoPhillips link up for biodiesel." CNETnews.com.

Li, H., Shen, B., Kabalu, J., Nchare, M. (2009). Enhancing the production of biofuels from cottonseed oil by fixed-fluidized bed catalytic cracking. Renewable Energy 34: 1033-1039.

Lima, D., Soares, V., Ribeiro, E., Carvalho, D., Cordoso, E., Rassi, F., Mundim, K., Rubim, J., Suarez, P. (2004). Diesel-like fuel obtained by pyrolysis of vegetable oils. J. Anal. Appl. Pyrolysis 71: 987-996.

Lua, A., Guo, J. (2002). Preparation and characterization of activated carbons from oil-palm stones for gas-phase adsorption. Colloids and Surfaces A: Physicochemical and Engineering Aspects 179: 151-162.

Ooi, Y., Zakaria, R., Mohamed, A., Bhatia, S. (2004). Catalytic conversion of palm oil-based fatty acid mixture to liquid fuel. Biomass and Bioenergy 27: 477-484.

Payne, Randy (2009). Tyson Foods, Inc., Cumming, GA. Personal communication.

Peacocke, G., Madrali, E., Li, C., Güell, A., Wu, F., Kandiyoti, R., Bridgwater, A. (1994). Effect of reactor configuration on the yields and structures of pine-wood derived pyrolysis liquids: A comparison between ablative and wire-mesh pyrolysis. Biomass and Bioenergy 7(1-6): 155-167.

Pütün, A. (2002). Biomass to bio-oil via fast pyrolysis of cotton straw and stalk. Energy Sources 24: 275-285.

Sena, R., Tambosi, J., Genena, A, Moreira, R., Schröder, H., José, H. (2009). Treatment of meat processing industry wastewater using dissolved air flotation and advanced oxidation processes monitored by GC-MS and LC-MS. Chemical Engineering Journal 152(1): 151-157.

Smith, J., Garcia-Perez, M., Das, K.C. (2009). Producing fuel and specialty chemicals from the slow pyrolysis of poultry DAF skimmings. J. Anal. Appl. Pyrolysis 86: 115-121.

Swisher, K. (2007). Market Report 2006. Render - The National Magazine of Rendering.

Twaiq, F., Mohamed, A. (2003). Liquid hydrocarbon fuels from palm oil by catalytic cracking over aluminosilicate mesoporous catalysts with various Si/Al ratios. Microporous and Mesoporous Materials 64(1-3): 95-107.

USDA (2009). Poultry – Production and Value, 2008 Summary; U.S. Department of Agriculture, U.S. National Agricultural Statistics Service. May 2009.

Valle, B., Gayubo, A., Atutxa, A., Alonso, A., Bilbao, J. (2007). Integration of thermal and catalytic transformation for upgrading biomass pyrolysis oil. International Journal of Chemical Reactor Engineering 5: 1-10.

Vitolo, S., Seggiani, M., Frediani, P., Ambrosini, G., Politi, L. (1999). Catalytic Upgrading of Pyrolytic Oils to Fuel over Different Zeolites. Fuel 78: 1147-1159.

Figure Captions

Figure 3.1. Reactor setup showing (1) DAF BO vessel, (2) hot plate, (3) peristaltic pump, (4) stainless steel reactor, (5) tube furnace, (6) collection flask, (7) ice bath, and (8) compressed N_2 tank.

Figure 3.2. Yield of products from batch pyrolysis of DAF skimmings (adapted from Smith et al, 2009).

Figure 3.3. Yield (% of DAF feed) of (a) oily liquid product and (b) un-condensed gases from catalytic cracking using both H-ZSM-5 (cat:oil = 0.4) and FCC (cat:oil = 0.6) catalysts. Note. Temperature and cat:oil scales are reversed for better viewing.

Figure 3.4. Yield of coke, char, and tar at 400, 450 and 500 °C after cracking with no catalyst, H-ZSM-5 and FCC catalyst.

Figure 3.5. GC chromatogram for (1) biodiesel, (2) DAF BO, and (3) FCC-upgraded DAF BO. Peaks were normalized to the largest peak in the spectrum. Peak identification is shown in Table 3.3.

Figure 3.6. Gases evolved during catalytic cracking of DAF using H-ZSM-5 catalyst at 450 °C and cat:oil of 0.4.

Tables

Table 3.1. Comparison of properties for various DAF treatments and B100.

Parameter	Raw DAF[a]	DAF BO[b]	400 ◦C		450 ◦C			500 ◦C		B100[c]
			Control	H-ZSM-5	Control	H-ZSM-5	FCC	Control	FCC	
C	64.6	73.2	72.7	72.5	72.9	70.7	73.1	74.5	71.5	77.2
H	8.61	11.1	11.3	10.4	11.0	9.7	10.9	9.91	9.9	12.2
N	3.65	4.3	4.9	4.1	4.0	4.0	3.6		3.7	0.0
S	0.43	0.1	0.1	0.1	0.2	0.1	0.1	0.1	0.1	0.0
O[d]	22.7	8.1	11.0	13.0	11.8	15.5	12.4	8.6	14.8	10.6
H:C	1.6	1.8	1.9	1.7	1.8	1.6	1.8	1.6	1.7	1.9
O:C	0.3	0.1	0.11	0.13	0.12	0.16	0.13	0.09	0.15	0.10
HHV (MJ kg^{-1})[e]	32.7	36.1	36.9	33.9	36.1	41.0	41.1	32.7	40.2	35.9
d.b.[f]	34.2	37.8	39.6	36.0	37.9	41.9	41.8	36.5	41.0	36.0
HHV (MJ L^{-1})[e]	–	33.2	32.8	31.2	32.1	36.5	35.3	31.2	35.0	30.8
d.b.	–	34.8	35.3	33.1	33.7	37.3	35.9	34.9	35.7	30.9
%H_2O	4.5	4.7	6.8	5.7	4.6	1.9	1.6	10.6	1.9	0.18
pH	–	7.0	7.0	7.7	5.8	9.3	8.6	7.7	8.9	7
Viscosity (cSt)[g]	–	37.8	41.4	8.5	20.6	1.5	2.6	18.5	1.6	2.0
OOT (°C)	–	–	229.6	235.0	228.2	196.0	252.5	181.9	197.2	212
Cloud Pt. (°C)	–	61.7	57.4	8.4	50.0	−4.5	−3.9	70.7	−2.7	12
Density (g mL^{-1})	–	0.9	0.89	0.92	0.89	0.89	0.86	0.96	0.87	0.86

[a] Untreated poultry DAF skimmings.
[b] DAF skimmings after pyrolysis at 600 °C.
[c] Biodiesel (100%) derived from poultry fat obtained from U.S. Biofuels, Inc. (Rome, Georgia).
[d] By difference.
[e] "As Received."
[f] "Dry Basis."
[g] Measured at 40 °C.

Table 3.2. Range of concentration for evolved gases (relative to N_2) from catalytic cracking of DAF bio-oil with H-ZSM-5 at cat:oil=0.4 and 450 °C during a 75 min experiment.

Evolved Gas	Molecular Formula	Relative Gas Concentration (0-100)[a]		M.W. (g mol^{-1})
		min	max	
Hydrogen	H_2	14.98	19.48	2
Methane	CH_4	7.74	8.27	16
Carbon monoxide	CO	1.00	2.66	28
Nitrogen	N_2	100	100	28
Ethylene	C_2H_4	2.80	3.22	28
Ethane	C_2H_6	5.61	6.46	30
Methyl acetylene	C_3H_4	0.00	1.58	40
Propylene	C_3H_6	1.43	1.61	42
Carbon dioxide	CO_2	2.99	4.83	44
Propane	C_3H_8	2.84	3.20	44
1,3-Butadiene	C_4H_6	0.44	0.48	54
trans-2-Butene	C_4H_8	0.43	0.47	56
iso-Butylene	C_4H_8	0.43	0.49	56
1-Butene	C_4H_8	0.43	0.49	56
cis-2-Butene	C_4H_8	0.43	0.48	56
n-Butane	C_4H_{10}	0.44	0.48	58
iso-Butane	C_4H_{10}	0.45	0.49	58
trans-2-pentene	C_5H_{10}	0.14	0.17	70
2-Methyl-2-butene	C_5H_{10}	0.07	0.08	70
1-Pentene	C_5H_{10}	0.15	0.16	70
cis-2-Pentene	C_5H_{10}	0.15	0.16	70
iso-Pentane	C_5H_{12}	0.15	0.17	72
n-Pentane	C_5H_{12}	0.15	0.16	72
n-Hexane	C_6H_{14}	0.00	0.08	86

[a]Relative to nitrogen (N_2)

Table 3.3. Compounds corresponding to peaks labeled in Fig. 3.4. Hit quality (0–100) for all compounds is greater than 90.

Peak	Compound	Molecular formula	Family	M.W. (g/mol)
A	Methyl dodecanoate	$C_{13}H_{26}O_2$	Saturated FAME[a]	214.3
B	Methyl tetradecanoate	$C_{15}H_{30}O_2$	Saturated FAME	242.4
C	9-Methyl hexadecanoate	$C_{17}H_{32}O_2$	Unsaturated FAME	268.4
D	Methyl hexadecanoate	$C_{17}H_{34}O_2$	Saturated FAME	270.5
E	Methyl octadecanoate	$C_{19}H_{38}O_2$	Saturated FAME	298.5
F	Methyl eicosenoate	$C_{21}H_{40}O_2$	Unsaturated FAME	310.5
G	Toluene	C_7H_8	AH[b]	92.1
H	Octane	C_8H_{18}	Alkane[c]	114.2
I	Nonane	C_9H_{20}	Alkane	128.3
J	Decane	$C_{10}H_{22}$	Alkane	142.3
K	Undecane	$C_{11}H_{24}$	Alkane	156.3
L	Dodecane	$C_{12}H_{26}$	Alkane	170.3
M	Tridecane	$C_{13}H_{28}$	Alkane	184.4
N	Tetradecane	$C_{14}H_{30}$	Alkane	198.4
O	Pentadecane	$C_{15}H_{32}$	Alkane	212.4
P	Hexadecane	$C_{16}H_{34}$	Alkane	226.4
Q	Heptadecane	$C_{17}H_{36}$	Alkane	240.5
R	Hexadecanenitrile	$C_{16}H_{31}N$	Fatty nitrile	237.4
S	Hexadecanoic acid	$C_{16}H_{32}O_2$	Saturated FFA[d]	256.4
T	Octadecanenitrile	$C_{18}H_{35}N$	Fatty nitrile	265.5
U	Octadecanoic acid	$C_{18}H_{36}O_2$	Saturated FFA	284.5
V	Hexadecanamide	$C_{16}H_{33}NO$	Amide	255.4
W	Benzene	C_6H_6	AH	78.1
X	Ethylbenzene	C_8H_{10}	AH	106.2
Y	p-Xylene	C_8H_{10}	AH	106.2
Z	Propylbenzene	C_9H_{12}	AH	120.2
AA	1-Ethyl-2-methylbenzene	C_9H_{12}	AH	120.2
AB	Butylbenzene	$C_{10}H_{14}$	AH	134.2
AC	Pentylbenzene	$C_{11}H_{16}$	AH	148.2
AD	Hexylbenzene	$C_{12}H_{18}$	AH	162.3
AE	1-Methylnaphthalene	$C_{11}H_{10}$	PAH[e]	142.2
AF	Heptylbenzene	$C_{13}H_{20}$	AH	176.3
AG	1,5-Dimethylnaphthalene	$C_{12}H_{12}$	PAH	156.2

[a] Fatty acid methyl ester.
[b] Aromatic hydrocarbon.
[c] Linear alkane hydrocarbon.
[d] Free fatty acid.
[e] Polycyclic aromatic hydrocarbon.

Figures

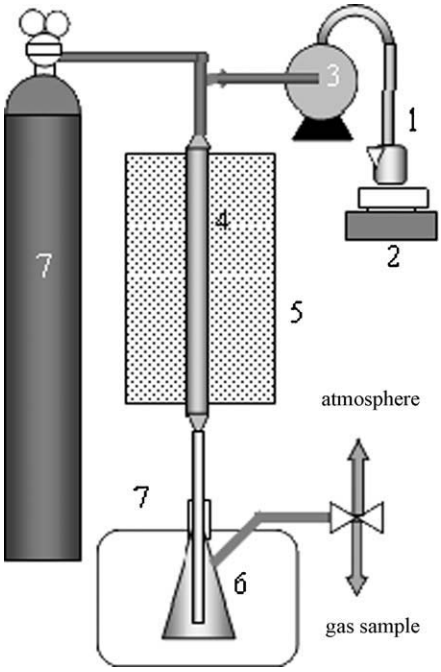

Figure 3.1. Reactor setup showing (1) DAF BO vessel, (2) hot plate, (3) peristaltic pump, (4) stainless steel reactor, (5) tube furnace, (6) collection flask, (7) ice bath, and (8) compressed N_2 tank.

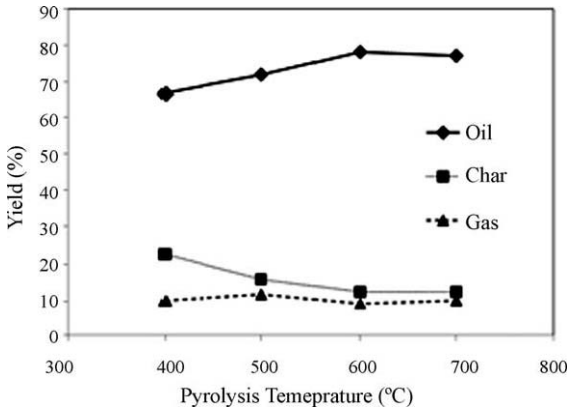

Figure 3.2. Yield of products from batch pyrolysis of DAF skimmings (adapted from Smith et al., 2009).

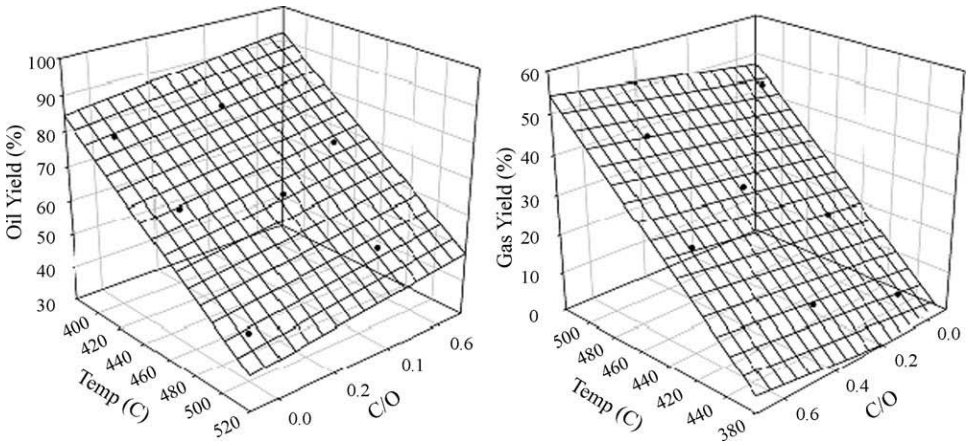

Figure 3.3. Yield (% of DAF feed) of (a) oily liquid product and (b) un-condensed gases from catalytic cracking using both H-ZSM-5 (cat:oil = 0.4) and FCC (cat:oil = 0.6) catalysts. Note. Temperature and cat:oil scales are reversed for better viewing.

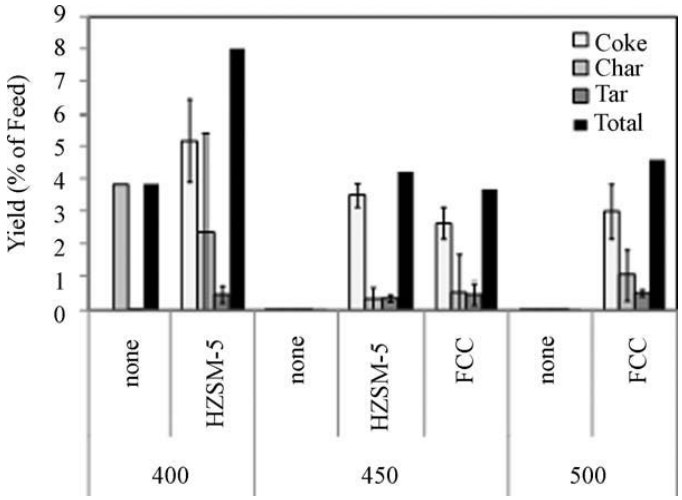

Figure 3.4. Yield of coke, char, and tar at 400, 450 and 500 °C after cracking with no catalyst, H-ZSM-5 and FCC catalyst.

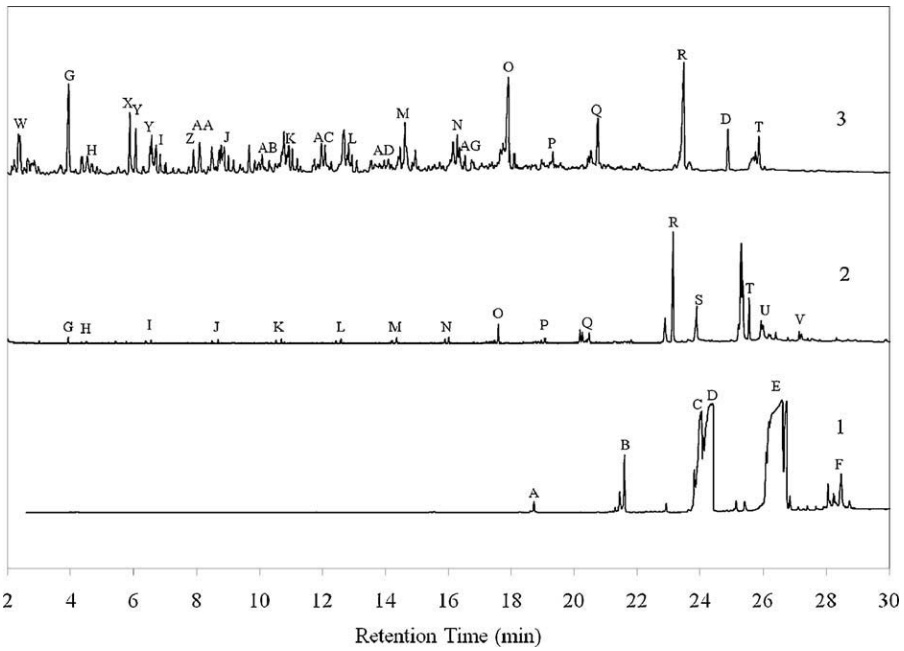

Figure 3.5. GC chromatogram for (1) biodiesel, (2) DAF BO, and (3) FCC-upgraded DAF BO. Peaks were normalized to the largest peak in the spectrum. Peak identification is shown in Table 3.3.

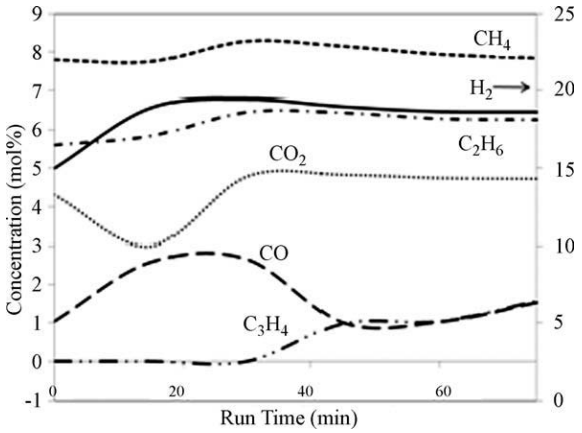

Figure 3.6. Gases evolved during catalytic cracking of DAF using H-ZSM-5 catalyst at 450 °C and cat:oil of 0.4.

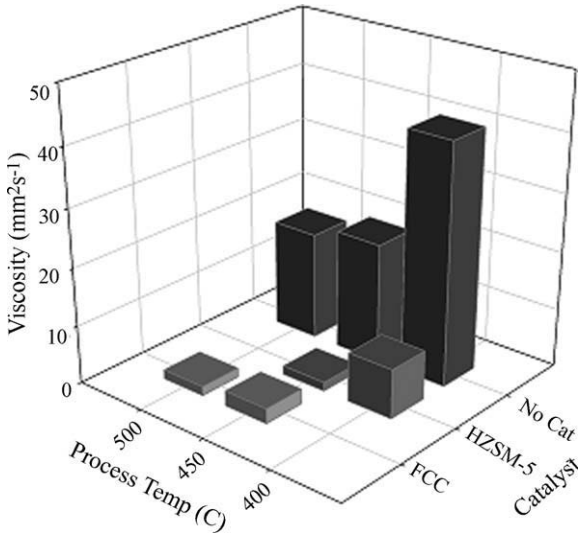

Figure 3.7. Viscosity (at 40 ◦C) of DAF BO before and after catalytic cracking with either FCC or H-ZSM-5 catalyst.

CHAPTER 4

PRODUCTION OF AROMATIC GREEN GASOLINE ADDITIVES VIA CATALYTIC PYROLYSIS OF ACIDULATED PEANUT OIL SOAP STOCK[3]

[3] Hilten, R., Speir, R., Kastner, J., Das, K.C. 2011, *Bioresource Technology*, 102: 8288-8294. Reprinted here with permission of the publisher.

Abstract

Catalytic pyrolysis was used to generate gasoline-compatible fuel from peanut oil soap stock (PSS), a high free fatty acid feedstock, using a fixed-bed reactor at temperatures between 450 and 550 °C with a zeolite catalyst (HZSM-5). PSS fed at 81 g h^{-1} along with 100 mL min^{-1} inert gas was passed across a 15 g catalyst bed (WHSV = 5.4 hr^{-1}, gas phase residence time = 34 s). Results indicate that fuel properties of PSS including viscosity, heating value, and O:C ratio were improved significantly. For PSS processed at 500 °C, viscosity was reduced from 59.6 to 0.9 mm^2 s^{-1}, heating value was increased from 35.8 to 39.3 MJ L^{-1}, and the O:C ratio was reduced from 0.07 to 0.02. Aromatic gasoline components (e.g., BTEX), were formed in concentrations as high as 94 % (v/v) in catalytically-cracked PSS with yields ranging from 22 to 35 % (v/v of PSS feed).

KEYWORDS: catalytic pyrolysis, soap stock, waste oil, free fatty acid, peanut processing

Introduction

Fats and vegetable oils are common feedstocks for biofuel production, particularly for biodiesel. Biodiesel can be produced from a variety of oils containing mono- (free fatty acids, or FFAs), di-, and tri-glyceride (i.e. lipid) feedstocks. Although a wide variety of plant- and animal-derived feedstocks is available, the cost is highly variable with feedstock ranging from 0.20 to 2.0 \$ lb^{-1} (between 2000 and 2006) (Ash and Wittenberger, 2010) which can make the cost of biodiesel production unpredictable and often unprofitable. In the U.S., soybean oil, containing lipids with mainly oleic and linoleic fatty acids, is a commonly-used feedstock. However, soybean oil is a traded commodity, and using soybean oil for biodiesel production directly competes with food uses, which increases the price for both uses. Mixtures of FFAs and lipids are common, especially in waste fats and oils (e.g., yellow grease, tallow, and soap stock) resulting in a much lower feedstock quality and cost. The estimated production cost of biodiesel generated from soybean oil, yellow grease and petroleum in 2011 is \$ 2.73, \$ 1.51, and \$ 0.76 gal^{-1}, respectively (Radich, 1998). However, mixtures of FFAs and lipids, as in yellow grease, present difficulties in biodiesel synthesis, since separate catalytic steps are required; esterification of the FFAs using an acid catalyst followed by transesterification of the triglycerides using a base catalyst.

An alternate method for producing biofuels from fats and oils is via a thermochemical pathway, such as pyrolysis or catalytic hydrotreatment. Kanellos (2007) indicates that commercial entities have shown interest in pursuing the development of fuels from fats, including Tyson Foods and ConocoPhillips who, in a collaborative effort set a target of producing 175 million gallons of diesel from animal fats using conventional hydrotreatment processes in existing refineries in 2008. The article states that the thermal technology used by Conoco, known as hydrotreatment, results in hydrocarbons of the desirable quality, although demand for pure hydrogen is high. However, this technology cannot be scaled down to distributed small units because of the difficulties in producing and handling hydrogen in small systems (Kanellos, 2007). Thus, there is a need to develop catalytic processes capable of transforming high FFA feedstocks to liquid fuels without the need for gaseous H_2 allowing for the design of distributed small or regional biorefineries.

Many studies have demonstrated thermochemical conversion as a means to generate liquid fuel from mono- (free fatty acid, or FFA), di-, and tri-glyceride (TG) feedstocks without costly hydrogen addition. Adebanjo and Mohamed (2005) explored pyrolysis of animal fat (mainly saturated TGs), which generated an oil exhibiting a very similar cetane number and heat of combustion as those specified by ASTM for diesel fuel. Hilten et al. (2010) produced a gasoline-like fuel via pyrolysis and catalytic cracking of poultry processing waste containing FFAs, TGs, and protein. Other studies have produced diesel-like fuels from pyrolysis of vegetable oil feedstocks, such as soybean oil (Lima et al., 2004; Wiggers et al., 2009). Many studies have added catalysts to the process in fixed-bed reactors to catalytically crack oils to produce fuels from plant-derived oils (Anjos et al., 1983; Dandik et al., 1998; Twaiq et al., 2003; Lima et al., 2004). Several studies (Twaiq et al., 1999; Twaiq et al., 2003; Twaiq et al., 2004; Tamunaidu and Bhatia, 2007) have used catalytic cracking to generate high yields of liquid hydrocarbons from palm oil waste. For example, Twaiq et al. (2003) cracked palm oil using a mesoporous acid catalyst and achieved an 80-90% yield of liquid hydrocarbons. Additionally, several studies have used solid acid zeolite catalysts to upgrade vegetable oils to liquid fuels via fluid catalytic cracking (FCC) (Li et al., 2009; Ooi et al., 2004; Padmaja et al., 2009). Cracking studies have used a

variety of acidic mono- and bi-functional catalysts at various pore size and functionality. Catalysts used in previous studies for cracking FFAs and TGs include MCM-41 (Twaiq et al., 2003), SBA-15 (Yean-Sang and Bhatia, 2007), and HZSM-5 (Dandik et al., 1998; Twaiq et al., 2004). Basic catalysts such as potassium carbonate (K_2CO_3) have also been used to upgrade vegetable oils including soybean oil (Xu et al., 2010).

A wide variety of waste and by-product oils could potentially be utilized for biofuel production via thermochemical pathways. For example, during peanut processing, waste oils are generated that could conceivably be converted to liquid fuels. One such waste material is peanut oil soap stock (PSS), a peanut processing by-product containing high levels of free fatty acids and emulsified water that is often underutilized due to the limited number of options for processing to higher-value products. Generated during vegetable oil refining, soap stock (SS) can be acidified to demulsify water while concentrating free fatty acids (FFAs). The FFA mixture, acidulated peanut oil soap stock (a.k.a. acid oil), can subsequently be used as feedstock for biodiesel production. Although there is some industrial use of SS, it is sporadic, and thus price can significantly fluctuate and generate little economic return (Haas et. al., 2003). A potentially more favorable route would be to directly convert PSS into a value-added product, such as a liquid transportation fuel via a thermochemical pathway.

Few studies can be found that attempt catalytic pyrolysis as a means to generate fuel or fuel additives from soap stock and no studies were found that attempt the process with soap stock from peanut-derived feedstock. One study found, Doll et al. (2008), generated biofuel from a soap stock (soybean-derived), but in a non-catalytic pyrolysis process. Use of catalysts for the conversion process could conceivably improve the process by both increasing yields and decreasing the temperature required for conversion.

For this study, we proposed to generate fuel quality product from a high FFA soap stock, PSS, by direct processing in a catalytic pyrolysis reactor. Using HZSM-5, an acidic microporous zeolite catalyst, we expected that the PSS upgrading process would result in the formation of fuel-like hydrocarbons. Additionally, we proposed that the fuel-like hydrocarbons would be in the form of aromatics (e.g.

benzene, xylene, toluene), components in gasoline representing approximately 20 % (v/v) (EPA, 2008), following several proposed reaction pathways. The resulting product would be in the form of a high-octane liquid fuel or fuel additive. Given our results, we believe the process could easily be integrated into peanut processing plants with the resultant products used as process fuel or sold as liquid transportation fuel.

Materials and Methods

Feedstock

Acidulated peanut oil soap stock (PSS) containing mainly free fatty acids (FFAs) was supplied by Golden Peanut Co., LLC. Table 4.1 provides the fatty acid profile for PSS. Oleic and linoleic acids are the main components in PSS. As such, a model compound mixture containing linoleic (70%) and oleic (30%) acid (denoted as LA for the linoleic acid in the mixture)) was chosen for comparison and supplied by Sigma-Aldrich. Table 2 provides additional compositional data for PSS, LA, gasoline, biodiesel and No. 2 diesel.

Free fatty acid conversion to fuel

FFA feedstocks including PSS and LA were preheated (unstirred) and injected using a peristaltic pump (Cole-Parmer, Model L/S Digital) at 2 mL min^{-1} into a 2.2 cm I.D. tubular reactor and passed across a fixed bed of HZSM-5 catalyst (see Figure 4.1). An inert gas flow (N_2) was maintained at 100 mL min^{-1} for all runs. The reactor was situated in a vertically oriented single-zone Lindberg/Blue M tube furnace where the catalyst zone temperature was held between 450-550 °C. Temperature was controlled using input from a thermocouple located at the center axis of the reactor and longitudinally at the center of the catalyst bed (TC1 in Figure 4.1). This temperature was measured every second with averages logged at 2 min intervals using a Campbell Scientific CR23X datalogger. Additionally, furnace temperature was measured at the outer diameter of the reactor (axially) and at the middle of the furnace (longitudinally) (TC2 in Figure 4.1). We have assumed plug flow reaction conditions, which implies that temperature is isothermal radially, although the temperature may vary minimally longitudinally due to the heat of reaction.

The HZSM-5 catalyst was produced by calcining NH_4-ZSM-5 (Zeolyst International, CBV 5524 G) at 550 ˚C for 4 h in air to produce the hydrogen form, HZSM-5, resulting in stronger acid pore sites. The pH was measured by mixing catalyst in water at a 50:50 ratio and then measuring the pH of the water using a standard pH probe. As a result of the calcining process, the pH was reduced from 4.98 to 3.06. The NH_4-ZSM-5 catalyst was received from the manufacturer as a fine powder. The catalyst powder has published values of 425 m^2 g^{-1}, 5 μm, and 50 for surface area, particle size and SiO_2/Al_2O_3 ratio, respectively. To minimize the pressure drop across the catalyst bed, the catalyst was granulated by mixing with water, drying, crumbling, and sieving to the desired size, ~ 0.5-1 mm. Products were collected in a flask (Figure 4.1-#7) in an ice bath (Figure 4.1-#8).

PSS and LA were catalytically pyrolyzed using a reactor and process similar to that described by ASTM D5154, "Standard test method for determining activity and selectivity of fluid catalytic cracking (FCC) catalysts by microactivity testing." For this work, changes that were made to the reactor described in ASTM D5154 as follows: a peristaltic pump was used as opposed to a syringe pump, the reactor size was increased to 25.4 mm O.D. (22.1 mm I.D.) as opposed to 18 mm O.D. (15.6 mm I.D.), fresh catalyst was used in all experiments (i.e. no catalyst were reused) as opposed to equilibrium (i.e. previously-regenerated) catalyst, furnace temperature control was accomplished using one thermocouple as opposed to three, catalyst temperature was monitored using one thermocouple as opposed to three, and a 15 g catalyst bed was used as opposed to 4 g. During processing, the feedstock was passed across a 15 g (7.5 cm depth, 28.5 cm^3 volume) fixed bed of HZSM-5 maintained at 450, 500, or 550 °C.

Catalyst to oil ratio (C/O) is defined by ASTM D5154 as the mass of catalyst in the bed divided by the mass of feed fed to the reactor, and was ~0.4 (15 g) for the PSS and LA experiments. The weight hourly space velocity (WHSV, units are hr^{-1}), is defined as the oil feed rate (2 mL min^{-1} or ~ 81 g h^{-1} based on measured density) divided by the mass of catalyst (g), and was 5.4 hr^{-1}. Catalyst contact time (i.e. time on stream), is defined as 3600/(WHSV · C/O), and was 1667 s (~30 min). Based on the catalyst bed height (7.5 cm) and carrier gas flow rate (100 mL min^{-1}), the gas phase residence time in the catalytic

zone was approximately 34 s. Control runs were accomplished by passing feedstock across an empty bed at each operating temperature (450, 500, and 550 °C) for comparison to catalyzed runs.

Reactor and catalyst were weighed before and after each run to determine the extent of residue formation. Residue was categorized and quantified as coke, char, or tar. Coke was considered the amount of material adhered to the catalyst after washing with acetone. Char was defined as the material that formed in the reactor, but not on the catalyst itself. Finally, tar was considered the acetone-soluble material that was removed from the catalyst by washing. Liquid yield was categorized as either oily or aqueous phase. The percent yield of oily and aqueous phase was determined relative to the total amount of oil introduced to the reactor.

Product Characterization Methods

Product parameters assessed included chemical composition of liquid product (via GC-MS, GC-FID) and gas (via GC-TCD), elemental content (C, H, N, S and O), H:C and O:C ratio, higher heating value (HHV), H_2O content, viscosity and density (ρ), and pH.

The formation of desired compounds, particularly aromatic green gasoline-range hydrocarbons, was verified using a Agilent (model HP-6890) gas chromatograph containing an HP-5 MS column, 30 m in length, with a 0.25 mm I.D. and 0.25 μm film thickness in conjunction with a Hewlett-Packard mass spectrometer (model HP-5973) with a mass selective detector. The method used was as follows: inlet temperature of 230 ˚C, detector temperature at 280 °C (MS interface temperature), a flow of 1 mL min^{-1} He, the oven initially at 40 °C for 2.5 min followed by a ramp at 8 °C min^{-1} to 250 °C (held for 5 min). Masses were scanned from 15-500 mass units. Sample size was 1 μL and was prepared for analysis by diluting to 2.5 % in a 50:50 acetone/methanol mixture.

Chromatograms and spectra were viewed and compounds were identified using Agilent Technologies software (MSD ChemStation D.03.00.611), which uses a probability-based matching (PBM) algorithm to match unknown spectra to those found in a library. The mass spectral library used was the National Institute of Standards and Technology's 1998 version (NIST 98).

BTEX compounds were quantified using an Hewlett Packard GC-FID (model HP-5890). The GC was equipped with an Agilent HP-5 column (crosslinked 5% PH ME Siloxane, 30 m x 0.25 mm x 0.25 um film thickness). A five-point standard calibration curve was developed using a BTEX standard (containing benzene, toluene, ethylbenzene, and o-, m-, and p-xylene) in methanol (Sigma-Aldrich). For the analysis, the inlet and detector temperatures were maintained at 220 and 230 °C, respectively. The oven temperature was held at 50 °C for 3 min, then ramped at 8 °C min^{-1} to 180 °C and held for 1 min. The injection volume was 1 μL. Samples were mixed in the same ratios as in the GC-MS analysis (2.5 % in 50:50 acetone:methanol). Yields were determined relative to the amount of feedstock injected and concentration was determined relative to liquid product.

Measurement of elemental CHNS-O content was accomplished by instrumental means using a CHNS analyzer (LECO, model CHNS932) following a modified version of ASTM D5291. Using CHNS results, oxygen was calculated by difference. Based on CHNS-O results, H:C and O:C ratios were obtained. The molar ratio of hydrogen to carbon is a good indicator of the existence of hydrocarbons in bio-oil. Given the average chemical formula of dodecane, $C_{12}H_{23}$, diesel fuel has an H:C ratio of 1.92. This is expected since compounds comprising diesel are mostly long-chain hydrocarbons where each "link" in the chain is composed of two hydrogen atoms attached to one carbon. Thus, the ratio should be approximately 2. For biodiesel, H:C is approximately 1.9, but varies with the level of saturation in the C-C bonds of the feedstock used to produce the material. For gasoline, H:C is approximately 2.3 assuming an average chemical formula, C_8H_{18} (octane). For unleaded gasoline, the maximum allowable sulfur content is 0.035 %. For ultra-low sulfur diesel, the maximum allowable sulfur content is 0.0015 %.

The ratio of oxygen to carbon, O:C, indicates the level of oxygenation in a material. For diesel fuel, the O:C ratio is essentially zero. Biodiesel FAMEs have an oxygen content of approximately 10 %, resulting in an O:C ratio of 0.1. For gasoline, the ratio varies depending on the amount of oxygenates added, which can include methyl tert-butyl ether (MTBE), ethyl tert-butyl ether (ETBE), or ethanol. Although fuel oxygenates increase combustion efficiency of, the heating value is decreased resulting in lower fuel economy. For comparison purposes, we will assume the O:C ratio to be zero for gasoline.

However, reformulated gasoline (RFG), a fuel designed to reduce air pollution, has additives that raise oxygen content to around 2% (EPA, 2006).

Reducing the oxygen content in biofuels is currently a primary goal for many researchers. Pyrolysis-derived bio-oils are no exception with bio-oils commonly containing > 20 % oxygen by weight. Catalytic upgrading using solid acid zeolites is one proposed method to decrease oxygen content and improve heating value.

HHV was determined by combusting a 0.5 g sample in a bomb calorimeter (Ika model C2000) following ASTM D240. It was desired to upgrade PSS such that the HHV was similar to that of conventional fuels. The HHV for diesel is about 45 MJ kg^{-1} or 38.6 MJ L^{-1}. Biodiesel's HHV is usually between 36-40 MJ kg^{-1} or 31-34 MJ L^{-1}. For gasoline, the value is 48.5 MJ kg^{-1} (34.9 MJ L^{-1}).

Water content in the oils was determined by Karl Fischer titration using a Mettler-Toledo titrator (model DL31), following ASTM E203 guidelines. Water content in diesel and gasoline is essentially 0.0 %, while in biodiesel, it is substantially less than 1 %.

Dynamic viscosity was measured using a Brookfield (model DV-I+) rotational viscometer with a ULA-ZY low-volume adapter. Kinematic viscosity was calculated by dividing dynamic viscosity by density as measured by a 2 mL Gay-Lussac pycnometer. Viscosity is important, since engine components (e.g. injectors, pumps, filters) are sized based on fuel properties such as viscosity. Higher viscosity fuels require larger fuel lines, more robust fuel filters, and larger injectors. According to ASTM D975, the acceptable range for diesel fuel kinematic viscosity is 1.9 – 4.1 $mm^2 s^{-1}$ measured at 40 °C. For biodiesel, kinematic viscosity can be as high as 6.0 $mm^2 s^{-1}$, and for gasoline kinematic viscosity should be less than 1 $mm^2 s^{-1}$. The suggested density for diesel and gasoline is 0.85 and 0.72 g mL^{-1}, respectively.

The pH of liquid product was measured directly using a Mettler-Toledo pH meter and probe. For fuels including diesel, biodiesel, and gasoline, pH values are near-neutral.

Results and Discussion

Free Fatty Acid conversion to fuel

Generally, cracking processes generate five products including a fuel-like oil, an acetone-soluble tar, reactor char, catalyst coke, an aqueous phase liquid, and non-condensable gases. Figure 4.2 illustrates the effect of catalyst, HZSM-5, on the yield of products and co-products from the catalytic cracking of PSS at 500 °C. No tar was recovered from LA or PSS upgrading. Other pyrolysis temperatures indicated similar trends in terms of product and by-product yield. The addition of catalyst affected PSS and LA similarly, with comparable drops in yield of oily product and an increase in non-condensable gas formation although the quality of the product was greatly improved. Feedstock significantly influenced char, oil, and aqueous phase yield at $\alpha = 0.05$ and gas yield at $\alpha = 0.1$, but it did not significantly affect coke yield at $\alpha = 0.1$. Specifically for PSS, char and gas yields were higher and oily and aqueous phase yields were lower relative to LA. With increasing conversion temperature, oil yield was significantly decreased while gas and coke yield were significantly increased at $\alpha = 0.05$ and $\alpha = 0.1$, respectively, but did not significantly affect char or aqueous product yield at $\alpha = 0.1$. The presence of HZSM-5 catalyst significantly increases coke, char, aqueous phase, and gas yield while significantly decreasing oil yield at $\alpha = 0.05$ (Figure 4.2). Additionally, no aqueous phase was formed for samples processed at 500 °C in the absence of catalyst.

Product Characterization

Although the yield of oily product decreased with the addition of catalyst, the quality of PSS oil was significantly improved due to catalytic cracking. Table 4.3 gives characterization results for both PSS and LA processed at 450, 500, and 550 °C with and without catalyst. The carbon content significantly increased for HZSM-5-processed PSS and LA at $\alpha = 0.05$. More importantly, oxygen content declined significantly, which led to significantly higher heating values. Another major improvement was a significant decrease in viscosity relative to unprocessed PSS and LA (compare Tables 4.2 and 4.3). After processing with HZSM-5, viscosity values for both PSS and LA were in the range

required for gasoline and significantly lower than values for materials processed at temperature without catalyst. Also, for catalytically-processed material, sulfur content was within specifications for gasoline (<0.035 %) for all feedstock/temperature combinations excluding PSS at 450 °C while control (non-catalyzed) products were not. From this observation, it is evident that HZSM-5 also promotes desulfurization thereby improving fuel properties.

While synergistically improving the heating value and viscosity of PSS, catalytic upgrading using HZSM-5 resulted in the formation of aromatic hydrocarbons indicated by the presence of BTEX. Figures 4.3A and 4.3B portray GC-MS spectra for heat-treated (control samples) and catalytically-cracked LA and PSS, respectively. Figure 4.3A indicates that under catalytic conditions, linoleic acid (peak L in Table 4.4) completely cracks (> 99 % conversion) and is rearranged to form predominantly aromatic hydrocarbons including benzene (peak A), toluene (peak C), ethylbenzene (peak D) and xylene (peak E) collectively known as BTEX. BTEX compounds are commonly-blended octane boosters for gasoline. A similar result was seen for PSS (Figure 4.3B); linoleic acid (peak L) completely cracks to form BTEX. This was expected since zeolites such as HZSM-5 are often incorporated with other materials into catalysts used in the petroleum industry for fluid catalytic cracking (FCC) operations to generate aromatics from heavy petroleum feedstocks. The inherent acidity and micropore structure of zeolites promote cracking of long chain hydrocarbons and size-selection of end-product molecules, leading to the formation of high octane product (Blauwhoff et al., 1999).

The formation of BTEX has been proposed to form via two reaction pathways involving either a carbenium or carbonium ion reaction mechanism. These pathways have been suggested in Blauwhoff et al. (1999) and Benson et al. (2008). For oleic acid ((9Z)-Octadec-9-enoic acid), as an example, the carbenium ion reaction pathway begins with a Brønsted acid site initiation step driven by a protonation mechanism on the catalyst surface as follows:

$$CH_3\text{-}(CH_2)_7\text{-}CH{=}CH\text{-}(CH_2)_7\text{-}COOH + HZ \rightarrow$$
$$CH_3\text{-}(CH_2)_7\text{-}CH_2\text{-}CH^+\text{-}(CH_2)_7\text{-}COOH + Z^- \quad \text{(Eq. 4.1)}$$

The next step, propagation via hydride transfer, involves the reaction of the carbenium ion with another oleic acid molecule to form a paraffin (stearic acid) and another carbenium ion as follows:

$$CH_3\text{-}(CH_2)_7\text{-}CH_2\text{-}CH^+\text{-}(CH_2)_7\text{-}COOH + CH_3\text{-}(CH_2)_7\text{-}CH{=}CH\text{-}(CH_2)_7\text{-}COOH \rightarrow$$

$$CH_3\text{-}(CH_2)_7\text{-}CH_2\text{-}CH_2\text{-}(CH_2)_7\text{-}COOH + CH_3\text{-}(CH_2)_7\text{-}CH_2\text{-}CH^+\text{-}(CH_2)_7\text{-}COOH \quad \text{(Eq. 4.2)}$$

Next, a β-scission cracking step forms another carbenium ion and an olefin as follows:

$$CH_3\text{-}(CH_2)_5\text{-}CH_2\text{-}CH^+\text{-}CH{=}CH\text{-}(CH_2)_7\text{-}COOH \rightarrow$$

$$CH_3\text{-}(CH_2)_5^+ + CH_2{=}CH\text{-}CH{=}CH\text{-}(CH_2)_7\text{-}COOH \quad \text{(Eq. 4.3)}$$

The carbenium ion is then free to react with another oleic acid molecule or enter the catalyst pore spaces where cyclization and aromatization occur:

$$CH_3\text{-}(CH_2)_6\text{-}CH_2^+ \rightarrow CH_3\text{-}CH{=}CH\text{-}C_6H_6 \text{ ((1E)-prop-1-en-1-ylbenzene)} \quad \text{(Eq. 4.4)}$$

$$CH_3\text{-}(CH_2)_6\text{-}CH_2^+ \rightarrow CH_2{=}CH_2\text{-}CH_3\text{-}CH_3\text{-}\ C_6H_6 \text{ (but-3-en-1-ylbenzene)} \quad \text{(Eq. 5.5)}$$

Alternately, following the carbonium ion pathway, the initiation step for the reaction is catalyzed by a Brønsted acid on a surface site as follows:

$$CH_3\text{-}(CH_2)_7\text{-}CH{=}CH\text{-}(CH_2)_7\text{-}COOH + HZ \rightarrow$$

$$CH_3\text{-}(CH_2)_7\text{-}CH_3\text{-}C^+\text{-}(CH_2)_7\text{-}COOH + Z^- \quad \text{(Eq. 4.6)}$$

Products from Eq. 4.6 undergo either β-scission or H_2 loss as follows:

$$CH_3\text{-}(CH_2)_7\text{-}CH_3\text{-}C^+\text{-}(CH_2)_7\text{-}COOH \rightarrow CH_3\text{-}(CH_2)_6\text{-}CH_2^+ + CH_3\text{-}CH_2\text{-}(CH_2)_7\text{-}COOH \quad \text{(Eq. 4.7)}$$

$$CH_3\text{-}(CH_2)_7\text{-}CH_3\text{-}C^+\text{-}(CH_2)_7\text{-}COOH \rightarrow CH_3\text{-}(CH_2)_7\text{-}CH_2\text{-}CH^+\text{-}(CH_2)_7\text{-}COOH + H_2 \quad \text{(Eq. 4.8)}$$

The non-carboxylic acid containing products from Eqs. 4.4, 4.5, 4.7, and 4.8 undergo further cracking and alkyl rearrangement to form final components including benzene, toluene, ethylbenzene, xylene, trimethylbenzene, and naphthalene.

The carboxylic acid-containing olefin undergoes decarboxylation to form CO_2 as follows:

$$CH_2{=}CH\text{-}(CH_2)_7\text{-}COOH \rightarrow CH_2{=}CH\text{-}(CH_2)_6\text{-}CH_3 + O{=}C{=}O, \quad \text{(Eq. 4.9)}$$

or decarbonylation to form CO:

$$CH_2{=}CH\text{-}(CH_2)_7\text{-}COOH \rightarrow CH_2{=}CH\text{-}(CH_2)_6\text{-}CH{=}O + C{\equiv}O \quad \text{(Eq. 4.10)}$$

$$CH_2=CH-(CH_2)_6-CH=O \rightarrow CH_2=CH-(CH_2)_5-CH_3 + C\equiv O \quad \text{(Eq. 4.11)}$$

Both $CH_2=CH-(CH_2)_6-CH_3$ and $CH_2=CH-(CH_2)_5-CH_3$ can then enter the HZSM-5 micropore spaces where they undergo carbenium and carbonium ion pathways shown above to form C_2H_4, C_3H_6, C_3H_8, and C_4H_8. These then undergo oligomerization, cyclization, and aromatization to form BTEX, trimethylbenzene and naphthalene as in the previous reaction set. To validate these reaction pathways, much more work would be required and is beyond the scope of the work outlined herein.

The presence of BTEX is a strong indication that the cracked free fatty acid product could be used as a green gasoline additive. Some polycyclic aromatic hydrocarbons such as naphthalene (peak G), which are also gasoline components, were identified, although not quantified, in the catalytically-cracked product both in LA and PSS but with qualitatively higher amounts in PSS, based on peak area. However based on these results, it is evident that very few by-product compounds (i.e. other than BTEX gasoline additives) were generated.

From Figure 4.4A, it appears that BTEX concentration for LA runs peak at 500 °C. Statistically, this is the case for both benzene and for combined BTEX where concentrations are significantly higher than for 450 or 550 °C processing. For toluene, the yield at 500 °C is significantly higher ($p<0.05$) than at 450 °C, but not significantly higher than at 550 °C. The remaining BTEX components show no significant difference in concentration due to process temperature. As seen in Figure 4.4B, yields of benzene and toluene and total BTEX generally increased with increasing pyrolysis temperature for PSS. There was a statistically significant increase in benzene concentration in PSS when process temperature was increased from 450 to 500 °C ($p < 0.001$) and from 500 to 550 °C ($p<0.001$), but not from 450 to 500 °C ($p=0.173$). The same was true for both toluene and total BTEX. For LA, the optimum temperature for BTEX formation appeared to be 500 °C, while for PSS, the optimum in the temperature range of the study was 550 °C. However, since BTEX yields were still increasing at 550 °C, the peak yields may occur at higher temperatures and is currently under investigation. The increase in benzene concentration at the expense of toluene and xylene, as in LA processing (Figure 4.4A) indicates that methylated aromatics, such as xylene, are undergoing further reactions (removal of side chains) due to higher

temperature resulting in greater formation the simplest aromatic, benzene. We propose that the increase in benzene formation occurred as a result of catalytic dealkylation of xylene and toluene as described in Weigert and Ragosta (1993) and Al-Khattaf (2006). The reaction is as follows for toluene (Ph-CH_3) dealkylation:

$$Ph\text{-}CH_3 + H_2O \rightarrow PhH + CO + 2H_2 \quad \text{(Eq. 4.12)}$$

Water for the reaction is derived from various cracking reactions. For xylene, the reaction above would occur twice sequentially; once to form toluene from xylene and once to form benzene from toluene. For PSS, if reactor residence times were increased or reaction temperature was increased, an increase in the yield of benzene relative to other BTEX compounds would likely be evident.

Conclusions

Our results demonstrate that green gasoline additives composed primarily of BTEX and with fuel properties comparable to gasoline can be generated from peanut soapstock. Biofuel yields ranged from 38-45 % (w/w) with BTEX selectivity approaching 94 % (v/v of product). By-product yields including non-condensable gas, catalyst coke and char were low. Processing PSS at 500 °C with HZSM-5 improved fuel properties relative to PSS feed as follows:

- kinematic viscosity was reduced 98% from 59.6 to 0.9 $mm^2\ s^{-1}$,
- heating value was increased 10% from 35.8 to 39.3 MJ L^{-1}, and
- O:C ratio was reduced 71% from 0.07 to 0.02.

Acknowledgements

The authors thank industry collaborator, DuBoise White of Golden Peanut Co. (Alpharetta, GA), for supplying PSS feedstock and feedstock characterization for material used for the work. Also, we thank Andrew Smola and Joby Miller for their work to analyze materials. The work was funded by the State of Georgia's Food Industry Partnership Program (FY2010). The funding agency played no role in the study design, in the collection, analysis and interpretation of data, in the writing of the report, or in the decision to submit this paper for publication.

References

Adebanjo, A.O., Dalai, A.K., 2005. Production of diesel-like fuel and other value-added chemicals from pyrolysis of animal fat. Energy Fuels 19(4), 1735-1741.

Al-Khattaf, S. (2006). Catalytic transformation of toluene over a high-acidity Y-zeolite based catalyst. Energy Fuels 20, 946-954.

Anjos, J., Gonzalez, W., Lam, Y., Frety, R. (1983). Catalytic decomposition of vegetable oil. Applied Catalysis 5, 299-308.

Ash, M., Wittenberger, K. (2010). Oil Crops Outlook. USDA Report OCS-10j, 18pp.

Benson, T., Hernandez, R., White, M., French, W., Alley, E., Holmes, W., Thompson, B., 2008. Heterogeneous cracking of an unsaturated fatty acid and reaction intermediates on H+ZSM-5 catalyst. Clean 36(8), 652-656.

Blauwhoff, P., Gosselink, J., Kieffer, E., Sie, S., Stork, W. (1999). Zeolites as Catalysts in Industrial Processes, in Weitkamp, J., Puppe, L. (Eds), Catalysis and Zeolites: Fundamentals and Applications. Springer-Verlag, Berlin, pp. 437-538.

Dandik, L, Aksoy, H., Erdem-Senatalar, A. (1998). Catalytic conversion of used oil to hydrocarbon fuels in a fractionating pyrolysis reactor. Energy Fuels 12, 1148-1152.

Doll, K., Sharma, B., Suarez, P., Erhan, S. (2008). Comparing biofuels obtained from pyrolysis, of soybean oil or soapstock, with traditional soybean biodiesel: density, kinematic viscosity, and surface tensions. Energy Fuels 22(3), 2061-2066.

EPA (2006). 1995-2006 RFG Surveys by Area. U.S. Environmental Protection Agency.

EPA (2008). Fuel Trends Report: Gasoline 1995-2005. Report number EPA420-R-08-002. U.S. Environmental Protection Agency.

Haas, M., Michalski, P., Runyon, S., Nunez, A., Scott, K. (2003). Production of FAME from Acid Oil, a By-product of Vegetable Oil Refining. JAOCS 80(1), 97-102.

Hilten, R., Speir, R., Kastner, J., Das, K.C. (2010). Production of fuel from the catalytic cracking of pyrolyzed poultry DAF skimmings. Journal of Analytical and Applied Pyrolysis 88, 30-38.

Kanellos, M. (2007). "Tyson, ConocoPhillips link up for biodiesel." CNETnews.com.

Li, H., Shen, B., Kabalu, J.C., Nchare, M. (1999). Enhancing the production of biofuels from cottonseed oil by fixed-fluidized bed catalytic cracking. Renewable Energy 34, 1033-1039.

Lima, D., Soares, V., Ribeiro, E., Carvalho, D., Cordoso, E., Rassi, F., Mundim, K., Rubim, J., Suarez, P. (2004). Diesel-like fuel obtained by pyrolysis of vegetable oils. J. Anal. Appl. Pyrolysis 71, 987-996.

Ooi, Y., Zakaria, R., Mohamed, A., Bhatia, S., 2004. Catalytic conversion of palm oil-based fatty acid mixture to liquid fuel. Biomass and Bioenergy 27, 477-484.

Padmaja, K., Atheya, N., Bhatnagar, A. (2009). Upgrading of Candelilla biocrude to hydrocarbon fuels by fluid catalytic cracking. Biomass and Bioenergy 33, 1664-1669.

Radich, A. (1998). Biodiesel Performance, Costs, and Use. Energy Information Administration.

Tamunaidu, P., Bhatia, S. (2007). Catalytic cracking of palm oil for the production of biofuels: optimization studies. Bioresour. Technol. 98, 3593–3601.

Twaiq, F., Zabidi, N.A.M., Bhatia, S. (1999). Catalytic conversion of palm oil to hydrocarbons: performance of various zeolite catalysts. Ind. Eng. Chem. Res. 38, 3230–3238.

Twaiq, F., Mohamed, A., Bhatia, S. (2003). Liquid hydrocarbon fuels from palm oil by catalytic cracking over aluminosilicate mesoporous catalysts with various Si/Al ratios. Microporous and Mesoporous Materials 64(1-3), 95-107.

Twaiq, F.A.A., Mohamad, A.R., Bhatia, S. (2004). Performance of composite catalysts in palm oil cracking for the production of liquid fuels and chemicals. Fuel Process. Technol. 85(11), 1283–1300.

Weigert, F., Ragosta, J. (1993). Nickel-on-alumina catalyzed polymethylbenzene dealkylation. J. Molec. Catal. 85, 237-251.

Wiggers, V., Meier, H., Wisniewski, A., Barros, A., Maciel, M. (2009). Biofuels from continuous fast pyrolysis of soybean oil: A pilot plant study. Bioresource Technology 100, 6570-6577.

Xu, J., Jiang, J., Sun, Y., Chen, J. (2010). Production of hydrocarbon fuels from pyrolysis using a basic catalyst. Bioresource Technology 101, 9803-9806.

Yean-Sang, O., Bhatia, S. (2007). Aluminum-containing SBA-15 as cracking catalyst for the production of biofuel from waste used palm oil. Micropor. Mesopor. Mater. 102, 310–317.

Figure Captions

Figure 4.1. Reactor setup showing (1) PSS vessel, (2) hot plate, (3) peristaltic pump, (4) stainless steel reactor with oil preheat zone, (5) catalyst bed, (6) tube furnace, (7) collection flask, (8) ice bath, (9) compressed N2 tank and thermocouples (TC1 and TC2).

Figure 4.2. Yield of products and co-products derived from FFA after catalytic pyrolysis at 500 °C.

Figure 4.3. GC-MS spectra for A) LA processed at 550 °C without catalyst (line a) and HZSM-5 (b) and B) PSS processed at 550 °C without catalyst (line a) and HZSM-5 (b).

Figure 4.4. Yield of BTEX components including total BTEX (a), toluene (b), benzene (c), p-xylene (d), m-xylene (e), and ethylbenzene (f) in A) LA and B) PSS relative to feed for catalytic processing using HZSM-5 at 450, 500, and 550 °C and a WHSV of 5.4 h^{-1}. Note: Values for p-xylene (d), m-xylene (e), and ethylbenzene (f) (i.e. dashed lines) are shown on the right-hand y-axis.

Tables

Table 4.1. Fatty acid profile for PSS.

Lipid #	Free Fatty Acid	Content
C16:0	Palmitic	13.0%
C18:0	Stearic	3.1%
C18:1	Oleic	51.3%
C18:2	Linoleic	22.7%
C20:0	Arachidic	1.6%
C20:1	Gadoleic	1.7%
C22:0	Behenic	4.3%
C24:0	Lignoceric	2.3%
	Total	100.0%

Table 4.2. Comparison of properties for LA, PSS, and conventional fuels.

Parameter	LA	PSS	Gasoline[a]	B100	No. 2 Diesel[b]
C	79.3	80.2	84.2	77.2	86.2
H	12.2	12.2	15.8	12.2	13.8
N	0.3	0.5	0	0	0
S	0.08	0.12	0	0	0
O[c]	8.1	7.0	0	10.6	0
H:C	1.85	1.83	2.3	1.9	1.9
O:C	0.08	0.07	0	0.1	0
HHV (MJ kg^{-1})[d]	39.6	39.8	48.5	35.9	45
d.b.[e]	39.6	39.9	48.5	36	45
HHV (MJ L^{-1})[d]	35.6	35.8	34.9	30.8	38.6
d.b.	35.7	35.9	34.9	30.9	38.6
% H_2O	0.1	0.2	0	0.18	0
pH	N/A	N/A	~7	7	~7
Viscosity (mm^2 s^{-1})[f]	22.9	59.7	< 1	2	1.9-4.1
Density (g mL^{-1})	0.9	0.9	0.72	0.86	0.85

[a] Assuming an average chemical formula, C_8H_{18}.
[b] Assuming an average chemical formula, $C_{12}H_{23}$.
[c] By difference.
[d] "As Received."
[e] "Dry Basis."
[f] Measured at 40 °C

Table 4.3. Comparison of properties for various LA and PSS treatments.

Parameter/ Temp., °C	LA						PSS					
	Control			HZSM-5			Control			HZSM-5		
	450	500	550	450	500	550	450	500	550	450	500	550
C	81.2	79.6	78.3	89.5	88.2	85.7	80.7	79.0	80.6	89.3	88.8	89.1
H	13.3	12.8	12.5	9.2	8.7	8.4	13.2	12.7	12.3	9.1	9.2	8.8
N	0.47	0.45	0.44	0.15	0.17	0.17	0.30	0.26	0.33	0.21	0.15	0.19
S	0.12	0.13	0.12	0.01	0.02	0.02	0.08	0.06	0.07	0.04	0.02	0.02
O[a]	4.90	7.01	8.63	1.09	2.99	5.72	5.81	8.01	6.71	1.41	1.84	1.87
H:C	1.90	1.94	1.91	1.24	1.18	1.17	1.96	1.93	1.84	1.22	1.24	1.19
O:C	0.11	0.07	0.08	0.01	0.03	0.05	0.05	0.08	0.06	0.01	0.02	0.02
HHV ($MJ\ kg^{-1}$)[b]	40.7	40.2	39.5	41.8	41.4	41.8	41.3	40.7	40.4	41.9	42.0	41.7
d.b.[c]	41.2	40.5	39.7	41.9	41.5	42.0	41.7	40.9	40.6	42.5	42.0	42.0
HHV ($MJ\ L^{-1}$)[b]	36.8	35.7	35.6	37.4	37.8	37.4	37.1	35.1	36.3	36.6	39.3	38.0
d.b.	37.2	36.0	35.7	37.5	37.9	37.6	37.4	35.2	36.5	37.1	39.3	38.3
% H_2O	1.2	0.7	0.4	0.2	0.3	0.5	1.0	0.5	0.5	1.5	0.1	0.7
pH	5.1	N/A	N/A	9.3	N/A	N/A	N/A	N/A	N/A	N/A	7.2	N/A
Viscosity ($mm^2\ s^{-1}$)[d]	11.6	10.6	5.7	0.7	0.7	0.7	10.7	9.9	5.1	0.9	0.9	0.8
Density ($g\ mL^{-1}$)	0.90	0.89	0.90	0.89	0.91	0.90	0.90	0.86	0.90	0.87	0.94	0.91

[a] By difference.
[b] "As Received."
[c] "Dry Basis."
[d] Measured at 40 °C.

Table 4.4. Compounds identified in LA and PSS catalytically upgraded using HZSM-5 (as labeled in Figures 3A and 3B).

Peak	Compound	Molecular Formula	Family	M.W. (g/mol)
A	benzene	C_6H_6	AH[a]	78.1
B	heptane	C_7H_{16}	alkane hydrocarbon	100.2
C	toluene	C_7H_8	AH	92.1
D	ethylbenzene	C_8H_{10}	AH	106.2
E	p-xylene	C_8H_{10}	AH	106.2
F	various benzene derivatives		AH	
G	various naphthalenes		PAH[b]	
H	cyclooctene	C_8H_{14}	AH	110.2
I	2-tetradecene	$C_{10}H_{28}$	alkene hydrocarbon	196.4
J	8-heptadecene	$C_{17}H_{34}$	alkene hydrocarbon	238.5
K	n-hexadecanoic acid	$C_{16}H_{32}O_2$	saturated fatty acid	256.4
L	9,12-octadecadienoic acid[c]	$C_{18}H_{32}O_2$	unsaturated fatty acid	280.5

[a] Aromatic hydrocarbon.
[b] Polycyclic aromatic hydrocarbon.
[c] Linoleic acid.

Figures

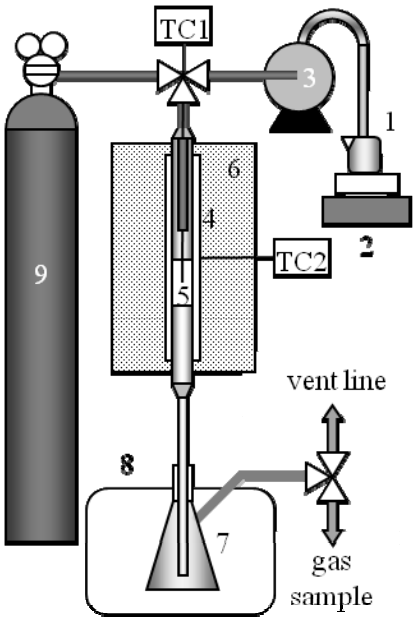

Figure 4.1. Reactor setup showing (1) PSS vessel, (2) hot plate, (3) peristaltic pump, (4) stainless steel reactor with oil preheat zone, (5) catalyst bed, (6) tube furnace, (7) collection flask, (8) ice bath, (9) compressed N2 tank and thermocouples (TC1 and TC2).

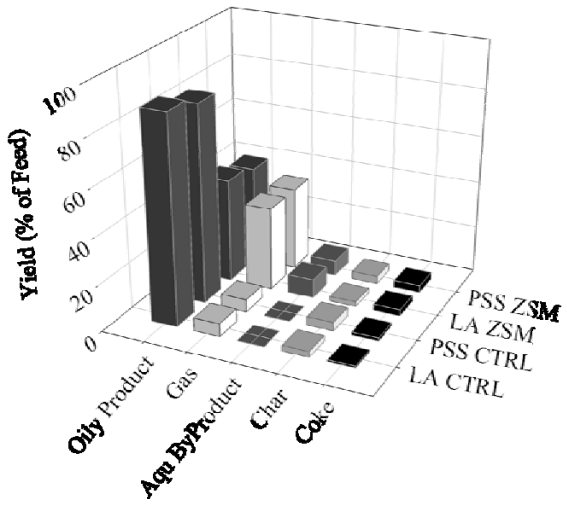

Figure 4.2. Yield of products and co-products derived from FFA after catalytic pyrolysis at 500 °C.

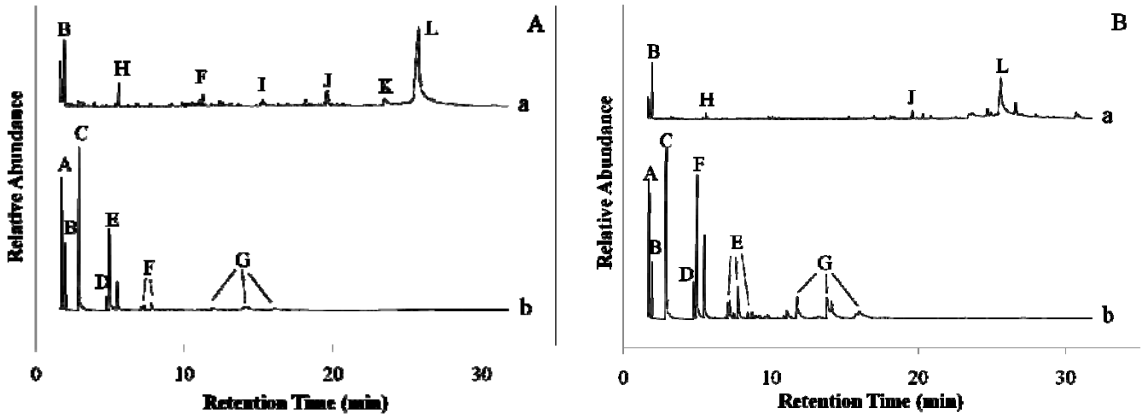

Figure 4.3. GC-MS spectra for A) LA processed at 550 °C without catalyst (line a) and HZSM-5 (b) and B) PSS processed at 550 °C without catalyst (line a) and HZSM-5 (b). Compounds are shown in Table 4.4.

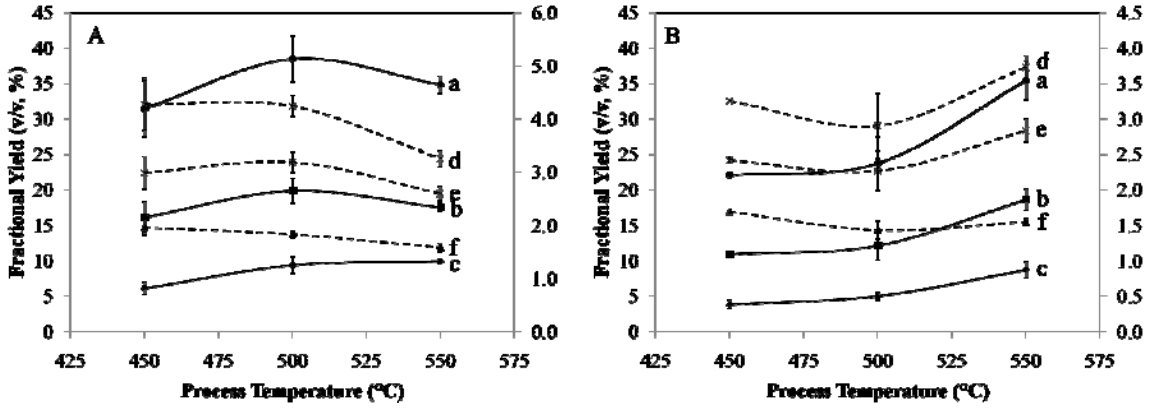

Figure 4.4. Yield of BTEX components including total BTEX (a), toluene (b), benzene (c), p-xylene (d), m-xylene (e), and ethylbenzene (f) in A) LA and B) PSS relative to feed for catalytic processing using HZSM-5 at 450, 500, and 550 °C and a WHSV of 5.4 h^{-1}. Note: Values for p-xylene (d), m-xylene (e), and ethylbenzene (f) (i.e. dashed lines) are shown on the right-hand y-axis.

CHAPTER 5

MODELING OLEIC ACID CONVERSION OVER A FIXED-BED OF HZSM-5 IN BOTH DIFFUSION AND REACTION RATE-LIMITED REGIMES[4]

[4] Hilten, R., Speir, R., Kastner, J., Das, K.C. To be submitted to *Catalysis Today*.

Abstract

A model was developed to determine the conversion of a model free fatty acid, oleic acid, over a fixed bed of a porous zeolite catalyst, HZSM-5. Conditions were modeled using reaction temperatures at 450, 500, and 550 °C with superficial gas velocity at 0.372, 0.743, and 1.49 cm s^{-1} and catalyst bed height at 0.05, 0.1, and 0.15 m. Concurrently, experimental data was generated using an oleic/linoleic acid mixture using the modeled process conditions to validate model predictions. Based on the calculated Thiele modulus (ca. 3600-23000), the system was mass transfer limited. Thus, the reaction theoretically occurred very quickly due to very fast reaction rates. One hundred percent conversion was modeled to occur in the first 4.5 mm of the catalyst bed. In experimental runs, oleic/linoleic acid conversion was 100 %, with yields of BTEX formation at 40-50 % of product.

KEYWORDS: catalytic cracking, free fatty acid, HZSM-5, modeling, reaction rate, mass transfer

Introduction

Fats and vegetable oils are common feedstocks for biofuel production, particularly for biodiesel production. Biofuels can be produced from a variety of oils containing mono- (free fatty acids, or FFAs), di-, and tri-glycerides (i.e. lipid). Although biodiesel production, a physicochemical pathway, has seen the most commercial development, thermochemical pathways are more robust in terms of the quality of feedstock that can be processed to fuel and the types of fuels that can be produced.

Many studies have demonstrated thermochemical conversion as a means to generate liquid fuel from mono- (free fatty acid, or FFA), di-, and tri-glyceride (TG) feedstocks without costly hydrogen addition. Adebanjo and Mohamed (2005) explored pyrolysis of animal fat (mainly saturated TGs), which generated an oil exhibiting a very similar cetane number and heat of combustion as those specified by ASTM for diesel fuel. Hilten et al. (2010) produced a gasoline-like fuel via pyrolysis and catalytic cracking of poultry processing waste containing FFAs, TGs, and protein. Other studies have produced diesel-like fuels from pyrolysis of vegetable oil feedstocks, such as soybean oil (Lima et al., 2004; Wiggers et al., 2009). Many studies have added catalysts to the process in fixed-bed reactors to catalytically crack oils to produce fuels from plant-derived oils (Anjos et al., 1983; Dandik et al., 1998;

Twaiq et al., 2003; Lima et al., 2004). Several studies (Twaiq et al., 1999; Twaiq et al., 2003; Twaiq et al., 2004; Tamunaidu and Bhatia, 2007) have used catalytic cracking to generate high yields of liquid hydrocarbons from palm oil waste. For example, Twaiq et al. (2003) cracked palm oil using a mesoporous acid catalyst and achieved an 80-90% yield of liquid hydrocarbons.

Additionally, several studies (Li et al., 2009; Ooi et al., 2004; Padmaja et al., 2009) have used solid acid zeolite catalysts to upgrade vegetable oils to liquid fuels via fluid catalytic cracking (FCC). Cracking studies have used a variety of acidic mono- and bi-functional catalysts at various pore size and functionality. Catalysts used in previous studies for cracking FFAs and TGs include MCM-41 (Twaiq et al., 2003), SBA-15 (Yean-Sang and Bhatia, 2007), and HZSM-5 (Dandik et al., 1998; Twaiq et al., 2004). Basic catalysts such as potassium carbonate (K_2CO_3) have also been used to upgrade vegetable oils including soybean oil (Xu et al., 2010).

Few studies can be found that attempt catalytic pyrolysis as a means to generate fuel or fuel additives from soap stock. One study found, Doll et al. (2008), generated biofuel from a soap stock (soybean-derived), but in a non-catalytic pyrolysis process. Use of catalysts for the conversion could conceivably improve the process by both increasing yields and decreasing the temperature required for conversion.

Several studies have attempted to elucidate reaction pathways for the conversion of FFAs to fuel via various catalytic thermochemical processing methods. Snåre et al. (2007) proposed kinetics and a reaction pathway for the conversion of ethyl stearate (with stearic acid as an intermediate) to aromatic end-products using a 5% Pd/C catalyst at temperatures 300-360 °C and pressures at 17-40 bar. Fu et al. (2011) decarboxylated palmitic and oleic acid to alkanes over activated carbon at 370 °C. Benson et al. (2008) proposed the reaction chemistry for oleic acid conversion to green fuels over HZSM-5 catalyst at 400 °C at atmospheric pressure. Figure 5.2 provides a simplified chemical pathway for the conversion of oleic acid to aromatics including benzene, toluene, ethylbenzene, and xylene (collectively, BTEX), trimethylbenzene, and naphthalene.

Additionally, a number of studies have explored the mass transfer aspects of conversion for a variety of feedstocks over zeolite catalysts. Studies involving mass transfer for zeolites have included alkane feedstocks such as n-hexane (Noordhoek et al., 1998), propane (Schwan and Möller, 2001), 2-methylpentane (Keipert and Baerns, 1998).

A wide variety of waste and by-product oils could potentially be utilized for biofuel production via thermochemical pathways. For example, during vegetable oil processing, by-products in the form of soap stock (SS), containing high levels of free fatty acids and emulsified water, are often underutilized due to the limited number of options for processing to higher-value products. Soap stock can be acidified to demulsify water while concentrating free fatty acids (FFAs). The FFA mixture, acidulated soap stock (a.k.a. acid oil), can subsequently be used as feedstock for biodiesel production using acid-catalyzed esterification. Although there is some industrial use of SS, it is sporadic, and thus price can significantly fluctuate and generate little economic return (Haas et. al., 2003). A potentially more favorable route would be to directly convert SS or acid oils into value-added products, such as a liquid transportation fuel via a thermochemical pathway.

In order to develop soap stocks as potential fuel feedstock, detailed information regarding the mass transfer and kinetic aspects during catalytic pyrolysis as a means to minimize processing costs. As such, for this study, HZSM-5, an acidic microporous zeolite catalyst, was used in a packed-bed tube reactor to process acidulated peanut soap stock (PSS) in an attempt to generate fuel-like hydrocarbons, particularly in the form of aromatics (e.g. benzene, xylene, toluene), components in gasoline representing approximately 20 % (v/v) (EPA, 2008). Several reaction pathways were proposed and a cursory exploration of mass transfer and kinetics has been attempted.

Theory

Reaction in porous media

The reaction system proposed, oleic acid (OA) cracking on microporous HZSM-5, can be described as diffusion with reaction in a porous solid media. This reaction system may be diffusion- or reaction rate-limited. The mass transfer model used for the mass transfer-limited system is that of Fogler

(1986). No matter the rate limiting step in a zeolite catalyst in a fixed bed, four phases of transport can be described. Figure 5.1 shows these phases. In the formulation in the following sections, models for predicting the concentration of OA in a single pellet and in a fixed-bed tubular reactor are developed.

Reaction in a spherical catalyst pellet

As shown in Figure 5.1E, the concentration of oleic acid also varies across individual catalyst pellets. A molar flux balance can be performed on a particle following Fogler (1986). Upon performing the shell balance, the following mole balance can be derived for a shell of thickness Δr for steady-state operation:

$$(\text{in at } r) - (\text{out at } r + \Delta r) + (\text{generation within } \Delta r) = 0$$

or,

$$\left(W_{Ar}(4\pi r^2|r)\right) - \left(W_{Ar}(4\pi r^2|r+\Delta r)\right) + \left(r_A''(A_i)(4\pi r_m^2 \Delta r)\right) = 0 \text{ (Eq. 5.1)}$$

In Eq. 5.1, A_i, is the surface area per volume of catalyst, can alternately be expressed as the catalyst's internal surface area per unit mass, S_a, by:

$$S_a = \frac{A_i}{\rho_p} \text{ (Eq. 5.2)}$$

Upon dividing by $-4\pi\Delta r$ and taking the limit when $\Delta r \rightarrow 0$, Eq. 1 takes the differential form:

$$\frac{d(W_{Ar}r^2)}{dr} - r_A'' A_i r^2 = 0 \text{ (Eq. 5.3)}$$

The rate of reaction per unit of surface area can be calculated as follows:

$$-r_{OA}'' = k_n C_{OA}^n \text{ (Eq. 5.4)}$$

where,

$$-r_{OA}'' = \frac{r_{OA}'}{S_a} \text{ (Eq. 5.5)}$$

In Eq. 5.5, r'_{OA} is the rate of reaction per unit mass of catalyst. In our system, we will assume dilute conditions such the concentration of product and reactant do not affect on another. With that assumption, the molar flow rate of OA is:

$$W_{Ar} = -cD_e \frac{dy_{OA}}{dr} = -D_e \frac{dC_A}{dr} \text{ (Eq. 5.6)}$$

Upon substituting Eqs. 5.4 and 5.6 into Eq. 5.3, the differential equation describing diffusion and reaction in a porous catalyst pellet becomes:

$$-\frac{d[r^2(dC_{OA}C_{OA}/dr)]}{dr}+\frac{r^2k_nA_iC_A^n}{D_e}=0 \text{ (Eq. 5.7)}$$

After differentiating the first term in Eq. 5.7 and dividing by r^2, the differential equation becomes:

$$\frac{d^2C_{\mathrm{OA}}}{dr^2}+\frac{2}{r}\left(\frac{dC_{\mathrm{OA}}}{dr}\right)-\frac{k_nA_i}{D_e}C_{\mathrm{OA}}^n=0 \text{ (Eq. 5.8)}$$

The boundary conditions that can be applied given the proposed reaction system are that at r=0, C_{OA} is finite, and that at r=R, C_{OA}=$C_{\mathrm{OA}s}$. In order to solve Eq. 5.8 analytically, it can be written in dimensionless form by introducing the new terms:

$$\varphi=\frac{C_{\mathrm{OA}}}{C_{\mathrm{OA}s}} \text{ (Eq. 5.9)}$$

$$\lambda=\frac{r}{R} \text{ (Eq. 5.10)}$$

Boundary conditions are thus transformed to:

$$\varphi=\frac{C_{\mathrm{OA}}}{C_{\mathrm{OA}s}}=1 \text{ at } r=R$$

and,

φ is finite at λ=0

After rewriting Eq. 5.6 in dimensionless form and using the chain rule, the equation becomes:

$$\frac{dC_{\mathrm{OA}}}{dr}=\frac{d\varphi}{d\lambda}\left(\frac{dC_{\mathrm{OA}}}{d\varphi}\right)\frac{d\lambda}{dr} \text{ (Eq. 5.11)}$$

Upon differentiating Eqs. 5.9 and 5.10 with respect to φ and r, respectively, and entering the new terms into Eq. 5.11, results in the following equation for the concentration gradient:

$$\frac{dC_{\mathrm{OA}}}{dr}=\frac{d\varphi}{d\lambda}\frac{C_{\mathrm{OA}s}}{R} \text{ (Eq. 5.12)}$$

The flux of OA is then:

$$W_{\mathrm{OA}r}=-D_e\frac{dC_{\mathrm{OA}}}{dr}=-\frac{D_eC_{\mathrm{OA}s}}{R}\left(\frac{d\varphi}{d\lambda}\right) \text{ (Eq. 5.13)}$$

Assuming steady-state conditions, i.e. all oleic acid that enters the pellet is completely reacted, the reaction rate can be assumed to be equal to the diffusion rate. With this consideration, the overall rate of reaction, M_{OA}, is obtained as follows:

$$M_{OA} = -4\pi R^2 W_{OAr}|_{r=R} = 4\pi R^2 \frac{dC_{OA}}{dr}\Big|_{r=R} = 4\pi R D_e C_{OAs} \frac{d\varphi}{d\lambda}\Big|_{\lambda=1} \text{ (Eq. 5.14)}$$

Upon differentiating the concentration gradient given in Eq. 5.12, the equation becomes:

$$\frac{d^2\varphi}{dr^2} = \frac{d^2\varphi}{d\lambda^2}\left(\frac{C_{OAs}}{R^2}\right) \text{ (Eq. 5.15)}$$

After substituting A_i into Eq. 5.14 and dividing by C_{OAs}/R^2, the dimensionless form of Eq. 5.15 becomes:

$$\frac{d^2\varphi}{d\lambda^2} + \frac{2}{\lambda}\frac{d\varphi}{d\lambda} - \frac{k_n R^2 S_a \rho_p C_{OAs}^{n-1}}{D_e}\varphi^n = 0 \text{ (Eq. 5.16)}$$

which can be written as:

$$\frac{d^2\varphi}{d\lambda^2} + \frac{2}{\lambda}\frac{d\varphi}{d\lambda} - \phi_n^2\varphi^n = 0 \text{ (Eq. 5.17)}$$

where,

$$\phi_n^2 = \frac{k_n R^2 S_a \rho_p C_{OAs}^{n-1}}{D_e} \text{ (Eq. 5.18)}$$

The square root of Eq. 5.18 is the also known as the Thiele modulus, a term that relates the surface reaction rate to the diffusion rate. High Thiele moduli indicate that diffusion limits the reaction, whereas small Thiele modulus values indicate that a reaction is surface reaction rate limited.

Assuming the conversion of oleic acid is first order, high temperatures are used (weak adsorption of OA and products) and OA and products are dilute, the rate law becomes:

$$-r_{OA}'' \cong k_1 C_{OA} \text{ (Eq. 5.19)}$$

Such that Eq. 5.17 becomes:

$$\frac{d^2\varphi}{d\lambda^2} + \frac{2}{\lambda}\frac{d\varphi}{d\lambda} - \phi_1^2\varphi = 0 \text{ (Eq. 5.20)}$$

Solving Eq. 5.20 using boundary conditions, φ=1 at λ=1 and φ is finite at λ=0, results in the dimensionless concentration profile:

$$\varphi = \frac{C_{OA}}{C_{OAs}} = \frac{1}{\lambda}\left(\frac{\sinh \phi_1 \lambda}{\sinh \phi_1}\right) \text{ (Eq. 5.21)}$$

Determining catalyst effectiveness factors

Internal effectiveness factor

The internal effectiveness factor, η, indicates the relative importance of diffusion or reaction limitation and is defined as:

$$\eta = \frac{\text{actual overall rate of reaction}}{\text{rate of reaction if the entire surface area were exposed to the external pellet surface concentration,} C_{OAs}} \text{ (Eq. 5.22)}$$

After some manipulation of Eqs. 5.14 and 5.21, η can be determined as:

$$\eta = \frac{3}{\phi_1^2}\left(\phi_1 \coth \phi_1 - 1\right) \text{ (Eq. 5.23)}$$

For large values of the Thiele modulus, η can be described as:

$$\eta = \frac{3}{R}\sqrt{\frac{D_e}{k_1 \rho_p S_a}} \text{ (Eq. 5.24)}$$

Overall effectiveness factor

The overall effectiveness factor, Ω, relates the actual overall rate to the rate if the entire catalyst area were exposed to C_{OAo}. For a first order reaction, Ω can be calculated as follows:

$$\Omega = \frac{\text{actual overall rate}}{\text{rate that would result if the entire surface were exposed to the bulk concentration,} C_{OAo}} \text{ (Eq. 5.25)}$$

or,

$$\Omega = \frac{\eta}{1+\eta\left(kA_s/k_c A_p\right)} \text{ (Eq. 5.26)}$$

where $\frac{A_s}{m} = \frac{\text{internal surface area}}{\text{mass of catalyst}} = S_a$

$$\frac{A_p}{m} = \frac{\text{external surface area}}{\text{mass of catalyst}} = a_c$$

where $a_c = 6(1-\epsilon_b)/\rho_p d_p$ (Eq. 5.27)

ρ_b = bulk density of the catalyst bed

d_p = pellet diameter

ϵ_b = bed void fraction

The overall effectiveness factor in terms of mass of catalyst is then:

$$\Omega = \frac{\eta}{1+\eta k S_a / k_c a_c} \text{ (Eq. 5.28)}$$

Reaction along a fixed-bed of particles – Diffusion-limited system

In Figure 5.1, the overall concentration of reactant and products changes moving down the length of the reactor (from z to $z+\Delta z$) as shown in Figure 5.1A. Bulk flow, shown in Figure 5.1A and Figure 5.1B, occurs between the macroparticles in the fixed-bed. At steady-state, bulk flow mole balance can be represented by:

$$[\text{molar rate in}] - [\text{molar rate out}] + [\text{molar rate of generation}] = [\text{molar rate of accumulation}]$$

or, at steady-state:

$$F_{\mathrm{OA}z|z} - F_{\mathrm{OA}z|z+\Delta z} + r''_{\mathrm{OA}} a(A_c \Delta z) = 0 \text{ (Eq. 5.29)}$$

In Eq. 5.29, F_{OAz} is the molar flow rate (mol s^{-1}) in the z-direction, r_{OA}'' is the rate of generation of OA per unit of catalytic surface area (mol s^{-1} m^{-2}), A_c is the cross-sectional area of the reactor (m^2), and a is the external surface area of the catalyst per volume of catalytic bed (m^2 m^{-3}) that can be calculated by:

$$a = \frac{6(1-\epsilon_b)}{d_p} \text{ (Eq. 5.30).}$$

In Eq. 5.30, ϵ_b is the porosity of the bed, d_p is the particle diameter (m). Upon dividing Eq. 5.30 by A_c and Δz and taking the limit as $\Delta z \rightarrow 0$, the equation reduces to:

$$-\frac{1}{A_c}\left(\frac{dF_{\mathrm{OA}z}}{dz}\right) + r''_{\mathrm{OA}} = 0 \text{ (Eq. 5.31)}$$

Expressing $F_{\mathrm{OA}z}$ and r''_{OA} in terms of concentration while neglecting axial diffusion results in the following equation:

$$F_{\mathrm{OA}z} = A_c W_{\mathrm{OA}z} = J_{\mathrm{OA}z}(A_c) = U C_{\mathrm{OA}} A_c \text{ (Eq. 5.32)}$$

In Eq. 5.32, $W_{\mathrm{OA}z}$ is the molar flux (mol m^{-2} s^{-1}), J_{OAz} is the concentration gradient, U is the superficial velocity (m s^{-1}), and C_{OA} is the concentration of oleic acid. Substituting the value for F_{OAz} in Eq. 5.32 into Eq. 5.31 and assuming constant superficial velocity results in the following formulation:

$$-U\frac{dC_A}{dz} + r''_{OA} = 0 \text{ (Eq. 5.33)}$$

At steady state, the molar flow rate of OA across the stagnant boundary layer to the surface equals the reaction rate on the surface such that:

$$-r_{OA}^{''} = W_{Ar} = k_c(C_{OA} - C_{OAs}) \text{ (Eq. 5.34)}$$

In Eq. 5.34, k_c is the mass transfer coefficient. The mass transfer coefficient and boundary layer thickness were found using the Frössling correlation which is a function of the Reynolds, Re, the Schmidt, Sc, and the Sherwood, Sh, number as follows:

$$\text{Re} = \frac{U\rho_{\text{N}_2} d_p}{\mu_{\text{N}_2}} \text{ (Eq. 5.36)}$$

$$\text{Sc} = \frac{\mu_{\text{N}_2}}{D_{\text{OA-N}_2}\rho_{\text{N}_2}} \text{ (Eq. 5.37)}$$

$$\text{Sh} = 2 + 0.6\text{Re}^{1/2}\text{Sc}^{1/3} \text{ (Eq. 5.38)}$$

$$k_c = \frac{\text{Sh}\cdot D_{\text{OA-N}_2}}{d_p} \text{ (Eq. 5.39)}$$

where, $D_{\text{OA-N2}}$ is the bulk mass transfer coefficient for oleic acid in N_2 ($m^2\ s^{-1}$), ρ_{N2} and μ_{N2} are the density and dynamic viscosity of N_2 at a given temperature.

The boundary layer thickness, δ(m), around the catalyst particle can be found as a function of the diffusion coefficient along with the mass transfer coefficient, k_c:

$$\delta = \frac{D_{\text{OA-N}_2}}{k_c} \text{ (Eq. 5.40)}$$

For mass transfer limited reaction systems, using Eq. 5.34, $C_{\text{OA}s}$ is negligible relative to C_{OA}. Taking this assumption and integrating using the boundary condition that at z=0, C_{OA}=C_{OA_0}, yields:

$$\frac{C_{\text{OA}}}{C_{\text{OA0}}} = \exp\left(-\frac{k_c a}{U} z\right) \text{ (Eq. 5.41)}$$

Reaction along a fixed-bed of particles – Reaction-limited system

The formulation of the reaction rate limited system follows that of the diffusion limited system. Starting with the mole balance at steady state:

$$[\text{rate in}] - [\text{rate out}] + [\text{rate of generation of OA}] = 0$$

$$A_c W_{OAz}|_z - A_c W_{OAz}|_{z+\Delta z} + r_{OA}^{'}\rho_b A_c \Delta z = 0 \text{ (Eq. 5.42)}$$

Upon dividing by Δz and taking the limit as $\Delta z \rightarrow 0$, Eq. 5.42 becomes:

$$-\frac{dW_{OAz}}{dz} + r'_{OA}\rho_p = 0 \text{ (43)}$$

With the assumption that the total concentration is constant, Fick's equation can be expressed as:

$$W_{OAz} = -D_{OA-N_2}\frac{dC_{OA}}{dz} + y_{OA}\left(W_{OAz} + W_{N_2z}\right) \text{ (Eq. 5.44)}$$

The bulk flow term, $y_{OA}\left(W_{OAz} + W_{N_2z}\right)$, can be rewritten as:

$$B_{OAz} = y_{OA}CU = UC_{OA} \text{ (Eq. 5.45)}$$

Using the flow term in Eq. 45, Eq. 5.44 becomes:

$$D_{OA-N_2}\frac{d^2C_{OA}}{dz^2} - U\frac{dC_{OA}}{dz} + r'_{OA}\rho_p = 0 \text{ (Eq. 5.46)}$$

Where r'_{OA} is the overall reaction rate within and on the pellet per unit mass of catalyst. From the overall rate, the rate if the entire surface was exposed to the bulk concentration, can be determined using the overall effectiveness factor, Ω, from Eq. 5.28. as follows:

$$-r'_{OA} = -r'_{OA0} \times \Omega \text{ (Eq. 5.47)}$$

Given a proposed first-order reaction, $-r'_{OA}$ can be calculated as:

$$-r'_{OA0} = -r''_{OA}S_a = kS_aC_{OA} \text{ (Eq. 5.48)}$$

As such, the overall rate of reaction can then be calculated as:

$$-r'_{\mathrm{OA}} = \Omega k S_a C_{\mathrm{OA}} \text{ (Eq. 5.49)}$$

When Eq. 5.49 is substituted into Eq. 5.46, the result is:

$$D_{\mathrm{OA-N_2}}\frac{d^2C_{\mathrm{OA}}}{dz^2} - U\frac{dC_{\mathrm{OA}}}{dz} + \Omega\rho_p k S_a C_{\mathrm{OA}} = 0 \text{ (Eq. 5.50)}$$

If superficial velocity is high enough, the first term, axial diffusion, can be neglected since the bulk diffusion term dominates. Neglecting axial diffusion and rearranging Eq. 5.50 yields:

$$\frac{dC_{\mathrm{OA}}}{dz} = -\left(\frac{\Omega\rho_p k S_a}{U}\right)C_{\mathrm{OA}} \text{ (Eq. 5.51)}$$

Assuming the boundary condition, C_{OA}=C_{OAo} at z=0, Eq. 5.51 can then be integrated to the following form:

$$C_{\mathrm{OA}} = C_{\mathrm{OA0}} \exp -(\rho_b k S_a \Omega z/U) \text{ (Eq. 5.52)}$$

Or, in terms of conversion, X, Eq. 5.52 can be rearranged to:

$$X = 1 - \frac{C_{\mathrm{OA}}}{C_{\mathrm{OAo}}} = 1 - \exp -(\rho_b k S_a \Omega z / U) \text{ (Eq. 5.53)}$$

Estimating the effective diffusivity

Gas phase diffusion (bulk)

The first calculation required to facilitate the model involved determining the gas phase diffusivity of the catalyst for the reactant, oleic acid in this case. The Wilke-Lee equation can be used for mixtures of non-polar gases and for mixtures of polar and non-polar gases. The Wilke-Lee equation in follows that the diffusion coefficient, $D_{\mathrm{OA\text{-}N2}}$, can be estimated as:

$$D_{\mathrm{OA-N_2}} = \frac{10^{-4}\left(1.084 - 0.249\sqrt{\frac{1}{M_{\mathrm{OA}}} + \frac{1}{M_{\mathrm{N_2}}}}\right) T^{3/2}\sqrt{\frac{1}{M_{\mathrm{OA}}} + \frac{1}{M_{\mathrm{N_2}}}}}{P_T(\sigma_{\mathrm{OA-N2}})^2 f\left(\frac{kT}{\varepsilon_{\mathrm{OA-N_2}}}\right)} \text{ (Eq. 5.54)}$$

In Eq. 5.54, M_{OA} and M_{N2} are the molecular weights of reactant (oleic acid) and solute (N_2) (g mol^{-1}), here take to be 282.46 and 28.0, respectively, T is the reaction temperature (K), P_T is the absolute pressure (Pa), σ is the collision diameter (nm), and $f(kT/\varepsilon_{\mathrm{AB}})$, the collision integral, also represented as Ω_{D}. The collision diameter, σ, is a function of molecular formula and more specifically, a function of the molecular volume as follows:

$$\sigma = 11.8V^{1/3} \text{ (Eq. 5.55)}$$

Part of the collision integral, $k/\varepsilon_{\mathrm{OA\text{-}N2}}$, the inverse of which is known as the energy of attraction, can be calculated by $0.826/T$ (1/K).

The effective bulk diffusion coefficient, $D_{\mathrm{OA-N_2,e}}$, can be found as follows:

$$D_{\mathrm{OA-N_2,e}} = D_{\mathrm{OA},K}\frac{\epsilon}{\tau} \text{ (Eq. 5.56)}$$

Since the catalyst pores were assumed to be small relative to the mean free path of the gas, Knudsen diffusivity was expected to contribute to the overall effective diffusion coefficient, as well. Generally, Knudsen diffusivity, $D_{\mathrm{OA},K}$, can be described as a function of pore radius, r_c (m), temperature,

T (K), and molecular weight of the diffusing component (i.e. oleic acid, abbreviated OA), M_{OA} (282.46 g mol^{-1}), as follows:

$$D_{OA,K} = 97.0 r_c \left(\frac{T}{M_{OA}}\right)^{1/2} \text{(Eq. 5.57)}$$

Given the catalyst used in these experiments, the diffusivity was adjusted to account for the tortuous path of the molecule and the porosity of the material as previously for bulk diffusion in Eq. 5.56:

$$D_{OA,K,e} = D_{OA,K} \frac{\epsilon}{\tau} \text{ (Eq. 5.58)}$$

Where $D_{OA,K,e}$ is the effective diffusivity, ϵ is the porosity of the solid, and τ is the tortuosity factor. Pore radius, r, and porosity, ϵ were measured using a surface area analyzer and found to be 1.08 x 10^{-9} (m) and 0.2, respectively. The tortuosity factor, τ, was not measured for the HZSM-5 catalyst, but was assumed to be 0.725 from the value taken from Barrer and Gabor (1959) for a silica-alumina cracking catalyst. Making the assumption that surface diffusion can be neglected, the overall effective diffusion coefficient can then be calculated as:

$$\frac{1}{D_{OA,e}} = \frac{1}{D_{OA-N_2}} + \frac{1}{D_{OA,K,e}} \text{ (Eq. 5.59)}$$

Oleic Acid cracking chemistry

The formation of BTEX has been proposed to form via two reaction pathways involving either a carbenium or carbonium ion reaction mechanism. These pathways have been suggested in Blauwhoff et al. (1999) and Benson et al. (2008). For oleic acid ((9Z)-Octadec-9-enoic acid), as an example (shown generally in Fig. 5.2), the carbenium ion reaction pathway begins with a Brønsted acid site initiation step driven by a protonation mechanism on the catalyst surface as follows:

$$CH_3\text{-}(CH_2)_7\text{-}CH{=}CH\text{-}(CH_2)_7\text{-}COOH + HZ \rightarrow$$

$$CH_3\text{-}(CH_2)_7\text{-}CH_2\text{-}CH^{+}\text{-}(CH_2)_7\text{-}COOH + Z^{-} \quad \text{(Eq. 5.60)}$$

The next step, propagation via hydride transfer, involves the reaction of the carbenium ion with another oleic acid molecule to form a paraffin (stearic acid) and another carbenium ion as follows:

$$CH_3\text{-}(CH_2)_7\text{-}CH_2\text{-}CH^{+}\text{-}(CH_2)_7\text{-}COOH + CH_3\text{-}(CH_2)_7\text{-}CH{=}CH\text{-}(CH_2)_7\text{-}COOH \rightarrow$$

$$CH_3\text{-}(CH_2)_7\text{-}CH_2\text{-}CH_2\text{-}(CH_2)_7\text{-}COOH + CH_3\text{-}(CH_2)_7\text{-}CH_2\text{-}CH^+\text{-}(CH_2)_7\text{-}COOH \quad \text{(Eq. 5.61)}$$

Next, a β-scission cracking step forms another carbenium ion and an olefin as follows:

$$CH_3\text{-}(CH_2)_5\text{-}CH_2\text{-}CH^+\text{-}CH{=}CH\text{-}(CH_2)_7\text{-}COOH \rightarrow$$

$$CH_3\text{-}(CH_2)_5^+ + CH_2{=}CH\text{-}CH{=}CH\text{-}(CH_2)_7\text{-}COOH \quad \text{(Eq. 5.62)}$$

The carbenium ion is then free to react with another oleic acid molecule or enter the catalyst pore spaces where cyclization and aromatization occur:

$$CH_3\text{-}(CH_2)_6\text{-}CH_2^+ \rightarrow CH_3\text{-}CH{=}CH\text{-}C_6H_6 \text{ ((1E)-prop-1-en-1-ylbenzene)} \quad \text{(Eq. 5.63)}$$

$$CH_3\text{-}(CH_2)_6\text{-}CH_2^+ \rightarrow CH_2{=}CH_2\text{-}CH_3\text{-}CH_3\text{-}\ C_6H_6 \text{ (but-3-en-1-ylbenzene)} \quad \text{(Eq. 5.64)}$$

Alternately, following the carbonium ion pathway, the initiation step for the reaction is catalyzed by a Brønsted acid on a surface site as follows:

$$CH_3\text{-}(CH_2)_7\text{-}CH{=}CH\text{-}(CH_2)_7\text{-}COOH + HZ \rightarrow$$

$$CH_3\text{-}(CH_2)_7\text{-}CH_3\text{-}C^+\text{-}(CH_2)_7\text{-}COOH + Z^- \quad \text{(Eq. 5.65)}$$

Products from Eq. 65 undergo either β-scission or H_2 loss as follows:

$$CH_3\text{-}(CH_2)_7\text{-}CH_3\text{-}C^+\text{-}(CH_2)_7\text{-}COOH \rightarrow$$

$$CH_3\text{-}(CH_2)_6\text{-}CH_2^+ + CH_3\text{-}CH_2\text{-}(CH_2)_7\text{-}COOH \quad (60)$$

$$CH_3\text{-}(CH_2)_7\text{-}CH_3\text{-}C^+\text{-}(CH_2)_7\text{-}COOH \rightarrow CH_3\text{-}(CH_2)_7\text{-}CH_2\text{-}CH^+\text{-}(CH_2)_7\text{-}COOH + H_2 \quad \text{(Eq. 5.66)}$$

The non-carboxylic acid containing products from Eqs. above undergo further cracking and alkyl rearrangement to form final components including benzene, toluene, ethylbenzene, xylene, trimethylbenzene, and naphthalene.

The carboxylic acid-containing olefin undergoes decarboxylation to form CO_2 as follows:

$$CH_2{=}CH\text{-}(CH_2)_7\text{-}COOH \rightarrow CH_2{=}CH\text{-}(CH_2)_6\text{-}CH_3 + O{=}C{=}O, \quad \text{(Eq. 5.67)}$$

or decarbonylation to form CO:

$$CH_2{=}CH\text{-}(CH_2)_7\text{-}COOH \rightarrow CH_2{=}CH\text{-}(CH_2)_6\text{-}CH{=}O + C{\equiv}O \quad \text{(Eq. 5.68)}$$

$$CH_2{=}CH\text{-}(CH_2)_6\text{-}CH{=}O \rightarrow CH_2{=}CH\text{-}(CH_2)_5\text{-}CH_3 + C{\equiv}O \quad \text{(Eq. 5.69)}$$

Both CH_2=CH-$(CH_2)_6$-CH_3 and CH_2=CH-$(CH_2)_5$-CH_3 can then enter the HZSM-5 micropore spaces where they undergo carbenium and carbonium ion pathways shown above to form C_2H_4, C_3H_6, C_3H_8, and C_4H_8. These then undergo oligomerization, cyclization, and aromatization to form BTEX, trimethylbenzene and naphthalene as in the previous reaction set. To validate these reaction pathways, much more work would be required and is beyond the scope of the work outlined herein.

Kinetics of Oleic Acid Cracking

In order to model the concentration of reactants and products, reaction rate expressions for the conversion were needed. Experiments were devised using differential data analysis for plug flow reactor data. The reaction was simplified to A → B, where A represents oleic acid and B represents products. The variable of interest however is (A), the concentration of oleic acid versus position or time.

Determining k from non-isothermal DSC data

A differential scanning calorimetry method (DSC) method was developed by Ozawa (1970) to determine activation energy (E), pre-exponential factor (k_0), rate constant, and half-like ($t_{1/2}$) for a given reaction. ASTM E698 provides an experimental procedure to follow to determine kinetic parameters based on formulations from Ozawa (1970). The approach assumes that the rate constant follows Arrhenius behavior such that k, the rate constant ($d\alpha/dt$), is a function of temperature, and can be determined by:

$$k = k_0 e^{-E_a/RT}(1-\alpha)^n \text{(Eq. 5.70)}$$

In Eq. 5.70, R is the gas constant (8.314 J mol^{-1} K^{-1}), T is the reaction temperature, α is the fractional conversion, and n is the reaction order. Eq. 5.70 can be modified to fit variable temperature DSC data by introducing a new term, the heating rate, β:

$$\beta = \frac{dT}{dt} \text{(Eq. 5.71)}$$

Whereby, $d\alpha/dt$ is simply $\beta\, d\alpha/dT$. When the heating rate (β), is used in Eq. 5.70, the equation changes to:

$$\beta \frac{d\alpha}{dT} = k_0 e^{E_a/RT}(1-\alpha) \text{(Eq. 5.72)}$$

According to ASTM E698, an iterative process is needed to determine the activation energy, E. Plotting $\log \beta$ versus $1/T$ produces a line with slope $d \log \beta / d\,(1/T)$. E can be calculated in the first iteration as:

$$E = -2.19R[d \log \beta / d\,(1/T)] \text{(Eq. 5.73)}$$

Next, E/RT is calculated and a tabulated value for a new term, D, is utilized to refine E in Eq. 5.73 in the next iteration as follows:

$$E = (-2.303\,R/D)[d \log \beta / d\ (1/T)] \text{(Eq. 5.74)}$$

This calculation is followed by another determination of E/RT corresponding to a new D value and a further re-calculation of E using Eq. 74. Iterations are continued until the value of E does not change from one iteration to the next. Using the final activation energy derived from the iterative process, the Arrhenius pre-exponential factor can then be calculated by:

$$k_0 = \beta E_a e^{E_a/RT} / RT^2 \text{(Eq. 5.75)}$$

Finally, the rate constant, k, can be calculated at multiple reaction temperatures using the Arrhenius equation from Eq. 5.70.

Determining r and k from isothermal reactor data

Using concentration data from the experimental reactor, the reaction rate, r, can be determined. The reaction rate, r, is defined by $r = kC_a^n$. Combining equations for r and Eq. 70 for k and linearizing yields:

$$\ln r = \ln k_a - \frac{E}{RT} + n \ln C_a \text{ (Eq. 5.76)}$$

Using multilinear regression, k_0, E, and n can be determined. For isothermal data, Eq 5.71 can be simplified to:

$$\ln r = \ln k + n \ln C_a \text{ (Eq. 5.77)}$$

where n and k are calculated as the intercept and slope of the best-fit line of the collected data. The pre-exponential factor, k_0, and the activation energy, E, can be determined by performing experiments at multiple temperatures and plotting the following equation where E is the slope and $\ln k_0$ is the y-intercept:

$$\ln k = \ln k_0 - \frac{E}{RT} \text{ (Eq. 5.78)}$$

Determining the rate limiting step

The Mear's criterion can be used to determine if mass transfer from the bulk phase to the catalyst surface is the rate limiting step. The Mear's criterion states that if:

$$\frac{-r_{OA}^{'}\rho_p Rn}{k_c C_{OA}} < 0.15 \text{ (Eq. 5.79)}$$

external mass transfer effects can be neglected.

Materials and Methods

Feedstock

Acidulated peanut oil soap stock (PSS) containing mainly free fatty acids (FFAs) was supplied by Golden Peanut Co., LLC. Table 5.1 provides the fatty acid profile for PSS. Oleic and linoleic acids are the main components in PSS. As such, a model compound mixture containing linoleic (70%) and oleic (30%) acid (denoted as LA for the linoleic acid in the mixture)) was chosen for comparison and supplied by Sigma-Aldrich. Table 5.2 provides additional compositional data for PSS, LA, gasoline, biodiesel and No. 2 diesel.

Free fatty acid conversion

Reactor Setup

PSS and LA were catalytically pyrolyzed using a reactor and process similar to that described by ASTM D5154, "Standard test method for determining activity and selectivity of fluid catalytic cracking (FCC) catalysts by microactivity testing." For this work, changes that were made to the reactor described in ASTM D5154 as follows: a peristaltic pump was used as opposed to a syringe pump, the reactor size was increased to 25.4 mm O.D. (22.1 mm I.D.) as opposed to 18 mm O.D. (15.6 mm I.D.), fresh catalyst was used in all experiments (i.e. no catalyst were reused) as opposed to equilibrium (i.e. previously-regenerated) catalyst, furnace temperature control was accomplished using one thermocouple as opposed to three, catalyst temperature was monitored using one thermocouple as opposed to three, and a different catalyst bed weight was used as opposed to 4 g. During processing, the feedstock was passed across a 5, 10, or 15 g (0.05, 0.10, or 0.15 m bed height) fixed bed of HZSM-5 maintained at 450, 500, or 550 °C.

FFA feedstocks including PSS and LA were preheated (unstirred) and injected using a peristaltic pump (Cole-Parmer, Model L/S Digital) at 2 mL min^{-1} into a 2.2 cm I.D. tubular reactor and passed across a fixed bed of HZSM-5 catalyst (see Figure 5.3). An inert gas flow (N_2) was maintained at 100 mL min^{-1} for all runs. The reactor was situated in a vertically oriented single-zone Lindberg/Blue M tube furnace where the catalyst zone temperature was held between 450-550 °C. Temperature was controlled using input from a thermocouple located at the center axis of the reactor and longitudinally at the center of the catalyst bed (TC1 in Figure 5.3). This temperature was measured every second with averages logged at 2 min intervals using a Campbell Scientific CR23X datalogger. Additionally, furnace temperature was measured at the outer diameter of the reactor (axially) and at the middle of the furnace (longitudinally) (TC2 in Figure 5.3). We have assumed plug flow reaction conditions, which implies that temperature is isothermal, although the temperature may actually vary somewhat due to heat of reaction.

Catalyst to oil ratio (C/O), defined by ASTM D5154 as the mass of catalyst in the bed divided by the mass of feed fed to the reactor, ranged from 0.11 to 0.34. The weight hourly space velocity (WHSV, units are hr^{-1}), is defined as the oil feed rate (2 mL min^{-1} or ~ 81 g h^{-1} based on measured density) divided by the mass of catalyst (g). Given catalyst weights at 5, 10, and 15 g, the WHSV value were 16.2, 8.1, and 5.4 hr^{-1}, respectively. Catalyst contact time (i.e. time on stream), defined as 3600/(WHSV • C/O), ranged from 1942 to 2000 s (32.4-33.3 min). Carrier gas flow rate was maintained at 50, 100, or 200 mL min^{-1}, which corresponded to superficial gas velocities of 0.372, 0.743, or 1.49 cm s^{-1}, respectively. Based on the catalyst bed height (0.05, 0.1, and 0.15 m) and superficial velocity (0.372, 0.743, or 1.49 cm s^{-1}), the gas phase residence time in the catalytic zone ranged from 3.3 s (at 0.05 m bed height and 0.372 cm s^{-1} velocity) to 40 s (at 0.15 m and 1.49 cm s^{-1}). Control runs were accomplished by passing feedstock across an empty bed at each operating temperature (450, 500, and 550 °C) and carrier gas flow rate (50, 100, and 200 mL min^{-1}) for comparison to catalyzed runs.

Catalyst Preparation

The HZSM-5 catalyst was produced by calcining NH_4-ZSM-5 (Zeolyst International, CBV 5524 G) at 550 ˚C for 4 h in air to produce the hydrogen form, HZSM-5, resulting in stronger acid pore sites.

The pH was measured by mixing catalyst in water at a 50:50 ratio and then measuring the pH of the water using a standard pH probe. As a result of the calcining process, the pH was reduced from 4.98 to 3.06. The NH_4-ZSM-5 catalyst was received from the manufacturer as a fine powder. To minimize the pressure drop across the catalyst bed, the catalyst was granulated by mixing with water, drying, crumbling, and sieving to the desired size, ~ 2-5 mm. The catalyst powder had published values of 425 m^2 g^{-1}, 5 μm, and 50 for surface area, particle size and SiO_2/Al_2O_3 ratio, respectively. In-house measurements of the catalyst surface characteristics were accomplished using a Quantachrome surface area analyzer that indicated a surface area of 345 m^2 g^{-1}, pore radius at 10.81 Å, and pore volume at 0.1851 cm^3 g^{-1} for fresh catalyst after calcination, drying, and granulation .

Yield Determination

Products were collected in a flask (Figure 5.1-#7) in an ice bath (Figure 5.1-#8). Reactor and catalyst were weighed before and after each run to determine the extent of residue formation. Residue was categorized and quantified as coke, char, or tar. Coke was considered the amount of material adhered to the catalyst after washing with acetone. Char was defined as the material that formed in the reactor, but not on the catalyst itself. Finally, tar was considered the acetone-soluble material that was removed from the catalyst by washing. Liquid yield was categorized as either oily or aqueous phase. The percent yield of oily and aqueous phase was determined relative to the total amount of oil introduced to the reactor.

Characterization Methods

Liquid product characterization

The chemical composition of liquid product was determined via GC-MS and selected compounds were quantified via GC-FID. The formation of product compounds, particularly aromatic green gasoline-range hydrocarbons, and the retention times for FFA's were verified and assessed using a Agilent gas chromatograph (model HP-6890) containing an HP-5 MS column, 30 m in length, with a 0.25 mm I.D. and 0.25 μm film thickness in conjunction with a Hewlett-Packard mass spectrometer (model HP-5973) with a mass selective detector. The method used was as follows: inlet temperature of 230 ˚C, detector

temperature at 280 °C (MS interface temperature), a flow of 1 mL min^{-1} He, the oven initially at 40 °C for 2.5 min followed by a ramp at 8 °C min^{-1} to 250 °C (held for 5 min). Masses were scanned from 15-500 mass units. Sample size was 1 μL and was prepared for analysis by diluting to 2.5 % in a 50:50 acetone/methanol mixture.

Chromatograms and spectra were viewed and compounds were identified using Agilent Technologies software (MSD ChemStation D.03.00.611), which uses a probability-based matching (PBM) algorithm to match unknown spectra to those found in a library. The mass spectral library used was the National Institute of Standards and Technology's 1998 version (NIST 98).

BTEX and free fatty acid content was quantified using a GC-FID. Prior to GC quantification, however, the product was esterified to convert the unreacted free fatty acids to fatty acid methyl esters (FAMEs) in order to increase volatility and thereby reduce the temperature required for the GC-FID analysis. In order to generate FAMEs from FFAs in the oils, a method was developed to esterify the oils using a 2% sulfuric acid (Sigma Aldrich, 98%) in methanol solution following . To this solution, oils were added at 1% and heated at 50 °C, while stirring, for 2 h. The reaction was proposed to follow classical Fischer esterification as shown below for oleic acid, e.g.:

$$CH_3(CH_2)_7CH=CH(CH_2)_7COOH + CH_3OH \Leftrightarrow$$

$$CH_3(CH_2)_7CH=CH(CH_2)_7COOCH3 + H_2O \text{ (Eq. 5.80)}$$

The formation of FAMEs was verified, and retention times were determined via GC-MS analysis using the GC described above. Esterified oils were then directly injected into a GC-FID for quantification.

The GC-FID (Hewlett Packard model HP-5890) was equipped with an Agilent HP-5 column (crosslinked 5% PH ME Siloxane, 30 m x 0.25 mm x 0.25 um film thickness). Five-point standard calibration curves for BTEX and FAME compounds were developed using BTEX (containing benzene, toluene, ethylbenzene, and o-, m-, and p-xylene) in methanol (Sigma-Aldrich) and FAME (oleic and linoleic acid methyl esters) standards. For the analysis, the inlet and detector temperatures were maintained at 220 and 230 °C, respectively. The oven temperature was held at 50 °C for 3 min, then

ramped at 10 °C min^{-1} to 300 °C and held for 10 min. The injection volume for calibration standards and samples was 1 μL. GC-FID analysis results were used to determine the concentration of individual BTEX and FAME compounds in the PSS feedstock, the LA model compound, and the liquid products. Yields of individual compounds in the product oils were then determined relative to the amount of feedstock injected to the reactor.

Catalyst characterization

Fresh and used catalyst was characterized using a Quantachrome Instruments (model Autosorb-1) surface area analyzer. Of particular interest were changes in pore radius, pore volume and BET-derived surface area as a function of process parameters including reaction temperature, WHSV, C/O, superficial velocity, and gas phase residence time. It was expected that as a result of processing, surface area and pore volume would decrease as result of coke formation and that average pore radius would increase due to filling of small pores with coke leaving only larger radius pores.

Results and Discussion

Modeling OA conversion

The concentration and conversion of oleic acid within a single catalyst pellet and in a fixed-bed reactor (plug flow reactor, PFR) was modeled as a function of reaction temperature (450, 500, 550 °C), superficial gas velocity (0.372, 0.743, or 1.49 cm s^{-1}), and catalyst bed height (0.05, 0.1, 0.15 m) following the procedure outlined in the Methods and Materials section.

Conversion within a porous catalyst particle

Following theoretical calculations, the concentration of OA within a catalyst pellet relative to the surface concentration (i.e. C_{OA}/C_{OAs}) was determined. In Table 5.1, estimates are provided for the diffusion coefficients used in subsequent calculations as predicted by previously-outlined equations.

Measured and estimated parameters related to the HZSM-5 catalyst used in the calculations are shown in Table 5.2.

Reaction parameters are given in Table 5.3 for reaction temperatures at 450, 500, and 550 °C. The high Thiele modulus indicates that the reaction at these conditions is rate-controlled by diffusion as

opposed to reaction. The very low effectiveness factors indicate that very little of the available surface area is being utilized for the reaction.

Based on the parameters in Tables 5.1, 5.2 and 5.3, C_{OA}/C_{OAs} as function of dimensionless radius (r/R) was determined for each reaction temperature. Figure 5.3 shows these results. It is clear from Fig. 5.3 that OA reacts mostly in the outer region of the catalyst particle. Given a proposed particle radius of 1.75 mm, the outer region where the reaction occurs is in the outer 0.2 mm shell. The reaction occurs on the outer shell as a result of the very high Thiele modulus (3600-23000) and low overall effectiveness factor associated with the reaction at these temperatures. Having a high Thiele modulus indicates that the surface reaction rate (as derived from the non-isothermal DSC experiment) is very high relative to the mass transfer rate. Thus, the mass transfer rate controls the overall rate.

Conversion in a fixed-bed reactor

Reactions were modeled in both reaction rate- and diffusion rate-limited formulations for three reaction temperatures (450, 500, and 550 °C) and three superficial gas velocities.

Reaction rate-limited case

For the reaction rate-limited case, the results are similar to the particle-only case (i.e. most conversion occurs in a very short section at the inlet of the reactor). Figure 5.3 shows the concentration of OA relative to the inlet concentration (C_{OA}/C_{OA0}) and the conversion of OA versus dimensionless reactor length (z/L) at reaction temperatures, 450, 500, and 500 °C.

It is clear that temperature has a major effect on the conversion of OA. However, the reaction still occurs mostly in the first 0.45 cm of the reactor. Again this is due to the high reaction rate relative to the diffusion rate of OA.

Results were similar when flow rate (i.e. superficial velocity) was varied. Figure 5.5 shows the relative concentration and conversion of OA versus dimensionless reactor length for gas flow rates at 50, 100, and 200 mL min^{-1} and a reaction temperature at 500 °C.

Assuming that the reaction was indeed reaction rate limited, the reactor length required for several conversion levels (X=0.5, 0.75, 0.9 and 0.99) was also modeled as function of temperature and

carrier gas flow rate. Results for reactor length versus temperature are shown in Figure 5.6. For X=0.99, the reactor length ranged from 0.08 to 4.5 mm.

Diffusion rate-limited case

For the reaction modeled as a diffusion-limited case, lower conversions were evident versus temperature or superficial velocity since the diffusion rate was much lower than the estimated reaction rate as determined by DSC. Figure 5.7 shows the concentration and conversion of OA relative to the inlet concentration for reaction temperatures at 300-600 °C.

For the diffusion limited case, temperature does not affect conversion greatly. Although temperature strongly affects the reaction rate, here we are assuming that the diffusion rate is the limiting factor. The diffusion rate is less strongly affected by temperature.

However, diffusion is strongly affected by the gas flow rate (i.e. superficial velocity) since the velocity controls the thickness of the stagnant boundary layer about the catalyst particles (i.e. higher velocities shrink the boundary layer and increase the diffusion rate). Figure 5.8 shows the effect of flow rate on the concentration and conversion of OA.

As with the rate-limited case, we also modeled the system in such a way as to determine the reactor length required for various levels of conversion. Figure 5.9 shows the reactor length versus superficial velocity of reactant and carrier gas across the bed. Again, it is clear that the majority of the conversion occurs in the first few millimeters of the catalyst bed.

Results of modeling for both the diffusion and reaction-limited case indicated that the proposed experimental reactor could be improved substantially. Changes including reducing the catalyst amount (length, z), decreasing the concentration, increasing the superficial velocity could make better use of the catalyst (i.e. deeper penetration of OA in the reactor particle and bed). However, conversions modeled were not always well-correlated with results from the experimental work (see following sections).

Experimental OA Conversion

Product yields

The cracking process generated six products including a fuel-like oil, an acetone-soluble tar, reactor char, catalyst coke, an aqueous phase liquid, and non-condensable gases. Figure 5.10 illustrates the effect of catalyst, HZSM-5, on the yield of products and co-products from the catalytic cracking of PSS at 500 °C. Minimal tar was recovered from LA or PSS upgrading. Other pyrolysis temperatures indicated similar trends in terms of product and by-product yield. The addition of catalyst affected PSS and LA similarly, with comparable drops in yield of oily product and an increase in non-condensable gas formation although the quality of the product was greatly improved. The presence of HZSM-5 catalyst significantly increases coke, char, aqueous phase, and gas yield while significantly decreasing oil yield at α=0.05. Additionally, no aqueous phase was formed for samples processed at 500 °C in the absence of catalyst.

Product characterization

Catalytic upgrading using HZSM-5 resulted in conversion of FFAs and the formation of aromatic hydrocarbons indicated by the presence of BTEX. Figures 5.3A and 5.3B portray GC-MS spectra for heat-treated (control samples) and catalytically-cracked LA and PSS, respectively. Figure 5.3A indicates that under catalytic conditions, linoleic acid (peak L in Table 4) completely cracks (>99 % conversion) and is rearranged to form predominantly aromatic hydrocarbons including benzene (peak A), toluene (peak C), ethylbenzene (peak D) and xylene (peak E) collectively known as BTEX. BTEX compounds are commonly-used octane boosters for gasoline. The same is true for PSS (Figure 5.3B); linoleic acid (peak L) completely cracks to form BTEX. This was expected since zeolites such as HZSM-5 are often incorporated with other materials into catalysts used in the petroleum industry for fluid catalytic cracking (FCC) operations to generate aromatics from heavy petroleum feedstocks. The inherent acidity and micropore structure of zeolites promote cracking of long chain hydrocarbons and size-selection end-product molecules, leading to the formation of high octane aromatic products (Blauwhoff et al., 1999).

The presence of BTEX is a strong indication that the cracked free fatty acid product could be used as a green gasoline additive. Some polycyclic aromatic hydrocarbons such as naphthalene (peak G), which are also gasoline components, were identified, although not quantified, in the catalytically-cracked

product both in LA and PSS but with qualitatively higher amounts in PSS, based on peak area. However based on these results, it is evident that very few by-product compounds (i.e. other than BTEX gasoline additives) were generated.

From Figure 5.4A, it appears that BTEX concentration for LA runs peak at 500 °C. Statistically, this is the case for both benzene and for combined BTEX where concentrations are significantly higher than for 450 or 550 °C processing. For toluene, the yield at 500 °C is significantly higher ($p<0.05$) than at 450 °C, but not significantly higher than at 550 °C. The remaining BTEX components show no significant difference in concentration due to process temperature. As seen in Figure 5.4B, yields of benzene and toluene and total BTEX generally increased with increasing pyrolysis temperature for PSS. There was a statistically significant increase in benzene concentration in PSS when process temperature was increased from 450 to 500 °C ($p<0.001$) and from 500 to 550 °C ($p<0.001$), but not from 450 to 500 °C ($p=0.173$). The same was true for both toluene and total BTEX.

For LA, the optimum temperature for BTEX formation appeared to be 500 °C, while for PSS, the optimum in the temperature range of the study was 550 °C. However, since BTEX yields were still increasing at 550 °C, the peak yields may occur at higher temperatures and is currently under investigation. The increase in benzene concentration at the expense of toluene and xylene, as in LA processing (Figure 5.4A) indicates that methylated aromatics, such as xylene, are undergoing further reactions (removal of side chains) due to higher temperature resulting in greater formation the simplest aromatic, benzene. We propose that the increase in benzene formation occurred as a result of catalytic dealkylation of xylene and toluene as described in Weigert and Ragosta (1993) and Al-Khattaf (2006). The reaction is as follows for toluene ($Ph\text{-}CH_3$) dealkylation:

$$Ph\text{-}CH_3 + H_2O \rightarrow PhH + CO + 2H_2 \quad \text{(Eq. 5.81)}$$

Water for the reaction is derived from various cracking reactions. For xylene, the reaction above would occur twice sequentially; once to form toluene from xylene and once to form benzene from toluene. For PSS, if reactor residence times were further increased or reaction temperature was increased, an increase in the yield of benzene relative to other BTEX compounds would likely be evident.

Catalyst Characterization

Fresh, used, and regenerated catalyst was analyzed using a Quantachrome (model Autosorb-1) surface area analyzer. Parameters assessed included pore radius, pore volume, surface area, and relative acid site strength and density (via NH_3 temperature programmed desorption, TPD).

It is clear from Figure 5.10 that catalyst is affected by both treatment and regeneration. Lower flow rates during treatment reduced the NH_3 adsorption capacity (i.e. number of acid pore sites) which indicates greater deactivation of catalyst. The fact that adsorption capacity then increased after the regeneration process (i.e. combustion/removal of coke) indicated that it was, indeed, the coke blocking acidic pores which caused the decrease in acidity. We conclude that the increase in coke was the result of deeper cracking of the OA reactant at higher temperatures and longer residence times. This was supported by the modeling results as in Figure 5.8 for which the fastest reaction rate was seen for the 50 mL min^{-1} flow rate.

Conclusions

The conversion of oleic acid (OA) over HZSM-5 was modeled for multiple temperatures and superficial velocities in both diffusion and reaction rate limited regimes. An experimental study is ongoing to determine the accuracy of the modeling using a fixed bed PFR with catalyst beds at 5, 10, and 15 cm and at gas flow rates of 50, 100, and 200 mL min^{-1}. Results from the modeling activities indicated that for both the diffusion rate- and the reaction rate-limited cases, the reaction occurs in a very short section of the proposed experimental reactor. Experimental results will verify if this is indeed the case. Results from the modeling of OA conversion indicated that the diffusion rate limited the reaction given that fact that the Thiele modulus was very high. Although both the reaction temperature and the superficial velocity affect conversion for both diffusion and reaction rate limited cases, temperature impacted the modeling results more strongly in the reaction rate limited case while superficial velocity more strongly affected the conversions for the diffusion-limited case.

For both cases, it was found that the reactor length required for the various conversion levels (X=0.5, 0.75, 0.9, and 0.99) was very short, much less than the experimental reactor length (L=0.0005,

0.0010, and 0.0015 m). However, initial results from GC-MS analysis of liquid product indicate that complete conversion was not achieved in the *L*=0005 m catalyst bed.

References

Abrams, L., Corbin, D., 1995. Probing Intrazeolite Space. J. Inclusion Phenom. Mol. Recognit. Chem. 21, 1-46.

Adebanjo, A.O., Dalai, A.K., 2005. Production of diesel-like fuel and other value-added chemicals from pyrolysis of animal fat. Energy Fuels 19(4), 1735-1741.

Ali, M., Siddiqui, M., Zaidi, S., 1998. Thermal analysis of crude oils and comparison with SIMDIST and TBP distillation data. Journal of Thermal Analysis and Calorimetry 51, 307-319.

Al-Khattaf, S., 2006. Catalytic transformation of toluene over a high-acidity Y-zeolite based catalyst. Energy Fuels 20, 946-954.

Anjos, J., Gonzalez, W., Lam, Y., Frety, R., 1983. Catalytic decomposition of vegetable oil. Applied Catalysis 5, 299-308.

Ash, M., Wittenberger, K., 2010. Oil Crops Outlook. USDA Report OCS-10j, 18pp.

Benson, T., Hernandez, R., White, M., French, W., Alley, E., Holmes, W., Thompson, B., 2008. Heterogeneous cracking of an unsaturated fatty acid and reaction intermediates on H+ZSM-5 catalyst. Clean 36(8), 652-656.

Blauwhoff, P., Gosselink, J., Kieffer, E., Sie, S., Stork, W., 1999. Zeolites as Catalysts in Industrial Processes, in Weitkamp, J., Puppe, L. (Eds), Catalysis and Zeolites: Fundamentals and Applications. Springer-Verlag, Berlin, pp. 437-538.

Dandik, L, Aksoy, H., Erdem-Senatalar, A., 1998. Catalytic conversion of used oil to hydrocarbon fuels in a fractionating pyrolysis reactor. Energy Fuels 12, 1148-1152.

Doll, K., Sharma, B., Suarez, P., Erhan, S., 2008. Comparing biofuels obtained from pyrolysis, of soybean oil or soapstock, with traditional soybean biodiesel: density, kinematic viscosity, and surface tensions. Energy Fuels 22(3), 2061-2066.

EPA, 2006. 1995-2006 RFG Surveys by Area. U.S. Environmental Protection Agency.

EPA, 2008. Fuel Trends Report: Gasoline 1995-2005. Report number EPA420-R-08-002. U.S. Environmental Protection Agency.

Fogler, H.S., 1986. Elements of Chemical Reaction Engineering. Prentice Hill, Englewood Cliffs, NJ, 769 pp.

Fuller, E., Schettler, P., Gidding, J., 1966. New method for prediction of binary gas phase diffusion coefficients. Ind. Eng. Chem. 58, 18–27.

Haas, M., Michalski, P., Runyon, S., Nunez, A., Scott, K., 2003. Production of FAME from Acid Oil, a By-product of Vegetable Oil Refining. JAOCS 80(1), 97-102.

Haynes, H. W., 1975. The determination of effective diffusivity by gas chromatography. Time domain solutions. Chem. Eng. Sci. 30, 995-961.

Hilten, R., Speir, R., Kastner, J., Das, K.C., 2010. Production of fuel from the catalytic cracking of pyrolyzed poultry DAF skimmings. Journal of Analytical and Applied Pyrolysis 88, 30-38.

Kanellos, M., 2007. "Tyson, ConocoPhillips link up for biodiesel." CNETnews.com.

Kärger, J., Ruthven, D., 1992. Diffusion in Zeolites and Other Microporous Solids. John Wiley & Sons: New York.

Keipert, O., Baerns, M., 1998. Determination of the intracrystalline diffusion coefficients of alkanes in H-ZSM-5 zeolite by a transient technique using the temporal-analysis-of-products (TAP) reactor. Chemical Engineering Science 53(20), 3623-3634.

Li, H., Shen, B., Kabalu, J.C., Nchare, M., 1999. Enhancing the production of biofuels from cottonseed oil by fixed-fluidized bed catalytic cracking. Renewable Energy 34, 1033-1039.

Lima, D., Soares, V., Ribeiro, E., Carvalho, D., Cordoso, E., Rassi, F., Mundim, K., Rubim, J., Suarez, P., 2004. Diesel-like fuel obtained by pyrolysis of vegetable oils. J. Anal. Appl. Pyrolysis 71, 987-996.

Noordhoek, N., van IJzendoorn, L., Anderson, B., de Gauw, F., van Santen, R., de Voigt, M., 1998. Mass transfer of alkanes in zeolite packed-bed reactors studied with positron emission profiling. 2. Modeling. Ind. Eng. Chem. Res 37, 825-833.

Ooi, Y., Zakaria, R., Mohamed, A., Bhatia, S., 2004. Catalytic conversion of palm oil-based fatty acid mixture to liquid fuel. Biomass and Bioenergy 27, 477-484.

Ozawa, T., 1970. Kinetic analysis of derivative curves in thermal analysis. Journal of Thermal Analysis 2, 301–324.

Padmaja, K., Atheya, N., Bhatnagar, A., 2009. Upgrading of Candelilla biocrude to hydrocarbon fuels by fluid catalytic cracking. Biomass and Bioenergy 33, 1664-1669.

Radich, A., 1998. Biodiesel Performance, Costs, and Use. Energy Information Administration.

Ruthven, D., 1984. Principles of Adsorption and Adsorption Processes. Wiley: New York.

Schwan, P., Möller, K., 2001. Analysis of the pulse response in a CSTR for diffusion measurement in bi-porous adsorbent pellets. Chemical Engineering Science 56, 2821-2830.

Tamunaidu, P., Bhatia, S., 2007. Catalytic cracking of palm oil for the production of biofuels: optimization studies. Bioresour. Technol. 98, 3593–3601.

Twaiq, F., Zabidi, N.A.M., Bhatia, S., 1999. Catalytic conversion of palm oil to hydrocarbons: performance of various zeolite catalysts. Ind. Eng. Chem. Res. 38, 3230–3238.

Twaiq, F., Mohamed, A., Bhatia, S., 2003. Liquid hydrocarbon fuels from palm oil by catalytic cracking over aluminosilicate mesoporous catalysts with various Si/Al ratios. Microporous and Mesoporous Materials 64(1-3), 95-107.

Twaiq, F.A.A., Mohamad, A.R., Bhatia, S., 2004. Performance of composite catalysts in palm oil cracking for the production of liquid fuels and chemicals. Fuel Process. Technol. 85(11), 1283–1300.

Weigert, F., Ragosta, J., 1993. Nickel-on-alumina catalyzed polymethylbenzene dealkylation. J. Molec. Catal. 85, 237-251.

Wiggers, V., Meier, H., Wisniewski, A., Barros, A., Maciel, M., 2009. Biofuels from continuous fast pyrolysis of soybean oil: A pilot plant study. Bioresource Technology 100, 6570-6577.

Xu, J., Jiang, J., Sun, Y., Chen, J., 2010. Production of hydrocarbon fuels from pyrolysis using a basic catalyst. Bioresource Technology 101, 9803-9806.

Yean-Sang, O., Bhatia, S., 2007. Aluminum-containing SBA-15 as cracking catalyst for the production of biofuel from waste used palm oil. Micropor. Mesopor. Mater. 102, 310–317.

Figure Captions

Figure 5.1. Fixed-bed reactor model showing modes of transport in bulk phase between macroparticles (A and B), through the stagnant layer on the macroparticle surface (C), through the macroparticle void spaces (D), and within the spherical macroparticle or microparticle (E). Based on Haynes (1975).

Figure 5.2. Thermochemical cracking chemistry the conversion of oleic acid to gasoline components, BTEX, trimethylbenzene, and naphthalene. From Benson et al. 2008.

Figure 5.3. Concentration of OA within a catalyst particle with properties shown in Table 2 as a function of dimensionless radius for three reaction temperatures.

Figure 5.4. Relative concentration of OA reacted over a fixed-bed reactor (L=0.0015 m) of HZSM-5 at a 100 mL min^{-1} gas flow rate for multiple temperatures as a function of dimensionless reactor length.

Figure 5.5. Relative concentration of OA reacted over a fixed bed of HZSM-5 (L=0.0015 m) at 450 °C for three gas flow rates as a function of dimensionless reactor length.

Figure 5.6. Reactor length required for four conversion levels of OA at temperatures between 300 and 600 °C.

Figure 5.7. Relative concentration of OA reacted over a fixed bed of HZSM-5 (L=0.0015 m) at a 100 mL min^{-1} flow rate for three temperatures as a function of reactor length for the diffusion-limited case.

Figure 5.8. Relative concentration of OA reacted over a fixed bed of HZSM-5 (L=0.0015 m) at 500 °C for three gas flow rates as a function of dimensionless reactor length.

Figure 5.9. Reactor length required for multiple conversion levels as a function of superficial velocity for the diffusion-limited case.

Figure 5.10. NH_3 TPD peak areas for untreated catalyst (---), Treated catalyst (solid triangles, diamonds, and squares), and regenerated catalyst (open triangles, diamonds, and squares).

Tables

Table 5.1. Diffusion coefficients for bulk, Knudsen and overall effective diffusion.

Diffusion Type	Abbreviation	D_{OA} (m^2 s^{-1}) at Reaction Temperature (°C)		
		450	500	550
Bulk	$D_{OA\text{-}N2}$	6.61E-05	7.30E-05	8.02E-05
Knudsen	$D_{OA,K}$	1.7E-07	1.7E-07	1.8E-07
Effective	D_{OAe}	4.62E-08	4.77E-08	4.93E-08

Table 5.2. Characterization data for granulated HZSM-5 catalyst.

Parameter	Abbreviation	Value
Particle diameter x 10^3 (m)	d_p	3.50
Particle radius x 10^3 (m)	R	1.75
Pore radius (m x 10^9)	r_c	1.08
Pore volume x 10^3 (m^3 kg^{-1})	V_c	185.1
Internal surface area x 10^5 (m^2 kg^{-1})	S_a	3.45
External surface area (m^2 kg^{-1})	a_c	1.24
Particle porosity	ε_p	0.204
Particle density (kg m^{-3})	ρ_p	1100

Table 5.3. Reaction parameters for HZSM-5 with OA at three reaction temperatures and three flow rates.

Parameter	Value at Reaction Temperature (°C) and Carrier Gas Flow Rate (mL min^{-1})								
	450			500			550		
	50	100	200	50	100	200	50	100	200
U (x 10^2 m s^{-1})	3.71	7.43	14.86	3.71	7.43	14.86	3.71	7.43	14.86
k[a] (x 10^3 s^{-1})	←-------5.15-------→			←-------36.4-------→			←------202.6------→		
ϕ[b] (x 10^{-4})	←-------6.9--------→			←-------17.9-------→			←-------41.6-------→		
η[c] (x 10^3)	←-------4.38-------→			←-------1.68-------→			←-------0.72-------→		
Re[d]	0.09	0.19	0.38	0.08	0.17	0.34	0.08	0.15	0.30
Sh[e]	2.19	2.26	2.37	2.18	2.25	2.35	2.17	2.24	2.34
Sc[f]	←-------1.047------→			←-------1.061------→			←------1.066------→		
k_c[g] (x 10^1 m s^{-1})	8.25	8.55	8.96	9.09	9.39	9.82	9.94	10.26	10.72
δ[h] x 10^3 m)	8.00	7.73	7.37	7.27	7.03	6.72	6.64	6.44	6.16
Ω[i] (x 10^3)	4.58	4.65	4.74	1.06	1.08	1.11	0.25	0.26	0.27

[a] Reaction rate constant.
[b] Thiele modulus.
[c] Effectiveness factor.
[d] Reynold's number.
[e] Sherwood number.
[f] Schmidt number.
[g] Mass transfer coefficient.
[h] Boundary layer thickness.
[i] Overall effectiveness factor.

Figures

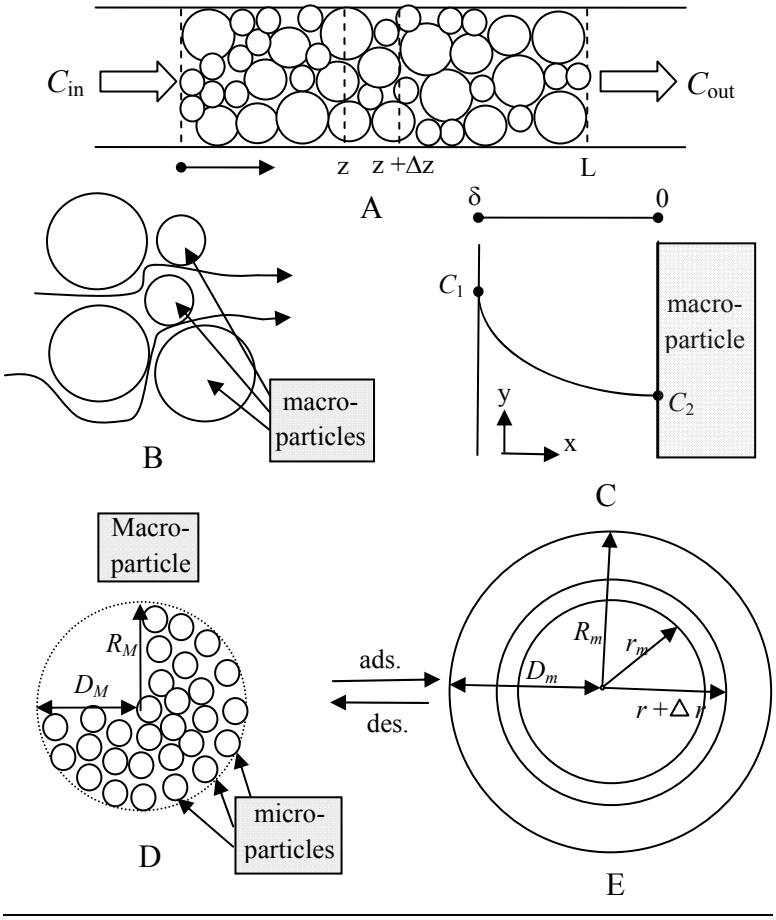

Figure 5.1. Fixed-bed reactor model showing modes of transport in bulk phase between macroparticles (A and B), through the stagnant layer on the macroparticle surface (C), through the macroparticle void spaces (D), and within the spherical macroparticle or microparticle (E). Based on Haynes (1975).

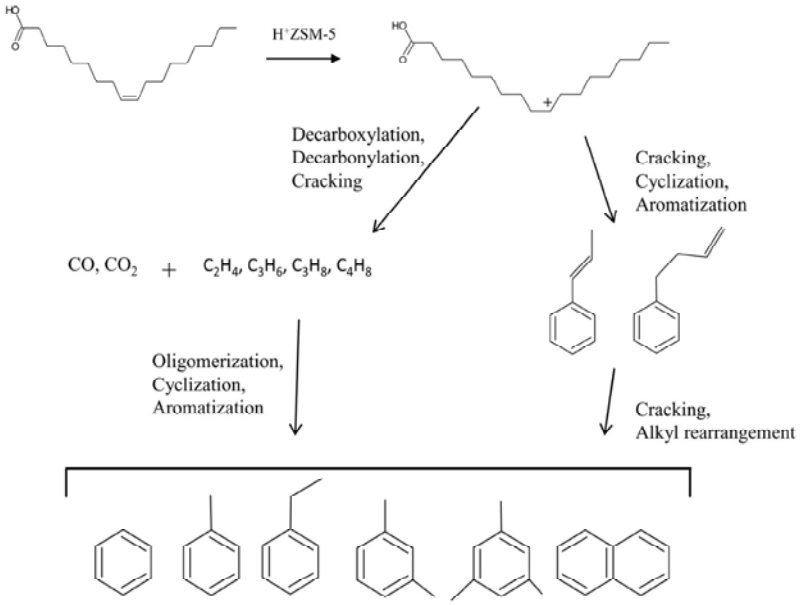

Figure 5.2. Thermochemical cracking chemistry the conversion of oleic acid to gasoline components, BTEX, trimethylbenzene, and naphthalene. From Benson et al. 2008.

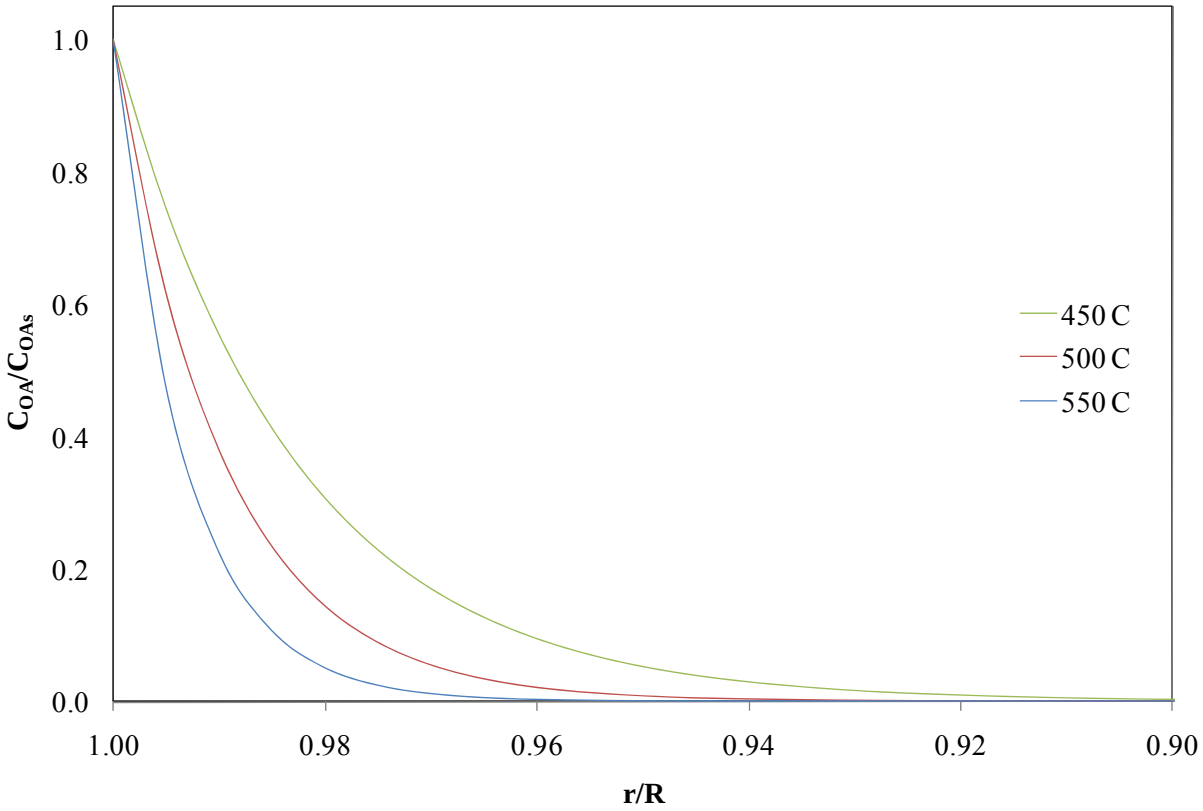

Figure 5.3. Concentration of OA within a catalyst particle with properties shown in Table 5.2 as a function of dimensionless radius for three reaction temperatures.

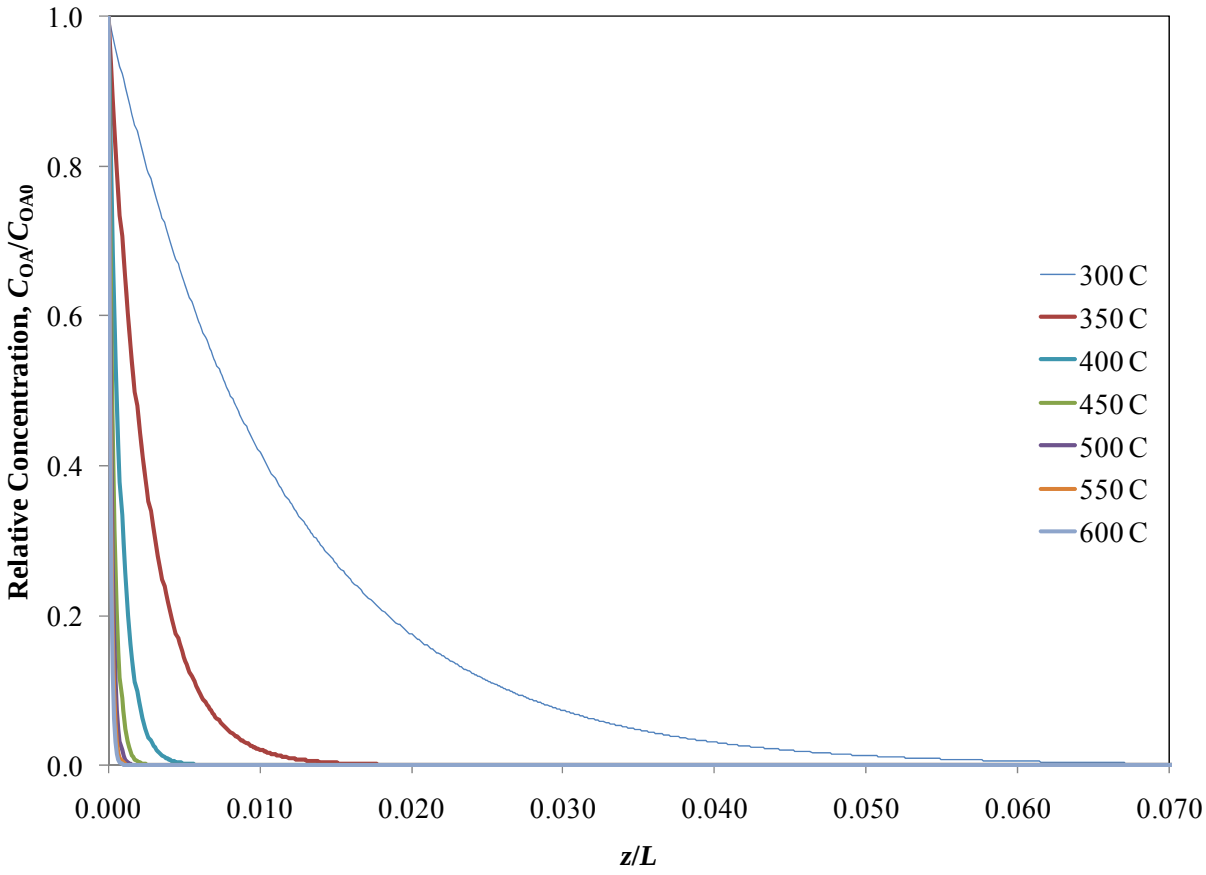

Figure 5.4. Relative concentration of OA reacted over a fixed-bed reactor (L=0.0015 m) of HZSM-5 at a 100 mL min^{-1} gas flow rate for multiple temperatures as a function of dimensionless reactor length.

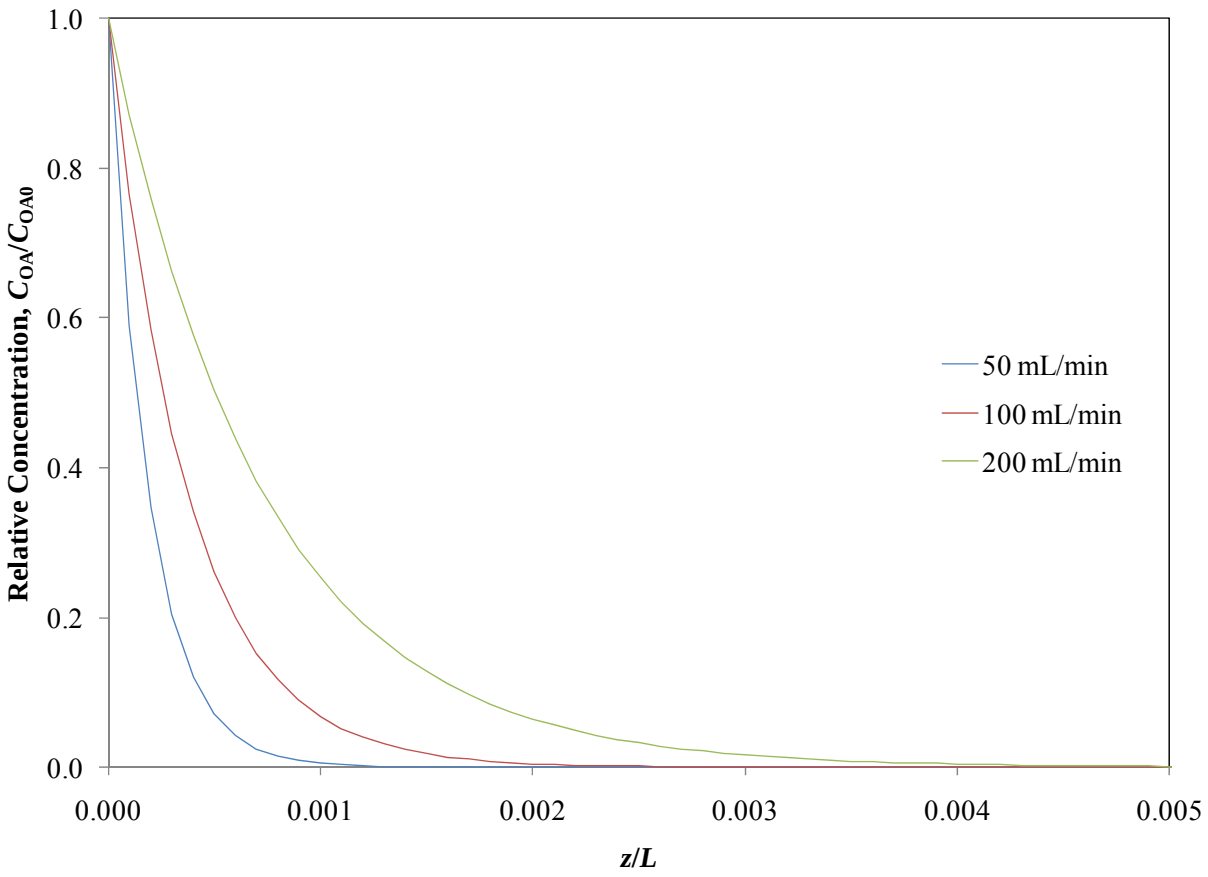

Figure 5.5. Relative concentration of OA reacted over a fixed bed of HZSM-5 (L=0.0015 m) at 450 °C for three gas flow rates as a function of dimensionless reactor length.

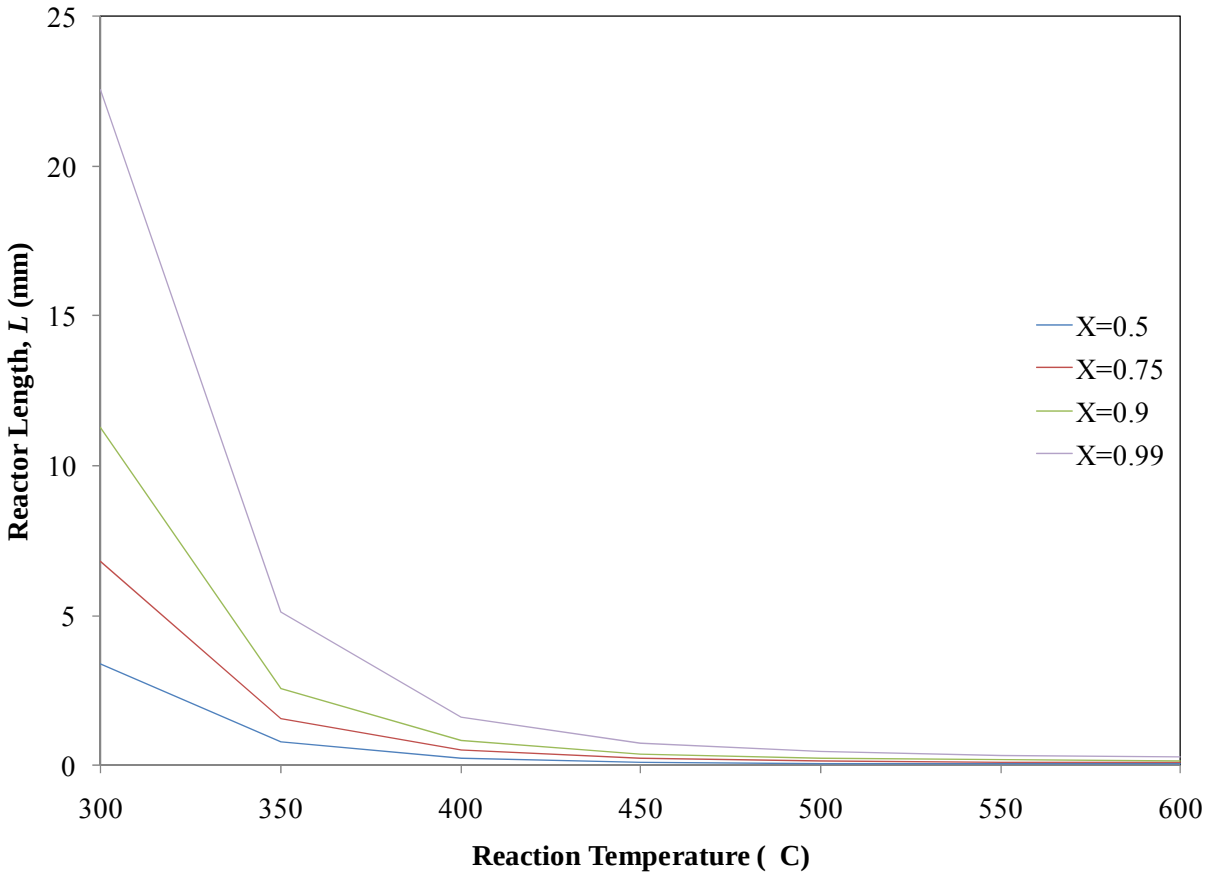

Figure 5.6. Reactor length required for four conversion levels of OA at temperatures between 300 and 600 °C.

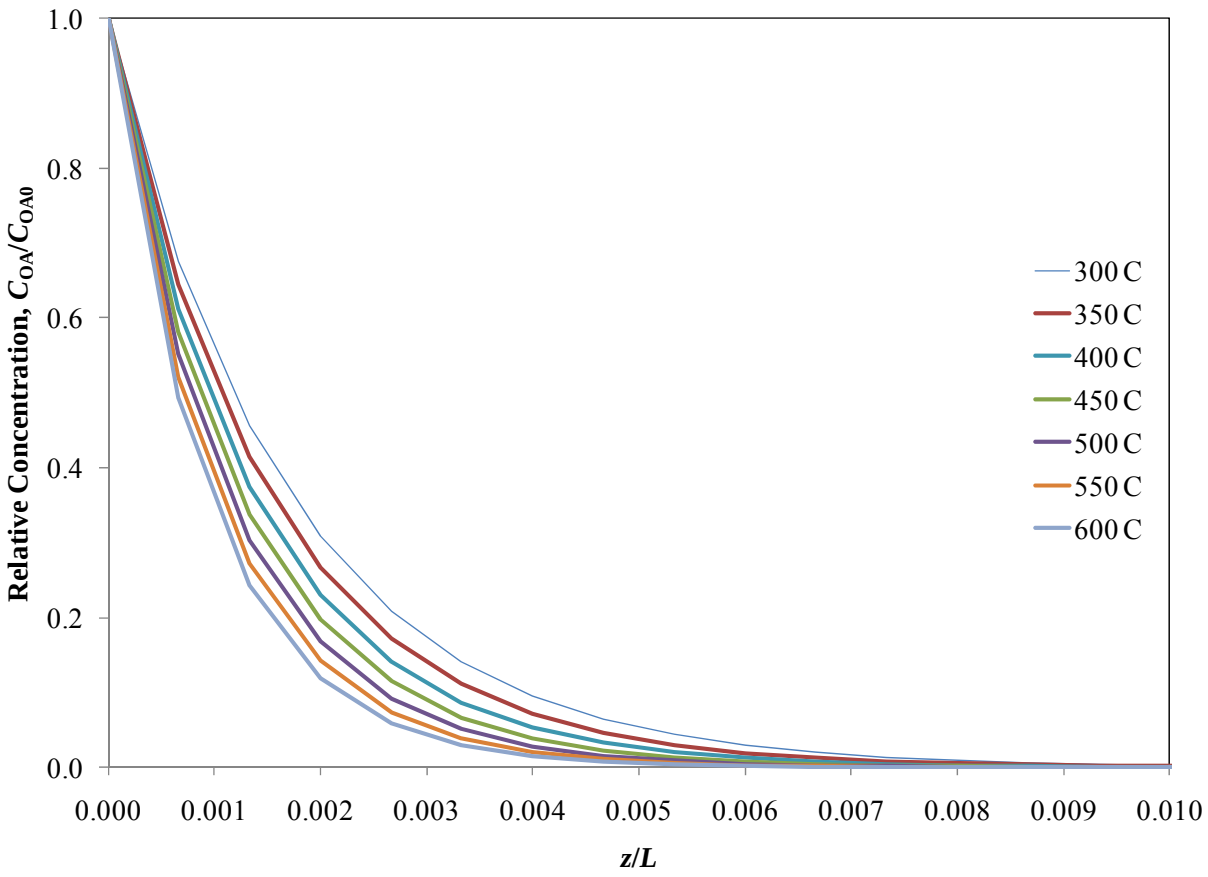

Figure 5.7. Relative concentration of OA reacted over a fixed bed of HZSM-5 (L=0.0015 m) at a 100 mL min^{-1} flow rate for three temperatures as a function of reactor length for the diffusion-limited case.

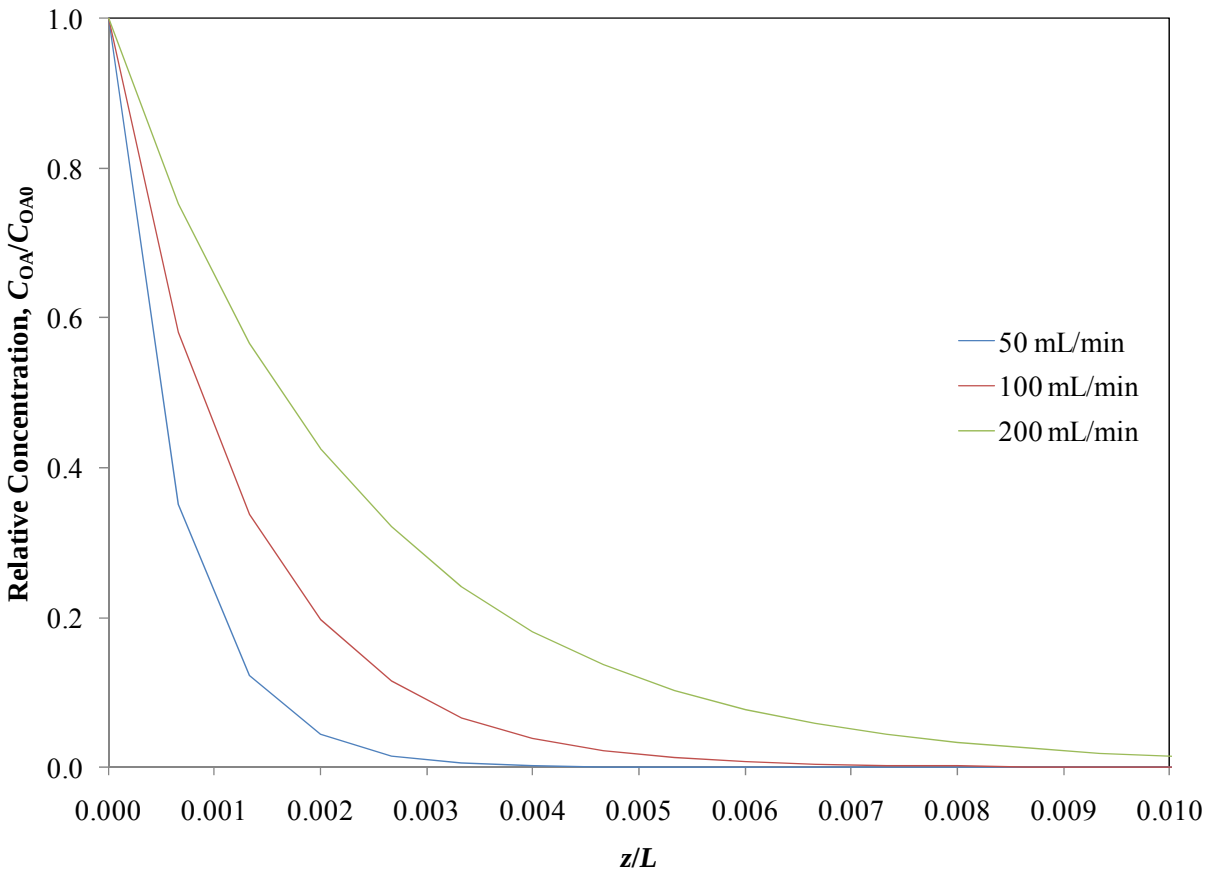

Figure 5.8. Relative concentration of OA reacted over a fixed bed of HZSM-5 (L=0.0015 m) at 500 °C for three gas flow rates as a function of dimensionless reactor length.

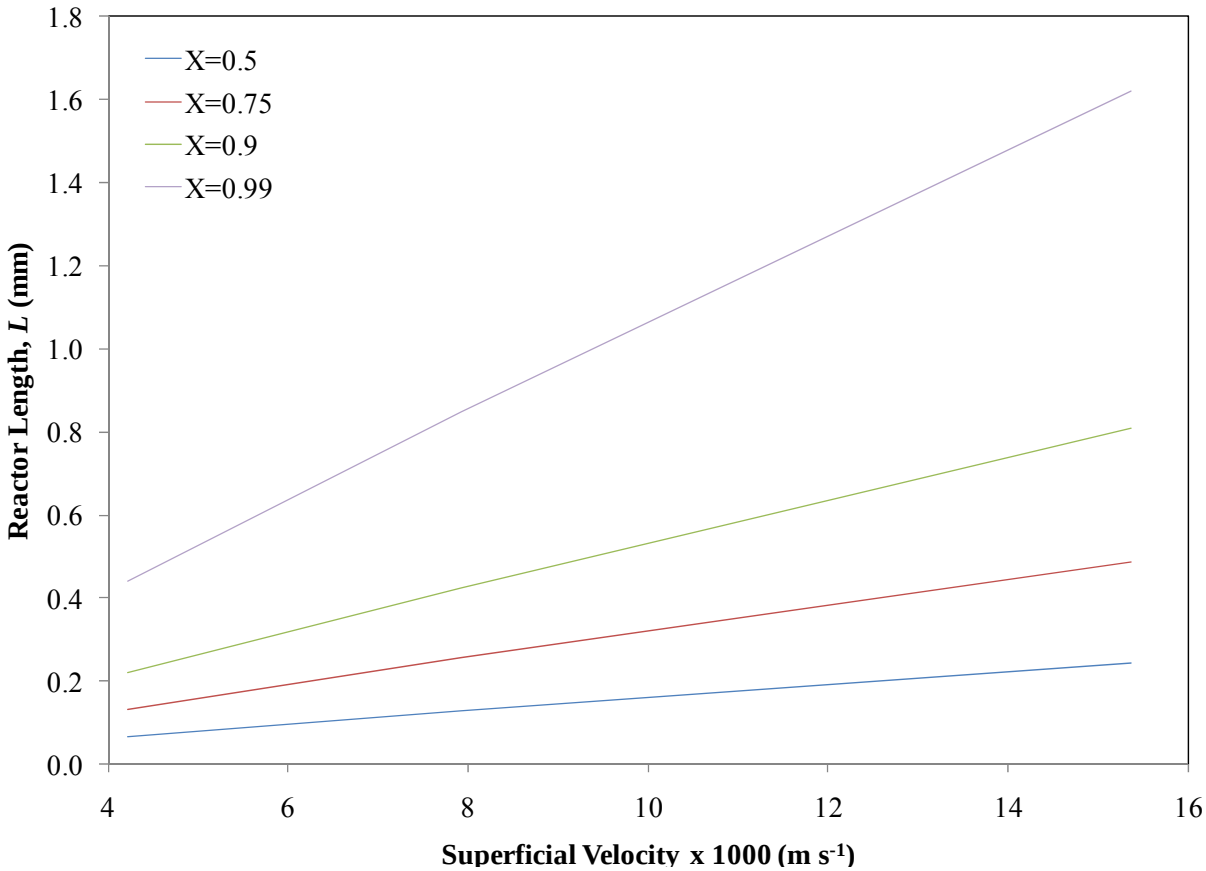

Figure 5.9. Reactor length required for multiple conversion levels as a function of superficial velocity for the diffusion-limited case.

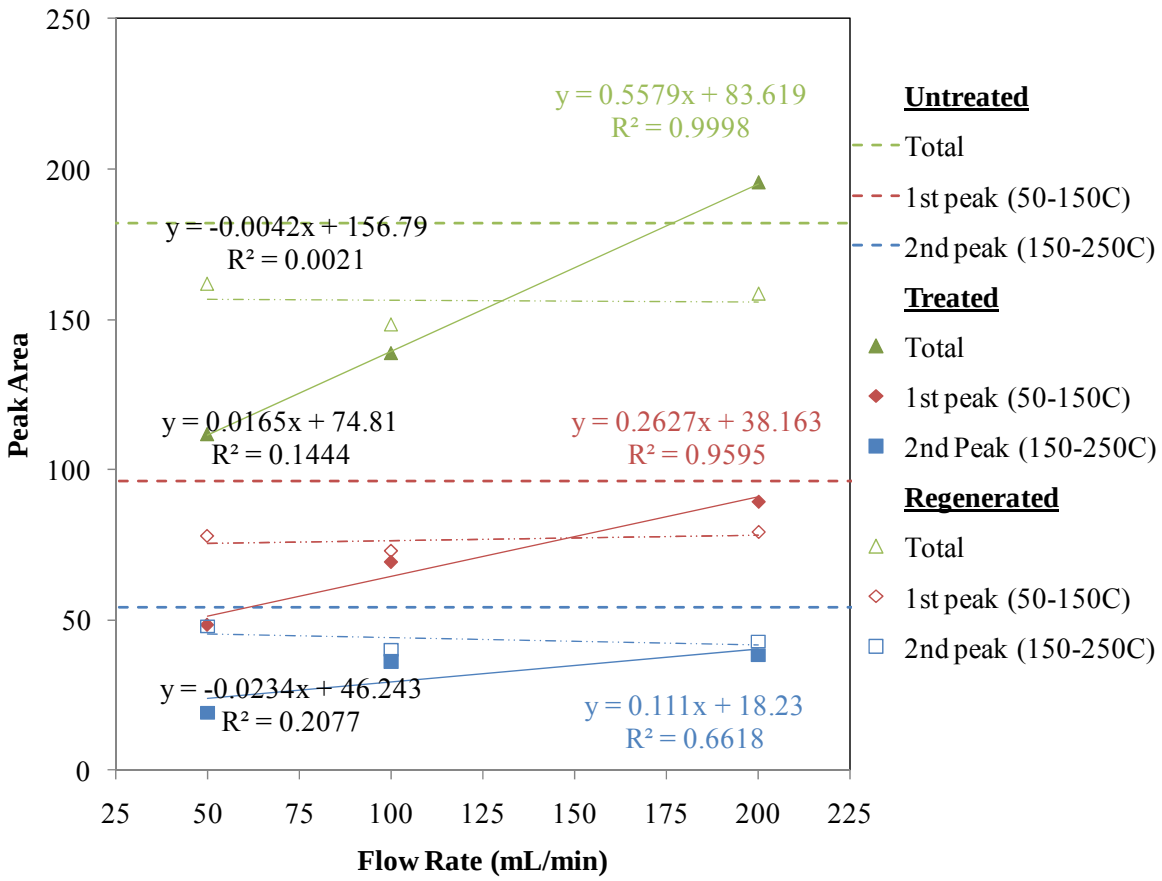

Figure 5.10. NH_3 TPD peak areas for untreated catalyst (---), Treated catalyst (solid triangles, diamonds, and squares), and regenerated catalyst (open triangles, diamonds, and squares).

CHAPTER 6

IN-LINE ESTERIFICATION OF PYROLYSIS VAPOR WITH ETHANOL IMPROVES BIO-OIL QUALITY[5]

[5] Hilten, R., Bibens, B., Kastner, J., Das, K.C. 2010, *Energy and Fuels*, 24: 673-682. Reprinted with permission from the publisher. Copyright 2010 American Chemical Society.

Abstract

A simple reactive condensation technique was developed to decrease the concentration of reactive species in the oily phase of two-phase pyrolysis oil as a means to increase the storage stability, heating value and overall quality of the oil. Bio-oil vapor was esterified from the reaction of in-situ organic acids with ethanol during condensation resulting in the production of water and esters. The research compared the quality of slow pyrolysis-produced bio-oils collected by condensing pyrolysis vapor using atomized ethanol (EtOH) at various weight hourly space velocity (WHSV). The resultant bio-oil exhibited two phases at room temperature, which were separated to obtain an oily and an aqueous phase. WHSV was varied from 8.3 – 33 (kg h^{-1} biomass per kg h^{-1} ethanol), which produced bio-oils with ethanol content ranging from 7.3 – 23.2 wt % of total oil. Increasing EtOH from 0 to 23 % (w/w) decreased water content and viscosity in the oily phase by 16 %and 56 %, respectively, while also increasing pH from 2.48 to 3.05. Results were consistent with the formation of esters. Using quantitative GC-MS analysis, the concentration of a carboxylic acid, acetic acid, and an ester, ethyl acetate, were determined and indicated a maximum 40% (v/v) conversion of acetic acid with 19 % (v/v) being converted to ethyl acetate. Other reactions predicted included acetalizations of formaldehyde and acetaldehyde with ethanol to form diethoxymethane and 1,1-diethoxyethane, respectively.

KEYWORDS: Bio-oil, esterification, reactive condensation, stability, biofuel, pyrolysis

Introduction

Pyrolysis oil, or bio-oil, is a potential source of renewable energy for electricity, heat generation, and as a transportation fuel. However, several obstacles must be overcome before bio-oil can be used reliably as a fuel. One of the main issues is poor storage stability of the oils. During storage, there is potential for bio-oils to undergo changes due to oxidative and thermal degradation. Oxidation can lead to polymerization resulting in viscosity increases. Thermal degradation causes partial decomposition of components and can lead to loss of volatiles. Storage in both oxidative and elevated temperature conditions lead to physical changes (e.g., viscosity increases and heating value decreases) and compositional changes (Boucher et al., 2000; Diebold and Czernik, 1997; Diebold, 2000; Oasmaa et al.,

2003). Most applications for bio-oils require that bio-oils retain favorable initial physical properties during storage, shipment and use (Diebold, 2000). Otherwise, filters, injectors, input lines, etc. may become obstructed. In addition, the high level of reactive species and water content of bio-oil makes it unstable under normal storage conditions, which lead to increased viscosity over time. In addition, high oxygen and water content also lower the heating value of the fuel (Oasmaa et al., 2003).

During aging, bio-oil viscosity and chemical composition change dramatically mainly due to polymerization reactions (Adjaye et al., 1992). A higher degree of polymerization results in an increase in viscosity. Polymerization reactions that lead to viscosity increases are accelerated at higher storage temperatures where it has been shown that viscosity can increase from 0.009 cP day^{-1} when stored at -20 °C to more than 300 cP day^{-1} at 90 ˚C (Adjaye et al., 1992). However, it has been shown that adding solvents after pyrolysis can increase the stability of bio-oil during aging. Diebold and Czernik (1997) showed that additions of solvents could significantly decrease viscosity changes during aging. Solvents used in the study included ethyl acetate, a mixture of methyl isobutyl ketone and methanol, acetone, methanol, a mixture of acetone and methanol, and ethanol. Their findings revealed that 10% (w/w) methanol enhanced bio-oil stability most effectively.

The immediate effects of adding an alcohol are decreased viscosity and increased heating value (Moens et al., 2009; Oasmaa et al., 2004; Stamatov et al., 2006). These improvements to bio-oil make it more favorable for combustion applications such as in furnaces, boilers and gas turbines, or as an alternative to diesel where untreated bio-oils can require major changes to existing systems (Stamatov et al., 2006; Gust et al., 1997). The increase in heating value for bio-oils mixed with ethanol is due to the fact that ethanol has a higher heating value of 27 MJ kg^{-1}, which is higher than that of most bio-oils.

Most studies have directly added alcohols after pyrolysis (Diebold and Czernik, 1997; Moens et al., 2009; Oasmaa et al., 2004) which works well to increase stability and heating value. However, several recent studies (Junming et al., 2008; Lu et al., 2007; Mahfud et al., 2007; Tang et al., 2008; Zhang et al., 2006) showed that using reactive distillation of bio-oil coupled with an alcohol and an acid or base catalyst resulted in bio-oil esterification. Esterifying bio-oil can significantly improve the quality of bio-

oil by lowering water content, viscosity, and the free-acid content. Additional improvements in bio-oil quality include an increase in heating value by as much as 50 % (Junming et al., 2008; Zhang et al., 2006) and an increase in stability due to the removal of acids that catalyze polymerization reactions. Junming et al. (2008) showed that after three months of aging, esterified bio-oil exhibited very little viscosity increase. Ji-lu (2007) introduced well-sprayed ethanol into a bio-oil condenser as a precursor to spraying bio-oil once enough was produced. The intent was to quickly cool vapors to prevent polymerization reactions, though esterification was not observed.

Fischer esterification is proposed to be the reaction pathway in conversion to esters. The esterification reaction follows the equation, $RCOOH + C_nH_{2n+1}OH \leftrightarrow RCOOC_nH_{2n+1} + H_2O$, leading to the formation of water and an ester. The simplest ester that can be produced is methyl formate, $HCOOCH_3$, when methanol (CH_3OH) is used as the alcohol and is reacted with formic acid, HCOOH. Industrially the reaction is always catalyzed by a strong acid. Several studies (Junming et al., 2008; Tang et al., 2008) have used solid acid catalysts to enhance the bio-oil esterification reaction which improved bio-oil quality by increasing HHV and pH and reducing specific gravity, viscosity and water content for esterified bio-oil.

Several studies (Chu et al., 1996; Kirumakki et al., 2006; Koster et al., 2001; Miao and Shanks, 2009) have shown the potential to use heterogeneous catalysts for esterifying model bio-oil compounds such as acetic acid. As an example, Miao and Shanks (2009) esterified acetic acid, a model bio-oil compound, using a mesoporous catalyst. Acetic acid conversion was close to 40 % at a 250 min reaction time at 50 °C using the catalyst. Zhang et al. (2006) esterified acetic acid in a reflux reactor and showed yields ranging from 15 % (no catalyst) to 100 % (solid acid catalyst). Koster et al. (2001) and Chu et al. (1996) performed vapor-phase esterifications of acetic acid with ethanol. Koster et al. (2001) performed gas-phase esterifications over several mesoporous catalysts, and showed moderate ester yields (< 25 %). Equilibrium for the reaction lies far to the right, especially in the vapor phase, for which the thermodynamic equilibrium constant is 367 for the reaction of ethanol and acetic acid to form ethyl acetate (Diebold, 2000).

In the current study, ethanol was atomized into a stream of uncondensed bio-oil vapor in order to rapidly and simultaneously cool, condense, and esterify carboxylic acids in the vapor phase. The intent was to increase the quality of bio-oil by effectively removing the undesired acidic compounds. In addition, it is proposed that adding an alcohol during condensation will better stabilize the bio-oil by quickly quenching bio-oil vapor to prevent secondary reactions and by simple dilution of reactive species before reactions can occur. In addition, we theorized that carboxylic acids, likely acetic acid which occurs in high concentration in bio-oil vapor (Gayubo et al., 2004; Milne et al., 1997) would undergo Fischer esterification upon mixing with ethanol at elevated temperature to produce esters and water. Water formation should be evident in the overall water balance of pyrolysis. Due to the lower polarity of esters compared to carboxylic acids, the solubility of water in the oily phase of the bio-oil will be reduced. Thus, we expect that water produced during esterification will be concentrated in the aqueous phase of the bio-oil thereby reducing the water content of the oily phase. We also propose that acetalization is occurring following the general equation: $RCOH + C_2H_5OH \leftrightarrow RCHC_2H_5O\text{-}C_2H_5O + H_2O$. Additionally, rapid condensation, esterification and acetalization will act to stabilize the bio-oil more effectively than simple condensation thereby increasing thermal and oxidative stability.

Since the reaction equilibrium constant in liquid phase is 4 (Simons, 1983) compared to 367 in vapor phase (Diebold, 2000), we have made the assumption that once bio-oil leaves the heated reaction zone and condenses, esterification essentially ceases. Without a strong acid catalyst, Moens et al. (2009) showed very little reduction in acid number and carbonyl content for bio-oil/methanol mixtures even under heating and proposed that high water content prevents the esterification reaction from going to completion. Though esterification reactions have been proposed to proceed at room temperature without a catalyst (Diebold and Czernik, 1997), no quantification has been attempted. The eventual goal is to power a diesel engine with bio-oil that has been upgraded via esterification alone or in combination with other upgrading techniques to improve quality.

Materials and Methods

Feedstock

The biomass feedstock used for all experiments was pine wood in the form of pellets supplied by the Southern Shaving Co. located in Cherryville, North Carolina. Pine pellets were subjected to pyrolysis "as received" with no pre-processing such as drying or grinding.

Bio-oil Production

Figure 6.1 shows the schematic of the transported-bed pyrolysis reactor used in the study. The reactor consisted of a 100 mm diameter stainless steel tube containing an auger driven by a ¼ hp electric motor. The auger continuously transported biomass feedstock through the reactor, which was externally-heated using a tube furnace (Lindberg/Blue M, model HTF55322A) The auger speed was maintained at 1.5 rpm which translated to a solid retention time of 8.3 min in the auger (residence time in the heated zone: 5.9 min).

Biomass feed was supplied to the reactor by a vibratory feeder (Eriez, model H036C). For pyrolysis experiments, the biomass feed rate was held constant to ensure consistent pyrolysis conditions. Pyrolysis vapors leaving the reactor were directed through a reactive condensation unit where ethanol was injected and then through a series of five ice-bath traps to condense any remaining bio-oil. In order to prevent high-boiling vapor (tar) from clogging the pyrolysis reactor and reactive condensation unit, the pyrolysis reactor's exhaust line was heated to maintain vapor temperature above 450 °C. Slow pyrolysis conditions were assumed based on the two phase-nature of the bio-oil end-product and the yield of char and gases. Non-condensable gases were removed from the system via a vacuum pump attached to the last ice-bath trap in the series and vented to atmosphere. Solids were collected in a stainless steel char collector at the outlet of the reactor where the material was cooled at room temperature under in an inert environment. An inert atmosphere was maintained in the reactor and char collector by supplying nitrogen to various inlets in the system. The nitrogen flow rate was 3.6 L min^{-1} distributed as follows: 2 L min^{-1} into the main reactor, 0.5 L min^{-1} into the hopper, 1 L min^{-1} into the char container, and 0.1 L min^{-1} into

the reactive condensing unit. Thermocouples were installed at various locations to monitor temperatures (see Figure 6.1).

Reactive Condensing System

Figure 6.1 also shows placement of the reactor (component 9) used in the experiments to condense and esterify acidic components in the pyrolysis vapor using ethanol. The reactive condensation unit consisted of a 102 mm I.D. stainless steel tube with a reaction zone length, L=457 mm, meaning the reaction zone volume was 3.8 L. In the reactor, vapors were contacted with atomized 100 % (200 proof) ethanol (C_2H_5OH, abbr. EtOH, supplied by Thermo Fisher Scientific) that was supplied using a peristaltic pump (Cole-Parmer L/S, model 7524-10) and input to the reactor by a small-bore (0.015 mm diameter) cone-spray atomizer nozzle. In order to achieve adequate atomization of EtOH at low flow rates (1.5 – 2.0 mL min^{-1}), 0.1 L min^{-1} pressurized N_2 at 377 kPa (40 psig) was mixed with the EtOH prior to entering the atomizer nozzle. Temperature was measured at the inlet of the reactive condensing unit and at two points along the condenser's length. Heavier liquids condensed in a drip trap directly beneath the reactor. At a carrier gas flow rate of 3.6 L min^{-1}, the effective reactor volume (3.8 L) translated to a vapor residence time of 63.3 s in the reaction zone before entering the drip trap. Un-condensed vapor and non-condensable gases were routed through a series of five ice-bath traps that collected the remaining condensable vapor. Non-condensable gases exited to the atmosphere.

Product Yield

The quantity of biomass in the vibratory feeder hopper was weighed before and after each pyrolysis run to determine the total amount supplied to the reactor. Biomass feed rate was assumed to be steady throughout each run. Solid material, namely char, was collected and weighed as was condensed liquid in the drip and ice-bath traps to determine product yield. A simple mass balance was used to calculate the quantity of non-condensable gases.

For the experimental runs, the biomass feed rate was kept constant to ensure equivalent characteristics for the vapor feed entering the reactive condensing unit, while the EtOH atomization rate was varied from 0 to 6 mL min^{-1}. These runs produced samples with a WHSV from 8.3 – 33 (7.3 - 23.2

% EtOH, w/w). Total yield of bio-oil was determined by weighing the whole product then subtracting the weight of EtOH added during the run. After total yield was determined, oily phase material from the drip and ice-bath traps was separated from aqueous phase by decanting, combined, quantified, and stored in a 4 °C refrigerator until characterized. Only oil phase material was evaluated for improvement in fuel quality. In all, five samples were generated during five one-hour pyrolysis runs. From the five samples, no less than three subsamples were taken for each characterization technique described below.

Characterization Methods

The pelletized pine feedstock used to generate bio-oil was extensively characterized prior to pyrolysis. Moisture, volatiles and ash content in the biomass and char was determined by ASTM D5142, "Standard Test Methods for Proximate Analysis of the Analysis Sample of Coal and Coke by Instrumental Procedures," using a proximate analyzer (LECO Model TGA701). Ultimate analysis (elemental C, H, N, S, and O (by difference) in % (w/w)) was performed in an ultimate analyzer (LECO, model CHNS-932) following ASTM D3176, "Standard Practice for Ultimate Analysis of Coal and Coke." Table 6.1 shows the characterization of the pine pellet biomass (PP BM) and pine pellet char (PP CH) produced during continuous pyrolysis at 500 ˚C.

Bio-oils produced by the five pyrolysis runs underwent several analyses in addition to those performed on the biomass and char. Ultimate analysis was performed using a modified version of method ASTM D5291, "Standard Test Methods for Instrumental Determination of Carbon, Hydrogen, and Nitrogen in Petroleum Products and Lubricants." In addition, water content in the oils was determined by Karl Fischer titration using a Mettler-Toledo titrator (Model DL31), following ASTM E203, "Standard Test Method for Water Using Volumetric Karl Fischer Titration." Higher heating value (HHV, in MJ kg^{-1}) was assessed using an isoperibol bomb calorimeter (Parr, model 1351) following ASTM D240, "Standard Test Method for Heat of Combustion of Liquid Hydrocarbon Fuels by Bomb Calorimeter." Dynamic viscosity, η (in cP), was measured at 40 and 60 ˚C using a dynamic viscometer (Brookfield, model DV-I+ with UL/YZ spindle adapter) at three shear rates using a modified version of ASTM D2983, "Standard Test Method for Low-Temperature Viscosity of Lubricants Measured by Brookfield

Viscometer." Kinematic viscosity, υ ($mm^2\ s^{-1}$), was determined by dividing η by density, ρ ($g\ mL^{-1}$), which was estimated using 2 mL Gay-Lussac pycnometers. The pH of the oil was measured directly using a Mettler-Toledo pH meter and probe.

We utilized a differential scanning calorimeter (DSC, Mettler-Toledo, model DSC823e) following ASTM E2009, "Standard Test Method for Oxidation Onset Temperature of Hydrocarbons by Differential Scanning Calorimetry," to determine bio-oil stability. The oxidation onset temperature (OOT) was determined by heating a sample under an oxygen environment from 25 – 350 °C during which time, the onset of oxidation was evidenced by a large exothermic peak. The extrapolated point formed by tangent lines extending from the baseline and from slope to the peak of oxidation was considered the OOT and higher OOTs indicate greater thermal stability. The DSC was also used to approximate the cold flow properties of the bio-oils; oils were cooled to -65 °C and then heated to 125 °C, above the melting point. Melting is indicated by an endothermic peak, and the extrapolated point where the endothermic melting peak ends is considered the cloud point. During cooling, this would be the point where crystals begin to form causing clouding. Lower cloud points indicate better cold flow properties.

The formation of esters was verified and quantified using a Hewlett-Packard (Model HP-6890) gas chromatograph containing an HP-5 MS column, 30 m in length, with a 0.25 mm I.D. and 0.25 μm film thickness in conjunction with a Hewlett-Packard mass spectrometer (Model HP-5973) with a mass selective detector. The method used was as follows: inlet temperature of 230 ˚C, detector temperature at 280 °C (MS interface temperature), a flow of 1 mL min^{-1} He, the oven initially at 40 °C for 2.5 min followed by a ramp at 8 °C min^{-1} to 250 °C (held for 5 min). Masses were scanned from 15-500 mass units. Sample size was 1 μL and was prepared for analysis by diluting to 2.5 % with acetone. An internal standard, heptane, was added to each sample-acetone mixture at 0.0625 % (v/v). Two model compounds in the bio-oil, acetic acid (AcOH, for acetyl hydroxide) and ethyl acetate (EA) were selected to represent an acid and an ester for quantification. Peak height ratios were calculated for AcOH and EA with the internal standard, heptane. It was assumed that some esters and acids were present in the aqueous phase.

No attempts were made to quantify acids and esters in the aqueous phase material. The intent of the work was to improve only the oily phase relative to non-esterified bio-oil.

Chromatograms and spectra were viewed and compounds were identified using Agilent Technologies software (MSD ChemStation D.03.00.611) which uses a probability-based matching (PBM) algorithm to match unknown spectra to those found in a library. The mass spectral library used was the National Institute of Standards and Technology's 1998 version (NIST 98). The quality of a match determined by ChemStation is defined as the probability that the unknown is correctly identified as the reference. The quality can be between 1 and 100 with values above 90 considered very good matches.

A quantification method was developed by producing a five-point standard curve using standard solutions containing mixtures of AcOH, EA, and heptane in acetone. The standard curve yielded a least-squares best-fit line showing the concentration of AcOH and EA versus peak height ratio with heptane. This correlation was then used to predict the concentration of each of the two compounds in the bio-oil samples based on the peak height ratio with heptane calculated for the bio-oils.

Results and Discussion

Bio-oil condensing system

The condensing system effectively lowered bio-oil vapor temperature such that a liquid formed in the collector below the condenser (drip trap) prior to the ice bath traps. Figure 6.2 shows the temperature profile obtained during the run producing a bio-oil condensed with 7.4 % EtOH (w/w). The start and end times for EtOH atomization during the pyrolysis run shown in Figure 6.2 were 60 and 150 minutes, respectively. The reaction zone is the region between thermocouples T6 and T7 in Figure 6.1, and we assume the reaction temperature to be approximately the average temperature as measured by the two thermocouples. Despite linearity, the relationship between upper condenser zone temperature and EtOH atomization rate (kg h^{-1}) was not statistically significant at $\alpha = 0.9$. The relationship between lower condenser zone temperature (˚C) and EtOH atomization rate was statistically significant at $\alpha = 0.95$. These are useful observations, since condensation temperature can be controlled by EtOH and biomass

feed rate to selectively condense various bio-oil components. For example, if it is desired to prevent water from condensing in the drip trap, spray volume can be adjusted such that the condenser temperature is higher than the condensing temperature of water.

Yield of Pyrolysis Products

Table 6.2 lists the yield of bio-oil components in % of original biomass (w/w) and % of total bio-oil (w/w) at each WHSV. The yield of un-condensed gas is calculated by difference such that the mass balance inevitably adds to 100 %. From Figure 6.3, it is evident that with increasing WHSV, total oily phase yield (% of biomass, w/w) decreases while aqueous phase increases. Although it appears that with increasing WHSV the oily phase increased and the aqueous phase decreased, neither relationship was significant at $\alpha = 0.95$. However, the apparent increase in aqueous phase with concurrent decrease in water content in the oily phase relative to non-esterified bio-oil (see next section) supports the hypothesis that esterification occurred.

Pyrolysis runs with the lowest WHSV (8.3 or 26.2 % EtOH (w/w)) produced a two-phase oil in the drip trap, although oily phase material condensed in the ice bath traps, as well. The aqueous phase yield in the drip trap indicated that the temperature in the reactive condensation unit was below the boiling point of some of the aqueous phase components. If desired, the temperature in the reactive condensing unit could be controlled using only EtOH in order to condense desired products in the drip trap.

Product Characterization

Table 6.3 shows characterization data for the bio-oil for each of the five pyrolysis experiments including a control run where no EtOH was added. Analysis results for untreated EtOH are also shown. Results from Table 6.3 indicate that the oily phase water content generally decreases with higher EtOH atomization rate, although the relationship is not statistically significant. In addition, as evidenced by the ultimate analysis of the oils, elemental oxygen content seemed to increase with increasing EtOH. A reduction in elemental oxygen would be consistent with formation of esters assuming that no ethanol remained unreacted in the product. If carboxylic acids react with EtOH to form esters as hypothesized,

the oxygen content should decrease. Theoretically, in the reaction of one mole of AcOH at 53.3 % oxygen (w/w), with one mole of EtOH at 34.8 % oxygen (w/w), one mole of ethyl acetate (EA) is formed with an oxygen content of 36.4 % (w/w), which is lower than that of AcOH. Some of the oxygen from AcOH is concentrated in the reaction by-product, water, and should partition in the aqueous phase of the condensed product and thus increase the aqueous phase yield, as seen in Figure 6.3 with decreasing WHSV. Since oxygen concentration does not decrease with increasing EtOH, it is likely that some ethanol remains unreacted in the bio-oil or that other reactions such as acetalizations could potentially generate higher oxygen content products.

Results indicated that as the EtOH % (w/w) was increased the water content in the oily phase decreased. Table 6.3 provides water content for oil collected and combined from both drip and ice bath traps. Here too, the water content decreased with increasing ethanol, although the relationship was not significant. The results are consistent with the formation of a more non-polar bio-oil and esters. With greater ethanol volume sprayed, a greater concentration of esters in the bio-oil is expected. Since esters are less polar than the organic acids from which they are formed, water solubility in the resultant bio-oil would be expected to decline. Decreased water solubility in the bio-oil should decrease the water content in the oily phase and increase the water content in the aqueous phase.

Although lower biomass feed to ethanol spray ratios (i.e., WHSV) lowered the water content at an undetermined threshold WHSV (denoted as the single-phase threshold) between 3.8 and 8.2, the bio-oil produced existed as a single phase with high water content. This was observed during a previous experiment in which two single-phase bio-oils were generated with WHSV at 1.5 and 4.8 (57 and 28 wt % EtOH) with water content at 11.5 and 26.2 wt %, respectively. More study is needed to accurately determine the single-phase threshold. For the oily phase samples of this study, the water content was reduced by as much as 16 %. Previous studies including Junming et al. (2008) and Zhang et al. (2006) witnessed greater reductions, although their starting material, fast pyrolysis oil, has a water content at 33 % compared to 10 % for our control bio-oil. Nonetheless, there was no great improvement in water content achieved through reactive condensation.

Table 6.3 also shows high heating value (HHV in MJ kg^{-1}) for the bio-oils generated. HHV in the bio-oil increases with increasing EtOH feed rate. The sample produced at WHSV 8.3 (23.2 wt % EtOH) showed similar HHV to EtOH. Since esters, particularly ethyl acetate (HHV = 25 MJ kg^{-1}), are formed in relatively high concentrations (1.89 to 3.42 μL mL^{-1}), it is expected that the increase in heating value is partially due to their presence. Additionally with decreasing water content, HHV should increase. For bio-oil collected from all traps, HHV ranged from 24.5 to 27.6 MJ kg^{-1} indicating little change in HHV due to esterification. Other studies (Zhang et al., 2006) have shown HHV increases as large as 52 % (from 16 to 24 MJ kg^{-1}) when using fast pyrolysis oil as the esterification reactant. Since our starting material, slow pyrolysis bio-oil, already had a relatively high HHV at 27 MJ kg^{-1} compared to fast pyrolysis oils (16 MJ kg^{-1}) and esters (~ 25 MJ kg^{-1}), an increase due to esterification was not clearly evident.

Another indication of the esterification reaction is the increase in pH with increasing EtOH % as shown in Figure 6.4. As acids such as acetic acid are consumed in the reaction with EtOH resulting in ester production, the overall acidity of the bio-oil is reduced. The relationship between pH and EtOH % is significant at $\alpha = 0.95$. Decreasing the acidity of bio-oil is a major goal for current research as a means to improve the fuel properties.

Another goal of bio-oil research involves lowering viscosity bio-oil such that it is similar to values specified for No. 2 diesel fuel (1.9-4.1 $mm^2\ s^{-1}$) by ASTM D975, "Standard Specification for Diesel Fuel Oils." Kinematic viscosity, υ, of the bio-oils is shown in Table 6.3. It can be seen that viscosity decreased substantially as more EtOH was added to the reactor relative to the whole oil. This is clearly evident in Figure 6.5 showing a non-linear decrease in viscosity at 40 and 60 °C as a function of EtOH concentration. An interesting phenomenon to note is that although water content in the oily phase is lower at lower WHSV, which generally results in higher viscosity, we have shown the opposite to be true of the esterified oils. Using fast pyrolysis bio-oil as the reactant, Zhang et al. (2006) saw a decrease in viscosity from 49 to 4.9 $mm^2\ s^{-1}$ when measured at 20 °C after the bio-oil was esterified with ethanol. Our reductions were similar using slow pyrolysis bio-oil as the reactant with a reduction from 300 to as

low as 37 mm^2 s^{-1} when measured at 40 °C. Moens et al. (2009) performed acid-catalyzed bio-oil esterifications while removing water by azeotropic distillation. Although they saw significant decreases in acidity (as measured by total acid number), the resulting oil was a semi-solid tar with poor flow characteristics.

Table 6.4 shows OOT (oxidation onset temperature) and cloud point (both in °C) for the reactively-condensed bio-oils. The trend for oxidation onset temperature is unclear. We expected that OOT would increase with increasing EtOH indicating an increase in stability. Other indices of stability may show improvement, but were not evaluated here. More study is needed to determine if esterification increases bio-oil stability. One measure of stability is the resistance to polymerization as evidenced by a viscosity increase. Junming et al. (2008) showed that after three months of aging, esterified bio-oil exhibited very little viscosity increase. Despite the lack of evidence for an increase in stability in the current study, cold flow properties were improved as evidenced by the linear decrease in cloud point as WHSV decreases (EtOH increases). A linear regression best-fit line showed an R^2=0.79 and a p-value<0.05. Thus, the relationship between cloud point and EtOH content is significant at $\alpha = 0.95$.

Improvements in fuel properties for esterified bio-oil as indicated by water content, HHV, pH, viscosity, and CP measurements show that progress has been made towards producing a fuel with properties more closely related to diesel fuel than un-esterified bio-oil. With additional study, we will show whether esterified bio-oil can be used in diesel engines alone and in blends with diesel and biodiesel.

Figure 6.6 shows the chromatogram for one of the calibration samples in which the EA, AcOH, and heptane peaks are clearly evident at retention times of 1.99, 2.05, and 2.8 min, respectively. For five calibration standards, peak height ratios for AcOH and EtOH with heptane were determined and used to calculate concentration in experimental samples. Although ethanol likely reacts with other carboxylic acids in the bio-oil (e.g., formic, propionic, butyric acid), with aldehydes (e.g., acetaldehyde, formaldehyde, propionaldehyde, furfural) and with ketones (e.g., acetone, propanone, butanone), forming multiple products, only the effects of EtOH addition on the yield of ethyl acetate are quantified here.

Figure 6.7 shows the chromatograms for the control sample and for the 23.2 % EtOH sample from retention times at 2 to 34 min. It is clear that two chromatograms are substantially similar but several key differences are clear. For one, a large peak at 9.7 min in the 23.2 % sample identified as 2,5-diethoxy-tetrahydrofuran (quality: 91) does not appear in the control. This compound was likely formed as product of several reactions stemming from the interaction between EtOH and furfural, an aldehyde. Furfural is visible at 5.6 min (quality > 90) in both spectra but with lower abundance in the esterified bio-oil indicating that the concentration of furfural has been reduced. Though not quantified, acetals, products of the reaction between ethanol and aldehydes, were identified in the chromatograms. Two acetalization products were identified by the ChemStation software; in Figure 6.8, diethoxymethane (2.58 min) and in Figure 6.9, 1,1-diethoxyethane (3.34 min) were identified in the spectrum of the 23.2 % EtOH sample but not in the 0 % EtOH sample. Diethoxymethane and 1,1-diethoxyethane are likely the products of EtOH with formaldehyde and acetaldehyde, respectively. However, ChemStation was not able to identify either formaldehyde or acetaldehyde in the bio-oil samples. This may be a limitation of the GC column used. An additional esterification reaction, that of propionic acid with ethanol, is indicated by the presence of propionic acid in the 0 % EtOH sample but not in the 23.2 % sample for which ethyl propionate, an ester, is evident.

Figure 6.10 shows example chromatograms for each of the EtOH concentrations. It is clear that AA (peak B) decreases with EtOH concentration increases producing a concurrent increase in EA abundance (peak A). Peak C, 1-hydroxy-2-propanone appears to decrease relative to the internal standard indicating a reduction in concentration. Also seen in Figure 6.10, the small peak (F) indicating the concentration of ethyl propionate increases with increasing EtOH concentration.

The yield results from the calibrated GC-MS method are shown in Figures 6.11 and 6.12. Fractional conversion of acetic acid in % (v/v) shown in Figure 6.11 is calculated as the change in concentration (in mmol mL^{-1}) divided by the concentration of acetic acid (mmol mL^{-1}) in the control sample for which no ethanol was added during condensation. Both reaction temperature and EtOH concentration relative to the whole oil significantly affect (at $\alpha = 0.95$) the conversion of acetic acid.

With better control of reaction zone temperature to achieve higher temperatures, it is expected that fractional conversion of acetic acid could be increased.

Figure 6.12 shows the fractional yield (%, v/v) of ethyl acetate assuming that the expected yield is equivalent to the fractional conversion of acetic acid. The concentration of EtOH is a significant predictor of EA fractional conversion at $\alpha = 0.9$ while reaction temperature is not. It is assumed that losses of ethyl acetate during storage and transfer of bio-oil due to high volatility of ethyl acetate account for some of the variability in fractional conversion. This is likely true of other esters, as well. However, the highest yield of EA was at 23.2 % EtOH and was 19 % which compares well with other studies. For example, Koster et al. (2001) observed EA yields that were at most 25 % when using a catalyst and long reaction times (> 250 min). Our method was successfully generated esters without a catalyst at reaction times of approximately 60 s.

It is clear from Figures 6.11 and 6.12 that the esterification reaction is a function of temperature and reactant concentration, since the conversion of acetic acid increased with reaction temperature (Fig. 6.11) and as more EtOH is added, acetic acid conversion EA formation (Figure 6.12) increased. Ultimately, the reaction will be limited by the amount of reactants in the bio-oil vapor available for esterification. Since the reaction is reversible, it will reach equilibrium between products and reactants. The removal of water shifts the equilibrium towards products. Equilibrium for esterification reactions lie far to the right, especially if conducted in vapor phase, for which the thermodynamic equilibrium constant is 367 for the reaction of ethanol and acetic acid to form ethyl acetate (Diebold, 2000). Because the reaction is carried out in the vapor phase, water vapor and bio-oil vapor containing reactants (e.g., acids, aldehydes, ketones) are spatially separated so water in the reaction medium affects reaction equilbria less than it would in liquid phase reactions. Thus, for the observed esterification reaction between AcOH and EtOH, the reaction strongly favors the product, ethyl acetate, with little potential for the reverse reaction between ethyl acetate and water to reform ethanol and acetic acid.

Conclusions

We have developed a method to improve the quality of bio-oil by coupling biomass pyrolysis with reactive condensation. By atomizing ethanol into uncondensed bio-oil vapor produced during pyrolysis, a single integrated step, a combined condensation and esterification process has been developed. Using a reactive condensation unit, we esterified bio-oil vapor with ethanol (EtOH) at elevated temperature (114-127 °C) and reactor residence times approximating 60 s without the use of a catalyst, although any primary alcohol (e.g., methanol) could conceivably be used. GC-MS results demonstrated the formation of esters including ethyl acetate and ethyl propionate and acetals including diethoxymethane and 1,1-diethoxyethane. Quantitative GC-MS results indicated that acetic acid concentration decreased by as much as 42 %, subsequently improving the pH, viscosity, and cold flow properties of the resultant bio-oil. Experiments showed the following improvements for bio-oil condensed with 23.2 % EtOH (w/w) relative to the control:

- pH was increased from 2.5±0.01 to 3.1±0.01
- viscosity was reduced from 24.4 to 9.7 cSt (measured at 40 °C)
- water content was reduced from 10±0.8 to 8.4± 2.3 % (w/w)
- the cloud point was reduced from -4.7±0.2 to -12.1±0.4 °C

The ability to reduce the concentration of reactive species in bio-oil is an important step in the development of stabile fuel-quality pyrolysis oils derived from biomass, and esterification is one way to do so. We have shown that esterification not only reduces the concentration of a key carboxylic acid, acetic acid, it also improves overall quality of the bio-oil. Additionally, esters can be easily removed by distillation due to higher volatility compared to the acids from which they are produced. Removed esters are highly valued products in the chemical industry. When left in the bio-oil, esters improve bio-oil quality compared to the carboxylic acids they replace. It was proposed that esterified bio-oil would be more stabile during aging, since acids that would normally catalyze condensation reactions leading to polymerization of bio-oil components were removed. Though not evident from the OOT results, an

increase in stability may yet be observed using other stability indices such as viscosity changes during storage. The OOT value is sensitive to large variations in specific gravity – the presence of lighter, volatile compounds, such as esters, often cause materials to oxidize more readily than heavier materials.

An additional benefit to the method developed in this study is that any alcohol may be used to condense and esterify the bio-oil vapor depending on what esters are desired as the end product. For example, if methanol, butanol or propanol is used, resulting esters will include methyl, butyl, or propyl acetate, respectively. Additionally due to the presence of other organic acids in the oils such as formic acid, propionic acid, and butyric acid, it is possible to produce esters including formates, butyrates, and propionates in addition to the acetates observed in the current study. The relative size of the esters determines the flash point and boiling point of the bio-oil produced. A bio-oil produced by reactive condensation with methanol will have the lowest flash and boiling points. One downside to longer chain alcohols is a significant reduction in the reaction rate (Simons, 1983). However, if an acidic catalyst is employed, the reaction rate can be increased if required.

We expect that the esterification of bio-oil using the method described herein can be optimized for greater conversion of carboxylic acids. With better reaction zone temperature control, the reaction rate will likely induce more complete carboxylic acid conversion. In addition, this esterification method could easily be integrated into a fast pyrolysis system to improve bio-oil quality. In fact, we are currently building a fluidized-bed reactor system with an in-line esterification reactor to test whether improvements can be made to fast pyrolysis oils. Additional studies will likely show further benefit for esterifying bio-oil, especially in further catalytic upgrading. We propose that esterified bio-oil will cause less coking on zeolite catalysts during upgrading to hydrocarbons since the cracking and deoxygenation of esters, ethyl, methyl or otherwise, has been successfully shown in many studies (Li et al., 2009: Lima et al., 2004; Ooi et al., 2004). The removal of organic acids is beneficial due to the fact that they may be precursors to coke formation on catalyst surfaces. In addition, the deoxygenation of carboxylic acids over zeolite catalysts is more difficult than esters, ketones, or aldehydes (Lu et al., 2007). Esterifying organic acids prior to upgrading alleviates the difficulty by removing oxygen in the form of water since esters compared

to the acids that produced them have much lower oxygen content. For example, the elemental oxygen content of acetic acid is 53.3 % while for its corresponding ester, ethyl acetate assuming ethanol was used for the esterification, the oxygen content is 36.4 %. The further removal of oxygen from esters during catalytic upgrading is much easier. Thus, once catalytically upgraded, the resulting esterified bio-oil will be more like a hydrocarbon than if no esterification had been attempted.

Acknowledgements

This research was conducted through partial support from the U.S. DOE Biorefinery Research Project grants, the State of Georgia Biorefinery grant, and the UGA Experiment Station. We thank Richard Speir for carrying out pyrolysis runs and bio-oil separations. We also thank Tom Lawrence for assistance in designing the novel condensing system. Finally, we thank Joby Miller, Damion Martell, Jenille Tulloch, Kate Lee, and Elizabeth Fortner for assistance in analyzing materials.

References

Adjaye, D., Sharma, R.K., Bakhshi, N.N. (1992). Characterization and stability analysis of wood-derived bio-oil. Fuel Processing Technology 31(3): 241-256

Boucher, M., Chaala, A., Pakdel, H., Roy, C. (2000). Bio-oils obtained by vacuum pyrolysis of softwood bark as a liquid fuel for gas turbines. Part II: Stability and ageing of bio-oil and its blends with methanol and a pyrolytic aqueous phase. Biomass Bioenergy 19: 351-361.

Chu, W., Yang, X., Ye, X., Wu, Y. (1996). Vapor phase esterification catalyzed by immobilized dodecatungstosilicic acid (SiW12) on activated carbon. Appl. Catal., A: General 145: 125-140.

Diebold, J. P. (2000). A Review of the chemical and physical mechanisms of the storage stability of fast pyrolysis bio-oils. Subcontractor Report for the National Renewable Energy Laboratory: Golden, CO, January 2000. NREL/SR-570-27613.

Diebold, J. P., Czernik, S. (1997). Additives to Lower and Stabilize the Viscosity of Pyrolysis Oils during Storage. Energy Fuels 11: 1081-1091.

Gayubo, A., Aguayo, A., Atutxa, A., Prieto, R., Bilbao, J. (2004). Deactivation of a HZSM-5 zeolite catalyst in the transformation of the aqueous fraction of biomass pyrolysis oil into hydrocarbons. Energy Fuels 18: 1640-1647.

Gust, S. (1997). Combustion experiences of flash pyrolysis fuel in intermediate size boiler. In Developments in thermal biomass conversion, Bridgewater A.V., Boocock D.G.B., Eds., Blackie Academic and Professional: London, UK, pp 481–488.

Ji-lu, Z. (2007). Bio-oil from fast pyrolysis of rice husk: Yields and related properties and improvement of the pyrolysis system. J. Anal. Appl. Pyrolysis 80: 30-35.

Junming, X., Jianchun, J., Yunjuan, S., Yanju, L. (2008). Bio-oil upgrading by means of ethyl ester production in reactive distillation to remove water and to improve storage and fuel characteristics. Biomass Bioenergy 32(11): 1056-1061.

Kirumakki, S., Nagaraju, N., Chary, K. (2006). Esterification of alcohols with acetic acid over zeolites, Hβ, HY and HZSM5. Appl. Catal., A: General 299: 185-192.

Koster, R., van der Linden, R.B., Poels, E., Bliek, A. (2001). The mechanism of the gas-phase esterification of acetic acid and ethanol over MCM-41. J. Catal. 204: 333-338.

Li, H., Shen, B., Kabulu, J., Nchare, M. (2009). Enhancing the production of biofuels from cottonseed oil by fixed-fluidized bed catalytic cracking. Renewable Energy 34: 1033-1039.

Lima, D., Soares, V, Ribeiro, E., Carvalho, D., Cardoso, E., Rassi, F., Mundim, K., Rubim, J., Suarez, P. (2004). Diesel-like fuel obtained by pyrolysis of vegetable oils. J. Anal. Appl. Pyrolysis 71: 987-996.

Lu, C.B., Yao, J.Z., Lin, W.G., Song, W.L. (2007). Study on biomass catalytic pyrolysis for the production of bio-gasoline by on-line FTIR. Chin. Chem. Lett. 18: 445-447.

Mahfud, F., Melián-Cabrera, I., Manurung, R., Heeres, H. (2007). Biomass to Fuels: Upgrading of flash pyrolysis oil by reactive distillation using a high boiling alcohol and acid catalysts. Process Safety & Environmental Protection: Transactions of the Institution of Chemical Engineers Part B 85(5): 466-472.

Miao, S., Shanks, B. (2009). Esterification of biomass pyrolysis model acids over sulfonic acid-functionalized mesoporous silicas. Appl. Catal., A: General 359, 113-120.

Milne, T. A., Agblevor, F., Davis, M., Deutch, S., Johnson, D. (1997). In Developments in Thermal Biomass Conversion, Bridgwater, A. V., Boocock, D.G.B., Eds., Blackie Academic and Professional: London, UK.

Moens, L., Black, S., Myers, M., Czernik, S. (2009). Study of the neutralization and stabilization of a mixed hardwood bio-oil. Energy Fuels 23: 2695-2699.

Oasmaa, A., Kuoppala, E. (2003). Fast Pyrolysis of Forestry Residue. 3. Storage Stability of Liquid Fuel. Energy Fuels 17(3): 1075-1084.

Oasmaa, A., Kuoppala, E., Selin, J., Gust, S., Solantausta, Y. (2004). Fast Pyrolysis of Forestry Residue and Pine. 4. Improvement of the Product Quality by Solvent Addition. Energy Fuels 18: 1578-1583.

Ooi, Y., Zakaria, R., Mohamed, A., Bhatia, S. (2004). Catalytic conversion of palm oil-based fatty acid mixture to liquid fuel. Biomass Bioenergy 27: 477-484.

Simons, R.M. (1983). In Encyclopedia of Chemical Processing and Design 19, J.J. McKetta and W.A. Cunningham, Eds., Marcel Dekker, N.Y., p 381.

Stamatov, V., Honnery, D., Soria, J. (2006). Combustion properties of slow pyrolysis bio-oil produced from indigenous Australian species. Renewable Energy 31: 2108–2121.

Tang, Y., Yu, W., Mo, L., Lou, H., Zheng, X. (2008). One-step hydrogenation-esterification of aldehyde and acid to ester over bifunctional Pt catalysts: A model reaction as novel route for catalytic upgrading of fast pyrolysis bio-oil. Energy Fuels 22(5): 3484-3488.

Zhang, Q., Chang, J., Wang, T., Xu, Y. (2006). Upgrading Bio-oil over Different Solid Catalysts. Energy Fuels 20: 2717-2720.

Figure Captions

Figure 6.1. Continuous pyrolysis reactor including components; (1) biomass hopper, (2) vibratory feeder, (3) reactor inlet, (4) auger motor, (5) auger conveyer, (6) water cooler, (7) furnace and furnace control, (8) char collector, (9) reactive condensation unit, (10) bio-oil drip trap, (11) ice bath trap, (12) vacuum pump, (13) ethanol container.

Figure 6.2. Cooling profile for bio-oil condensed with 7.4 % EtOH (w/w) injected at 1.5 mL min^{-1}. Furnace temperature is shown on secondary vertical axis.

Figure 6.3. Relationship between WHSV and yield (wt % of original biomass) of whole oil (▲, ···), oily phase (◊) with best-fit line (---, R^2=0.71, p-value>0.05) and aqueous phase (□) with best-fit line (—, R^2=0.79, p-value>0.05).

Figure 6.4. Relationship between pH and EtOH % (w/w).

Figure 6.5. Viscosity at 40 °C (×, —) and at 60 °C (▲, ---) as a function of EtOH fitted with a 5-parameter sigmoidal line at R^2=0.999 and R^2=0.996 ($p<0.05$), respectively.

Figure 6.6. Gas chromatogram for calibration standard containing EA (rt=1.999, quality: 72), AcOH (rt=2.142, quality: 90), and heptane (rt=2.8, quality: 90).

Figure 6.7. Bio-oil samples with 0 and 23.2 % (w/w) EtOH including internal standard, heptane (rt=2.798 min), showing EA (rt=1.996) and AcOH (rt=2.046) peaks.

Figure 6.8. Gas chromatogram for 0 and 23.2 % EtOH (w/w) bio-oil samples showing EA (quality: 72), AA (quality: 90), heptane (quality: 94 and 90, respectively) and various other compounds.

Figure 6.9. Chromatogram for bio-oil condensed with 0 and 23.2 % (w/w) EtOH.

Figure 6.10. Stacked plot showing normalized gas chromatograms for each EtOH concentration. Compounds include EA (A), AcOH (B), 1-hydroxy-2-propanone (C), diethoxymethane (D), heptane (E), and ethyl propionate (F).

Figure 6.11. Fractional conversion of acetic acid (AA) as a function of reaction temperature (°C) and EtOH concentration (mmol mL^{-1}) (R^2=0.996, $p<0.01$).

Figure 6.12. Fractional conversion of acetic acid to ethyl acetate (EA) as a function of reaction temperature (°C) and EtOH concentration (mmol mL^{-1}) (R^2=0.89, $p<0.1$).

Tables

Table 6.1. Characterization of solid feedstock and pyrolysis char.

Analysis[a]	Biomass	Char
Moisture (w.b.)	7.45	3.20
Volatiles	74.83	27.58
Ash	0.13	2.70
Fixed Carbon	17.59	69.12
C	52.60	79.1
H	5.66	3.1
N	0.18	0.2
S	0.02	0.0
O[b]	38.90	12.6
HHV (MJ/kg)	20.6	34.1

[a]Measured as a % (w/w, d.b.) unless otherwise stated.
[b]By difference.

Table 6.2. Product yield for reactive condensation experiments.

Product	% Yield (w/w) at % EtOH				
	0.0	7.3	10.3	16.4	23.2
Char	21.8	23.5	23.5	24.4	24.4
Gases[a]	20.6	17.8	17.0	27.2	13.9
Bio-oil	57.7	58.7	59.5	48.4	61.7
Oily Phase					
(% of BO[b])	17.5	21.6	17.1	19.2	9.0
(% of BM[c])	9.0	11.6	9.6	9.5	6.0
Aqueous Phase					
(% of BO)	82.5	78.4	82.9	80.8	91.0
(% of BM)	42.4	42.0	36.5	40.0	40.4

[a]Calculated by difference.
[b]Bio-oil.
[c]Biomass.

Table 6.3. Characterization data for oily-phase bio-oils produced at various WHSV.

Parameter	Oily Phase Characteristics at WHSV					
	∞	33.3	25	16.7	8.3	0
EtOH (wt %)	0	7.4	10.3	16.4	23.2	100
C	65 ± 1.7[b]	58 ± 2	56 ± 0.5	57 ± 0.4	56 ± 1.4	47 ± 3.4
H	7.1 ± 0.4	5.6 ± 0.6	5.6 ± 0.4	6.4 ± 0.1	6 ± 0.1	12 ± 0.7
N	0.2 ± 0	0.2 ± 0	0.3 ± 0	0.2 ± 0	0.2 ± 0	0 ± 0
S	0 ± 0	0 ± 0	0 ± 0	0 ± 0	0 ± 0	0 ± 0
O[a]	28 ± 1.4	36 ± 1.9	38 ± 0.5	37 ± 0.4	38 ± 1.6	42 ± 0
HHV (MJ kg^{-1})	28 ± 0.2	25 ± 0.1	26 ± 0.6	25 ± 0.1	27 ± 0.2	27 ± 3.8
% H_2O	10 ± 0.8	16 ± 2.6	11 ± 0.2	14 ± 0.9	8.4 ± 2.3	0.4 ± 0
pH	2.5 ± 0	2.7 ± 0	2.7 ± 0	2.8 ± 0	3.1 ± 0	5.3 ± 0.4
Viscosity (mm^2 s^{-1})						
40 °C	300.1	151.2	41.3	37.2	49.2	3.75[c]
60 °C	24.4	13.7	13.5	11.2	9.7	3.99
Density (g mL^{-1})	1.2 ± 0.2	1.2 ± 0.2	1.2 ± 0.1	1.1 ± 0.2	1.1 ± 0.1	0.8 ± 0

Table 6.4. Oxidation onset temperature (°C) and cloud point temperature (°C) for EtOH-condensed bio-oils.

EtOH (wt %)	Oxidation Onset Temperature (°C)		Cloud Point (°C)	
	Ave	S.D.	Ave	S.D.
0	174.3	1.1	-4.7	0.2
7.4	167.7	0.5	-7.3	0.4
10.3	157.1	3.1	-7.9	0.3
16.4	169.9	2.5	-6.7	1.0
23.2	172.2	1.6	-12.1	0.3

Figures

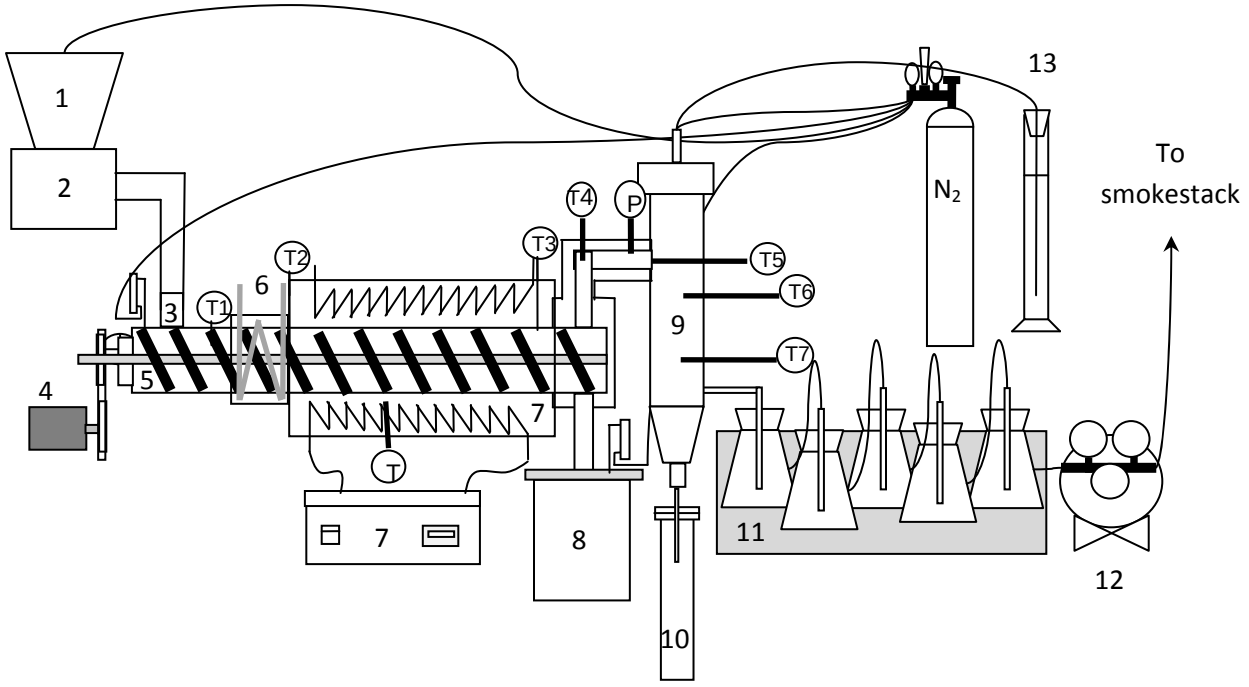

Figure 6.1. Continuous pyrolysis reactor including components; (1) biomass hopper, (2) vibratory feeder, (3) reactor inlet, (4) auger motor, (5) auger conveyer, (6) water cooler, (7) furnace and furnace control, (8) char collector, (9) reactive condensation unit, (10) bio-oil drip trap, (11) ice bath trap, (12) vacuum pump, (13) ethanol container.

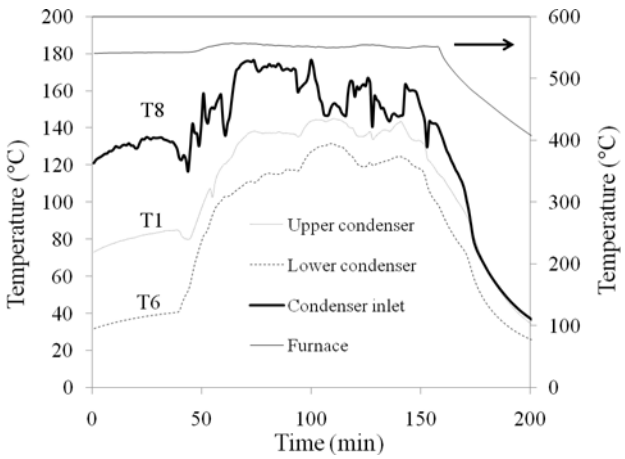

Figure 6.2. Cooling profile for bio-oil condensed with 7.4 % EtOH (w/w) injected at 1.5 mL min^{-1}. Furnace temperature is shown on secondary vertical axis.

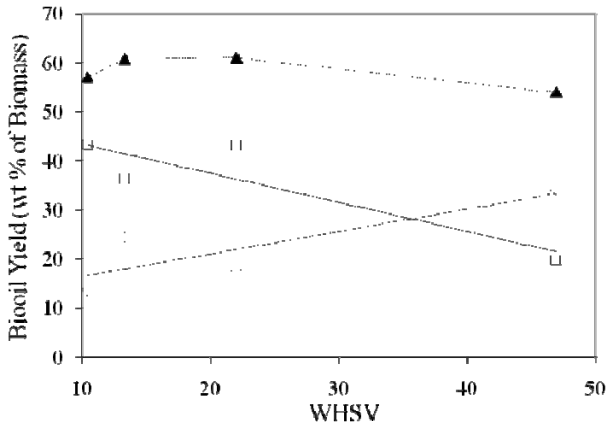

Figure 6.3. Relationship between WHSV and yield (wt % of original biomass) of whole oil (▲, ···), oily phase (◊) with best-fit line (---, R^2=0.71, p-value>0.05) and aqueous phase (□) with best-fit line (—, R^2=0.79, p-value>0.05).

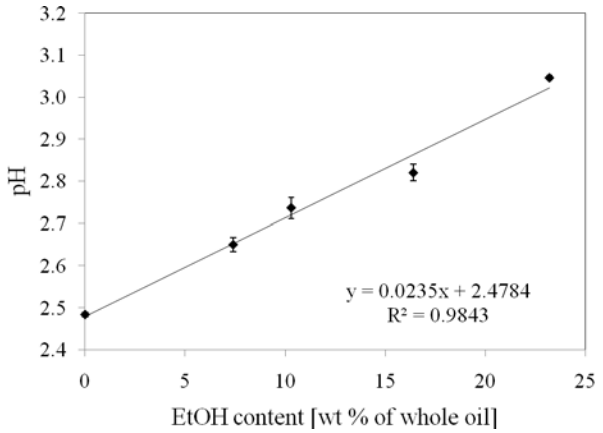

Figure 6.4. Relationship between pH and EtOH % (w/w).

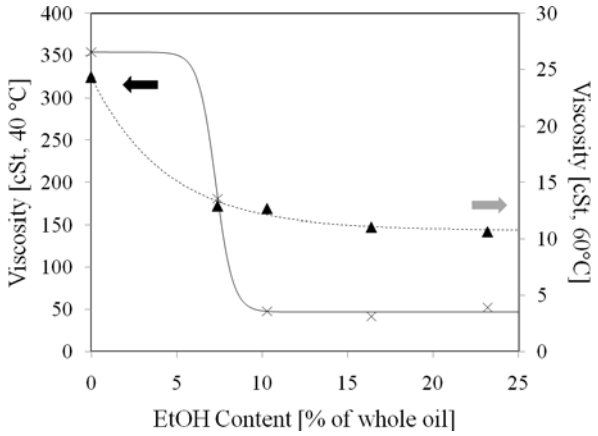

Figure 6.5. Viscosity at 40 °C (×, —) and at 60 °C (▲, ---) as a function of EtOH fitted with a 5-parameter sigmoidal line at R^2=0.999 and R^2=0.996 ($p<0.05$), respectively.

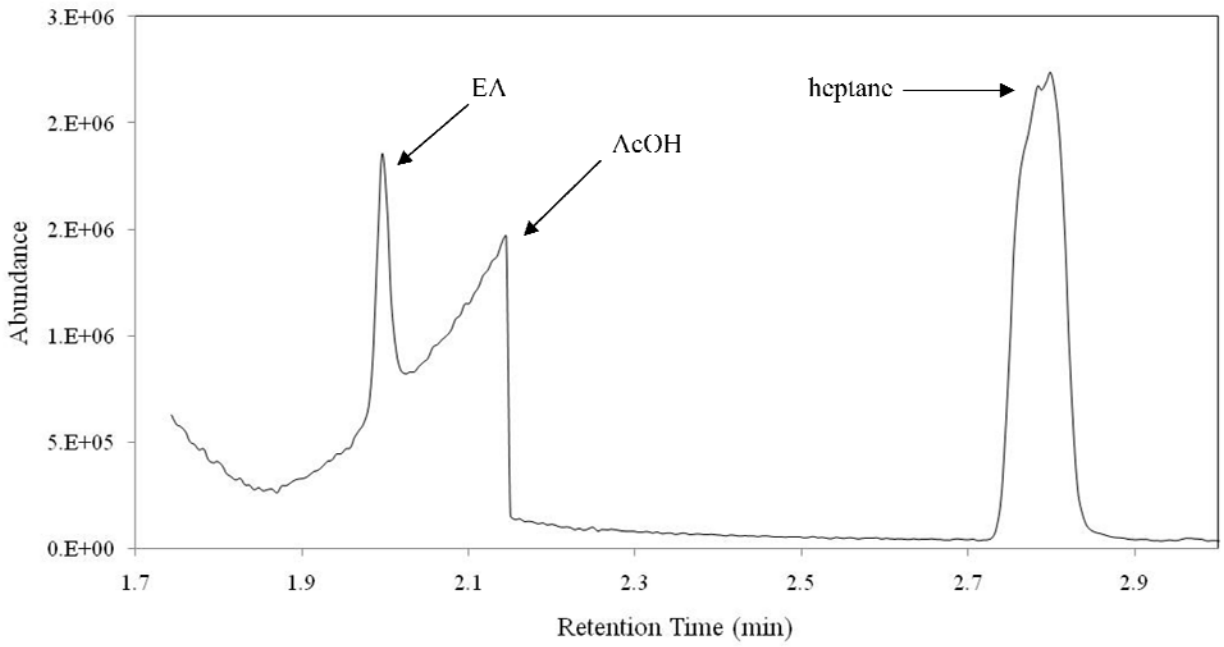

Figure 6.6. Gas chromatogram for calibration standard containing EA (rt=1.999, quality: 72), AcOH (rt=2.142, quality: 90), and heptane (rt=2.8, quality: 90).

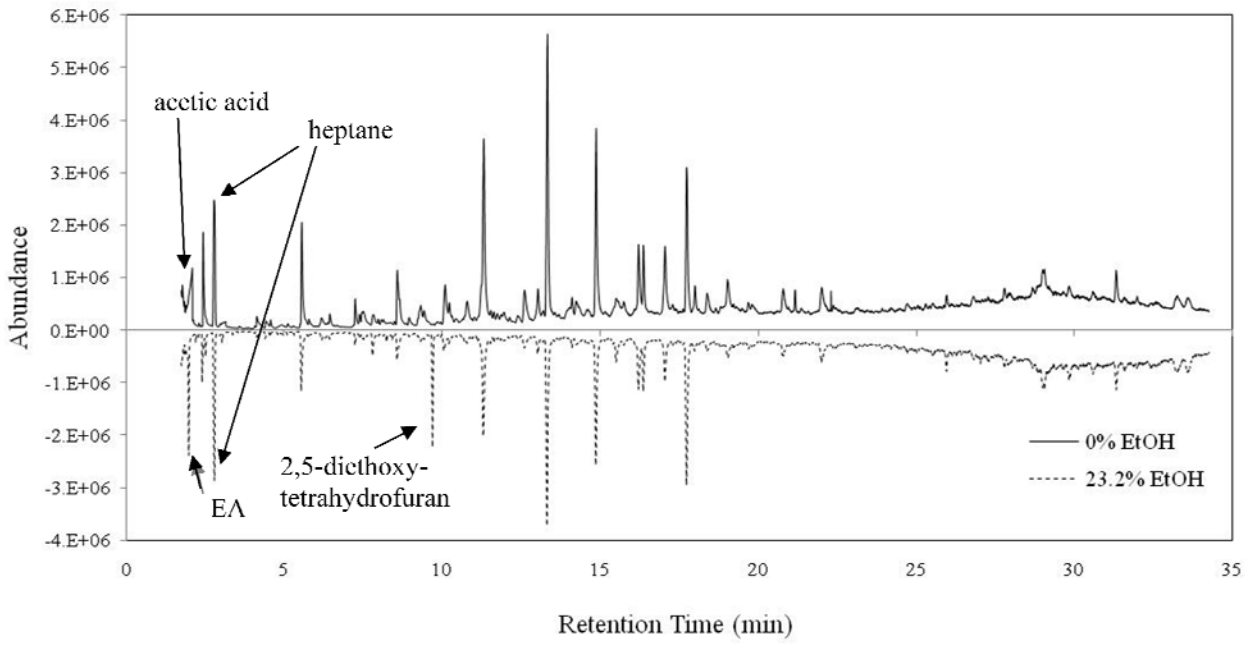

Figure 6.7. Bio-oil samples with 0 and 23.2 % (w/w) EtOH including internal standard, heptane (rt=2.798 min), showing EA (rt=1.996) and AcOH (rt=2.046) peaks.

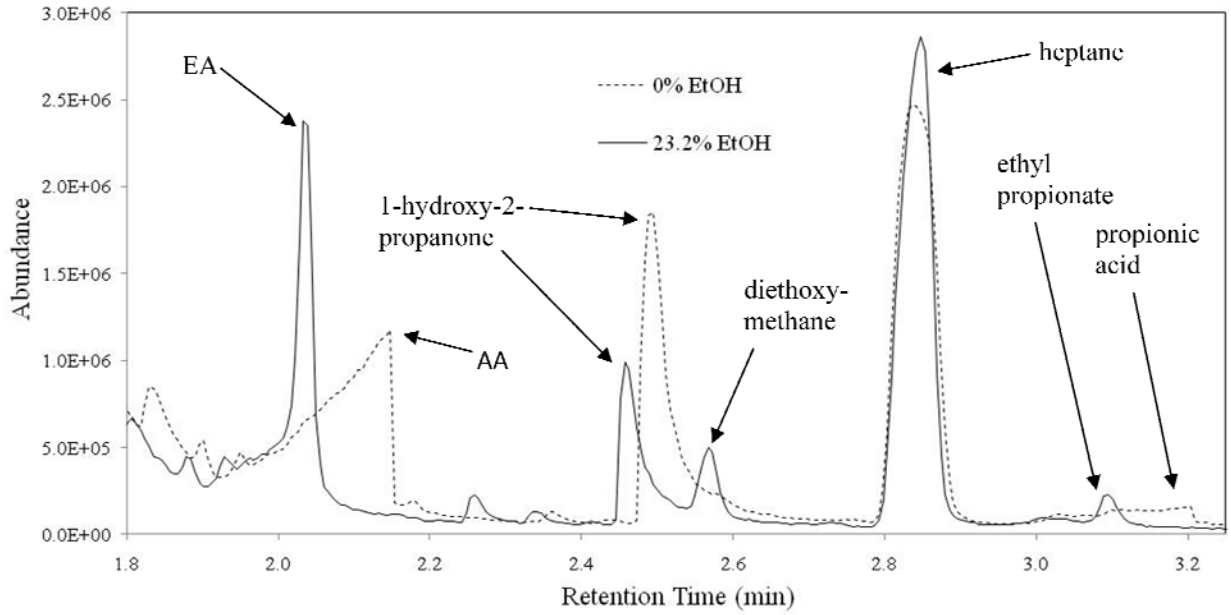

Figure 6.8. Gas chromatogram for 0 and 23.2 % EtOH (w/w) bio-oil samples showing EA (quality: 72), AA (quality: 90), heptane (quality: 94 and 90, respectively) and various other compounds.

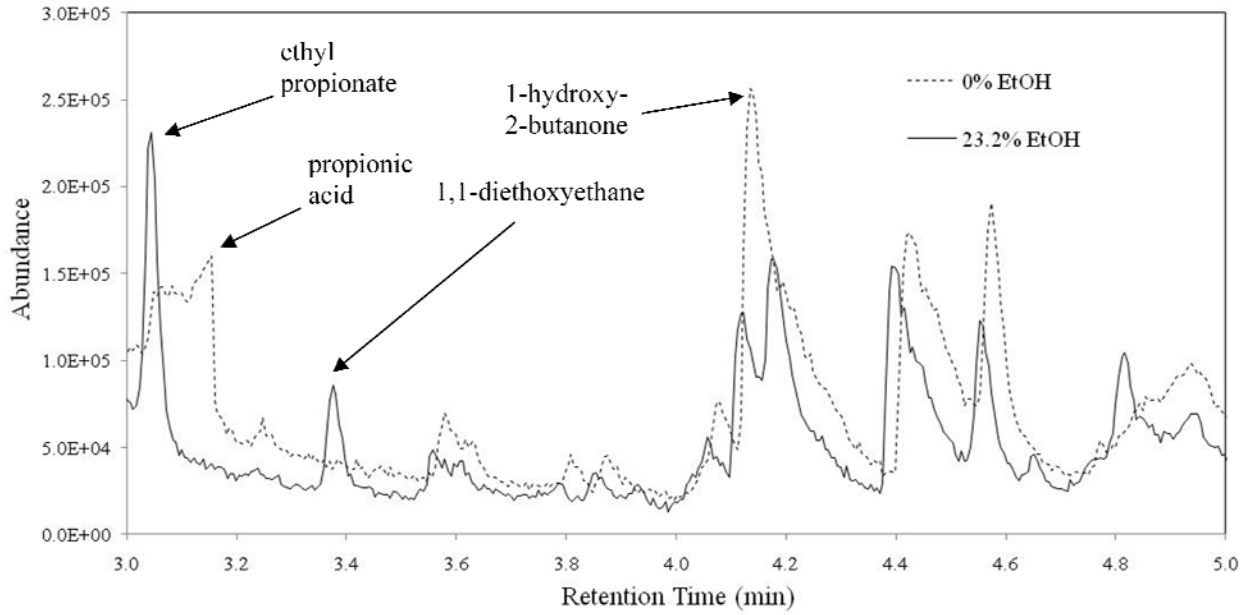

Figure 6.9. Chromatogram for bio-oil condensed with 0 and 23.2 % (w/w) EtOH.

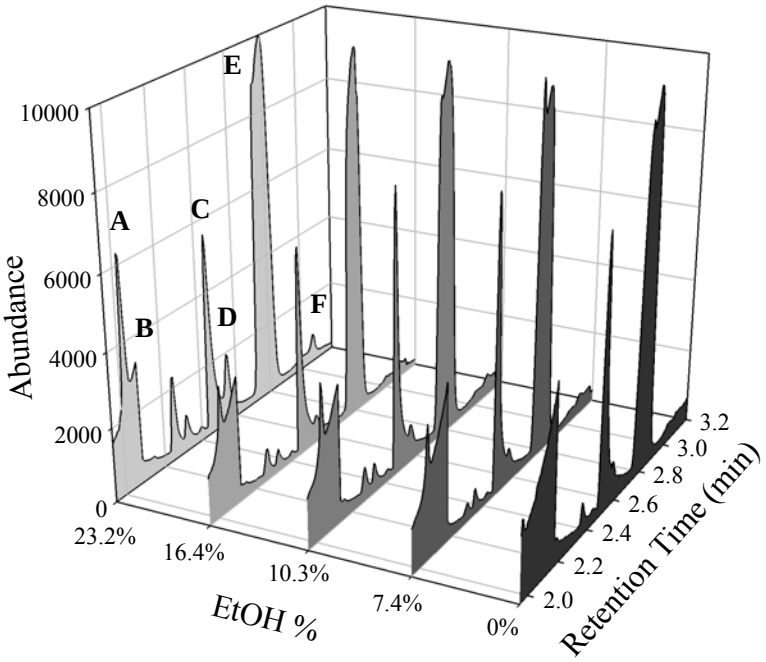

Figure 6.10. Stacked plot showing normalized gas chromatograms for each EtOH concentration. Compounds include EA (A), AcOH (B), 1-hydroxy-2-propanone (C), diethoxymethane (D), heptane (E), and ethyl propionate (F).

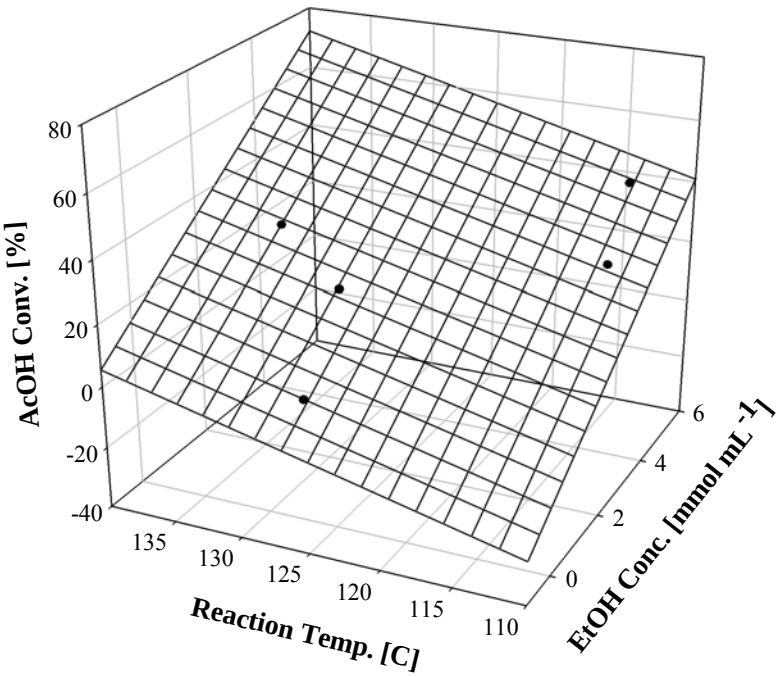

Figure 6.11. Fractional conversion of acetic acid (AA) as a function of reaction temperature (°C) and EtOH concentration (mmol mL^{-1}) (R^2=0.996, $p<0.01$).

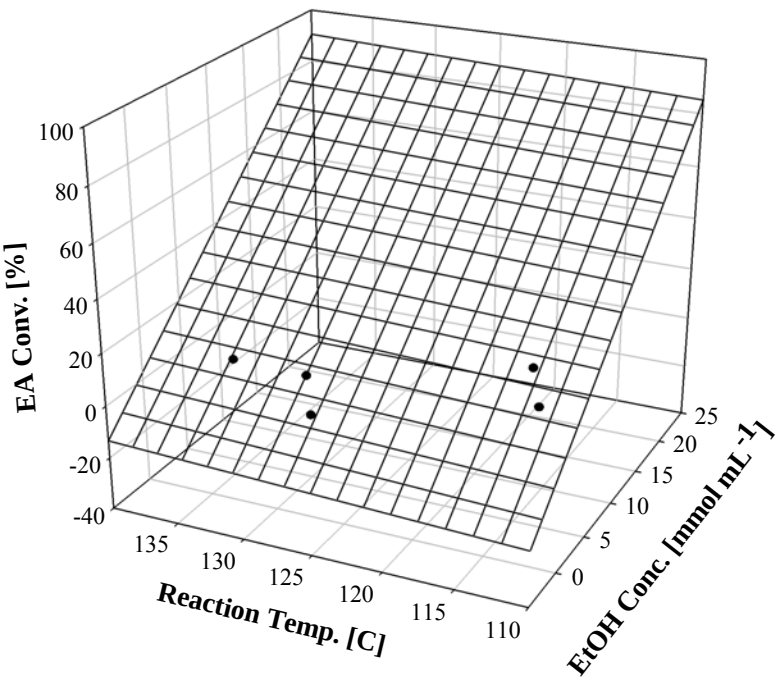

.

Figure 6.12. Fractional conversion of acetic acid to ethyl acetate (EA) as a function of reaction temperature (°C) and EtOH concentration (mmol mL^{-1}) (R^2=0.89, $p<0.1$).

CHAPTER 7

IMPROVING SLOW PYROLYSIS BIO-OIL QUALITY AND STABILITY VIA CATALYTIC CRACKING[6]

[6] Hilten, R., Speir, R., Kastner, J., Das, K.C. To be submitted to *Fuel*.

Abstract

Upgraded pyrolysis oils were produced from pine (PP) and peanut hull (PH) biomass with similar properties to traditional liquid fuels with potential for use in stationary power/heat generation or in liquid transport fuel applications. Bio-oil vapors were cracked and upgraded over a packed bed of HZSM-5 (ZSM) or commercially available fluid catalytic cracking (FCC) catalyst. Liquid product yield was higher for FCC-processed versus ZSM-processed bio-oil. Increasing catalytic cracking temperature reduced liquid and coke yield while increasing the yield of gas and reactor char. Parameters assessed included H/C_{eff} and O/C ratios, oxidative stability, energy density, and chemical composition. H/C_{eff} was significantly higher for PH although unaffected by cracking temperature or catalyst type. Elemental O/C ratio was significantly reduced in PH- versus PH-derived products and reduced due to catalytic cracking with ZSM being somewhat more effective. Chemical composition assessed for 500 °C catalytic processing experiments was significantly affected by both feedstock and catalyst type. FCC was more effective for reactant conversion (guaiacol and creosol) while ZSM was more effective in maximizing the yield of products (BTEX gasoline additives).

KEYWORDS: pyrolysis, catalytic cracking, fluid catalytic cracking, HZSM-5, pine, peanut hull

Introduction

Due to recent increases in fossil fuel costs, biomass-derived fuels are receiving much more attention than in the past. Many alternatives to conventional liquid hydrocarbon fuels have been proposed including bioethanol, biodiesel, and pyrolysis oil. The latter, pyrolysis oil, or bio-oil, can be produced relatively cheaply using any biomass feedstock. For some applications such as turbines, furnaces, and boilers, it may be possible to use bio-oil without upgrading. However, some problems may arise due to the nature of un-upgraded bio-oils. Problems occur for a variety of reasons including high ash content that can block filters, high viscosity that can affect pumping and injection, possible phase separation due to water, and corrosion due to low pH (Bridgwater, 1996; Adam et al., 2006). However, by upgrading pyrolysis oils, it is possible to produce liquid fuels from biomass that can more easily replace or supplement conventional hydrocarbon fuels (Sharma and Bakhshi, 1991; Bridgwater, 1996). Upgrading is

generally accomplished by catalytic cracking and reforming and hydrotreating of bio-oils to produce high quality liquid fuels.

Catalytic processes can either be integrated with pyrolysis systems to upgrade all vapors, or applied after pyrolysis on selected compounds extracted from pyrolysis products. Studies using in situ upgrading are abundant. Major work with catalytic pyrolysis began in the mid-eighties with the advent of zeolite catalysts – ZSM-5, in particular. ZSM-5 was developed by Mobil to convert methanol to gasoline (MTG) with a patent registered by Arguer and Landolt (1972). ZSM-5 is particularly effective in producing gasoline-range hydrocarbons due to shape-selective pores in the surface (Renaud et al., 1987). Diebold and Scahill (1987) produced gasoline boiling range hydrocarbons by upgrading fast pyrolysis vapors from softwood sawdust in a vortex reactor using ZSM-5 catalyst. Renaud et al. (1987) converted vapor from pyrolysis of populus deltoids wood over ZSM-5. More recently, Williams and Nugranad (2000) pyrolyzed rice husks in a fluidized bed reactor with pyrolysis vapors being upgraded using a zeolite ZSM-5 catalyst. The study showed that in upgraded oils, molecular weight distribution decreased and the concentration of single ring and polycyclic aromatic hydrocarbons increased markedly compared to bio-oils produced during non-catalytic pyrolysis. Lu et al. (2007) used online FT-IR to show the formation of bio-gasoline from the catalytic pyrolysis of wheat straw using HUSY, REY, and HZSM-5 catalysts. Gasoline was indicated by the relative increase in the concentration of iso-alkanes and aromatics. Adam et al. (2006) upgraded pyrolysis vapors from spruce and Miscanthus biomass using several catalysts including several Al-MCM-41 catalysts and a commercial FCC catalyst. The quality of bio-oil was assessed for each catalyst by observing the yields of eight desirable and undesirable components in bio-oils produced including hydrocarbons, phenols, furans, acids, alcohols, carbonyls, PAHs, and heavy compounds.

Many studies have investigated upgrading of fast pyrolysis oil over catalysts (Baker and Elliott, 1988; Sharma and Bakhshi, 1991; Sharma and Bakhshi, 1993a; Sharma and Bakhshi, 1993b; Adjaye and Bakhshi, 1995; Valle et al., 2007). Other studies have attempted upgrading of selected bio-oil components separated after pyrolysis. Several studies have observed the effects of upgrading only the

non-phenolic fraction (NPF) over HZSM-5 (Sharma and Bakhshi, 1993a; Sharma and Bakhshi, 1993b) to alleviate the coking effects caused by phenolic compounds. Several articles upgrade only the aqueous fraction or components making up the aqueous fraction of bio-oil. Gayubo et al. (2004a) transformed alcohols and phenol components over HZSM-5. Gayubo et al. (2004b) upgraded aldehydes, ketones, and acids. Corma et al. (2007) used several catalysts including FCC, Al_2O_3, USY, and ZSM-5-based FCC to upgrade representative biomass oxygenates including glycerol and sorbitol.

The current study sought to upgrade the organic fraction of a bio-oil produced from the slow pyrolysis of pelletized pine and peanut hull biomass. Two catalysts were used in a secondary packed bed reactor (PBR) with the goal of improving the quality of bio-oil. Catalysts used included a commercially available FCC catalyst (Grace Chemical) and H-ZSM-5 (Zeolyst International).

Materials and Methods

Experimental Design

Slow pyrolysis bio-oil was generated in a batch reactor (Figure 7.1) at 500 °C using pelletized pine (PP) and peanut hull (PH) feedstock. Biomass characteristics are given in Table 7.1. The bio-oil collected exhibited two phases; an organic, oily phase, and a high water content aqueous phase. The organic phase of bio-oil was used in all subsequent upgrading endeavors. In an effort to improve the quality and stability of the oils, PP and PH bio-oil were passed across a fixed bed of zeolitic catalyst.

Reactor and catalyst were weighed before and after each run to determine the amount of catalyst coke, catalyst tar, and reactor char. Catalyst coke was determined by first rinsing the catalyst in acetone to remove tar (which was also quantified) then subjecting the dried catalyst in combustion conditions in a thermogravimetric analyzer (TGA) to determine mass loss. Mass loss was attributed to the combustion of coke. The yield of oily product and aqueous phase byproduct was also determined relative to the total amount of bio-oil introduced to the reactor.

Catalytic Cracking Process

Previously produced and phase-separated bio-oil is pumped continuously into a tubular reactor (shown in Figure 7.2) and across a 15 g catalyst bed (28.5 cm^3) maintained at 400, 450, or 500 ˚C using a

tube furnace. Pumping was accomplished using a peristaltic pump at a flow rate of 1.5 mL min^{-1} (~ 100 g h^{-1}) corresponding to a weight hourly space velocity (WHSV, h^{-1}) of 6.6 h^{-1}. Catalyst to oil ratio ranged from 0.25 to 0.3. Catalyst contact time (3600/(WHSV · C/O) thus ranged from 1818 to 2182 s. Given a carrier gas flow rate of 50 cm^3 min^{-1}, gas phase residence time in the catalytic zone (V = 28.5 cm^3) was approximately 34 s. Samples that were highly viscous at room temperature, particularly the PH bio-oils, were heated during pumping using a hot plate.

Bio-oil vapor was condensed in a series of glass flasks in an ice bath. Non-condensable vapors were subsampled and analyzed every 10 min during runs by micro-GC while the bulk will be emitted to outside air.

Catalysts

The reactor contained a fixed bed of catalyst, either H-ZSM-5 or FCC variety. The H-ZSM-5 catalyst was produced by calcining NH_4-ZSM-5 that was supplied by Zeolyst International (CBV 5524 G). The catalyst has published values of 425 m^2 g^{-1}, 5 μm, and 50 for surface area, particle size and SiO_2/Al_2O_3 ratio, respectively, in powdered form. The NH_4-ZSM-5 was calcined at 550 ˚C for 4 h to produce the hydrogen form, H-ZSM-5, resulting in stronger acid pore sites. The process reduced the overall pH from 4.98 to 3.06. In-house measurements of the catalyst surface characteristics were accomplished using a Quantachrome surface area analyzer and indicated a surface area of 345 m^2 g^{-1}, pore radius at 10.81 Å, and pore volume at 0.1851 cm^3 g^{-1} for fresh catalyst after calcination, drying, and granulation . HZSM-5 will be henceforth referred to as ZSM. The FCC catalyst was supplied by Grace Chemical – composition is proprietary.

Product Characterization

Bio-oil products were characterized for CHNS-O (%, w/w), higher heating value (HHV, in MJ kg^{-1}), storage stability via oxidation onset temperature (OOT, °C), and chemical composition via GC-MS. Both H/C_{eff} and O/C ratios were determined based on CHNS-O results, assessed in a CHNS analyzer

(Thermoscientific, Flash 2000), as indicators of hydrocarbon formation and deoxygenation, respectively. Effective H/C ratio, H/C_{eff} was calculated as follows:

$$H/C_{eff} = \frac{mol\ H - (2\ x\ mol\ O)}{mol\ C} \quad \text{(Eq. 7.1)}$$

It was expected that catalytic cracking would effectively increase H/C_{eff} and reduce O/C. As an effect, HHV should increase as well as OOT. HHV was measured in a bomb calorimeter (IKA, C2000) using benzoic acid as the calibration standard. OOT was assessed using a differential scanning calorimeter (DSC, Mettler-Toledo, DSC823e) following ASTM E2009. Details of the method as used for bio-oils are provided in Hilten and Das (2010). Essentially, oils were heated in an oxidative atmosphere until combustion began. The temperature at the onset of combustion was designated as OOT.

GC-MS determination of the chemical composition was accomplished by developing six-point calibration curves to quantify several reactants and products in the bio-oils. All chemicals were purchased from Sigma-Aldrich. Here, we chose 2-methoxyphenol (guaiacol, >98% purity) and 2-methoxy-4-methylphenol (creosol, ≥ 98% purity) as representative reactants and benzene, toluene, ethylbenzene, and xylene (o-, m-, and p-xylene), collectively known as BTEX, as products. The GC-MS unit (Agilent, HP-6890) contained an HP-5 MS column, 30 m in length, with a 0.25 mm I.D. and 0.25 μm film thickness in conjunction with a Hewlett-Packard mass spectrometer (HP-5973) with a mass selective detector. The method used was as follows: inlet temperature of 230 ˚C, detector temperature at 280 °C (MS interface temperature), a flow of 1 mL min^{-1} He, the oven initially at 40 °C for 2.5 min followed by a ramp at 8 °C min^{-1} to 250 °C (held for 5 min). Masses were scanned from 15-500 mass units. Sample size was 1 μL and was prepared for analysis by diluting to 2.5 % in a 50:50 acetone/methanol mixture.

Statistical Design

The experimental design was planned such that a 3-way ANOVA could be used to determine the effects of three factors, biomass type (2 levels – PP and PH), catalyst type (3 levels - CTRL, FCC, and ZSM), and catalytic cracking temperature (3 levels – U450, U500, and U550 for temperatures at 450 and 500, and 550 °C), on yields and product composition and quality. The null hypothesis for all analyses was

that factors at any level had no affect on product yield or composition. Rejection of the null hypothesis was concluded at p-values less than a level of significance, $\alpha = 0.05$. The Holm-Sidak method of multiple comparisons was used to determine effects of levels for each factor.

Results and Discussion

Pyrolysis and Catalytic Cracking Yield

Table 7.2 provides yield data for pyrolysis runs using PH and PP biomass. Yields were similar for the two biomass types, although char yield for PH was somewhat higher than PP most likely due to higher ash content in PH (2.34 versus 0.34 % for PP). However, the yield of whole bio-oil (oily and aqueous phases) was equivalent. Yields for oily phase bio-oil at 7.5 and 9.2 % for PH and PP, respectively, are low, and catalytic cracking was performed on only this fraction. This means that the maximum product yield relative to original biomass is limited to less than 10 %.

Figures 7.3A and 7.3B provide product liquid yields for PH and PP, respectively. Yield of liquid did not significantly vary due to biomass type ($p=0.552$), although yield was significantly affected by both temperature and catalyst variety. The cracking of bio-oil generates liquid product as well as catalyst coke, reactor char, and non-condensable gases. Since no major cracking occurs for the control, liquid yield is highest, higher than for bio-oil cracked over ZSM ($p<0.001$) or FCC ($p<0.001$). Yield of liquid for bio-oil cracked over FCC was significantly higher than for ZSM ($p<0.001$). Temperature significantly affected yield, i.e. increasing temperature caused a requisite decrease in liquid yield and an increase in non-condensable gas yield for both feedstock types. Gas yield was significantly higher ZSM than for the control or for FCC.

Coke and char yields were also significantly affected by catalyst type and process temperature, although feedstock type had no significant effect. Coke yield, shown in Figure 7.4, was significantly reduced with increasing temperature for most temperature comparisons. For example, bio-oil processed at 450 °C formed significantly more coke than that formed from processing at either 500 or 550 °C. However, coke yields at 500 and 550 °C were not significantly different ($p=0.569$). Coke yield was

significantly higher for FCC than for ZSM (p=0.018). Figure 7.4 indicates coke yields for all samples. The opposite effect was seen for char yield, i.e. char yield increased with increasing temperature although there was no significant difference between 500 and 550 °C (p=0.212).

Composition, Quality, and Stability Results

CHNS

Table 7.3 shows CHNS-O, H/C_{eff}, and O/C for control and processed bio-oils. The 3-way ANOVA test indicated that elemental carbon (C) was significantly affected by biomass type, catalyst type, and catalytic cracking temperature. PH-derived bio-oils had higher C content than did PP-derived bio-oils. In both FCC- and ZSM-catalyzed cracking experiments, elemental C was higher relative to the control. Also, C for ZSM-derived oils was higher than for FCC-derived oils. Elemental hydrogen (H) was influenced significantly by biomass type, catalyst type, and catalytic cracking temperature, as well. Again, PH-derived oils had higher H-content. However, in the comparison of catalyst type, bio-oils generated using the control catalyst type indicated the highest H-content compared to either FCC- or ZSM-catalyzed experiments. Indicating an inverse relationship, lower temperature catalytic cracking favored higher H-content. Elemental nitrogen (N) was also significantly influenced by biomass type (PH bio-oil had higher N) and mildly influenced by catalyst type (p=0.05). No sulfur was detected for any of the oil types. Elemental oxygen (O) was significantly affected by biomass and catalyst type. PP-derived oils had higher oxygen content as did the control relative to the catalyzed cracking experiment. Results indicated that oils generated in FCC-catalyzed experiments had lower O compared to ZSM-catalyzed reactions.

Both H/C_{eff} and O/C were also significantly affected by the experimental factors. However, H/C_{eff} was only affected by biomass type and not catalyst type or catalytic upgrading temperature. H/C_{eff} was significantly higher for PH-derived liquid product. O/C was significantly influenced by both biomass type and catalyst type. PP-derived bio-oils showed higher O/C ratios than PH-derived oils. Both catalyst types generated bio-oils with lower O/C than the un-catalyzed control experiments. Results also showed

that ZSM was relatively more effective than FCC in reducing O/C. Catalytic cracking temperature had no significant effect on O/C ratio.

HHV

A major indicator of bio-oil quality was chosen here to be HHV. Table 7.4 provides heating values for liquid products derived from PH and PP bio-oil. HHV significantly increased with increasing process temperature ($p<0.001$) although the multiple comparisons test revealed there to be no statistical difference in HHV between oils processed at 500 and 550 °C ($p=0.108$). However, both feedstock type ($p<0.001$) and catalyst type ($p<0.001$) significantly affected HHV. Multiple comparisons tests revealed that PH bio-oils had greater HHV values than PP bio-oils. HHV for oils processed using HZSM-5 was also higher relative to control or FCC-processed oils. Figures 7.5A and 7.5B indicate these trends for upgraded PH and PP bio-oils, respectively. For all catalytically cracked samples, the HHV was higher than for untreated bio-oil (dashed lines in Figures 7.5A and 7.5B).

Results indicated that if the highest yield of liquid product is desired, the combination of FCC catalyst and 450 °C processing was most effective. For generating liquid product with the greatest HHV, the combination of PH feedstock, HZSM-5 catalyst, and 500 °C processing was most effective. Alternately if coke minimization is desired, the combination of FCC catalyst and processing at 500 °C was most effective.

Storage stability (OOT)

A three-way ANOVA test indicated that both biomass type and catalytic cracking temperature significantly affected OOT while catalyst type was not a significant predictor for OOT. Multiple comparisons tests showed that OOT was significantly higher for PP compared to PH biomass. OOT was significantly affected by catalytic upgrading temperature, as well. For most temperature comparisons, OOT was inversely related to catalytic cracking temperature. OOT for U450 was significantly higher than for U550, and U500 was higher than for U550. OOT for U450 versus U500 showed no significant difference.

Chemical composition (GC-MS)

Product liquids from one catalytic cracking temperature (500 °C) were assessed via GC-MS to determine the yield of BTEX and the conversion of guaiacol and creosol. Table 7.5 provides yields of total BTEX and conversion of combined guaiacol and creosol for PP- and PH-derived upgraded bio-oils. FCC catalyst was more effective for the conversion of guaiacol and creosol, but selectivity to BTEX was lower, hence higher yields of BTEX, the only products for which quantification was attempted, for ZSM. This was expected since HZSM-5 is particularly suited for the production of low boiling aromatics due to small pore size and distinctive pore shape (Renaud et al., 1987). Yield of BTEX from the FCC-processed oils was not significantly different than the control (non-catalytically-processed sample).

Conclusions

Catalytic upgrading has been proposed as a way to generate hydrocarbon fuels from bio-oil. Work described here confirms that catalytic cracking using zeolite-containing catalysts including HZSM-5 and commercial FCC catalyst significantly improves the higher heating value of slow pyrolysis bio-oils by reducing the oxygen content and increasing the H/C_{eff} ratio.

Results showed the yield of bio-oil and liquid product from pyrolysis and catalytic cracking, respectively, did not differ for the two biomass types. However, for catalytic processing, yield of liquid product did vary as a function of both catalytic cracking temperature and catalyst variety. Yield of liquid was highest for the control since little cracking was achieved (i.e. little conversion of reactants). For catalyzed runs, FCC processed experiments resulted in higher liquid yields than for ZSM-processed experiments. Liquid yield was inversely related to catalytic processing temperature while gas yield was directly related.

Yield of solid material including catalyst coke and reactor char also varied as a function of process conditions, but no effect was evident due to feedstock type. Catalyst coke was inversely related to catalytic processing temperature for both FCC- and ZSM-processed bio-oils. FCC-catalyzed bio-oil processing resulted in the largest yield of coke. While catalyst coke decreased with increasing

temperature, reactor char indicated a direct relationship with process temperature – char increased with increased temperature.

The two reactants chosen for quantification, guaiacol and creosol, were shown in be completely converted in the best case scenario, PH-derived oil processed using FCC catalyst at 500 °C. For the equivalent PP-derived oil, conversion of guaiacol plus creosol was 92.7 %. However, the yield of BTEX was higher for ZSM-processed oils. At 500 °C, the yield of BTEX for PP ZSM500 was 3.1 % (v/v of oil fed) versus 0.23 % for FCC-processed (PP FCC500) bio-oil.

References

Adam, J., Antonakou, E., Lappas, A., Stocker, M., Nilsen, M., Bouzga, A., Hustad, J., Oye, G. (2006). In situ catalytic upgrading of biomass derived fast pyrolysis vapours in a fixed bed reactor using mesoporous materials. Microporous and Mesoporous Materials 96: 93–101.

Adjaye, J., Bakhshi, N. (1996). Production of hydrocarbons by catalytic upgrading of a fast pyrolysis bio-oil. Part I: Conversion over various catalysts. Fuel Processing Technology 45 (1995) 161-183

Bridgwater, A. (1996). Production of high grade fuels and chemicals from catalytic pyrolysis of biomass. Catalysis Today 29: 285-295.

Corma, A., Huber, G., Sauvanaud, L., O'Connor, P. (2007). Processing biomass-derived oxygenates in the oil refinery: Catalytic cracking (FCC) reaction pathways and role of catalyst. Journal of Catalysis 247: 307–327.

Diebold, J., Scahill, J. (1987). Biomass to gasoline (BTG): upgrading pyrolysis vapors to aromatic gasoline with zeolite catalysis at atmospheric pressure. ACS, Div. Fuel Chem. 32(2): 297-307.

Gayubo,A., Aguayo, A., Atutxa, A., Aguado, R., Bilbao, J. (2004a). Transformation of Oxygenate Components of Biomass Pyrolysis Oil on a HZSM-5 Zeolite. I. Alcohols and Phenols. Ind. Eng. Chem. Res. 43: 2610-2618.

Gayubo, A., Aguayo, A., Atutxa, A., Aguado, R., Bilbao, J. (2004b). Transformation of Oxygenate Components of Biomass Pyrolysis Oil on a HZSM-5 Zeolite. II. Aldehydes, Ketones, and Acids. Ind. Eng. Chem. Res. 43: 2619-2626.

Lu, C., Yao, J., Lin, W., Song, W. (2007). Study on biomass catalytic pyrolysis for production of bio-gasoline by on-line FTIR. Chinese Chemical Letters 18: 445 – 448.

Renaud, M., Grandmaison, J. L., Roy, Ch., Kaliaguine, S. (1987). Conversion of vacuum pyrolytic oils from populus deltoids over HZSM-5. ACS, Div. Fuel Chem., 32(2): 276-86.

Sharma, R., Bakhshi, N. (1991). Upgrading of wood-derived bio-oil over HZSM-5. Bioresource Technology 35: 57-66.

Sharma, R., Bakhshi, N. (1993a). Catalytic conversion of fast pyrolysis oil to hydrocarbons over HZSM-5 in a dual reactor system. Biomass and Bioenergy 5(6): 445-455.

Sharma, R., Bakhshi, N. (1993b). Conversion of non-phenolic fraction of biomass-derived pyrolysis oil to hydrocarbons over HZSM-5 using a dual reactor system. Bioresource Technology 45: 195-203.

Valle B., Gayubo, A., Atutxa, A., Alonso, A., Bilbao, J. (2007). Integration of Thermal Treatment and Catalytic Transformation for Upgrading Biomass Pyrolysis Oil. International Journal of Chemical Reactor Engineering 5: Article A86.

Williams P., Nugranad, N. (2000). Comparison of products from the pyrolysis and catalytic pyrolysis of rice husks. Energy 25: 493–513.

Figure Captions

Figure 7.1. Batch pyrolysis unit used to generate biochar and bio-oil from peanut hulls – 1) nitrogen sweep gas, 2) gas flow controller, 3) reactor holding biomass, and 4) condensation unit to collect bio-oil.

Figure 7.2. Reactor setup showing 1) PSS vessel, 2) hot plate, 3) peristaltic pump, 4) stainless steel reactor with oil preheat zone, 5) catalyst bed, 6) tube furnace, 7) collection flask, 8) ice bath, 9) compressed N_2 tank and thermocouples (TC1 and TC2).

Figure 7.3. Yield of liquid product from the catalytic cracking of A) PH and B) PP bio-oil at 400-550 °C.

Figure 7.4. Yield of catalyst coke for PH and PP bio-oils catalytically cracked at 400-550 °C over HZSM-5 or FCC catalyst.

Figure 7.5. Higher heating values for A) PH and B) PP bio-oils processed at catalytic cracking temperatures between 400 and 550 °C.

Tables

Table 7.1. Feedstock characteristics for PH and PP biomass used in pyrolysis and catalytic cracking experiments.

Parameter	Feedstock Characteristics (dry basis)					
	PH			PP		
	AVE	±	95% CI	AVE	±	95% CI
Moisture[a]	8.60	±	0.74	7.45	±	0.09
Volatiles	71.75	±	6.79	80.85	±	0.14
Ash	4.21	±	9.03	0.14	±	0.08
Fixed Carbon	24.04	±	2.26	19.01	±	0.07
C	53.34	±	0.13	52.60	±	0.12
H	5.58	±	0.06	5.66	±	0.06
N	0.18	±	0.00	0.18	±	0.00
S	0.02	±	0.01	0.02	±	0.01
O[b]	38.19	±	0.81	38.90	±	0.80
HHV ($MJ\ kg^{-1}$)	20.34	±	0.30	20.60	±	0.11

[a]Wet basis

[b]By difference

Table 7.2. Yield of products from pyrolysis of PH and PP at 500 °C.

Product	Yield (%, w/w of BM[a])	
	PH[b]	PP[c]
Char	32.1	28.0
Gases	22.1	26.4
Whole BO[d]	45.8	45.8
Oily phase	7.5	9.2
Oily phase (%, w/w of BO)	17.9	20.0
Aqueous phase (%, w/w of BO)	82.1	80.0

[a]Biomass
[b]Peanut hull
[c]Pine pellet
[d]Bio-oil

Table 7.3. Characterization data for PP- and PH-derived bio-oils catalytically processed at 450, 500, or 550 °C.

Biomass Type	PH									PP								
Catalyst Type	CTRL			FCC			ZSM			CTRL			FCC			ZSM		
CatUp Temp (°C)	450	500	550	450	500	550	450	500	550	450	500	550	450	500	550	450	500	550
C	70.3	71.2	71.8	73.0	73.3	75.9	73.6	74.3	76.8	66.3	64.4	66.5	70.0	69.5	70.5	71.6	73.6	76.3
H	8.60	8.90	8.71	8.46	8.47	7.54	8.20	8.04	7.65	7.43	7.52	7.24	7.52	7.53	6.42	7.16	7.62	7.16
N	2.12	2.39	2.26	2.25	3.12	3.17	2.48	2.70	2.49	0.49	0.0	0.0	0.49	0.0	1.16	0.0	0.0	0.0
S	0.0	0.0	0.0	0.0	0.0	0.0	0.0	0.0	0.0	0.0	0.0	0.0	0.0	0.0	0.0	0.0	0.0	0.0
O[a]	19.0	17.5	17.2	16.3	15.1	13.4	15.7	14.9	13.0	25.7	28.1	26.2	22.0	22.9	22.0	21.2	18.8	16.5
H/C_{eff}	1.06	1.13	1.10	1.06	1.08	0.93	1.02	1.00	0.94	0.76	0.75	0.71	0.82	0.81	0.63	0.76	0.86	0.80
O/C	0.20	0.18	0.18	0.17	0.15	0.13	0.16	0.15	0.13	0.29	0.33	0.30	0.24	0.25	0.23	0.22	0.19	0.16
OOT (°C)	149.1	160.0	161.5	150.4	152.6	147.4	153.9	143.8	135.5	163.6	163.9	167.6	168.2	167.8	153.0	183.2	172.4	153.7

[a] By difference.

Table 7.4. Higher heating value for PH and PP bio-oils processed at 400-550 °C.

Catalyst Type	Process Temp (°C)	HHV (MJ kg^{-1})					
		PH			PP		
		AVE	±	95% CI	AVE	±	95% CI
CTRL	CTRL	31.22	±	0.59	28.38	±	0.22
	450	33.59	±	0.14	29.50	±	0.06
	500	33.34	±	0.45	29.60	±	0.11
	550	33.05	±	0.20	29.74	±	0.08
ZSM	400	34.20	±	0.09	30.87	±	0.66
	450	34.07	±	0.09	32.16	±	0.14
	500	34.85	±	0.04	34.37	±	0.72
	550	35.55	±	0.00	36.30	±	0.22
FCC	450	34.53	±	0.10	31.33	±	0.03
	500	35.10	±	0.16	32.15	±	0.03
	550	35.13	±	0.42	32.12	±	0.06

Table 7.5. Conversion (%, v/v) of combined guaiacol and creosol (G + C) and yield of BTEX (%, v/v of slow pyrolysis bio-oil) as result of catalytic cracking at 500 °C with no catalyst (CTRL), HZSM-5 (ZSM), and FCC catalyst.

Feedstock	Catalyst Type	Yield	Conversion
		BTEX	G + C
PH	CTRL	0.19	0.0
	ZSM	1.36	31.2
	FCC	0.31	100
PP	CTRL	0.41	0.0
	ZSM	3.08	83.7
	FCC	0.23	92.7

Figures

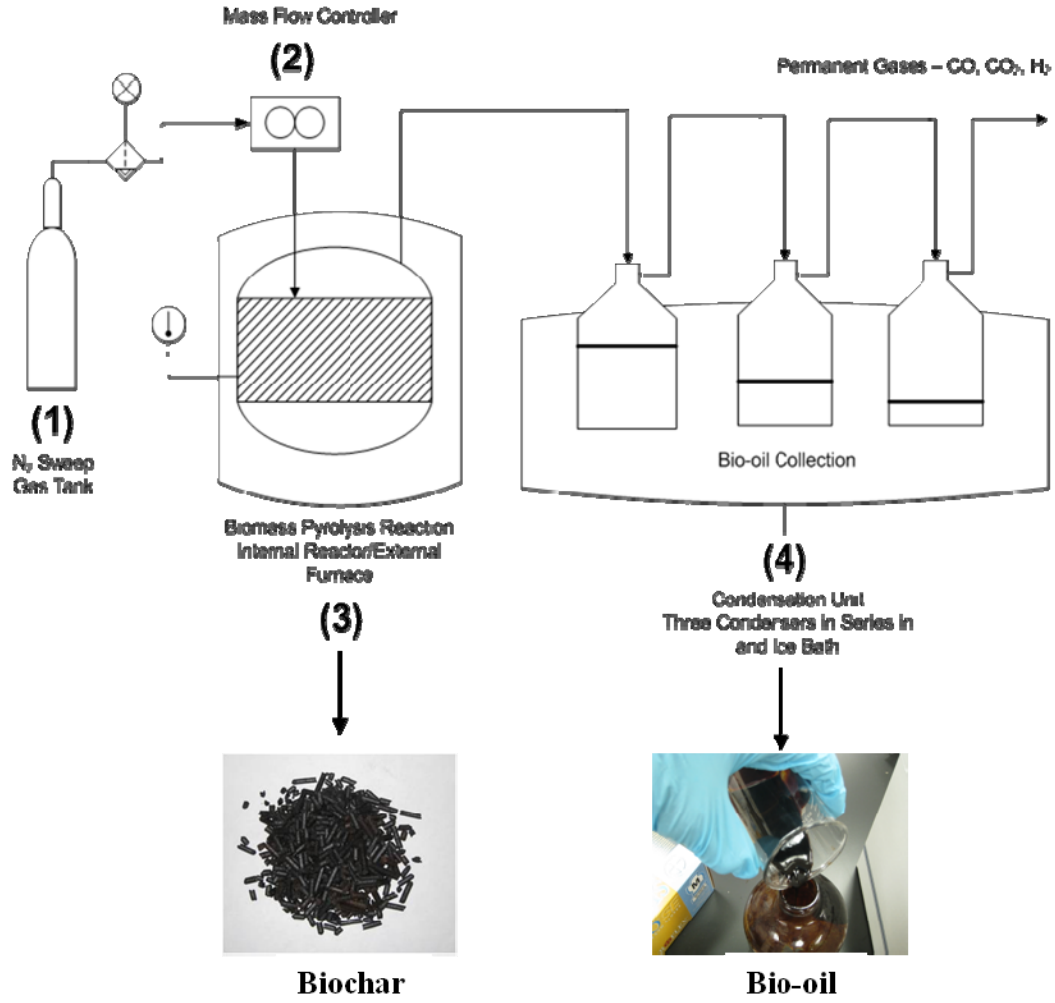

Figure 7.1. Batch pyrolysis unit used to generate biochar and bio-oil from peanut hulls – 1) Nitrogen sweep gas, 2) gas flow controller, 3) reactor holding biomass, and 4) condensation unit to collect bio-oil.

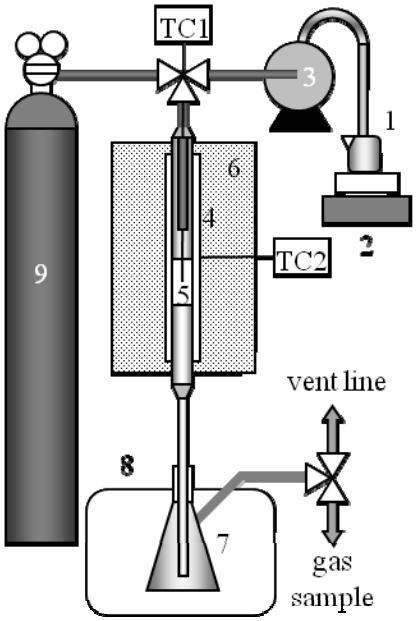

Figure 7.2. Reactor setup showing 1) bio-oil vessel, 2) hot plate, 3) peristaltic pump, 4) stainless steel reactor with oil preheat zone, 5) catalyst bed, 6) tube furnace, 7) collection flask, 8) ice bath, 9) compressed N_2 tank and thermocouples (TC1 and TC2).

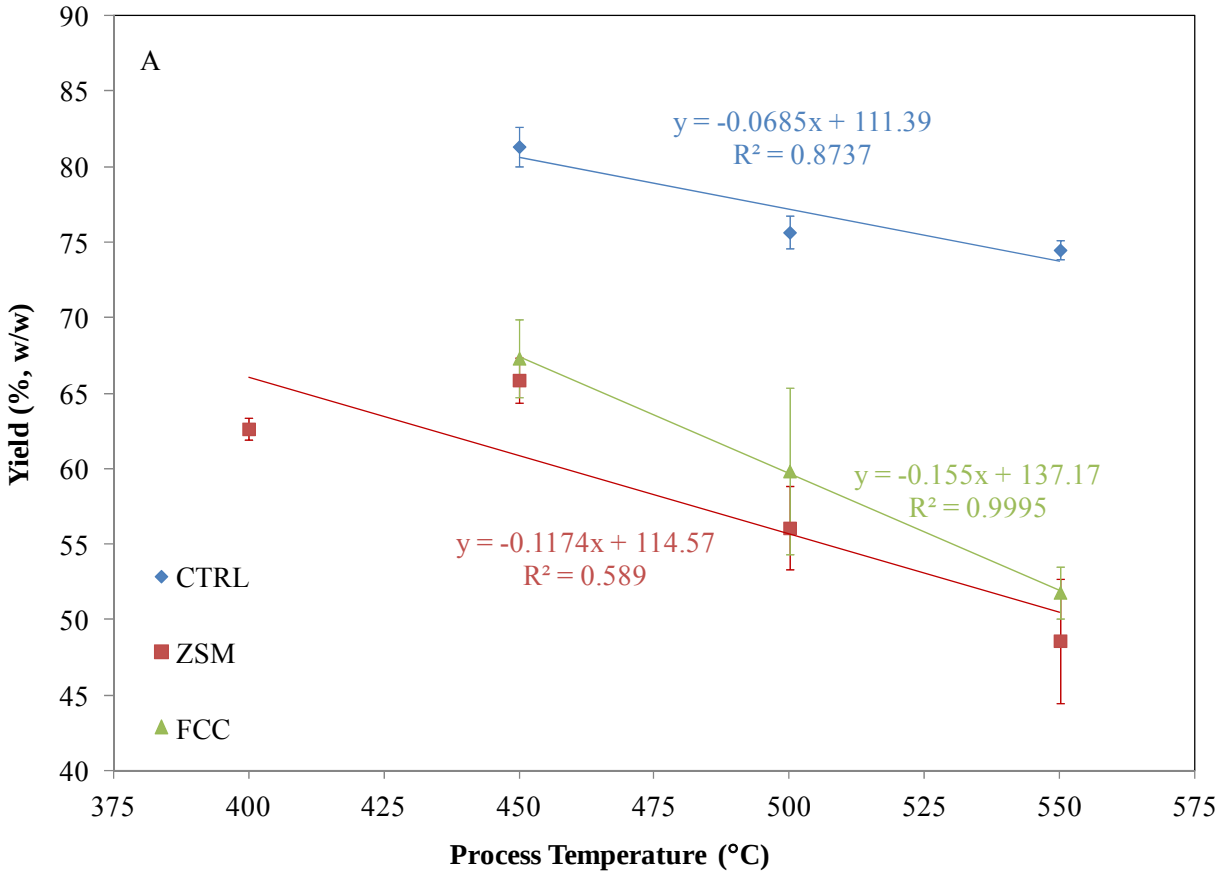
A
y = -0.0685x + 111.39
R² = 0.8737
y = -0.155x + 137.17
R² = 0.9995
y = -0.1174x + 114.57
R² = 0.589
CTRL
ZSM
FCC
Yield (%, w/w)
Process Temperature (°C)
90
85
80
75
70
65
60
55
50
45
40
375
400
425
450
475
500
525
550
575

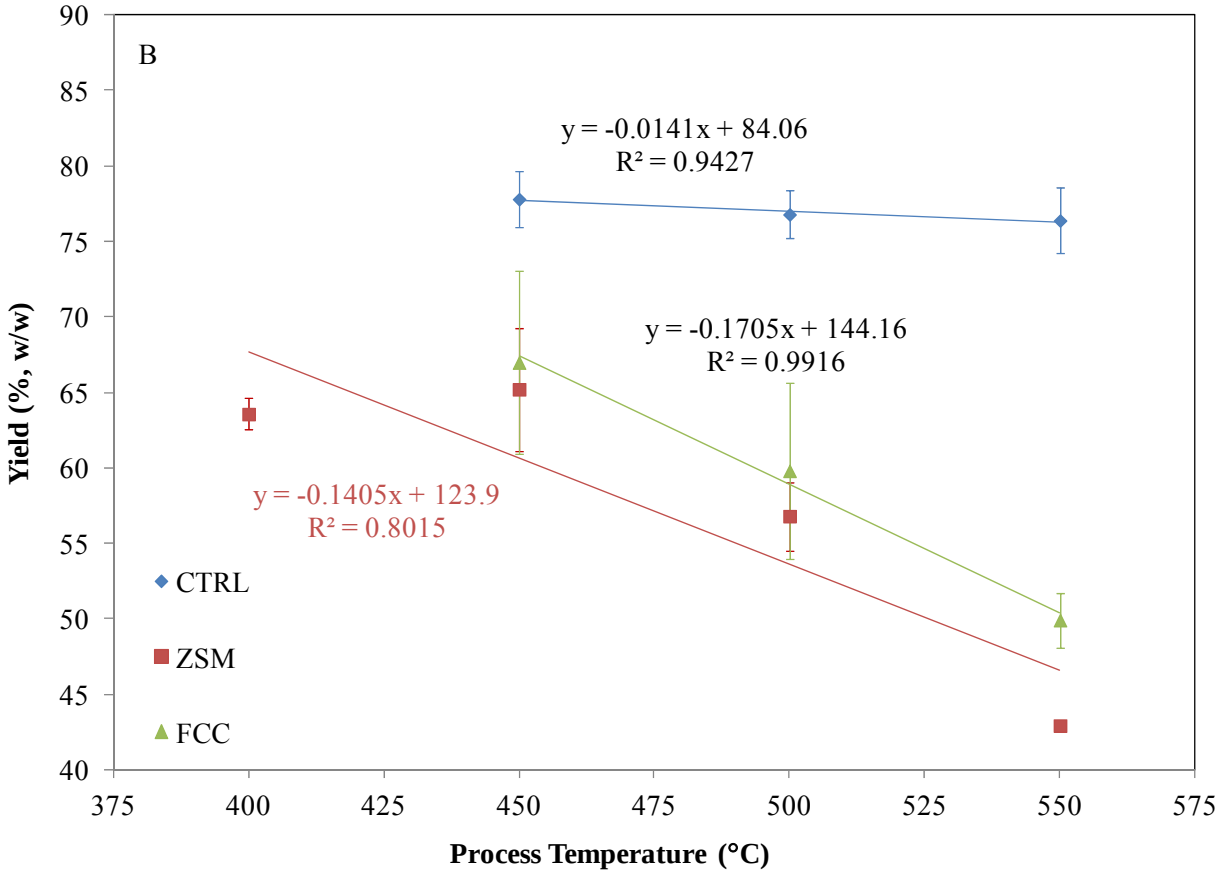

Figure 7.3. Yield of liquid product from the catalytic cracking of A) PH and B) PP bio-oil at 400-550 °C.

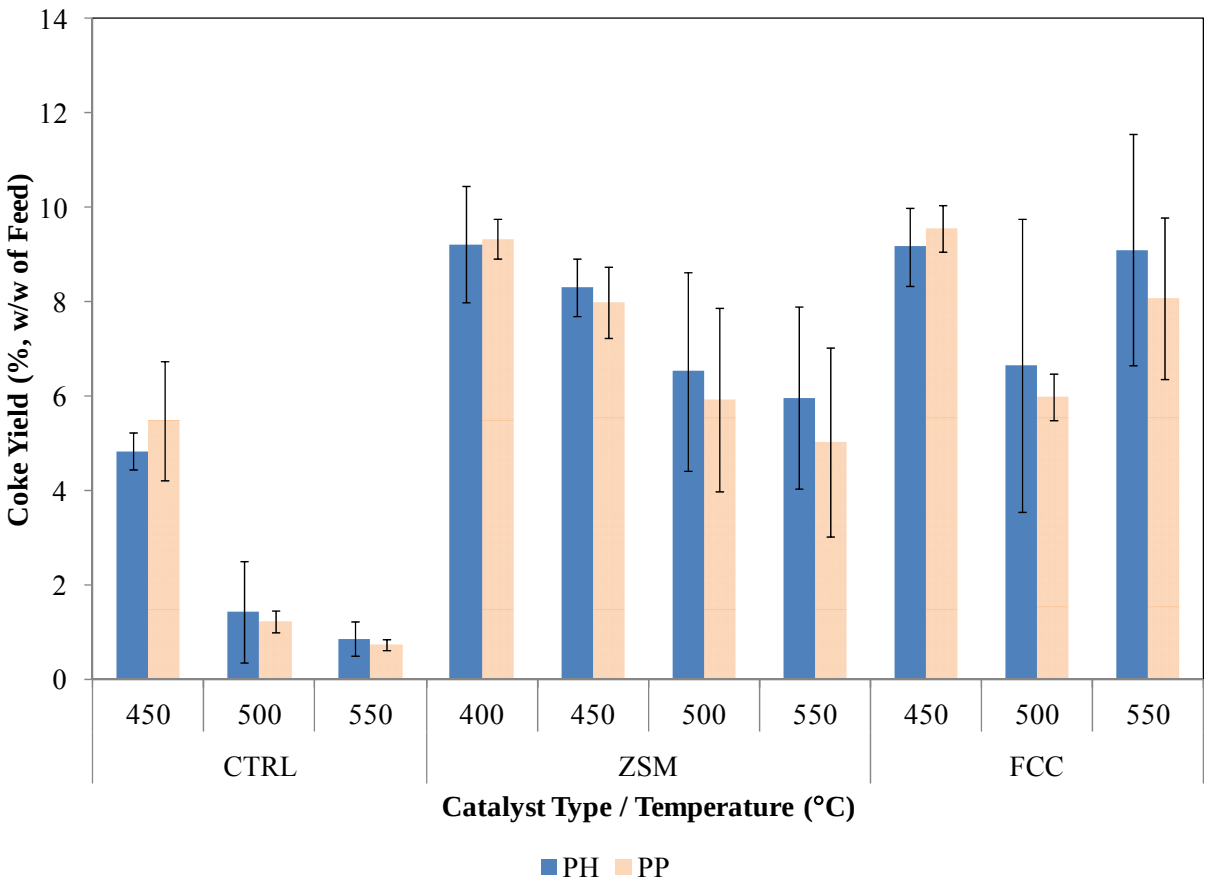

Figure 7.4. Yield of catalyst coke for PH and PP bio-oils catalytically cracked at 400-550 °C over HZSM-5 or FCC catalyst.

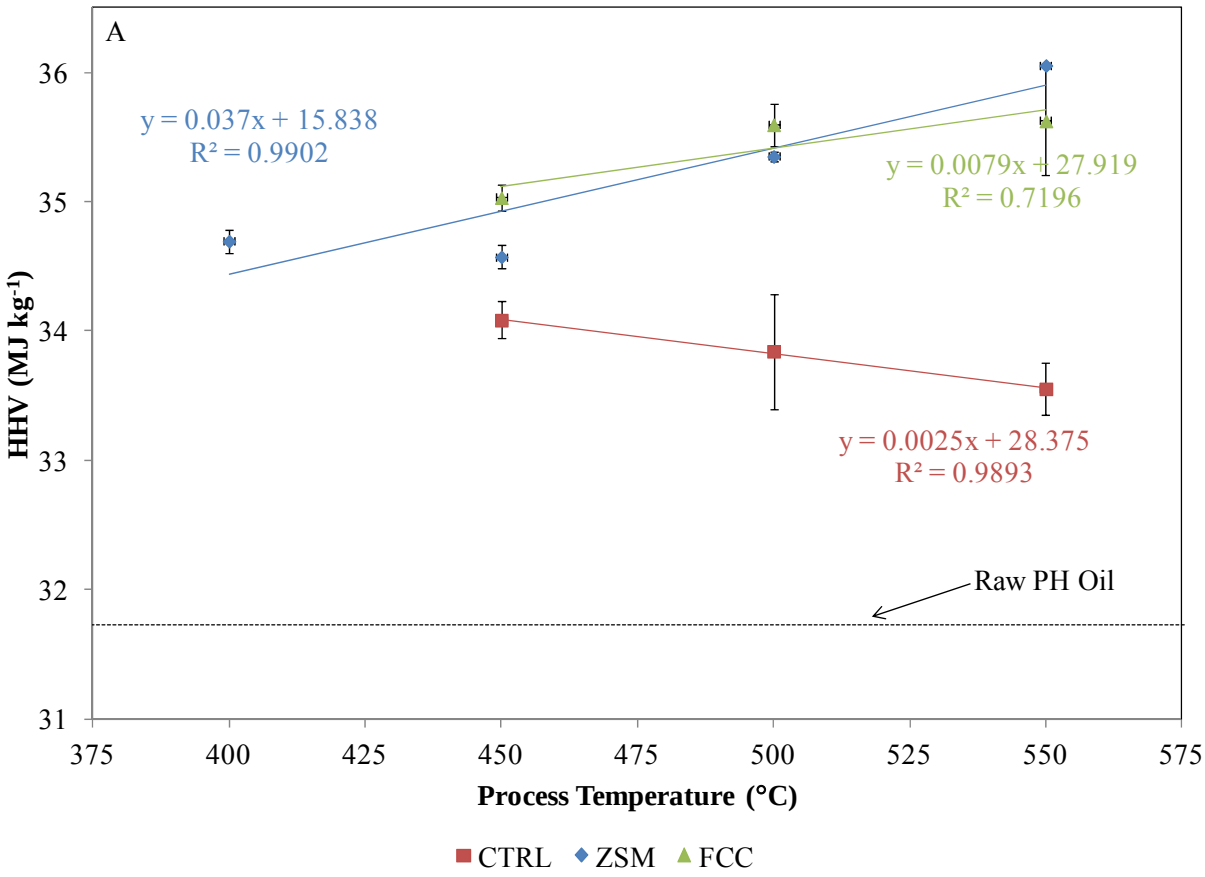
A
y = 0.037x + 15.838
R² = 0.9902
y = 0.0079x + 27.919
R² = 0.7196
y = 0.0025x + 28.375
R² = 0.9893
Raw PH Oil
HHV (MJ kg-1)
Process Temperature (°C)
CTRL
ZSM
FCC

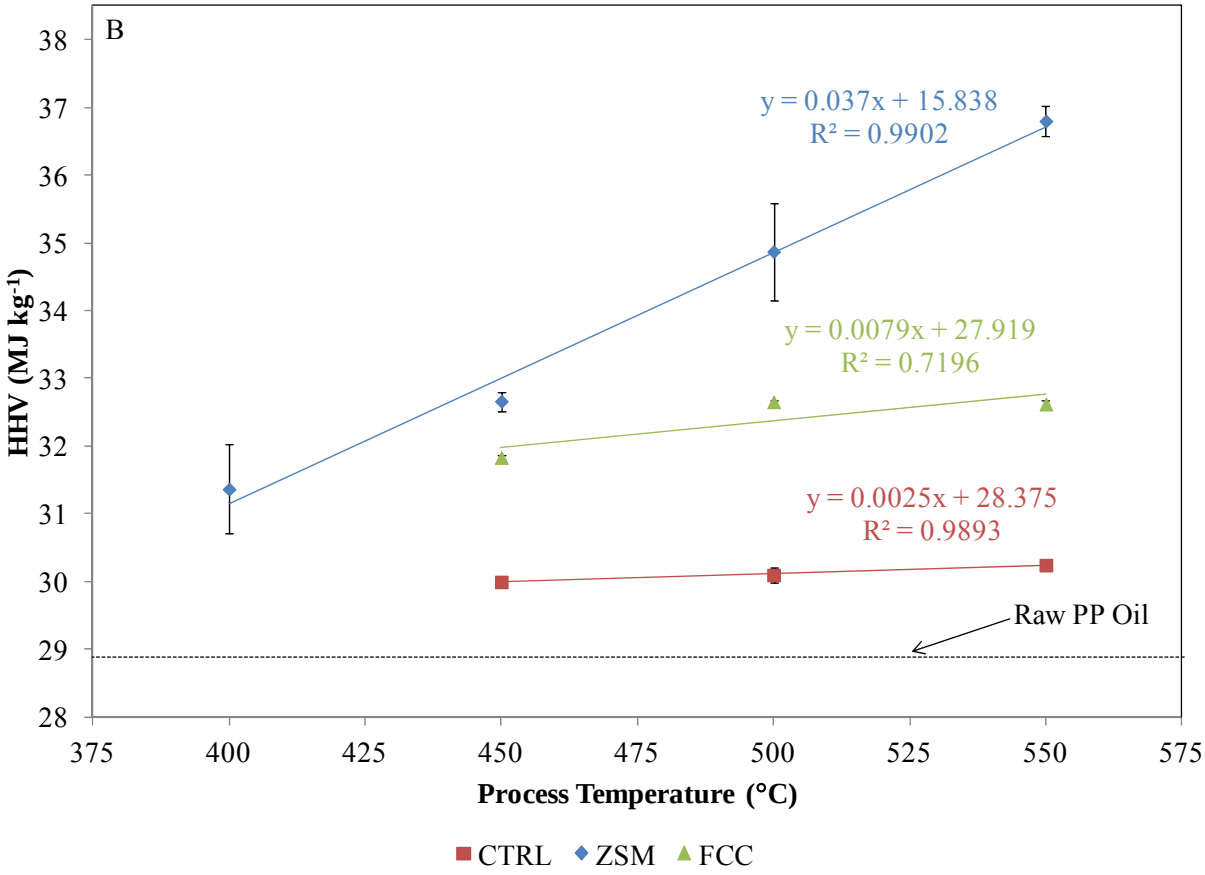

Figure 7.5. Higher heating values for A) PH and B) PP bio-oils processed at catalytic cracking temperatures between 400 and 550 °C.

CHAPTER 8

PRELIMINARY INVESTIGATION ON CATALYTIC UPGRADING OF BIO-OIL GENERATED FROM TORREFIED BIOMASS[7]

[7] Hilten, R., Speir, R., Kastner, J., Mani, S., Das, K.C. Submitted to *Biomass Conversion and Biorefinery*, 02/21/2012.

Abstract

In an effort to improve yield and quality of catalytically upgraded pyrolysis oil, biomass was thermally pre-treated (torrefied) at 275 ºC prior to slow pyrolysis. Torrefaction of biomass removes major coke precursors including organic acids (e.g. acetic acid, formic acid), aldehydes (e.g. acetaldehyde, formaldehyde) and furfural and resulted in a cleaner feedstock for pyrolysis. In this study, pyrolysis was performed at a low heating rate (8 °C min^{-1}) to a final temperature of 500 °C. Bio-oils were catalytically cracked by re-vaporizing them and passing them through a tubular reactor across a packed-bed of zeolite, HZSM-5, maintained at 450 °C at a WHSV at 10.8 h^{-1}. For catalytically cracked oils, acidity as measured by pH was significantly improved, increasing from 3.2 to 3.5 as a result of torrefaction pretreatment, and elemental oxygen content was reduced from 18.4 to 18 %. In addition, torrefaction pretreatment resulted in reduced catalyst coking during the catalytic cracking process, although reactor char (solid material on reactor walls) was increased. Compositionally, a variety of changes were observed as a result of torrefaction. Although trends were unclear for most compounds, torrefaction clearly increased the number of potential gasoline additives including branched aromatics (e.g. m-xylene, mesitylene, cyclopropylbenzene, 1-propynylbenzene, 1,4-diethylbenzene) in catalytically cracked bio-oil.

KEYWORDS: torrefaction, pyrolysis, catalytic cracking, HZSM-5, BTEX, biofuel

Introduction

Currently, pyrolysis oil, or bio-oil, derived from lignocellulosic feedstock cannot be used directly to fuel internal combustion engines without extensive upgrading. High oxygen content components including alcohols, ketones, and aldehydes lower the heating value, increase corrosivity, and reduce thermal stability in bio-oils compared to hydrocarbon fuels (Chiaramonti et al., 2007; Czernik and Bridgwater, 2004). Catalytic hydrotreatment and zeolite catalytic upgrading are often used separately or in conjunction to convert oxygenated bio-oils into hydrocarbons.

During hydrotreating, bio-oil is contacted with large quantities of hydrogen at high pressure (> 5 MPa) which makes the process expensive and difficult to scale-up. Hydrotreating bio-oil in the presence of a variety of catalysts has been successfully shown to reduce oxygen content in the product oils in many studies (Elliot et al., 1984; Sheu et al., 1988; Elliot, 1996). Elliot (1996) showed using a two step hydrotreating process at a pressure of 21 MPa with consecutive processes at 150-200 and 300-400 °C could effectively drive complete deoxygenation of the product oil. However, technoeconomic analyses have shown that costs for the hydrotreating process, particularly the cost for H_2 and catalyst, are prohibitively high (Mahfud, 2007).

Alternately, catalytic cracking is another process shown to greatly improve the quality of pyrolysis oils generated from high oxygen content feedstocks including rice husks, rice straw (Chen et al., 2003), pine wood (Carlson et al., 2011; Chen et al., 2003; Valle et al., 2007), maple wood (Adjaye and Bakhshi, 1995a; Adjaye and Bakhshi, 1995b), poplar wood (Lu et al., 2010) and many others. The cracking process was developed by the petroleum industry to deoxygenate and crack heavy petroleum crude oil feedstock to predominantly gasoline and other light hydrocarbons (Corma et al., 2007). The catalysts generally used for treating biomass-derived oils during catalytic cracking are acidic zeolites that hydrogenate oxygenates and act as molecular sieves to impact the range of molecule size and shape in the end-product. Catalytic upgrading of pyrolysis oils using the petroleum process with zeolite catalysts can be very effective, although catalyst coking is a major issue, and resolving the catalyst coking issue is a major research goal (Corma et al., 2007; Valle et al., 2007; Elliott et al., 1996). Adjaye and Bakhshi (1995a, 1995b) attempted to catalytically crack fast pyrolysis bio-oil with five different catalysts (ZSM-5, H-Y-zeolite, H-mordenite, silicalite, and silica-alumina). Yield of organic liquid product was highest with ZSM-5 (34 % w/w of feed) although coke yield was as high as 29 %. If coking could be reduced, catalytic upgrading could become a viable method to produce hydrocarbon fuels from lignocellulosic feedstocks able to power internal combustion engines.

One potential way to minimize coke formation on zeolite catalysts is to remove coke precursors from the oil prior to upgrading. Compounds that are thought to promote coke formation include

aldehydes, oxyphenols, furfural, and lignin-derived oligomers (Gayubo et al., 2005; Lu et al., 2010). Other studies (Gagnon et al., 1988; Laurent and Delmon, 1994a; Centeno et al., 1995; Wildschut et al., 2009) have indicated that the carbohydrate fraction is a major contributor to coke formation. There is currently very little research that attempts to remove coke precursors from bio-oil prior to upgrading. Pretreatment of biomass by torrefaction prior to pyrolysis could conceivably remove coke precursors from bio-oil prior to upgrading and thus reduce coke formation and improve bio-oil quality.

Biomass torrefaction is a low temperature pyrolysis process, similar to coffee roasting, in which the biomass is heated in an inert environment (N_2) from ~200-275 °C. Torrefaction generates a hydrophobic, friable solid biomass that requires less energy for grinding relative to untorrefied biomass (Phanphanich and Mani, 2010). Torrefied biomass has lower elemental oxygen content (CO, H_2O, and CO_2 are emitted during torrefaction) compared to untreated biomass, and torrefaction drives off a fraction of reactive and acidic intermediate components , such as acetic acid, furfural, and acetaldehyde (Phanphanich and Mani, 2010; Mani et al., 2009). Although some of these reactive gases generate coke on acid catalysts, leading to deactivation (Gayubo et al., 2004a, Gayubo et al., 2005), and that the NSF/DOE Roadmap (2008, p. 44) has indicated that the impact of torrefaction on thermochemical processing should be investigated, to date no research has been performed to determine the effect of torrefaction as a pretreatment for pyrolysis and catalytic cracking of biomass. Torrefaction, when coupled with pyrolysis and catalytic cracking, could provide synergistic effects not realized with drying and/or catalytic treatment alone.

Torrefaction effectively dries the biomass and decomposes hemicellulose. Several hemicellulose-derived compounds that are thought to produce coke in the subsequent upgrading step, such as acetyl groups that form acetic acid, would be effectively removed via torrefaction. Reactions of the acetic acid component during subsequent catalytic upgrading of the bio-oil can lead to severe catalyst coking. In addition, after upgrading, some acetic acid is left unreacted, and thus, the acid ends up in the product causing high acidity (low pH). As such, it was proposed that a hemicellulose-depleted feedstock would result in a pyrolysis oil containing less acetic acid resulting in less coke formation during subsequent

catalytic upgrading. The main objective of this study was to investigate the catalytic upgrading of pyrolysis bio-oil generated from torrefied wood pellets in an effort to improve the quality of upgraded pyrolysis bio-oil.

Methods and Materials

Biomass used during the experiments was in the form of pelletized pine (PP-BM). Bio-oil was produced in three ways including a one-, two- and a three-step process. Steps included biomass pretreatment (torrefaction), pyrolysis, and catalytic cracking. Fig. 8.1 provides details for the processes and products generated.

The one-step process involved subjecting untreated PP-BM to pyrolysis at an end temperature of 500 °C in the reactor shown in Fig. 8.2. The batch reactors shown in Fig. 8.2 had dimensions, 20 H x 20 W x 20 D cm, with two 1.3 cm ports for the introduction of inert gas and the removal of evolved gases and vapors. A low heating rate (8 °C min^{-1}) was used, and evolved vapors were condensed with ice bath vapor condensation. The two-phase liquid obtained was separated in a separatory funnel, and the heavier lower phase was considered the product and was collected and assessed for initial quality and long-term stability.

The two-step process was based on a conventional bio-oil production and upgrading scheme. Bio-oil was generated by pyrolysis, and the liquid was collected and phase-separated using a separatory funnel. The aforementioned lower, heavy phase was used in upgrading experiments. An uncoupled catalytic cracking process was used in the second step during which previously-generated bio-oil was re-vaporized and injected at 1.5 mL min^{-1} along with 100 mL min^{-1} inert carrier gas (N_2, minimum purity=99.6%, typical purity=99.99%) into a 2.21 cm I.D. reactor (L=38 cm) containing a fixed bed of HZSM-5 zeolite catalyst (10 g bed weight, WHSV=10.8 h^{-1}). The reactor was maintained at 450 °C using input from a thermocouple centrally-located in the catalyst bed.

The catalyst, HZSM-5, was produced by calcining NH_4-ZSM-5 (Zeolyst International, CBV 5524 G) at 550 ˚C for 4 h in air to produce the hydrogen form, H-ZSM-5, resulting in stronger acid pore sites. The pH was measured by mixing catalyst in water at a 50:50 ratio and then measuring the pH of the water

using a standard pH probe. As a result of the calcining process, the pH was reduced from 4.98 to 3.06. The NH_4-ZSM-5 catalyst was received from the manufacturer as a fine powder. To minimize the pressure drop across the catalyst bed, the catalyst was granulated by mixing with water, drying, crumbling, and sieving to the desired size, ~ 2-5 mm. The catalyst powder had published values of 425 m^2 g^{-1}, 5 μm, and 50 for surface area, particle size and SiO_2/Al_2O_3 ratio, respectively. In-house measurements of the catalyst surface characteristics were accomplished using a Quantachrome surface area analyzer that indicated a surface area of 345 m^2 g^{-1}, pore radius at 10.81 Å, and pore volume at 0.1851 cm^3 g^{-1} for fresh catalyst after calcination, drying, and granulation.

The three-step process added torrefaction as a biomass pretreatment step. Torrefaction was performed at 275 °C, a commonly-used temperature for the removal of hemicellulose, in the same reactor as that used for pyrolysis (see Fig. 8.2). After torrefaction, the resulting torrefied biomass ("PP T275") was characterized and then subjected to pyrolysis at 500 °C. The resulting condensable bio-oil was then catalytically cracked as previously described.

In all, four bio-oil (BO) types were produced and were labeled P-BO (Pyrolysis Bio-Oil), PU-BO (Pyrolysis + catalytic Upgrading), TP-BO (Torrefaction + Pyrolysis), and TPU-BO (Torrefaction + Pyrolysis + catalytic Upgrading). Fig. 8.1 shows the materials produced at each step. Bio-oil produced by the one-step process, P-BO, was used as a control to compare to the various treatments.

The yield of liquid for each step including torrefaction, pyrolysis and catalytic cracking was determined as the weight change of the collection vessel. Phase yield, oily and aqueous, was determined by weighing separatory funnel-separated fractions. The total yield of catalytic cracking byproducts including tar, catalyst coke, and reactor char was quantified by measuring the change in weight of the reactor. The yield of individual byproduct components was also quantified. Tar was considered to be the acetone-soluble material adhered to the catalyst and was quantified by washing the catalyst with acetone after catalytic runs, drying the catalyst, and measuring the change in mass. Catalyst coke formation was determined by heating the catalyst under a flow of oxygen in a thermogravimetric analyzer (TGA). The

change in mass of catalyst was assumed to be due to the complete combustion of coke. The weight of reactor char was then determined as the difference between reactor weight change and coke and tar yield.

Solid materials including biomass, torrefied biomass and pyrolysis char were subsampled and analyzed. Other solids generated during catalytic cracking including reactor char, catalyst coke, and tar were not analyzed compositionally, only quantified. Yield of non-condensable gas was determined by difference.

Feedstock and products were analyzed by an assortment of methods. Biomass feedstock was analyzed for gross calorimetric value (HHV), proximate composition (moisture, volatiles, ash and fixed carbon), and elemental composition (CHNS-O). The initial quality of bio-oils was assessed by measuring HHV, water content (by Karl Fischer titration), pH, CHNS-O, specific gravity and chemical composition (GC-MS).

Results and Discussion

Table 8.1 shows the yield of products from each of the processes shown in Fig. 8.1. Characteristics for untreated and treated (by torrefaction) biomass are shown in Table 8.2. Results show that as torrefaction treatment temperature increases, so does fixed carbon, elemental carbon, and HHV. Concurrently, oxygen content and volatile content reduces with increasing treatment temperature. Volatile content is a good indicator of bio-oil yield, so as pretreatment temperature increases, the yield of bio-oil after pyrolysis decreases (see Table 8.3). However by reducing oxygen content in the treated material, the oxygen content should also be lower in the bio-oil product. As seen in Table 8.4, oxygen content in the product is indeed reduced as a result of torrefaction pretreatment.

Byproduct (i.e. coke, char, and tar) quantification is shown in Table 8.3. Catalyst coke and upgraded bio-oil yield from torrefied feedstock were significantly reduced relative to non-torrefied feedstock-derived oil. However, reactor char and noncondensable gas yields were significantly higher for torrefied feedstock-derived bio-oil.

Fuel property effects

In Table 8.4, results are shown for the characterization of various bio-oils produced by one-, two-, and three-step processes. For all treatments, the oxygen content in bio-oil is reduced compared to the one-step control process (i.e. pyrolysis only) represented by sample, P. It is clear that catalytic upgrading improves the quality of bio-oil generated by both pyrolysis and by torrefaction plus pyrolysis processes. HHV, carbon content, and pH are increased, and oxygen content is reduced. Furthermore, HHV is increased despite an increase in water content for both catalytically upgraded bio-oils. A key improvement for bio-oils generated by first pretreating biomass using torrefaction is the significant increase in pH. Multiple comparisons were made between pH values as a function of treatment using a Tukey HSD multiple comparisons test. The Tukey test indicates that all comparisons of pH among treatments show that differences are statistically significant at $\alpha = 0.05$ except for the comparison between the pH values for TP and TPU which are not statistically different. Most notably, TP and TPU oils had significantly higher pH when compared to their respective non-torrefied oils, P and PU, as hypothesized.

Compositional changes

Fig. 8.4 through Fig. 8.7 show typical GC spectra and MS-matched compounds for TP, TPU, P and PU bio-oils from 2-33 minute retention times. Although many peaks are identifiable, comparing differences between oils is difficult since few compounds occur in high concentration. Although peaks at retention times less than 10 min are similar for each of the four bio-oil products, several notable exceptions are evident. Table 8.5 indicates some of the major compositional differences between oils produced by the various processes. The first notable difference in bio-oil composition is the existence of 2-methylfuran (C_5H_6O) in both the catalytically upgraded samples (TPU and PU) in the 2-5 minute retention time range (Fig. 8.4) and not in P or PU. Another noticeable difference in the oils is the presence of tetrahydrofuran (THF, $[CH_2]_4O$) in the non-torrefied bio-oils but not in the torrefied. The next exception is the existence of acetic acid (CH_3COOH) in both the torrefied bio-oils (TP and TPU) at 2.3-2.5 min whereas no acetic acid is identified in either non-torrefied bio-oil. The existence of acetic acid in the non-torrefied oils is contrary to our hypothesis. We expected that acetic acid would be

removed by the torrefaction process (i.e. the removal of hemicellulose). The fact that acetic acid was increased indicates that its formation is a result of the thermal degradation of biomass components other than hemicellulose. Also, benzene (C_6H_6) appears in all samples except TP. Propanoic acid appears in TP and TPU as very small peaks. In the 5-10 minute range, the most notable difference is that for torrefied bio-oils, furfural ($C_5H_4O_2$) is not evident, whereas, in non-torrefied bio-oils (P and PU), there is a pronounced peak identified as furfural at about 5.2 min. At approximately 6.2 min, a large peak representing m-xylene (1,3-dimethylbenzene) appears in TPU with a very small peak in P, but not in TP or PU.

Above 10 min, many compounds are evident and comparison is difficult. However, it is clear that the torrefaction pretreatment affects the formation of lignin-derived phenolic compounds including creosol, eugenol, dihydroeugenol, and isoeugenol. These phenolic compounds likely have been degraded to form the benzene derivatives (peaks 71, 103, 120, 122-124) that appear in TPU and not in the other treatments. These benzene derivatives in addition to toluene and xylene are customary reaction products for pyrolysis oils that have been catalytically cracked with HZSM-5. These can also be used as high octane, gasoline additives.

Conclusions

Torrefaction has been proposed as a means to improve biomass quality so that processing and quality of end products from thermochemical conversion could be improved. The process was improved in some ways, but worsened in others. For example, the amount of catalyst coke was significantly reduced for the upgrading of the TP bio-oil. However, reactor char was significantly increased as was the yield of permanent gases. As such, the yield of condensable oil relative to original biomass was reduced when torrefied biomass-derived bio-oil was catalytically upgraded.

In this study, the pH of bio-oil intermediate (after torrefaction but before catalytic cracking) and bio-oil end product was significantly increased indicating a substantial improvement in quality. However, we had expected to see a complete disappearance of acetic acid. However, it is clear that not all the acetic

acid was converted to other constituents. Since acetic acid was not quantified specifically, it may be that acetic acid was significantly reduced in concentration.

Fuel properties were similar between pyrolysis oils from torrefied biomass and untreated biomass (P and TP), and from both bio-oils after catalytic cracking (PU and TPU). Catalytic cracking for both P and TP bio-oil increased heating value and reduced oxygen content significantly. Oxygen content was lowest for the TPU bio-oil indicating a substantial improvement, certainly over non-catalytically cracked oil (P and TP), but also over bio-oil derived from non-torrefied biomass that was subsequently upgraded (PU).

Acknowledgements

This work was supported by a United States Department of Energy Biorefinery Grant. We thank Andrew Smola and Joby Miller for their work to analyze materials.

References

Chiaramonti, D., Oasmaa, A., Salantausta, Y., 2007. Power Generation Using Fast Pyrolysis Liquids from Biomass. Renew. Sust. Energy Rev. 11, 1056-1086.

Czernik, S., Bridgwater, A.V., 2004. Overview of Applications of Biomass Fast Pyrolysis Oil. Energy Fuels 18, 590-598.

Lu, Q., Zhang, Y., Tang, Z., Li, W., Zhu, X., 2010. Catalytic upgrading of biomass fast pyrolysis vapors with titania and zirconia/titania based catalysts. Fuel 89, 2096-2103.

Sheu, Y., Anthony, R., Soltes, E., 1988. Fuel Processing Technology 19, 31-50.

Elliott, D., Baker, E., 1984. Upgrading Biomass Liquefaction Products through Hydrodeoxygenation. Biotechnology and Bioengineering Symp. 14, 159-174.

D. C. Elliott, G. G. N. In Developments in Thermochemical Biomass Conversion; Boocock, A. V. B. a. D. G. B., Ed.; Blackie Academic & Professional, 1996, pp. 611-621.

Mahfud, F., 2007. Exploratory studies on fast pyrolysis oil upgrading. Ph.D. dissertation, University of Groningen.

Corma, A., Huber, G., Sauvanaud, L., O'Connor, P., 2007. Processing biomass-derived oxygenates in the oil refinery: Catalytic cracking (FCC) reaction pathways and role of catalyst. Journal of Catalysis 247, 302-327.

Gayubo, A.G., Aguayo, A.T., Atutxa, A., Valle, B., Bilbao, J., 2005. Undesired components in the transformation of biomass pyrolysis oil into hydrocarbons on an HZSM-5 zeolite catalyst. Journal of Chemical Technology and Biotechnology 80, 1244-1251.

Valle, B., Gayubo, A., Atutxa, A., Alonso, A., Bilbao, J., 2007. Integration of thermal treatment and catalytic transformation for upgrading biomass pyrolysis oil. International Journal of Chemical Reactor Engineering 5, A86.

Elliott, D. C.; Neuenschwander, G. G., 1996. Liquid Fuels by Low-Severity Hydrotreating of Biocrude, in: Bridgwater, A. V., Boocock, D. G. B. (Eds.), Developments in Thermochemical Biomass Conversion. Blackie Academic & Professional, London, Vol. 1, p. 611.

Adjaye, J., Bakhshi, N., 1995a. Production of hydrocarbons by catalytic upgrading of a fast pyrolysis bio-oil. Part II: Comparative catalyst performance and reaction pathways. Fuel Processing Technology 45, 185-202.

Adjaye, J., Bakhshi, N., 2011. Production of hydrocarbons by catalytic upgrading of a fast pyrolysis bio-oil. Part I: Conversion over various catalysts. Fuel Processing Technology 45 (1995b): 161-183.

Phanphanich, M.; Mani, S. Impact of torrefaction on the grindability and fuel characteristics of forest biomass. Bioresource Technology 102, 1246–1253.

Mani, S.; Das, K.C.; Kastner, J.R., 2009. Development of biomass torrefaction technology to produce biocoal for electricity production. Final Report to State of Georgia, Traditional Industries Program.

Gayubo, A.G., Aguayo, A.T., Atutxa, A., Prieto, R., Bilbao, J. 2004. Deactivation of a HZSM-5 Zeolite Catalyst in the Transformation of the Aqueous Fraction of Biomass Pyrolysis Oil into Hydrocarbons. Energy and Fuels 18, 1640-1647.

NSF, 2008. Breaking the Chemical and Engineering Barriers to Lignocellulosic Biofuels: Next Generation Hydrocarbon Biorefineries. Ed.George W. Huber, University of Massachusetts Amherst. National Science Foundation, Chemical, Bioengineering, Environmental, and Transport Systems Division. Washington D.C. 180 p.

Figure Captions

Tables

Table 8.1. Yield of products from torrefaction (T), sequential torrefaction and pyrolysis (TP) and sequential torrefaction, pyrolysis and catalytic upgrading (TPU) processes.

Product	Yield (%, w/w)				
	T	P	TP	PU	TPU
solids	65.5	28.0	43.9	1.9[b]	4.2[b]
Non-condensable gas	15.5	26.4	21.6	8.7	14.3
BO[a]	19.0	45.8	34.5	81.2	78.4
oily (of BO)	0	20.0	28.9	86.3	90.5
oily (of feed)	0	9.2	9.4	62.8	69.0
oily (of BM)	0	22.9	22.6	14.4	15.6
aqu (of BO)	100	80.0	71.1	15.5	9.6

[a] Bio-oil

[b] Char material formed on the reactor walls.

Table 8.2. Characterization of solid fraction of untreated (BM), torrefied (T250, 300, and 350 °C), and pyrolyzed (P500 °C) pine pellet (PP) biomass.

Characteristic	Material Composition (%, w/w)				
	PP BM	PP T250	PP T300	PP T350	PP P500
C	52.6	53.9	73.2	78.0	82.5
H	5.7	5.3	4.7	3.7	2.6
N	0.2	0.1	0.2	0.2	0.2
S	0.0	0.1	0.1	0.1	0.0
O	38.9	37.6	19.6	15.0	4.4
Moisture	7.2	0.0	1.0	2.0	3.2
Volatiles	79.8	71.2	42.4	32.2	28.1
Ash	0.5	3.0	2.2	2.9	2.8
Fixed Carbon	19.7	25.8	55.4	64.9	69.1
HHV (MJ/kg)	20.6	20.9	28.8	29.7	31.0

Table 8.3. Yield of catalytic upgrading products.

Material	Yield (% of feed)			
	Reactor Char[a]	Catalyst Coke	Gases	Bio-oil
PU	1.9	8.1	8.7	81.2
TPU	4.2	3.0	14.3	78.4

[a] Material formed on the reactor walls.

Table 8.4. Characterization of bio-oils.

Parameter	Bio-Oil Characteristics			
	P[a]	PU[b]	TP[c]	TPU[d]
Ultimate analysis (%, w/w d.b.)				
C	69.6	73.1	71.3	73.9
H	7.65	8.1	7.97	7.93
N	0.74	0.4	0.19	0.17
S	0.05	0.0	0.01	0.02
O[e]	22.0	18.4	20.5	18.0
HHV (MJ kg^{-1}, w.b.)	29.1	30.9	28.6	30.7
H_2O (%, w/w w.b.)	2.4	4.0	9.3	6.7
pH	3.1	3.2	3.7	3.5

[a] P: Pyrolysis (catalytic upgrading feedstock, no torrefaction)
[b] PU: Pyrolysis + catalytic Upgrading (no torrefaction)
[c] TP: Torrefaction + Pyrolysis (catalytic upgrading feedstock)
[d] TPU: Torrefaction + Pyrolysis + catalytic Upgrading
[e] By difference.

Table 8.5. Major chemical compositional differences (an "X" indicates the component was identified). Peak numbers are in reference to Fig.s 2-5.

Component[a]	Chem. Form.	P	PU	TP	TPU	Peak No.	Retention Time
acetic acid	$C_2H_4O_2$		X	X	X	1	2-2.3
2-methyl-furan	C_5H_6O		X		X	5	2-2.1
tetrahydrofuran (THF)	C_4H_8O	X	X			7	2.2
benzene	C_6H_6	X	X		X	12	2.5
acetol	$C_3H_6O_2$			X	X	14	2.6
furfural	$C_5H_4O_2$	X	X			56	5.2
2-cyclopenten-1-one	C_5H_6O			X	X	60	5.3
furanmethanol	$C_5H_6O_2$	X	X	X		64, 65	5.7
m-xylene	C_8H_{10}				X	71	6-6.5
mesitylene	C_9H_{12}				X	103	8.8
cyclopropylbenzene	C_9H_{10}				X	120	9.6
1-propynylbenzene	C_9H_8				X	122	9.8
1,4-diethylbenzene	$C_{10}H_{14}$				X	123	9.9
1-methyl-3-propylbenzene	$C_{10}H_{14}$				X	124	9.9
creosol	$C_8H_{10}O_2$	X	X	X		157, 160-162	12.4-12.6
1,2-benzenediol	$C_6H_6O_2$			X	X	170	13
Eugenol	$C_{10}H_{12}O_2$	X	X	X		212	16.2
dihydroeugenol	$C_{10}H_{14}O_2$	X	X	X		217	15.6-15.8
isoeugenol	$C_{10}H_{12}O_2$	X		X		228	16.5-17.2

[a] Common names are used when available.

Figures

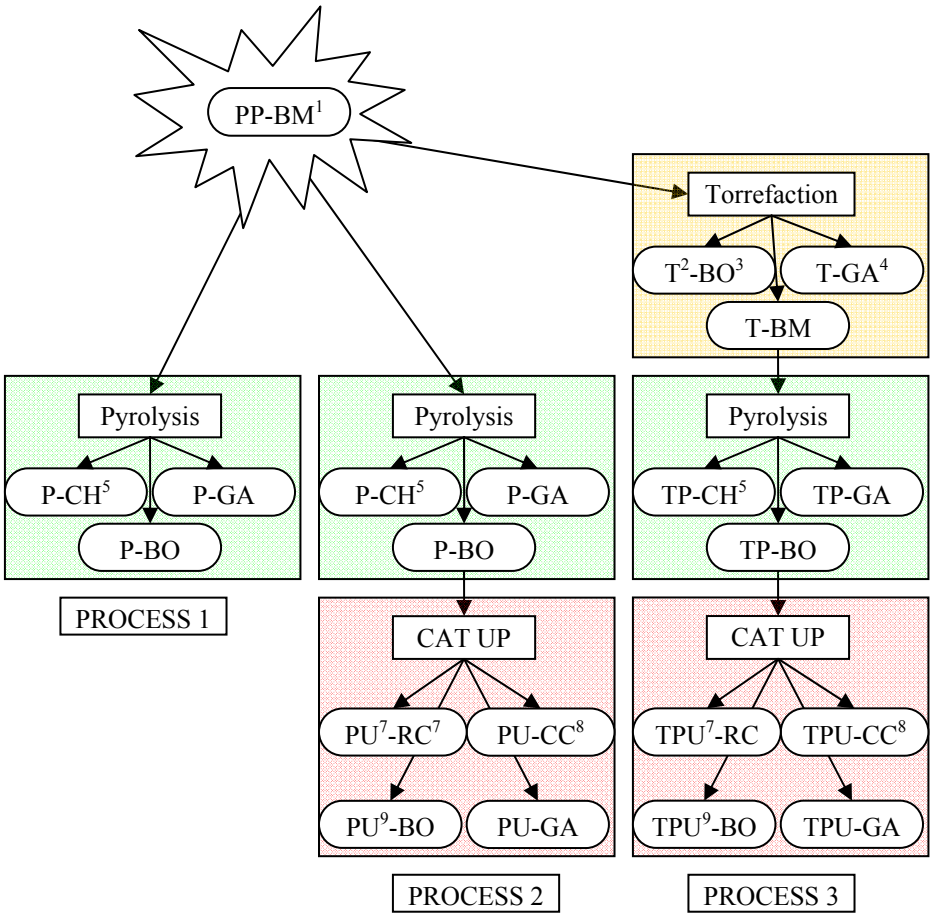

[1]BM ≡ biomass
[2]T ≡ torrefied
[3]BO ≡ bio-oil
[4]GA ≡ non-condensable gas
[5]CH ≡ char
[6]P ≡ pyrolyzed
[7]RC ≡ reactor char
[8]CC ≡ catalyst coke
[9]U ≡ upgraded

Figure 8.1. Products from torrefaction, pyrolysis and catalytic upgrading processes.

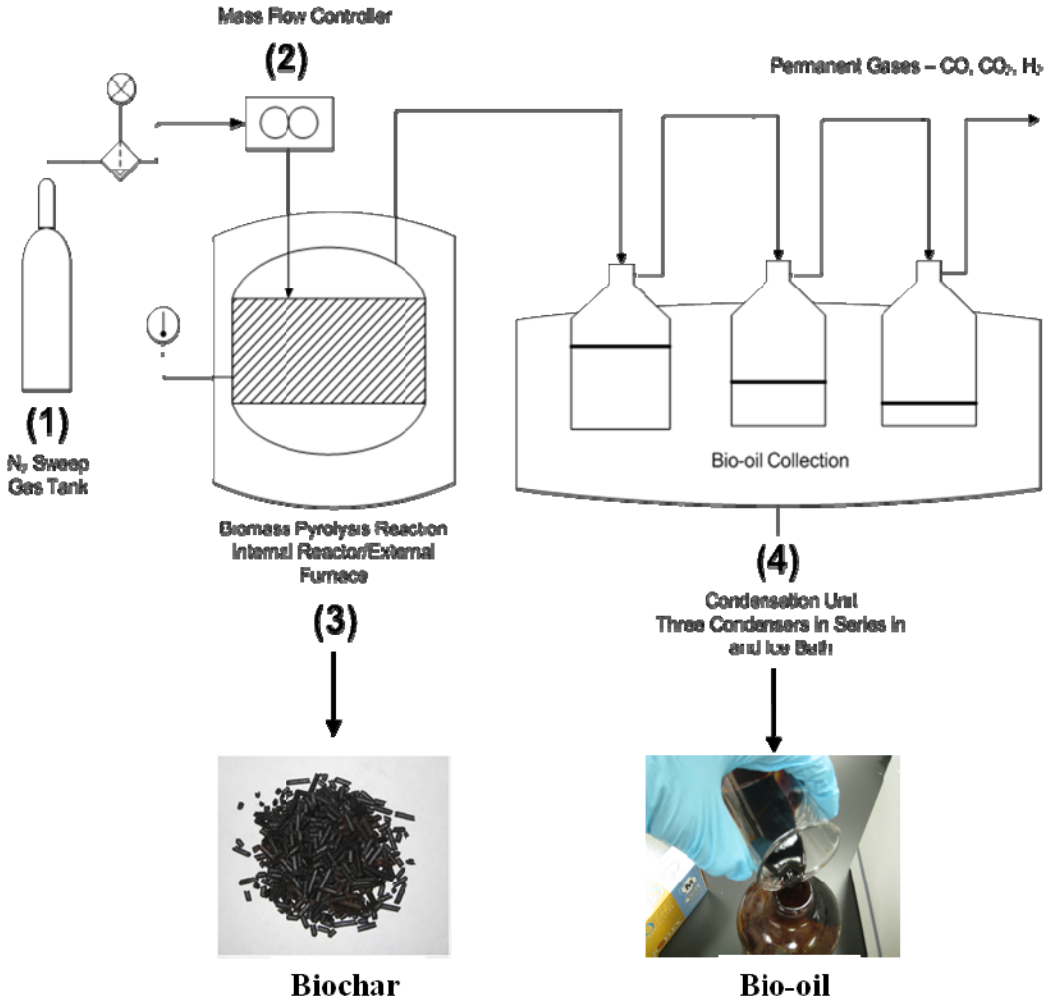

Figure 8.2. Batch pyrolysis unit used to generate biochar and bio-oil from peanut hulls – 1) Nitrogen sweep gas, 2) gas flow controller, 3) reactor holding biomass, and 4) condensation unit to collect bio-oil

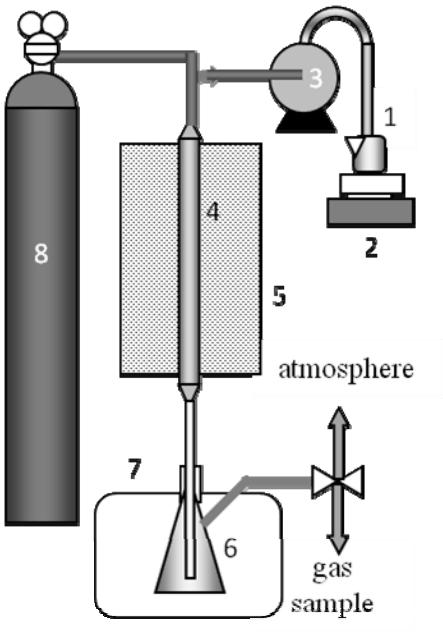

Figure 8.3. FCCU showing: 1) sample container, 2) sample preheater, 3) pump, 4) reactor, 5) furnace, 6) sample collector, 7) ice bath, and 8) inert gas source

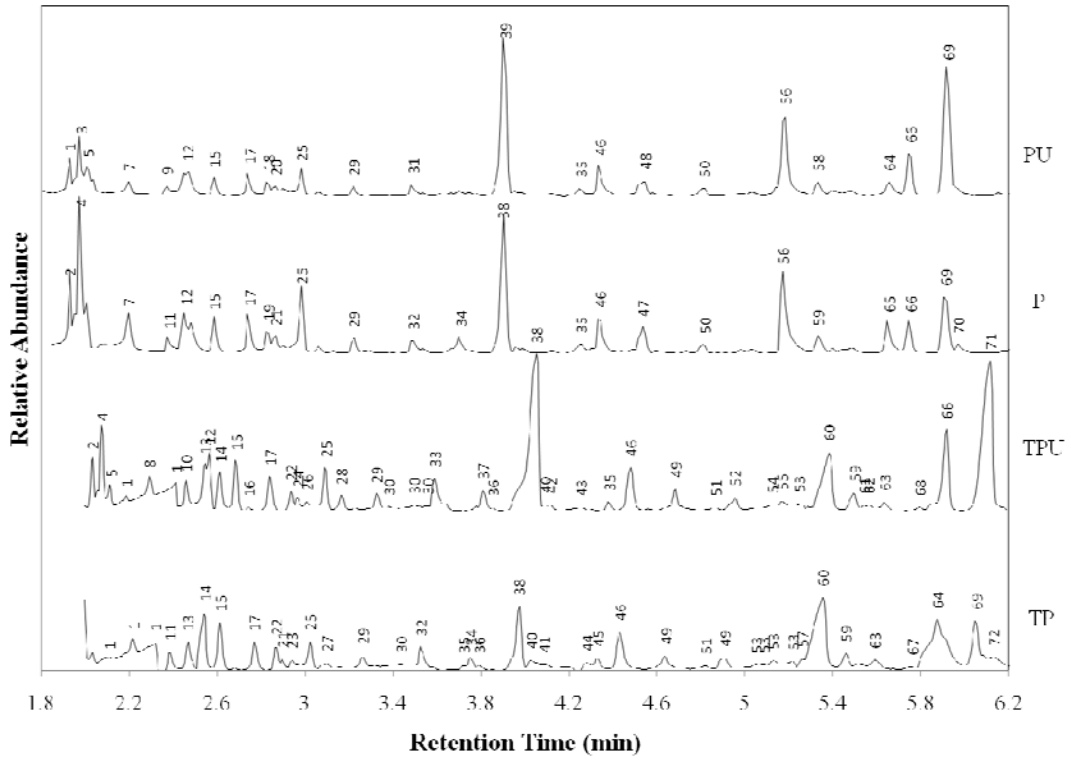

Figure 8.4. GC results from 2 to 6 minute retention time for bio-oils produced by torrefaction plus pyrolysis (TP), torrefaction plus pyrolysis plus catalytic upgrading (TPU), pyrolysis (P), and pyrolysis plus catalytic upgrading (PU).

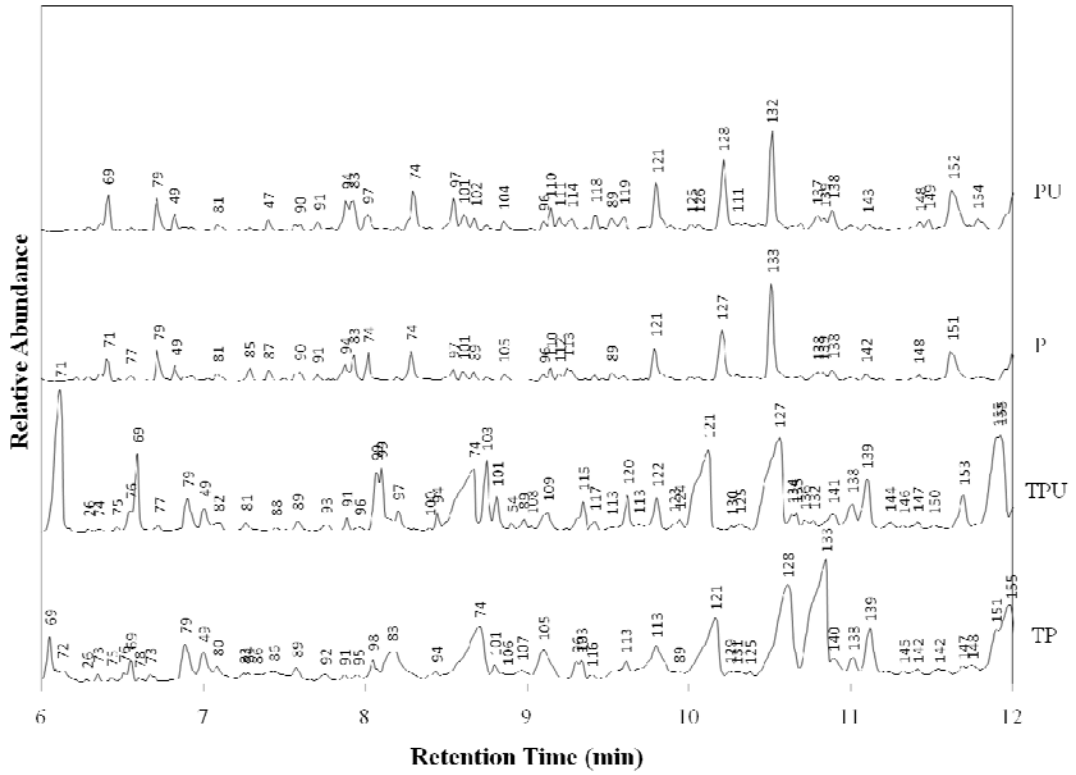

Figure 8.5. GC results from 6 to 12 minute retention time for bio-oils produced by torrefaction plus pyrolysis (TP), torrefaction plus pyrolysis plus catalytic upgrading (TPU), pyrolysis (P), and pyrolysis plus catalytic upgrading (PU).

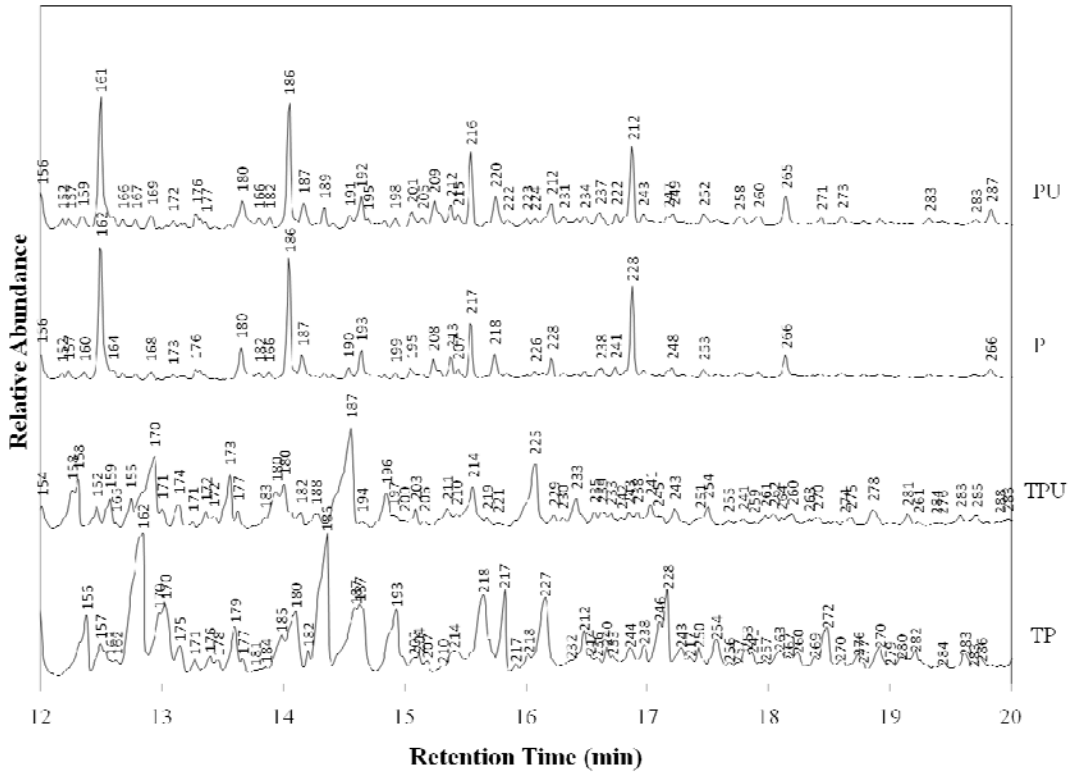

Figure 8.6. GC results from 12 to 20 minute retention time for bio-oils produced by torrefaction plus pyrolysis (TP), torrefaction plus pyrolysis plus catalytic upgrading (TPU), pyrolysis (P), and pyrolysis plus catalytic upgrading (PU).

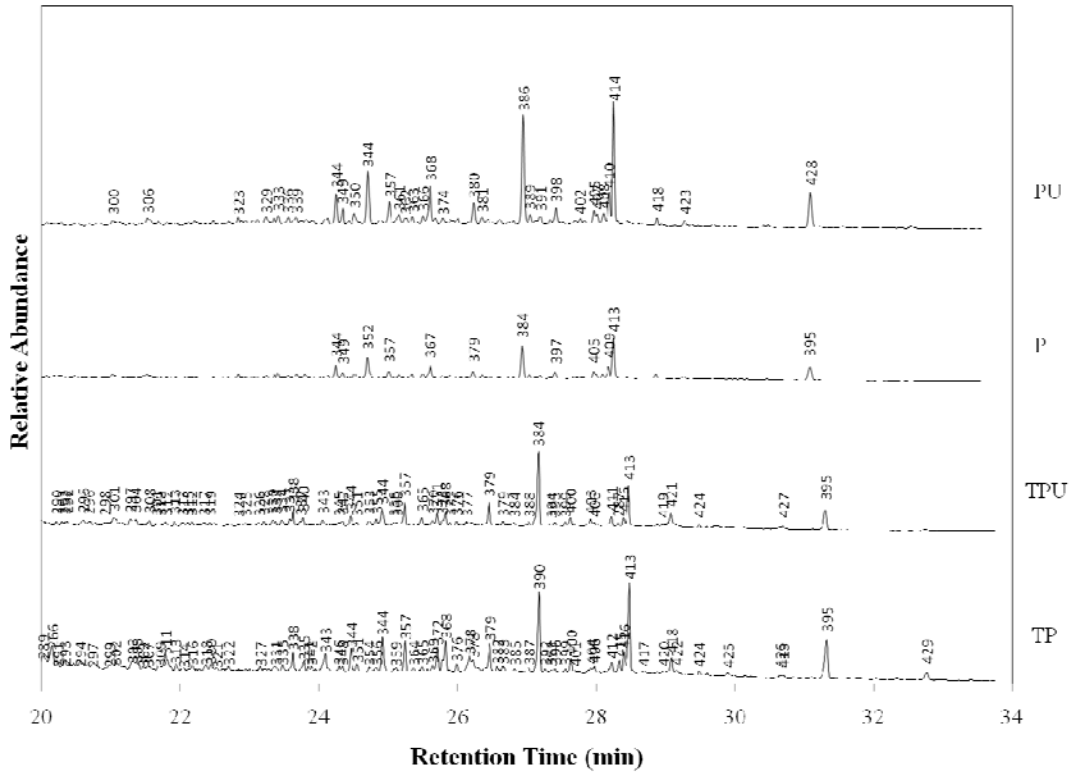

Figure 8.7. GC results from 20 to 34 minute retention time for bio-oils produced by torrefaction plus pyrolysis (TP), torrefaction plus pyrolysis plus catalytic upgrading (TPU), pyrolysis (P), and pyrolysis plus catalytic upgrading (PU).

CHAPTER 9

EFFECT OF TORREFACTION ON THE CATALYTIC CRACKING EFFECTIVENESS FOR FAST AND SLOW PYROLYSIS BIO-OIL[8]

[8] Hilten, R., Speir, R., Kastner, J., Mani, S., Das, K.C. To be submitted to *Bioresource Technology*.

Abstract

To improve processing and end product quality for fast and slow pyrolysis bio-oils, torrefaction pretreatment and secondary catalytic were attempted as a means to produce an improved biofuel. Pine chip biomass was pretreated by torrefaction at 225, 250 or 275 °C with a 20 minute hold time prior to pyrolysis (fast and slow) and catalytic cracking (at 400, 450, and 500 °C). Results indicated that torrefaction significantly reduced reactor char, catalyst coke, and catalyst tar during the catalytic upgrading process, and increased carbon content and HHV. Increasing pyrolysis heating rate from 0.13 to 100 C s^{-1} increased pyrolysis oil yield, and gas, coke, char, and BTEX yield and increased carbon content while reducing oil product yield and oxidative stability. Catalytic cracking significantly improved bio-oil yield (total product and BTEX) while reducing tar, coke and char yield. Quality was also improved. Carbon content and HHV were increased while O/C was reduced. Increased conversion of guaiacol and increased selectivity for benzene and toluene were also indicated.

Keywords: torrefaction, catalytic cracking, pyrolysis, HZSM-5, BTEX, biofuel, bioenergy

Introduction

Catalytic cracking is a process shown to greatly improve the quality of pyrolysis oils generated from high oxygen content feedstocks including rice husks, rice straw (Chen et al., 2003), pine wood (Carlson et al., 2011; Chen et al., 2003; Valle et al., 2007), maple wood (Adjaye and Bakhshi, 1995a; Adjaye and Bakhshi, 1995b), poplar wood (Lu et al., 2010) and many biomass feedstocks. The cracking process was developed by the petroleum industry to deoxygenate and crack heavy petroleum crude oil feedstock to predominantly gasoline and other light hydrocarbons (Corma et al., 2007). The catalysts generally used for treating biomass-derived oils during catalytic cracking are acidic zeolites that hydrogenate oxygenates and act as molecular sieves to impact the range of molecule size and shape in the end-product. Catalytic upgrading of pyrolysis oils using the petroleum process with zeolite catalysts can be very effective, although catalyst coking is a major issue, and resolving the catalyst coking issue is a major research goal (Corma et al., 2007; Valle et al., 2007; Elliott et al., 1996). Adjaye and Bakhshi

(1995a, 1995b) attempted to catalytically crack fast pyrolysis bio-oil with five different catalysts (ZSM-5, H-Y-zeolite, H-mordenite, silicalite, and silica-alumina). Yield of organic liquid product was highest with ZSM-5 (34 % w/w of feed) although coke yield was as high as 29 %. If coking could be reduced, catalytic upgrading could become a viable method to produce hydrocarbon fuels from lignocellulosic feedstocks able to power internal combustion engines.

One potential way to minimize coke formation on zeolite catalysts is to remove coke precursors from the oil prior to upgrading. Compounds that are thought to promote coke formation include aldehydes, oxyphenols, furfural, and lignin-derived oligomers (Gayubo et al., 2005; Lu et al., 2010). Other studies (Gagnon et al., 1988; Laurent and Delmon, 1994a; Centeno et al., 1995; Wildschut et al., 2009) have indicated that the carbohydrate fraction is a major contributor to coke formation. There is currently very little research that attempts to remove coke precursors from bio-oil prior to upgrading. Pretreatment of biomass by torrefaction prior to pyrolysis could conceivably remove coke precursors from bio-oil prior to upgrading and thus reduce coke formation and improve bio-oil quality.

Biomass torrefaction is a low temperature pyrolysis process, similar to coffee roasting, in which the biomass is heated in an inert environment (N_2) from ~200-275 °C. Torrefaction generates a hydrophobic, friable solid biomass that requires less energy for grinding relative to untorrefied biomass (Phanphanich and Mani, 2010). Torrefied biomass has lower elemental oxygen content (CO, H_2O, and CO_2 are emitted during torrefaction) compared to untreated biomass, and torrefaction drives off a fraction of reactive and acidic intermediate components , such as acetic acid, furfural, and acetaldehyde (Phanphanich and Mani, 2010; Mani et al., 2009). Although some of these reactive gases generate coke on acid catalysts, leading to deactivation (Gayubo et al., 2004a, Gayubo et al., 2005), and despite the fact that the NSF/DOE Roadmap (2008, p. 44) has indicated that the impact of torrefaction on thermochemical processing should be investigated, to date no research has been performed to determine the effect of torrefaction as a pretreatment for pyrolysis and catalytic cracking of biomass. Torrefaction, when coupled with pyrolysis and catalytic cracking, could provide synergistic effects not realized with drying and/or catalytic treatment alone.

Torrefaction effectively dries biomass and decomposes hemicellulose. Several hemicellulose-derived compounds that are thought to produce coke in the subsequent upgrading step, such as acetyl groups that form acetic acid, would be effectively removed via torrefaction. Reactions of the acetic acid component during subsequent catalytic upgrading of the bio-oil can lead to severe catalyst coking. In addition, after upgrading, some acetic acid is left unreacted, and thus, the acid ends up in the product causing high acidity (low pH). As such, it was proposed that a hemicellulose-depleted feedstock would result in pyrolysis oils containing less acetic acid resulting in less coke formation during subsequent catalytic upgrading. The main objective of this study was to investigate the catalytic upgrading of fast pyrolysis bio-oil generated from torrefied pine wood in an effort to improve the quality of upgraded pyrolysis bio-oil.

Materials and Methods

A one-, two-, or three-step process used to generate bio-oil with characteristics similar to gasoline. Steps included feedstock pretreatment (via torrefaction), pyrolysis (fast and slow), and secondary catalytic cracking. Torrefaction was undertaken in a pilot scale (1000 kg per batch) rotating kiln torrefaction unit. Fast pyrolysis was accomplished in a fluidized bed pyrolysis unit (FBPU, see Figure 9.1). Slow pyrolysis was performed in a batch reactor system (see Figure 9.2). For catalytic cracking, a fixed bed plug flow reactor (PFR, see Figure 9.3) unit was used to process bio-oil generated via the fast pyrolysis of pine chip (PC) or torrefied pine chip (TPC) biomass. A generalized process flowchart is presented in Figure 9.4.

The one-step process involved fast pyrolysis of PC biomass at 500 °C in a fluidized bed fast (100 °C s^{-1}) pyrolysis unit (Figure 9.1) or slow pyrolysis in a batch slow (8 °C min^{-1} heating rate) pyrolysis unit. Prior to pyrolysis, biomass was ground in a hammer mill to 1-2 mm and dried at 105 °C for 4 h. Subsamples of bio-oil were taken for analysis, while the bulk was used in the subsequent catalytic cracking process, the as-named two-step process.

Previously produced and phase-separated bio-oil was pumped continuously into a tubular reactor (shown in Figure 9.3) and across a 15 g catalyst bed (28.5 cm^3) maintained at 400, 450, or 500 ˚C using a tube furnace. Pumping was accomplished using a peristaltic pump at a flow rate of 1.5 mL min^{-1} (~ 100 g h^{-1}) corresponding to a weight hourly space velocity (WHSV, h^{-1}) of 6.6 h^{-1}. Catalyst to oil ratio ranged from 0.34 to 0.65. Catalyst contact time (3600/(WHSV · C/O) thus ranged from 844 to 1582 s. Given a carrier gas flow rate of 50 cm^3 min^{-1}, gas phase residence time in the catalytic zone (V = 28.5 cm^3) was approximately 34 s.

The catalyst, HZSM-5, was produced by calcining NH_4-ZSM-5 (Zeolyst International, CBV 5524 G) at 550 ˚C for 4 h in air to produce the hydrogen form, H-ZSM-5, resulting in stronger acid pore sites. The pH was measured by mixing catalyst in water at a 50:50 ratio and then measuring the pH of the water using a standard pH probe. As a result of the calcining process, the pH was reduced from 4.98 to 3.06. The NH_4-ZSM-5 catalyst was received from the manufacturer as a fine powder. To minimize the pressure drop across the catalyst bed, the catalyst was granulated by mixing with water, drying, crumbling, and sieving to the desired size, ~ 2-4 mm. The catalyst powder had published values of 425 m^2 g^{-1}, 5 μm, and 50 for surface area, particle size and SiO_2/Al_2O_3 ratio, respectively. In-house measurements of the catalyst surface characteristics were accomplished using a Quantachrome surface area analyzer that indicated a surface area of 345 m^2 g^{-1}, pore radius at 10.8 Å, and pore volume at 0.1851 cm^3 g^{-1} for fresh catalyst after calcination, drying, and granulation.

The three-step process added torrefaction as a biomass pretreatment step. Torrefaction was performed at 225, 250, and 275 °C, a commonly-used temperature range for the partial or complete removal of hemicellulose, in a large-scale rotary kiln. Once each end temperature was reached, a soak of 20 min was used to drive complete devolatilization of components. Air-dried, coarsely ground pine chips were processed directly in the torrefaction unit. After torrefaction, the resulting torrefied feedstock (PC T225, PC T250, PC T275) were characterized (see Table 9.1), ground to 1-2 mm, then subjected to fast pyrolysis at 500 °C as discussed previously. The resulting condensable bio-oil was then catalytically cracked as previously described.

Including control samples, 32 bio-oil (BO) types were produced and were labeled torrefaction temperature (T100, T225, T250, or T275), pyrolysis heating rate (fast pyrolysis: FP, or slow pyrolysis: SP), and catalytic upgrading temperature (U400, U450, or U500). Figure 9.4 shows the materials produced at each step. Bio-oil produced by the one-step process, FP500 and SP500, were used as a control to compare to the various treatments.

The yield of liquid for each step including torrefaction, pyrolysis and catalytic cracking was determined as the weight change of the collection vessel. Phase yield, oily and aqueous, was determined by weighing separatory funnel-separated fractions. The total yield of catalytic cracking byproducts including tar, catalyst coke, and reactor char was quantified by measuring the change in weight of the reactor. The yield of individual byproduct components was also quantified. Tar was considered to be the acetone-soluble material adhered to the catalyst and was quantified by washing the catalyst with acetone after catalytic runs, drying the catalyst, and measuring the change in mass. Catalyst coke formation was determined by heating the catalyst under a flow of oxygen in a thermogravimetric analyzer (TGA). The change in mass of catalyst was assumed to be due to the complete combustion of coke. The weight of reactor char was then determined as the difference between reactor weight change and coke and tar yield. All yields were calculated relative to dry PC feedstock unless otherwise stated.

Product Characterization

Solid materials including biomass, torrefied biomass and pyrolysis char were subsampled and analyzed. Other solids generated during catalytic cracking including reactor char, catalyst coke, and tar were not analyzed compositionally, only quantified. Yield of non-condensable gas was determined by difference.

Feedstock and products were analyzed by an assortment of methods. Biomass feedstock was analyzed for proximate composition (moisture, volatiles, ash and fixed carbon), and elemental composition (CHNS-O). The initial quality of bio-oils was assessed by measuring CHNS-O and calculating molar H/C_{eff} and O/C ratios which provide good indications of fuel applicability and the level of deoxygenation, respectively, as a result of catalytic cracking. H/C_{eff} was calculated as follows:

$$H/C_{eff} = \frac{mol\ H - 2\ x\ mol\ O}{mol\ C} \quad \text{(Eq. 9.1)}$$

Storage stability was assessed in a differential scanning calorimeter (DSC), in which oxidation onset temperature (OOT) was determined following Hilten et al. (2010) and ASTM E2009, "Standard Test Method for oxidation onset temperature of hydrocarbons by differential scanning calorimetry". Using the method, oils are heated from room temperature to 250 °C under an oxygen environment. At a material-specific temperature, combustion (oxidation) begins. Oxidation onset is determined by extrapolating the baseline and the slope of the oxidation peak. The point of intersection is the oxidation onset temperature. Higher temperature at the onset of oxidation implies greater storage stability.

Chemical composition was determined using a calibrated GC-MS method. The calibrated GC-MS method (see Figure 9.5 for calibration factors) was used to determine conversion of proposed reactants including guaiacol (2-methoxyphenol), creosol (2-methoxy-4-methylphenol), and acetic acid and yield of products including benzene, toluene, ethylbenzene, and xylene (collectively, BTEX) products based on 6-point calibrations with pure compound mixtures with internal standard, heptane. Upon calculating peak areas relative to heptane and using the calibration factor from Figure 9.5, the concentration of BTEX and reactants in the product liquid was found for all samples from each process condition combination. Product selectivity to benzene, toluene, ethylbenzene, p-, m-, and o-xylene, total BTEX, and other non-BTEX compounds was found by assuming all product formation resulted from the conversion of guaiacol and creosol. This simplification allowed for the determination of product yield, as well. With knowledge of liquid yield catalytic cracking process, the yield of each component was determined relative to the combined conversion of reactants, guaiacol and creosol, whose concentrations were derived relative to the bio-oil fed to the catalytic cracking reactor.

Statistical Design

The experimental design was planned such that a 3-way ANOVA could be used to determine the effects of three factors, pretreatment temperature (4 levels – denoted T100, T225, T250, and T275 for temperatures at 100, 225, 250, and 275 °C), pyrolysis heating rate (2 levels – denoted SP or FP for slow

pyrolysis and fast pyrolysis at 0.13 or 100 °C s^{-1}), and catalytic cracking temperature (4 levels – CTRL, U400, U450, and U500 for temperatures at 0, 400, 450 and 500 °C), on yields and product composition and quality. The null hypothesis for all analyses was that factors at any level had no affect on product yield or composition. Rejection of the null hypothesis was concluded at p-values less than a level of significance, alpha=0.05. The Holm-Sidak method of multiple comparisons was used to determine effects of levels for each factor.

Results and Discussion

Effect of torrefaction on solid feedstock

Yields of solid material at T225, T250, and T275 were 71.2, 69.7, and 55.7 % (w/w of PC biomass) after a hold time of 20 min as shown in Table 9.1. As expected, solid product yield significantly ($p<0.001$) decreased with increasing torrefaction temperature as a result of greater volatilization. As indicated in Table 9.1, volatile matter remaining was indeed less for PC having undergone higher temperature torrefaction. At the same time, fixed carbon and elemental carbon are concentrated in the solid and oxygen content is reduced meaning that energy density is increased. Higher energy density in solid biomass feedstocks make them better candidates from thermal energy applications.

Effect of torrefaction on pyrolysis and catalytic cracking product yield

With less volatile matter remaining, feedstock generated at higher torrefaction temperature generated lower liquid yields ($p<0.001$) and higher char yields upon pyrolysis. Table 9.2 provides yield results for the pyrolysis processes. Aqueous phase and oily phase liquid showed a significant inverse relationship with pretreatment temperature (i.e. yield was reduced with increasing temperature). Concurrently, non-condensable gas and solid yields increased significantly with increasing pretreatment temperature. Despite lower oily phase liquid yield, the quality of the oils generated was expected to be higher.

Torrefaction had a significant effect on the yield of all products of catalytic cracking including liquid product (oily and aqueous), non-condensable gas, catalyst coke, catalyst tar, and reactor char.

Liquid product (oily phase) decreased significantly with increasing temperature for two temperature comparisons: T225 versus T275 and T100 versus T275. All other pretreatment temperature comparisons were statistically insignificant. Liquid product yield for SP-derived oils was significantly higher than for FP-derived oils. Gas yield significantly increased with increasing pretreatment temperature for all temperature comparisons. Tar yield also significantly decreased with increasing temperature for all pretreatment temperature comparisons except for T250 versus T275. A particularly important effect observed was a significant reduction in catalyst coke with increasing pretreatment temperature for all temperature comparisons. All torrefaction temperatures reduced coke and tar relative to the control, T100. Increasing torrefaction also significantly reduced reactor char production for all temperature comparisons except for T225 versus T250.

From a perspective of yield from catalytic cracking, torrefaction appears to be beneficial in the reduction of unwanted byproducts including tar, char, and coke. Liquid yield is largely unaffected by torrefaction although gas yield does increase with torrefaction. If byproduct minimization is desired, pretreatment at 275 °C is the best temperature to utilize, while pretreatment temperatures at 100, 225, and 250 °C maximize product liquid production.

Effect of pyrolysis heating rate on product yield

Pyrolysis heating rate significantly affected the pyrolysis yield of aqueous phase liquid ($p<0.001$) and the oily phase liquid ($p<0.001$), as well as char and non-condensable gas. Aqueous phase liquid was significantly reduced in fast pyrolysis (0 %, w/w) versus slow pyrolysis oils (27 %, w/w). Alternately, oily phase yield was significantly increased ($p<0.001$) as a result of fast pyrolysis processing (14.8 %, w/w) relative to slow pyrolysis (6.5 %, w/w).

Additional yield effects resulting from pyrolysis heating rate were evident in the secondary catalytic cracking process, as well. Product liquid, non-condensable gas, tar, coke, and char yields were all significantly affected (<0.001 for all) as a result to pyrolysis heating rate. Product liquid and tar yields were significantly higher and gas, coke, and char yields were lower for slow pyrolysis-derived oils

relative to fast pyrolysis processing. If maximization of product and minimization of byproduct (except tar) is desired irrespective of product quality, slow pyrolysis is optimal.

Effect of catalytic upgrading temperature on product yield

Liquid product yield significantly increased with increasing catalytic cracking temperature. At the same time, gas yield also significantly increased. Concurrently, tar, coke and char yields were significantly reduced. From this perspective, the highest catalytic cracking temperature was optimal.

Effect of process conditions on intermediate and final product quality

Tables 9.3 and 9.4 show characterization results for SP- and FP-derived liquid products, respectively. Intermediate and final product quality was assessed via a variety of measures. First, the change in elemental C, H, N, S, and O (by difference) and in particular, H/C_{eff} and O/C ratios, was utilized to indicate improvement in oil quality as a function of process conditions. Given CHNS-O values, heating values were also calculated following Channiwala and Parikh (2002). Secondly, quality was also indicated in relation to OOT, an indicator of storage stability. Finally, quality was determined relative to the yield of desirable end product compounds, specifically, BTEX, in the product liquid and the conversion of proposed reactants (i.e. undesired components) as determined via a calibrated GC-MS routine.

Effect of process conditions on CHNS-O, H/C_{eff}, O/C, and HHV

Pretreatment temperature, pyrolysis heating rate and catalytic cracking temperature all significantly affected elemental C, N, and O as well as O/C ratio and HHV. Elemental H was affected significantly only by catalytic upgrading temperature. H/C_{eff} was significantly affected by both pyrolysis heating rate and catalytic upgrading temperature. Bio-oil intermediate and end product characteristics are given in Tables 9.3 and 9.4.

Carbon content significantly increased with increasing catalytic cracking temperature, and was higher for SP- than for FP-derived oils. C-content for T275, T250, and T100 were all higher than for T225. In both SP- and FP-derived oils, the control had significantly lower H/C_{eff} ratio than upgraded oils. The SP-derived catalytic upgrading control indicated a higher H/C_{eff} than did the FP-derived control oils.

However, for all catalytic upgrading temperatures other than the control, FP-derived oils had higher H/C_{eff}.

The reduction of O/C is a good indicator of deoxygenation. The catalytic upgrading process significantly reduced O/C. Overall, SP-derived oils had lower O/C than FP-derived oils. As a function of torrefaction, significant reduction in O/C was seen for T275, T250 and T100 relative to T225. No other pretreatment temperature comparisons proved significant. Catalytic cracking temperature also significantly impacted O/C. All upgrading temperatures had lower O/C than the control. In addition, U500 reduced O/C more than U400. Results indicated that torrefaction pretreatment did not significantly affect O/C, although catalytic upgrading was effective at all upgrading temperatures.

HHV, a good indicator of the potential applicability of pyrolysis oils and of the optimal levels for CHNS-O, was affected by process conditions in a multitude of ways. HHV increased with increasing catalytic processing temperature for all temperature comparisons except for T500 versus T450. Within heating rate groups, HHV varied significantly. For SP, higher catalytic cracking temperature resulted in significantly higher HHV except for U450 versus CTRL, U400 versus CTRL, and U500 versus U450. Within catalytic processing temperature groups, HHV varied as result of pyrolysis heating rate. Within the catalytic cracking control group, HHV for slow pyrolysis oil was significantly higher than for fast pyrolysis oil. However, for all other catalytic processing temperatures (U400, U450, and U500), the HHV for upgraded fast pyrolysis oil was significantly higher.

Effect of process conditions on OOT

All process variables (i.e. pyrolysis heating rate, pretreatment temperature, and catalytic cracking temperature) significantly affected the storage stability of the product liquids as measured via OOT. OOT for SP-derived oils was significantly higher than for FP-derived oils ($p=0.024$). Catalytic cracking temperature comparisons indicated that OOT for U500 > CTRL, U500 > U400, U450 > CTRL, and U450 > U400. OOT for T100 bio-oils was significantly greater than for oils derived from T225, T250, or T275. Results indicated that torrefaction pretreatment did not have a positive effect on product stability.

However, catalytic cracking did have a positive effect, although the temperature at which cracking was accomplished was irrelevant.

Effect of process conditions on conversion and yield of reactants/products

Three-way ANOVA tests were also used to determine if variables including torrefaction temperature, heating rate, and catalytic cracking temperature significantly affected the final concentration of reactants and products, conversion of reactants, and yield of BTEX and non-BTEX (Total product yield minus BTEX product yield) products. Table 9.5 shows the p-values for the comparisons and indicates whether direct or inverse relationships were present. Values for yield are also represented visually in Figure 9.6.

It is clear from Table 9.5 that catalytic cracking had the greatest effect on the concentration, selectivity, and yield of components although heating rate also affected concentration and yield. The only effect on components as a function of torrefaction temperature was a decrease in the concentration of p-xylene with increasing torrefaction temperature. Acetic acid concentration was higher for the FP-derived oils as were the concentrations of toluene, ethylbenzene, and p-xylene. The yield of toluene, ethylbenzene, p-xylene, m-xylene, and total BTEX was also higher for FP-derived oil. As such, if maximizing BTEX is desired, FP processing is most effective.

Catalytic cracking temperature was inversely related to the concentration of guaiacol although no clear relationship with the conversion of guaiacol was evident. Concurrently, the concentration of all BTEX components increased with increasing catalytic processing temperature as did the yield (relative to conversion of guaiacol and creosol) of all BTEX compounds. The selectivity to benzene and toluene was also directly related to catalytic cracking temperature. For the maximization of BTEX, and of benzene and toluene, in particular, catalytic cracking at U500 was most effective followed in order of most to least effective: U450 < U400 < CTRL.

Conclusions

An upgrading scheme was proposed to improve the yield, quality and stability of biomass-derived pyrolysis oils involving biomass pretreatment and catalytic cracking for fast and slow pyrolysis bio-oils.

Process conditions varied included biomass pretreatment temperature (100, 225, 250, and 275 °C), pyrolysis heating rate (0.13 and 100 °C s^{-1}), and catalytic cracking temperature (400, 450, and 500 °C). Effects seen as a result of torrefaction included:

- reduced total liquid yield of pyrolysis bio-oil and increased solid yield
- increased carbon content and heating value for the pyrolysis feedstock
- increased gas yield upon catalytic cracking
- reduced reactor char and catalyst coke and tar formation
- negative effect on OOT-assessed stability

Pyrolysis heating rate also significantly affected yield and quality of products. Results relative to slow pyrolysis included:

- reduced aqueous phase and increased oily phase yield after pyrolysis
- reduced liquid and tar yield upon catalytic cracking
- increased gas, coke, and char yield from catalytic cracking
- higher carbon content in the product liquid
- lower H/C_{eff} ratio and reduced HHV but increased O/C ratio for non-catalytically treated oils
- higher H/C_{eff} and HHV and lower O/C ratio for catalytically-treated oils
- reduced OOT-assessed stability
- increased yield of toluene, ethylbenzene, p-xylene, and m-xylene

Catalytic cracking temperature affected processing and end product, as well. Results relative to the control included:

- increased gas and liquid product yield
- reduced tar, coke and char yield
- increased carbon content and HHV in liquid product
- reduced O/C ratio

- increased yield of BTEX
- increased conversion of guaiacol
- increased selectivity for benzene and toluene

References

Adjaye, J., Bakhshi, N. (1995a). Production of hydrocarbons by catalytic upgrading of a fast pyrolysis bio-oil. Part II: Comparative catalyst performance and reaction pathways. Fuel Processing Technology 45: 185-202.

Adjaye, J., Bakhshi, N. (1995b). Production of hydrocarbons by catalytic upgrading of a fast pyrolysis bio-oil. Part I: Conversion over various catalysts. Fuel Processing Technology 45: 161-183.

Carlson, T., Cheng, Y., Jae, J., Huber, G. (2011). Production of green aromatics and olefins by catalytic fast pyrolysis of wood sawdust. Energy Environ. Sci. 4: 145-161.

Centeno, A., Laurent, E., Delmon, B. (1995). Influence of the support of CoMo sulfide catalysts and of the addition of potassium and platinum on the catalytic performances for the hydrodeoxygenation of carbonyl, carboxyl, and guaiacol-type molecules. J. Catalysis 154: 288-298.

Channiwala, S., Parikh, P. (2002). A unified correlation for estimating HHV of solid, liquid and gaseous fuels. Fuel 81: 1051-1063.

Chen, G., Andries, J., Luo, Z., Spliethoff, H. (2003) Biomass pyrolysis/gasification for product gas production: the overall investigation of parametric effects. Energy Conversion and Management 44: 1875-1884.

Corma, A., Huber, G., Sauvanaud, L., O'Connor, P. (2007). Processing biomass-derived oxygenates in the oil refinery: Catalytic cracking (FCC) reaction pathways and role of catalyst. Journal of Catalysis 247: 302-327.

Elliott, D.C., Neuenschwander, G.G. (1996). Liquid Fuels by Low-Severity Hydrotreating of Biocrude. In: Bridgwater AV, Boocock DGB (eds) Developments in Thermochemical Biomass Conversion, Blackie Academic & Professional, London, Vol. 1, pp 611-621

Gagnon, J., Kaliaguine, S. (1988). Catalytic hydrotreatment of vacuum pyrolysis oils from wood. Ind. Eng. Chem. Res. 27(10): 1783-1788.

Gayubo, A., Aguayo, A., Atutxa, A., Prieto, R., Bilbao, J. (2004a) Deactivation of a HZSM-5 Zeolite Catalyst in the Transformation of the Aqueous Fraction of Biomass Pyrolysis Oil into Hydrocarbons. Energy and Fuels 18: 1640-1647.

Gayubo, A., Aguayo, A., Atutxa, A., Valle, B., Bilbao, J. (2005). Undesired components in the transformation of biomass pyrolysis oil into hydrocarbons on an HZSM-5 zeolite catalyst. Journal of Chemical Technology and Biotechnology 80: 1244-1251.

Laurent, E., Delmon, B. (1994a). Study of the hydrodeoxygenation of carbonyl, carboxylic and guaiacyl groups over sulfided CoMo/γ-Al2O3 and NiMo/γ-Al2O3 catalysts: I. Catalytic reaction schemes. Applied Catalysis A: General 109(1): 77-96.

Lu, Q., Zhang, Y., Tang, Z., Li, W., Zhu, X. (2010). Catalytic upgrading of biomass fast pyrolysis vapors with titania and zirconia/titania based catalysts. Fuel 89: 2096-2103.

Mani, S., Das, K.C., Kastner, J. (2009). Development of biomass torrefaction technology to produce biocoal for electricity production. Final Report to State of Georgia, Traditional Industries Program

NSF (2008). Breaking the Chemical and Engineering Barriers to Lignocellulosic Biofuels: Next Generation Hydrocarbon Biorefineries, Huber GW (ed), University of Massachusetts Amherst. National Science Foundation, Chemical, Bioengineering, Environmental, and Transport Systems Division, Washington D.C. 180 p.

Phanphanich, M., Mani, S. (2010). Impact of torrefaction on the grindability and fuel characteristics of forest biomass. Bioresource Technology 102: 1246–1253.

Valle, B., Gayubo, A., Atutxa, A., Alonso, A., Bilbao, J. (2007). Integration of thermal and catalytic transformation for upgrading biomass pyrolysis oil, International Journal of Chemical Reactor Engineering 5 (2007): 1-10.

Wildschut, J., Mahfud, F., Venderbosch, R., Heeres, H. (2009). Hydrotreatment of fast pyrolysis oil using heterogeneous noble-metal catalysts. Ind. Eng. Chem. Res. 48: 10324-10334.

Figure Captions

Figure 9.1. Fluidized-bed pyrolysis unit showing components: 1) biomass hopper/feeder, 2) gas pre-heater, 3) riser reactor, 4) cyclone separators, 5) char collector, 6) hot gas filter, 7) shell and tube condenser, 8) ice-bath condensers, and 9) exhaust fan.

Figure 9.2. Batch pyrolysis unit used to generate biochar and bio-oil from peanut hulls – 1) Nitrogen sweep gas, 2) gas flow controller, 3) reactor holding biomass, and 4) condensation unit to collect bio-oil.

Figure 9.3. Catalytic cracking reactor setup showing 1) bio-oil vessel, 2) hot plate, 3) peristaltic pump, 4) stainless steel reactor with oil preheat zone, 5) catalyst bed, 6) tube furnace, 7) collection flask, 8) ice bath, 9) compressed N_2 tank and thermocouples (TC1 and TC2).

Figure 9.4. Process flow diagram showing products from torrefaction, pyrolysis and catalytic upgrading processes.

Figure 9.5. Calibration factors for quantification of BTEX, acetic acid, guaiacol, and creosol.

Figure 9.6. Yield of BTEX and non-BTEX products relative to guaiacol plus creosol converted.

Tables

Table 9.1. Feedstock characteristics for torrefied and untorrefied PC biomass.

Parameter	Feedstock Characteristics (%, w/w d.b)														
	PC			PC T100			PC T225			PC T250			PC T275		
	AVE	±	95% CI	AVE	±	95% CI	AVE	±	95% CI	AVE	±	95% CI	AVE	±	95% CI
Yield[a]	100	±	N/A	86.0	±	N/A	71.2	±	N/A	69.7	±	N/A	55.6	±	N/A
Moisture[b]	14.0	±	0.32	0.03	±	0.02	0.48	±	0.28	0.35	±	0.10	0.01	±	0.02
Volatiles	82.0	±	0.42	81.4	±	0.02	80.0	±	0.22	77.9	±	1.20	72.3	±	0.47
Ash	0.2	±	0.028	0.30	±	0.04	0.36	±	0.03	0.39	±	0.05	0.20	±	0.16
Fixed Carbon	17.9	±	0.39	18.3	±	0.02	19.6	±	0.24	21.7	±	1.15	27.5	±	0.31
C	46.9	±	0.2	46.9	±	0.2	48.3	±	0.5	48.4	±	0.1	53.3	±	0.6
H	5.98	±	0.1	5.98	±	0.1	5.88	±	0.1	5.83	±	0.1	5.6	±	0
N	0.45	±	0.1	0.45	±	0.1	0.88	±	0.2	0.82	±	0.1	1	±	0.3
S	0	±	0	0	±	0	0	±	0	0	±	0	0	±	0
O[c]	46.3	±	0.2	46.3	±	0.2	44.6	±	0.2	44.6	±	0.1	39.9	±	0.5
HHV[d] ($MJ\ kg^{-1}$)	18.6	±	0.1	18.6	±	0.1	19.1	±	0.1	19.1	±	0.1	21.1	±	0.3

[a]Yields are calculated versus air dried PC biomass.
[b]Wet basis.
[c]By difference.
[d]Calculated following Channiwala and Parikh (2002).

Table 9.2. Yield of material after pretreatment and pyrolysis.

Fraction	Yield (%, w/w Pretreated Biomass)							
	Fast Pyrolysis				Slow Pyrolysis			
	100 °C	225 °C	250 °C	275 °C	100 °C	225 °C	250 °C	275 °C
Oil	22.4	13.8	13.8	11.0	8.5	8.1	7.4	7.8
Aqu	0.0	0.0	0.0	0.0	34.1	35.1	34.3	27.0
Char	21.0	17.8	31.1	66.5	29.6	29.4	30.2	37.8
Gas	56.6	68.4	55.1	22.4	27.3	26.7	26.1	26.1

Table 9.3. Characteristics of product bio-oil generated via pretreatment, pyrolysis and catalytic cracking using pretreated PC as the slow pyrolysis feedstock.

Parameter	Slow Pyrolysis															
	100				225				250				275			
	CTRL	400	450	500	CTRL	400	450	500	CTRL	400	450	500	CTRL	400	450	550
C	63.4	67.9	70.1	69.0	60.5	66.4	70.8	72.4	60.8	66.8	67.0	72.3	62.4	68.4	68.0	70.0
H	6.3	7.8	7.9	7.6	6.5	7.1	7.9	7.7	6.5	7.6	7.4	7.7	6.2	7.4	7.7	7.9
N	0.2	0.1	0.0	0.0	0.7	0.3	0.4	0.5	0.5	0.2	0.0	0.2	0.2	0.2	0.1	0.0
S	0.0	0.0	0.0	0.0	0.0	0.0	0.0	0.0	0.0	0.0	0.0	0.0	0.0	0.0	0.0	0.0
O[a]	30.1	24.3	23.4	22.2	32.4	26.3	20.9	19.8	32.2	25.5	25.6	19.7	31.2	24.1	24.2	22.1
H/C_{eff}	0.5	0.8	0.8	0.8	0.5	0.7	0.9	0.9	0.5	0.8	0.8	0.9	0.4	0.8	0.8	0.9
O/C	0.4	0.3	0.3	0.2	0.4	0.3	0.2	0.2	0.4	0.3	0.3	0.2	0.4	0.3	0.3	0.2
HHV ($MJ\ kg^{-1}$)[b]	26.4	30.3	31.3	30.8	25.4	28.8	31.9	32.4	25.5	29.6	29.5	32.3	25.8	30.0	30.2	31.4
OOT (°C)	161.5	145.5	160.5	163.9	157.1	145.5	160.5	156.5	159.4	140.9	151.4	156.6	158.0	153.0	154.5	160.4

[a]Calculated by difference.

[b]Calculated following Channiwala and Parikh (2002).

Table 9.4. Characteristics of product bio-oil generated via pretreatment, pyrolysis and catalytic cracking using pretreated PC as the fast pyrolysis feedstock.

Parameter	Fast Pyrolysis															
	100				225				250				275			
	CTRL	400	450	500	CTRL	400	450	500	CTRL	400	450	500	CTRL	400	450	500
C	35.1	71.6	74.2	80.4	35.8	39.7	57.2	71.9	39.3	71.5	72.7	71.1	42.0	75.6	72.0	80.1
H	6.5	7.9	7.8	8.1	6.2	8.8	7.9	7.0	6.1	7.5	7.7	7.7	6.0	7.4	7.6	8.0
N	0.0	0.0	0.0	0.0	0.1	0.0	0.0	0.1	0.2	0.0	0.0	0.0	0.1	0.0	0.0	0.0
S	0.0	0.0	0.0	0.0	0.0	0.0	0.0	0.0	0.0	0.0	0.0	0.0	0.0	0.0	0.0	0.0
O[a]	58.4	33.1	18.0	11.6	57.9	53.6	34.9	21.1	53.8	32.0	19.6	20.7	52.0	18.8	20.4	11.9
H/C_{eff}	-0.3	0.6	0.9	1.0	-0.3	0.6	0.7	0.7	-0.2	0.6	0.9	0.9	-0.2	0.8	0.8	1.0
O/C	1.3	0.3	0.2	0.1	1.2	1.0	0.5	0.2	1.0	0.3	0.2	0.2	0.9	0.2	0.2	0.1
HHV ($MJ\ kg^{-1}$)[b]	13.9	30.9	33.2	36.4	13.8	18.7	25.7	31.1	15.4	30.5	32.5	31.7	16.3	33.2	32.0	36.2
OOT (°C)	168.6	161.0	160.7	159.7	135.8	145.9	157.7	163.3	130.0	162.2	154.9	164.9	126.4	149.7	151.2	149.1

[a]Calculated by difference.

[b]Calculated following Channiwala and Parikh (2002).

Table 9.5. P-values for 3-way ANOVA results comparing concentration, selectivity/conversion, and yield of component compounds to torrefaction temperature, pyrolysis heating rate, and catalytic cracking temperature. Green blocks indicate a significant positive correlation, red indicates a significant negative correlation, and blue indicates both positive and negative correlations within a group.

Component	Torr Temp (°C)			Heating Rate (°C s^{-1})			CatUp Temp (°C)		
	Concentration	Selectivity / Conversion	Yield	Concentration	Selectivity / Conversion	Yield	Concentration	Selectivity / Conversion	Yield
Acetic Acid	0.46			0.01			0.02		
Guaiacol	0.15	0.17		0.12	0.38		0.03	0.96	
Creosol	0.16	0.25		0.51	0.46		0.01	0.76	
G + C		0.31			0.15			0.97	
Benzene	0.52	0.46	0.08	0.94	0.72	0.59	<0.01	0.01	0.00
Toluene	0.12	0.60	0.10	0.02	0.10	0.00	<0.01	0.02	<0.01
Ethyl-benzene	0.16	0.72	0.19	0.00	0.04	<0.01	<0.01	0.06	<0.01
p-Xylene	0.01	0.46	0.30	<0.01	0.32	0.00	<0.01	0.37	0.01
m-Xylene	0.37	0.46	0.14	0.11	0.34	0.04	<0.01	0.41	0.00
Total BTEX		0.54	0.03		0.23	<0.01		0.24	<0.01
Other		0.42	0.29		0.46	0.69		0.56	0.07

Figures

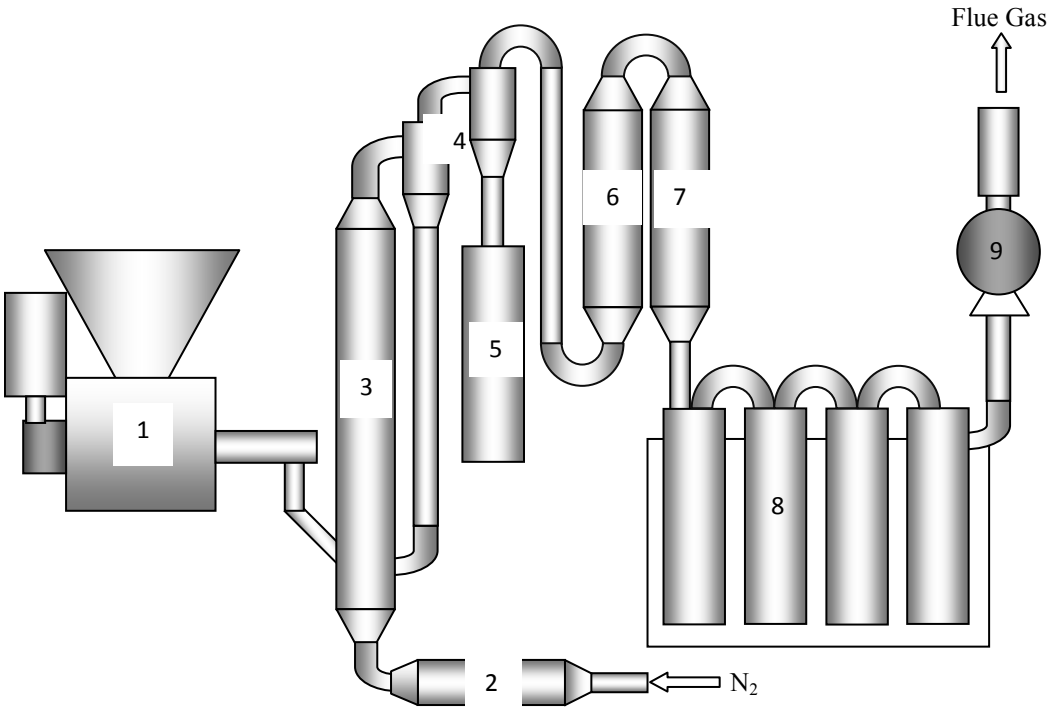

Figure 9.1. Fluidized-bed pyrolysis unit showing components: 1) biomass hopper/feeder, 2) gas pre-heater, 3) riser reactor, 4) cyclone separators, 5) char collector, 6) hot gas filter, 7) shell and tube condenser, 8) ice-bath condensers, and 9) exhaust fan.

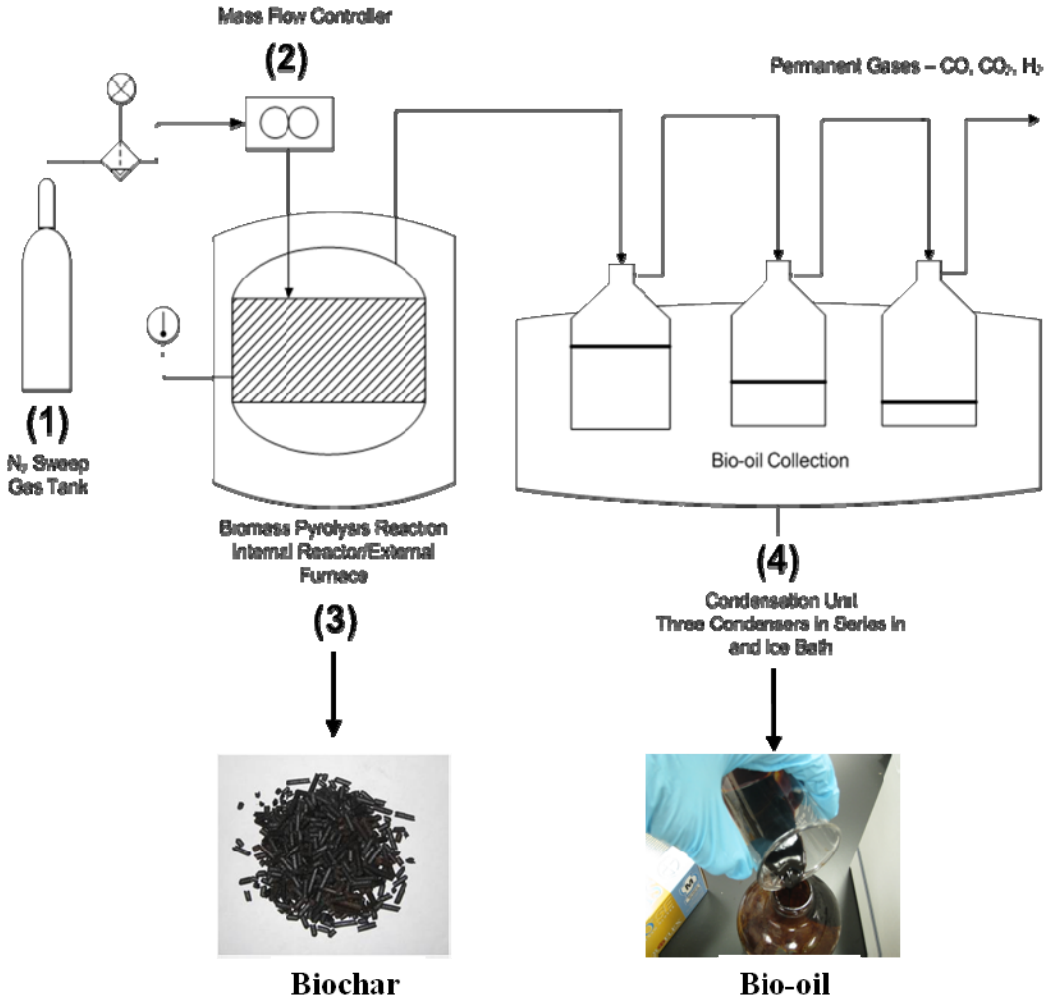

Figure 9.2. Batch pyrolysis unit used to generate biochar and bio-oil from peanut hulls – 1) Nitrogen sweep gas, 2) gas flow controller, 3) reactor holding biomass, and 4) condensation unit to collect bio-oil.

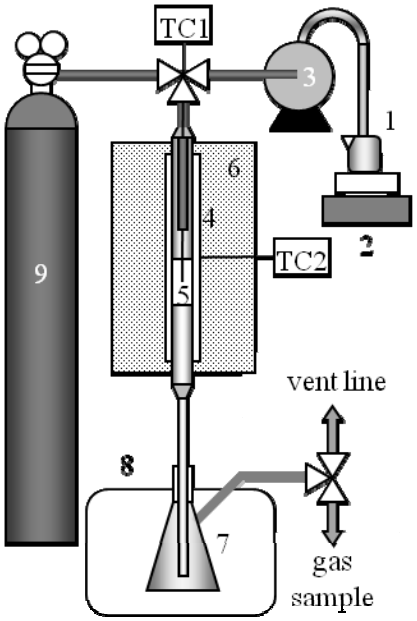

Figure 9.3. Catalytic cracking reactor setup showing 1) bio-oil vessel, 2) hot plate, 3) peristaltic pump, 4) stainless steel reactor with oil preheat zone, 5) catalyst bed, 6) tube furnace, 7) collection flask, 8) ice bath, 9) compressed N_2 tank and thermocouples (TC1 and TC2).

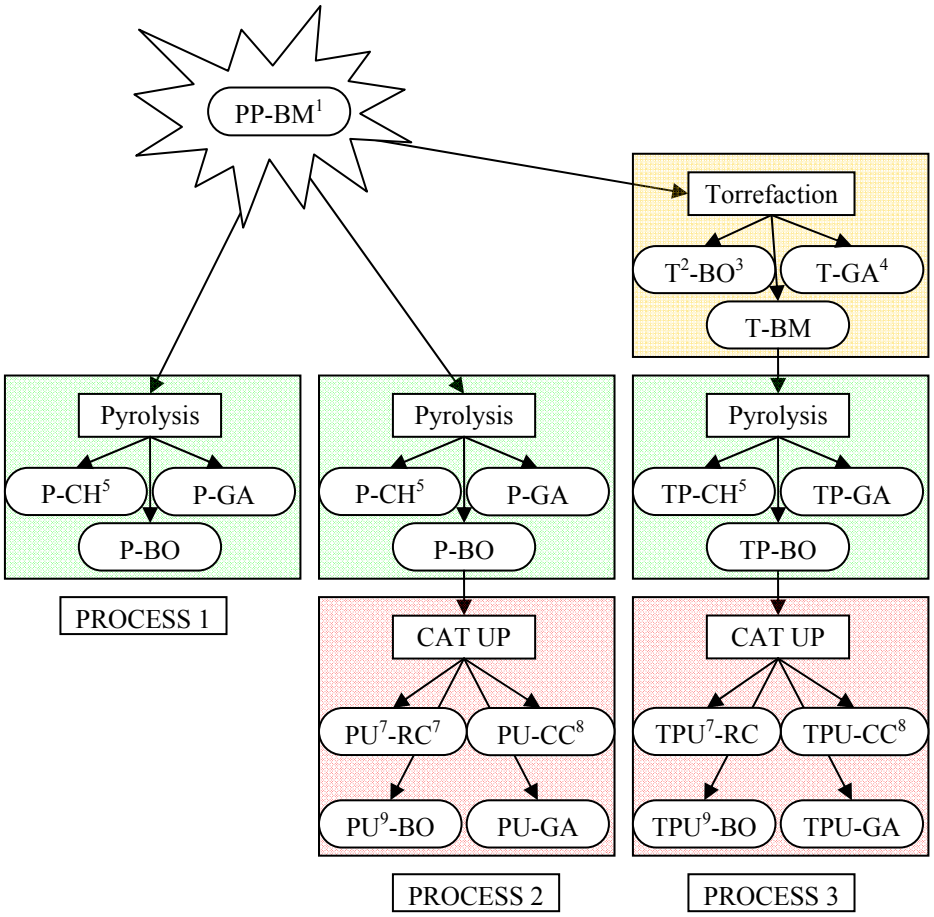

[1]BM ≡ biomass
[2]T ≡ torrefied
[3]BO ≡ bio-oil
[4]GA ≡ non-condensable gas
[5]CH ≡ char
[6]P ≡ pyrolyzed
[7]RC ≡ reactor char
[8]CC ≡ catalyst coke
[9]U ≡ upgraded

Figure 9.4. Products from torrefaction, pyrolysis and catalytic upgrading processes.

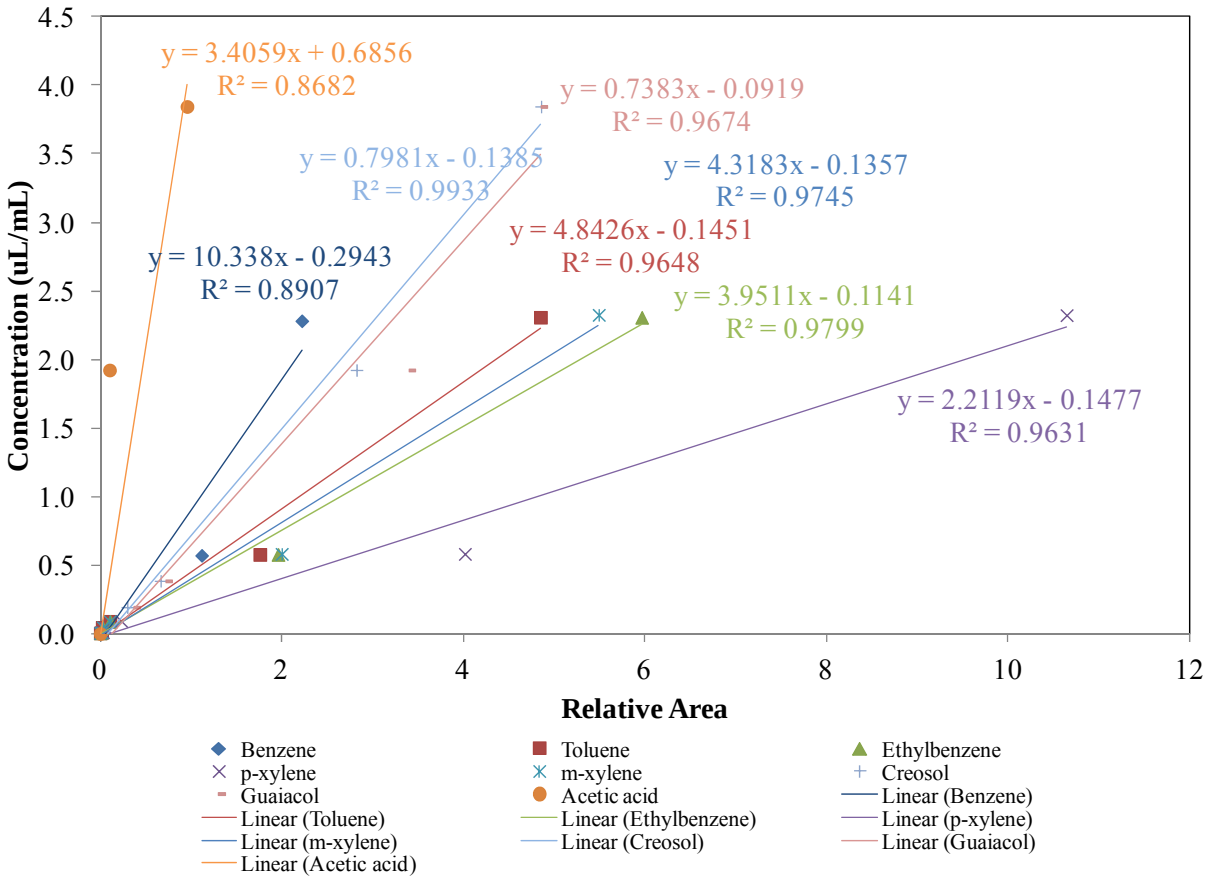

Figure 9.5. Calibration factors for BTEX, acetic acid, guaiacol, and creosol.

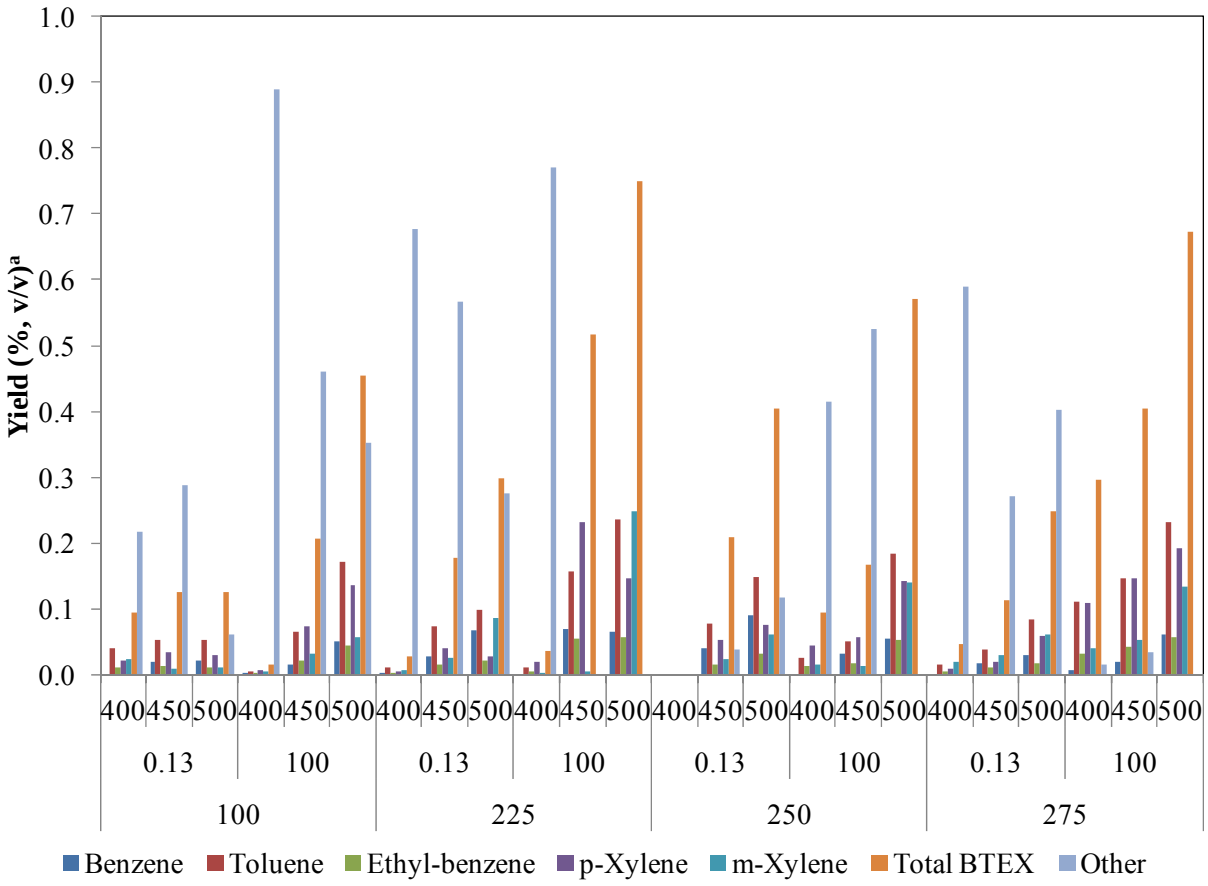

Figure 9.6. Yield of BTEX and non-BTEX products. [a]Yield was determined relative to bio-oil fed to the catalytic reactor.

CHAPTER 10

CONCLUSIONS

Results from the work described herein have indicated the potential for processing biomass-derived oils to liquid fuels. Three upgrading methods were proposed for liquids from a variety of underutilized feedstocks including waste oils (DAF and PSS) and lignocellulosic biomass (pine pellet, pine chip and peanut hull pellets in an effort to generate value-added products. Upgrading methods included biomass pretreatment by torrefaction, pyrolysis-linked catalytic esterification, and secondary catalytic pyrolysis (cracking). Both fast and slow pyrolysis processes were utilized to generate oils from feedstock. These were used for DAF (slow pyrolysis only) and for lignocellulosic biomass. Of the three upgrading methods, only catalytic cracking was used for all material types and as such received the most attention.

The goal was to improve processing to generate fuel compatible liquids (i.e. hydrocarbons) in gasoline and diesel boiling point ranges including monoaromatics, polycyclic aromatics, and linear aliphatics. These were verified and quantified via GC-MS and GC-FID. Other fuel properties analyzed included H/C and O/C ratio, high heating value, H_2O content, viscosity and storage stability. Results indicated definite improvements in fuel properties. For FFA-derived products, the main shortcoming is high viscosity of untreated feedstock. Catalytic cracking effectively reduced viscosity to the range of gasoline in most cases and below that of diesel in all cases. For lignocellulosic feedstock-derived pyrolysis liquids, poor stability, low heating value, and high water content limit utilization in liquid fuel applications. For bio-oils from lignocellulose, fuel properties were improved markedly, water content and heating value, in particular.

Chapters in this work are separated as standalone manuscripts, but when linked, a clear theme emerges. The overall effort was devised to not only to develop a process to produce a petroleum

compatible fuel from biomass but to also develop the methods by which to determine if actual improvements were made.

Chapter 2 – Stability assessment method development

Because storage stability is of particular importance for biofuels since biofuel use has historically been limited due to undesirable changes occurring during transport and long-term storage, efforts were made to develop a method to determine stability quickly and accurately. In the current study, stability was assessed from both a physical standpoint (viscosity change, OOT) and from a chemical standpoint (FT-IR). It was clear that stabilization techniques such as adding methanol affected the stability of pine and peanut hull-derived slow pyrolysis bio-oils. The stability assessment methods developed as part of the study described in Ch. 2 were used in work outlined in subsequent chapters of this dissertation to determine if upgrading endeavors were successful.

Chapter 3 –Catalytic cracking of DAF

Poultry processing waste derived from dissolved air flotation (DAF) is a particularly low-value material. The majority is landfilled after separation from wastewater. Pyrolysis and catalytic cracking were shown to significantly improve the fuel properties of DAF waste. Catalytic cracking was particularly effective in reducing the viscosity of pyrolyzed DAF (37.8 to 1.5 $mm^2 s^{-1}$ at 40 °C) and increasing the heating value of DAF (from 32.7 to 41.1 MJ kg^{-1}).

This research effort showed that there is strong potential to upgrade low value feedstock including complex mixtures of fat and protein to liquid fuels using catalytic cracking. These fuels could be used as process fuels at the point of generation/production or further upgraded to transportation fuels in conventional petroleum refineries.

Chapter 4 – Catalytic cracking of PSS

As in the study outlined in Chapter 3, the study described in Chapter indicated very good improvements in fuel properties for a high free fatty acid feedstock, in this case an acidulated peanut oil soap stock (PSS). Where PSS was unlike DAF was in the level of protein, which for PSS was essentially zero. As a result, no fatty nitriles were apparent and the elemental N content was much lower than for

upgraded DAF bio-oil. For PSS, elemental C (at close to 90 %, w/w) was very much like diesel as were the heating values (~42 MJ kg^{-1}). Viscosity was reduced, as well, from ~10 to less than 1 mm^2 s^{-1}. Gasoline additives, BTEX in particular, were formed in high concentrations as a result of catalytic cracking. With minor changes to the processing methodology, selectivity to other fuel components (e.g. linear alkanes, cyclic alkanes, PAHs) could likely be improved if gasoline additives were not desired.

Chapter 5 – Modeling PSS cracking

The major result from the modeling efforts was the discovery that the reaction was highly mass transfer limited given the reaction conditions. Combined with a very high reaction rate, modeling indicated that the majority of FFA conversion occurred in the first few millimeters of the reactor.

Chapter 6 – Reactive condensation

An alternate method was proposed for upgrading bio-oil in Ch. 6. Initially devised as a way to quickly cool and condense bio-oil vapor, an evaporative cooling reactor was designed to atomize a liquid into a stream of bio-oil vapor. Upon injecting a primary alcohol into the reactor, it became clear that esterification was occurring (a sweet smelling bio-oil was collected). After further analysis, the formation of esters including ethyl acetate and ethyl propionate was confirmed and the concentration of esters was measured. The conversion of acetic acid was measured at 40 % relative to the control. In addition to acetic acid and propionic acid, other acids were likely undergoing esterification, although only acetic acid was quantified. The esterification reaction as proposed is catalyzed by an acid, so as the acids are consumed, the reaction rate slows. With the addition of a mineral or solid acid catalyst, conversion of acids and yield of esters could likely be significantly improved.

Fuel properties were also improved as a result of esterification. Viscosity was reduced from 24.4 to 9.7 mm^2 s^{-1}, pH was increased from 2.5 to 3.1, and cloud point was reduced from -4.7 to -12.1 °C.

Chapter 7 – Slow pyrolysis bio-oil cracking

Given the success of catalytic cracking for FFA feedstocks, attempts were made to similarly improved bio-oils derived from lignocellulosic feedstocks. Although yields were much lower for liquid product from cracking lignocellulosic-derived bio-oil, the quality of oil was significantly improved. From

both pine and peanut hull feedstocks, liquids were produced over commercially-available zeolite and FCC catalyst. Yields of BTEX and conversion of guaiacol and creosol were determined as were H/C_{eff} and O/C ratios. Conversion of guaiacol plus creosol for PH feedstock was 31.2 and 100 % for ZSM and FCC catalyst, respectively. Conversion of guaiacol and creosol in PP-derived liquid product was 83.7 and 92.7 % for ZSM and FCC catalyst, respectively.

Although elemental C was higher for catalytically cracked oils, H/C_{eff} was not significantly affected by catalyst type or catalytic cracking temperature. O/C was significantly reduced as a result of processing using either ZSM or FCC catalyst relative to the control. Higher heating value, HHV, was also significantly improved as a result of catalytic cracking. In the best-case-scenario upgrading conditions, HHV was increased from 31.2 to 35.6 MJ kg^{-1} for PH-derived liquids and from 28.4 to 36.3 MJ kg^{-1} for PP-derived liquid product. In both cases, HHV was maximized using ZSM as the catalyst and 550 °C as the process temperature. In all processes, coke yield was less than 10 % (w/w).

Chapter 8 – Preliminary torrefaction pretreatment experiment

Ch. 8 describes preliminary work involving an additional treatment to improve processing to liquid bio-oil via slow pyrolysis followed by catalytic cracking and to improve quality of liquid product. For this effort, torrefaction biomass pretreatment was explored. From a process standpoint, torrefaction reduced liquid yield relative to dry biomass for pyrolysis since torrefaction results in greater evolution of volatiles. However, torrefaction resulted in increased overall liquid yield after catalytic cracking. In addition, torrefaction pretreatment resulted in lowered catalyst coke formation during catalytic cracking. However, reactor char was increased.

From a product quality standpoint, catalytically upgraded bio-oils derived from torrefied biomass indicated greater quality than bio-oils from non-torrefied feedstock. For example, pH of bio-oil product after cracking was reduced as a result of torrefaction, a result proposed to be due the removal of organic acids which would likely have evolved during torrefaction. In addition, torrefaction resulted in greater concentrations of a variety of branched aromatics in product oil including m-xylene, mesitylene, cyclopropylbenzene, 1-propynylbenzene and others.

Since a minimal number of experiments were accomplished during this preliminary study, in-depth statistical analyses were not attempted. Also, bio-oils generated as the feedstock for catalytic cracking were produced via slow pyrolysis, a process that seems to be ill-favored in industry for the production of bio-oil since liquid yields are somewhat low. As such, the work was mainly accomplished to determine what, if any, glaringly obvious improvements may be possible as a result of biomass torrefaction prior to pyrolysis and catalytic cracking.

Chapter 9 – Culminating torrefaction experiment

Moving the torrefaction work further, the subsequent study outlined in Ch. 9 improved upon the work in Ch. 8 in a variety of ways. Firstly, fast pyrolysis processing was used in addition to slow pyrolysis processing. Additionally, the effect of both torrefaction temperature and catalytic cracking temperature was assessed in terms of yield of bulk products and liquid components. In all, 3 factors were assessed: pyrolysis heating rate (2 levels), torrefaction pretreatment temperature (4 levels), and catalytic cracking temperature (4 levels). Three-way ANOVA analysis was used to determine if factors significantly affected product and byproduct yield and conversion and yield of reactants and products. Additionally, the Holk-Sidak method of multiple comparisons was used to determine differences within factors as a result of varied levels.

The yield of bulk products was significantly affected by the experimental factors. Torrefaction pretreatment reduced pyrolysis liquid yield. Upon catalytic cracking, char and catalyst coke significantly reduced with increasing torrefaction pretreatment temperature as did liquid yield. At the same time, non-condensable gas yield increased. Increasing heating rate from slow to fast pyrolysis (0.13 to 100 °C s^{-1}) increased pyrolysis liquid yield, but reduced liquid product yield from catalytic cracking. The yield of gas, coke, and char were also increased. Liquid product and non-condensable gas yield increased with increasing catalytic cracking temperature. Concurrently, tar, coke and char yields were reduced.

The effects of the three factors on product quality were also assessed in terms of H/C_{eff} and C/O ratio, HHV, and oxidative stability. Both elemental C and HHV increased with increasing torrefaction temperature. However, oxidative stability as measured by OOT significantly decreased with increasing

torrefaction temperature. Increasing heating rate to fast pyrolysis conditions resulted in higher elemental C, H/C_{eff}, and HHV and lower O/C in catalytically cracked product. However, oxidative stability was reduced for fast versus slow pyrolysis. Increasing catalytic cracking temperature significantly increased elemental C, and HHV in catalytically cracked product while reducing O/C. Conversion of two reactants (guaiacol and creosol) was determined and yield of BTEX product was determined as in Ch. 7. Torrefaction had no significant effect on yield and conversion of chemical components. Increased heating rate significantly increased the yield of BTEX components including toluene, ethylbenzene, p-xylene, and m-xylene. Increased catalytic cracking temperature increased the conversion of guaiacol and the selectivity towards benzene and toluene.

Torrefaction appeared to have positive process-related improvements (reduced catalyst coke and tar and reactor char), but quality improvements were not clearly indicated. However, since only large scale torrefaction (~ 500 kg per batch) was attempted, temperature gradients in the reactor leading to inconsistent torrefied product may have been the cause of poor statistical significance for the measured parameters. Smaller-scale processing with greater temperature control may be able to improve these results.

Future directions

Each study presented here was devised to answer a research question. However, as in all research, more questions arise as a result of the work than can be answered in a single study. This was indeed the case for each study here. One major concern that arose here was the low yield afforded by catalytic cracking. For DAF, liquid yield was highest, but it was clear that many compounds remained unconverted in the liquid product, fatty nitriles, in particular. Although fatty nitriles have fuel-level energy density, high nitrogen content results in the emission of excessive NO_x upon combustion. As such, a question arises as to how to remove the nitriles from the product or to remove the proteins in DAF prior to processing to prevent the formation of nitriles. Although removing these nitrogenous compounds would reduce yield, the overall quality of the product should be improved.

In experiments using PSS, as evidenced by the modeling exercise, diffusion limitations were predicted as a result of the process conditions (i.e. reactant molecule size, catalyst pore size, flow rates, temperature). Thus, the question becomes how to improve the reactor setup to minimize mass transfer and diffusion limitations such that the system becomes reaction rate limited – a requirement to determine actual reaction kinetics. One way to reduce mass transfer limitation would be to increase the catalyst pore size and particle size to decrease diffusion rates. However, in increasing pore size, the overall reaction would change, particularly the selectivity to BTEX, meaning that the using the system to determine reaction kinetics would no longer be valid for a conversion from FFAs to BTEX. Another way to decrease diffusion limitation would be to increase carrier gas flow rate to reduce the boundary layer thickness about the catalyst particles.

The next step for the reactive condensation work would be to improve conversion of acids and the yield of esters by introducing an acidic- or basic-functionalized catalyst. A fixed catalytic bed could be added to the reactive condensation reactor in a manner such that reactants, bio-oil vapor and an alcohol, would thoroughly mix prior to passing across the catalyst bed. A variety of catalyst types would serve to catalyze the reaction including a char-based, solid acid derived from the pyrolysis of the feedstock. Using a low-value pyrolysis co-product would help to improve the process economics for a pyrolysis to liquid fuel pathway.

A variety of research questions arise from the catalytic cracking of bio-oil derived from pyrolysis lignocellulosic material. Firstly, how can yield be improved? Fast pyrolysis is likely capped in terms of increasing liquid yield further. However for the upgrading processes, major yield gains could be made, likely in the area of bio-oil pretreatment. Hydrogenation prior to catalytic cracking may do just that by simultaneously increasing H/C_{eff} and driving off oxygen. As such during subsequent conversion, less oxygenated byproduct, CO_2 in particular, is emitted. The catalytic effect is focused on cracking of carbon-carbon bonds to generate lower molecular weight compounds. Hydrogenation would lessen the number of oxygenated functional groups that would need to be expelled prior to cracking and deoxygenation of core molecules. Work we would like to pursue involves the use of a hydrogen donor

such as 2-propanol or formic acid as opposed to H_2 gas to hydrogenate under more mild conditions prior to catalytic cracking.

Another way to improve yields is to reduce coke formation which forms in substantial quantities during catalytic cracking, a shortcoming that has plagued zeolitic catalytic cracking processing (Corma et al., 2007; Valle et al., 2007; Elliott et al., 1996). As we proposed and attempted, one way to reduce coke is to remove coke precursors that normally exist in bio-oil. The way we attempted to remove coke precursors, via torrefaction, was effective. Coke formation was inversely related to torrefaction temperature. One aspect we did not vary was torrefaction hold time. A 20-minute hold time was used in all pretreatment processing. Longer hold times may be even more effective at removing coke precursors. At the same time, efforts would need to balance coke reduction with overall yield of product. In all experiments we attempted here, yield of liquid bio-oil from pyrolysis was reduced. However, the yield of liquid product relative to bio-oil fed was largely unaffected by pretreatment temperature. It was also unclear what effect torrefaction had on bio-oil quality.

Another aspect related to torrefaction pretreatment is what compounds are removed as a result of the process. We claim that the compounds removed are coke precursors since coke formation is reduced, but the compounds that are actually removed are only proposed. A more in-depth study of torrefaction is needed to state with any assurance which specific compounds are removed. One way to do this is using thermogravimetric analysis with mass spectral analysis of the gaseous products formed. What we would expect to see is a preponderance of acetic acid, furfural, and other light alcohols and ketones in the product gas. In small-scale experiments we would also have greater temperature control during torrefaction.

Yet another aspect of torrefaction that begs understanding is how torrefaction affects the structure of biomass and how the change in structure affects pyrolysis, and in particular, the kinetics of decomposition. Again, a TG experiment could be used to answer these questions. As to the actual structural change, we propose that not only is hemicellulose decomposed but the structure of cellulose likely changes, as well, and in particular, the crystallinity of cellulose. Future work would involve

determining crystallinity index of biomass after torrefaction at various temperatures and holding times. An extensive TG experiment would supplement crystallinity determination work and better explain how changes in crystallinity affect Arrhenius decomposition parameters including decomposition rate, activation energy, and pre-exponential factor.

In addition, we would like to do a broader study of the effects of torrefaction, reactive esterification, and catalytic cracking on stability in terms of parameters other than OOT including viscosity, solids formation and carbonyl content (via FT-IR), procedures that were attempted for non-upgraded bio-oil in Ch. 2 but not for upgraded oils. The hope, of course, would be to increase stability by way of upgrading using some combination of processes explored in this body of work.

Finally, we claim that the processes and feedstocks here are intended to be petroleum substitutes. None of our work thus far has involving testing these materials as liquid fuels in test engines. Work would entail blending studies to determine miscibility with conventional gasoline and diesel and testing the fuel blends in stationary engines to determine fuel economy, cetane number/octane number, and emissions.

REFERENCES

Abrams, L., Corbin, D. (1995). Probing Intrazeolite Space. J. Inclusion Phenom. Mol. Recognit. Chem. 21: 1-46.

Achten, W., Almeida, J., Fobelets, V., Bolle, E., Mathijs, E., Singh, V., Tewari, D., Verchot, L., Muys, B. (2010). Life cycle assessment of Jatropha biodiesel as transportation fuel in rural India. Applied Energy 87: 3652-3660.

Adam, J., Antonakou, E., Lappas, A., Stocker, M., Nilsen, M., Bouzga, A., Hustad, J., Oye, G. (2006). In situ catalytic upgrading of biomass derived fast pyrolysis vapours in a fixed bed reactor using mesoporous materials. Microporous and Mesoporous Materials 96: 93–101.

Adebanjo, A., Dalai, A., Bakhshi, N. (2005). Production of diesel-like fuel and other value-added chemicals from pyrolysis of animal fat. Energy Fuels 19(4): 1735-1741.

Adjaye, D., Sharma, R.K., Bakhshi, N.N. (1992). Characterization and stability analysis of wood-derived bio-oil. Fuel Processing Technology 31(3): 241-256.

Adjaye, J., Bakhshi, N. (1995a). Production of hydrocarbons by catalytic upgrading of a fast pyrolysis bio-oil. Part II: Comparative catalyst performance and reaction pathways. Fuel Processing Technology 45: 185-202.

Adjaye, J., Bakhshi, N. (1995b). Production of hydrocarbons by catalytic upgrading of a fast pyrolysis bio-oil. Part I: Conversion over various catalysts. Fuel Processing Technology 45: 161-183.

Ali, M., Siddiqui, M., Zaidi, S. (1998). Thermal analysis of crude oils and comparison with SIMDIST and TBP distillation data. Journal of Thermal Analysis and Calorimetry 51: 307-319.

Al-Khattaf, S., 2006. Catalytic transformation of toluene over a high-acidity Y-zeolite based catalyst. Energy Fuels 20, 946-954.

Anjos, J., Gonzalez, W., Lam, Y., Frety, R. (1983). Catalytic decomposition of vegetable oil, Applied Catalysis 5: 299-308.

Arguer, R.J., Landolt G.R. (1972). US Patent 3 702 886.

Ash, M., Wittenberger, K., 2010. Oil Crops Outlook. USDA Report OCS-10j, 18pp.

ASTM D 1744 – 92 (Withdrawn 2000). Standard Test Method for Determination of Water in Liquid Petroleum Products by Karl Fischer Reagent. Easton, MD: American Society for Testing and Materials, 1992.

ASTM D 2983-04a (2004). Standard Test Method for Low-Temperature Viscosity of Lubricants Measured by Brookfield Viscometer. Easton, MD: American Society for Testing and Materials, 2004.

ASTM D 3176-89 (2002). Standard Practice for Ultimate Analysis of Coal and Coke. Easton, MD: American Society for Testing and Materials, 2002.

ASTM D 4809-06 (2006). Standard Test Method for Heat of Combustion of Liquid Hydrocarbon Fuels by Bomb Calorimeter (Precision Method). Easton, MD: American Society for Testing and Materials, 2006.

ASTM D 5291-02 (2007). Standard Test Methods for Instrumental Determination of Carbon, Hydrogen, and Nitrogen in Petroleum Products and Lubricants. Easton, MD: American Society for Testing and Materials, 2007.

ASTM D 5304-06 (2006). Standard Test Method for Assessing Middle Distillate Fuel Storage Stability by Oxygen Overpressure. Easton, MD: American Society for Testing and Materials, 2006.

ASTM D 5865-07a (2007). Standard Test Method for Gross Calorific Value of Coal and Coke. Easton, MD: American Society for Testing and Materials, 2007.

ASTM E 2009-02 (2002). Standard Test Method for Oxidation Onset Temperature of Hydrocarbons by Differential Scanning Calorimetry. Easton, MD: American Society for Testing and Materials, 2002.

ASTM E 203-01 (2001). Standard Test Method for Water Using Volumetric Karl Fischer Titration. Easton, MD: American Society for Testing and Materials, 2001.

ASTM E 698-05 (2005). Standard test method for Arrhenius kinetic constants for thermally unstable materials using differential scanning calorimetry and the Flynn/Wall/Ozawa method. Easton, MD: American Society for Testing and Materials, 2005.

Baquero, M., Giraldo, L., Moreno, J., Suárez-García, F., Martínez-Alonso, A., Tascón, J. (2003). Activated carbons by pyrolysis of coffee bean husks in presence of phosphoric acid, J. Anal. Appl. Pyrolysis 70: 779-784.

Benson, T., Hernandez, R., White, M., French, W., Alley, E., Holmes, W., Thompson, B. (2008). Heterogeneous cracking of an unsaturated fatty acid and reaction intermediates on H+ZSM-5 catalyst. Clean 36(8): 652-656.

Blauwhoff, P., Gosselink, J., Kieffer, E., Sie, S., Stork, W. (1999). Zeolites as Catalysts in Industrial Processes, in Weitkamp, J., Puppe, L. (Eds), Catalysis and Zeolites: Fundamentals and Applications. Springer-Verlag, Berlin, pp. 437-538.

Boucher, M., Chaala, A., Pakdel, H., Roy, C. (2000). Bio-oils obtained by vacuum pyrolysis of softwood bark as a liquid fuel for gas turbines. Part II: Stability and ageing of bio-oil and its blends with methanol and a pyrolytic aqueous phase. Biomass Bioenergy 19: 351-361.

Bridgwater, A. (1996). Production of high grade fuels and chemicals from catalytic pyrolysis of biomass. Catalysis Today 29: 285-295.

Bridgwater, A., Meier, D., Radlein, D. (1999). An overview of fast pyrolysis of biomass, Organic Geochemistry 30(12): 1479-1493.

Carlson, T., Cheng, Y., Jae, J., Huber, G. (2011). Production of green aromatics and olefins by catalytic fast pyrolysis of wood sawdust. Energy Environ. Sci. 4: 145-161.

Centeno, A., Laurent, E., Delmon, B. (1995). Influence of the support of CoMo sulfide catalysts and of the addition of potassium and platinum on the catalytic performances for the hydrodeoxygenation of carbonyl, carboxyl, and guaiacol-type molecules. J. Catalysis 154: 288-298.

Channiwala, S., Parikh, P. (2002). A unified correlation for estimating HHV of solid, liquid and gaseous fuels. Fuel 81: 1051-1063.

Chen, G., Andries, J., Luo, Z., Spliethoff, H. (2003) Biomass pyrolysis/gasification for product gas production: the overall investigation of parametric effects. Energy Conversion and Management 44: 1875-1884.

Chiaramonti, D., Oasmaa, A., Salantausta, Y. (2007). Power Generation Using Fast Pyrolysis Liquids from Biomass. Renew. Sust. Energy Rev. 11: 1056-1086.

Chu, W., Yang, X., Ye, X., Wu, Y. (1996). Vapor phase esterification catalyzed by immobilized dodecatungstosilicic acid (SiW12) on activated carbon. Appl. Catal., A: General 145: 125-140.

Corma, A., Huber, G., Sauvanaud, L., O'Connor, P. (2007). Processing biomass-derived oxygenates in the oil refinery: Catalytic cracking (FCC) reaction pathways and role of catalyst. Journal of Catalysis 247: 302-327.

Czernik, S., Bridgwater, A. (2004). Overview of Applications of Biomass Fast Pyrolysis Oil. Energy Fuels 18: 590-598.

Czernik, S., Johnson, D., Black, S. (1994). Stability of wood fast pyrolysis oil. Biomass Bioenergy 7(1-6): 187-192.

Dandik, L., Aksoy, H., Erdem-Senatalar, A. (1998). Catalytic conversion of used oil to hydrocarbon fuels in a fractionating pyrolysis reactor. Energy Fuels 12: 1148-1152.

Das, P., Sreelatha, T., Ganesh, A. (2004). Bio-oil form pyrolysis of cashew nut shell – characterization and related properties. Biomass and Bioenergy 27: 265-275.

Demirbas, A., Sahin-Demirbas, A., Demirbas, A. (2004). Liquid fuels from agricultural residues via conventional pyrolysis, Energy Sources 26(9): 821-827.

Diebold, J. P., Czernik, S. (1997). Additives to Lower and Stabilize the Viscosity of Pyrolysis Oils during Storage. Energy Fuels 11: 1081-1091.

Diebold, J., Scahill, J. (1987). Biomass to gasoline (BTG): upgrading pyrolysis vapors to aromatic gasoline with zeolite catalysis at atmospheric pressure. ACS, Div. Fuel Chem. 32(2): 297-307.

Diebold, J.P. (2000). A Review of the chemical and physical mechanisms of the storage stability of fast pyrolysis bio-oils. Subcontractor Report for the National Renewable Energy Laboratory: Golden, CO, January 2000. NREL/SR-570-27613.

Doll, K., Sharma, B., Suarez, P., Erhan, S. (2008). Comparing biofuels obtained from pyrolysis, of soybean oil or soapstock, with traditional soybean biodiesel: density, kinematic viscosity, and surface tensions. Energy Fuels 22(3), 2061-2066.

Domínguez, A., Menéndez, J., Fernández, J., Pis, J., Valente Nabais, J., Carrott, P., Ribeiro Carrott, M. (2007). Conventional and microwave induced pyrolysis of coffee hulls for the production of a hydrogen rich fuel gas, J. Anal. Appl. Pyrolysis 79: 128-135.

EIA (2010a). U.S. Energy Information Administration. World Oil Balance, 2006-2010. International Petroleum Monthly, August 2010.

EIA (2010b). U.S. Energy information Administration. Non-renewable energy: U.S. Energy Information Administration (EIA), Monthly Energy Review (MER) March 2010, DOE/EIA-0035 (2010/03) (Washington, DC, March 2010).

Elliott, D., Baker, E. (1984) Upgrading Biomass Liquefaction Products through Hydrodeoxygenation. Biotechnology and Bioengineering Symp. 14: 159-174.

Elliott, D., Baker, E. (1988). "Catalytic Hydrotreating Processes for Upgrading Biocrude Oils." In: Thermochemical Conversion Program Annual Meeting, pp 45-56.

Elliott, D.C., Neuenschwander, G.G. (1996). Liquid Fuels by Low-Severity Hydrotreating of Biocrude. In: Bridgwater AV, Boocock DGB (eds) Developments in Thermochemical Biomass Conversion, Blackie Academic & Professional, London, Vol. 1, pp 611-621

EPA (2006). 1995-2006 RFG Surveys by Area. U.S. Environmental Protection Agency.

EPA (2008). Fuel Trends Report: Gasoline 1995-2005. Report number EPA420-R-08-002. U.S. Environmental Protection Agency.

Fogler, H.S. (1986). Elements of Chemical Reaction Engineering. Prentice Hill, Englewood Cliffs, NJ, 769 pp.

Fuller, E., Schettler, P., Gidding, J. (1966). New method for prediction of binary gas phase diffusion coefficients. Ind. Eng. Chem. 58: 18-27.

Gagnon, J., Kaliaguine, S. (1988). Catalytic hydrotreatment of vacuum pyrolysis oils from wood. Ind. Eng. Chem. Res. 27(10): 1783-1788.

Gayubo, A., Aguayo, A., Atutxa, A., Prieto, R., Bilbao, J. (2004a) Deactivation of a HZSM-5 Zeolite Catalyst in the Transformation of the Aqueous Fraction of Biomass Pyrolysis Oil into Hydrocarbons. Energy and Fuels 18: 1640-1647.

Gayubo, A., Aguayo, A., Atutxa, A., Aguado, R., Bilbao, J., (2004b). Transformation of Oxygenate Components of Biomass Pyrolysis Oil on a HZSM-5 Zeolite. I. Alcohols and Phenols. Ind. Eng. Chem. Res. 43, 2610-2618.

Gayubo, A., Aguayo, A., Atutxa, A., Aguado, R., Bilbao, J. (2004c). Transformation of Oxygenate Components of Biomass Pyrolysis Oil on a HZSM-5 Zeolite. II. Aldehydes, Ketones, and Acids. Ind. Eng. Chem. Res. 43: 2619-2626.

Gayubo, A., Aguayo, A., Atutxa, A., Valle, B., Bilbao, J. (2005). Undesired components in the transformation of biomass pyrolysis oil into hydrocarbons on an HZSM-5 zeolite catalyst. Journal of Chemical Technology and Biotechnology 80: 1244-1251

Gust, S. (1997). Combustion experiences of flash pyrolysis fuel in intermediate size boiler. In Developments in thermal biomass conversion; Bridgewater A.V., Boocock D.G.B., Eds.; Blackie Academic and Professional: London, UK, 1997; pp 481-488.

Haas, M., Michalski, P., Runyon, S., Nunez, A., Scott, K. (2003). Production of FAME from Acid Oil, a By-product of Vegetable Oil Refining. JAOCS 80(1): 97-102.

Harwood, H.J. (1984). Oleochemicals as a fuel: Mechanical and economic feasibility. JAOCS 61: 315-324.

Haynes, H. W. (1975). The determination of effective diffusivity by gas chromatography. Time domain solutions. Chem. Eng. Sci. 30: 995-961.

Hilten, R., Bibens, B., Kastner, J., Das, K.C. (2010). In-line esterification of pyrolysis vapor with ethanol improves bio-oil quality. Energy Fuels 24: 673-682.

Hilten, R., Das, K.C. (2010). Comparison of three accelerated aging procedures to assess bio-oil stability. Fuel 89: 2741-2749.

Hilten, R., Speir, R., Kastner, J., Das, K.C. (2010). Production of fuel from the catalytic cracking of pyrolyzed poultry DAF skimmings. Journal of Analytical and Applied Pyrolysis 88: 30-30.

Hilten, R., Speir, R., Kastner, J., Das, K.C. (2011). Production of aromatic green gasoline additives via catalytic pyrolysis of acidulated peanut oil soap stock. Bioresource Technology 102: 8288-8294.

IATA (2009). International Air Transport Association. 2nd Generation biomass conversion efficiency.

Ji-lu, Z. (2007). Bio-oil from fast pyrolysis of rice husk: Yields and related properties and improvement of the pyrolysis system. J. Anal. Appl. Pyrolysis 80: 30-35.

Junming, X., Jianchun, J., Yunjuan, S., Yanju, L. (2008) Bio-oil upgrading by means of ethyl ester production in reactive distillation to remove water and to improve storage and fuel characteristics. Biomass Bioenergy 32(11): 1056-1061.

Kanellos, M. (2007). "Tyson, ConocoPhillips link up for biodiesel." CNETnews.com.

Kärger, J., Ruthven, D. (1992). Diffusion in Zeolites and Other Microporous Solids. John Wiley & Sons: New York.

Keipert, O., Baerns, M., 1998. Determination of the intracrystalline diffusion coefficients of alkanes in H-ZSM-5 zeolite by a transient technique using the temporal-analysis-of-products (TAP) reactor. Chemical Engineering Science 53(20), 3623-3634.

Kirumakki, S., Nagaraju, N., Chary, K. (2006). Esterification of alcohols with acetic acid over zeolites, Hβ, HY and HZSM5. Appl. Catal., A: General 299: 185-192.

Koster, R., van der Linden, R.B., Poels, E., Bliek, A. (2001). The mechanism of the gas-phase esterification of acetic acid and ethanol over MCM-41. J. Catal. 204: 333-338.

Laurent, E., Delmon, B. (1994a). Study of the hydrodeoxygenation of carbonyl, carboxylic and guaiacyl groups over sulfided CoMo/γ-Al2O3 and NiMo/γ-Al2O3 catalysts: I. Catalytic reaction schemes. Applied Catalysis A: General 109(1): 77-96.

Laurent, E., Delmon, B. (1994b). Influence of water in the deactivation of a sulfided NiMo/γ-Al_2O_3 catalyst during hydrodeoxygenation. J. Catal. 146: 281.

Lédé, J., Broust, F., Ndiaye, F., Ferrer, M. (2007). Properties of bio-oils produced by biomass fast pyrolysis in a cyclone reactor. Fuel 86: 1800-1810.

Li, H., Shen, B., Kabalu, J., Nchare, M. (2009). Enhancing the production of biofuels from cottonseed oil by fixed-fluidized bed catalytic cracking, Renewable Energy 34: 1033-1039.

Lima, D., Soares, V., Ribeiro, E., Carvalho, D., Cordoso, E., Rassi, F., Mundim, K., Rubim, J., Suarez, P. (2004). Diesel-like fuel obtained by pyrolysis of vegetable oils. J. Anal. Appl. Pyrolysis 71: 987-996.

Lima, D., V. Soares, V., E. Ribeiro, E., D. Carvalho, D., E. Cordoso, E., F. Rassi, F., K. Mundim, K., Rubim, J., Suarez, P. (2004). Diesel-like fuel obtained by pyrolysis of vegetable oils, J. Anal. Appl. Pyrolysis 71: 987-996.

Lu, C.B., Yao, J.Z., Lin, W.G., Song, W.L. (2007). Study on biomass catalytic pyrolysis for the production of bio-gasoline by on-line FTIR. Chin. Chem. Lett. 18: 445-447.

Lu, Q., Zhang, Y., Tang, Z., Li, W., Zhu, X. (2010). Catalytic upgrading of biomass fast pyrolysis vapors with titania and zirconia/titania based catalysts. Fuel 89: 2096-2103.

Lua, A., Guo, J. (2002). Preparation and characterization of activated carbons from oil-palm stones for gas-phase adsorption. Colloids and Surfaces A: Physicochemical and Engineering Aspects 179: 151-162.

Mahfud, F. (2007) Exploratory studies on fast pyrolysis oil upgrading. Dissertation, University of Groningen.

Mahfud, F., Melián-Cabrera, I., Manurung, R., Heeres, H. (2007). Biomass to Fuels: Upgrading of flash pyrolysis oil by reactive distillation using a high boiling alcohol and acid catalysts. Process Safety & Environmental Protection: Transactions of the Institution of Chemical Engineers Part B 85(5): 466-472.

Mani, S., Das, K.C., Kastner, J. (2009). Development of biomass torrefaction technology to produce biocoal for electricity production. Final Report to State of Georgia, Traditional Industries Program

Miao, S., B. Shanks, B. (2009). Esterification of biomass pyrolysis model acids over sulfonic acid-functionalized mesoporous silicas. Appl. Catal., A: General 359: 113-120.

Milbrandt, A. (2005). A geographic perspective on the current biomass availability in the United States. NREL Technical Report, NREL/TP-560-39181, December 2005.

Milne, T. A., Agblevor, F., Davis, M., Deutch, S., Johnson, D. (1997). In Developments in Thermal Biomass Conversion; Bridgwater, A. V., Boocock, D.G.B., Eds.; Blackie Academic and Professional: London, UK, 1997.

Moens, L., Black, S., Myers, M., Czernik, S. (2009). Study of the neutralization and stabilization of a mixed hardwood bio-oil. Energy Fuels 23: 2695-2699.

Mohebby, B. (2005). Attenuated total reflection infrared spectroscopy of white-rot decayed beech wood. International Biodeterioration and Biodegradation 55: 247–251.

Noordhoek, N., van IJzendoorn, L., Anderson, B., de Gauw, F., van Santen, R., de Voigt, M. (1998). Mass transfer of alkanes in zeolite packed-bed reactors studied with positron emission profiling. 2. Modeling. Ind. Eng. Chem. Res 37: 825-833.

NSF (2008). Breaking the Chemical and Engineering Barriers to Lignocellulosic Biofuels: Next Generation Hydrocarbon Biorefineries, Huber GW (ed), University of Massachusetts Amherst. National Science Foundation, Chemical, Bioengineering, Environmental, and Transport Systems Division, Washington D.C. 180 p.

Oasmaa, A., Kuoppala, E. (2003). Fast pyrolysis of forestry residue. 3. Storage stability of liquid fuel. Energy Fuels 17: 1075-1085.

Oasmaa, A., Kuoppala, E., Selin, J., Gust, S., Solantausta, Y. (2004). Fast Pyrolysis of Forestry Residue and Pine. 4. Improvement of the Product Quality by Solvent Addition. Energy Fuels 18: 1578-1583.

Oasmaa, A., Leppämäki, E., Koponen, P., Levander, J., Tapola, E. (1997). Physical characterization of biomass-based pyrolysis liquids – Application of standard fuel oil analyses. VTT, Technical Research Centre of Finland, ESPOO.

Oasmaa, A., Peacocke, C. (2001). A guide to the physical property characterization of biomass-derived fast pyrolysis liquids. VTT Research Publications. VTT Technical Research Center of Finland.

Ooi, Y., Zakaria, R., Mohamed, A., Bhatia, S. (2004). Catalytic conversion of palm oil-based fatty acid mixture to liquid fuel, Biomass and Bioenergy 27: 477-484.

Ou, X., Zhang, X., Chang, S., Guo, Q. (2009). Energy consumption and GHG emissions of six biofuel pathways by LCA in (the) People's Republic of China. Applied Energy 86: S197-S208.

Ou, X.M., Zhang, X.L., Chang, S.Y. (2008). Life-cycle analysis of energy consumption, GHG emissions and regulated pollutants emissions of automotive fuel pathways in (the) PRC. Center of Automotive Energy Research Center, Tsinghua University, Beijing.

Ozawa, T. (1970). Kinetic analysis of derivative curves in thermal analysis. Journal of Thermal Analysis 2: 301-324.

Padmaja, K., Atheya, N., Bhatnagar, A. (2009). Upgrading of Candelilla biocrude to hydrocarbon fuels by fluid catalytic cracking. Biomass and Bioenergy 33: 1664-1669.

Payne, Randy (2009). Tyson Foods, Inc., Cumming, GA. Personal communication.

Peacocke, G., Madrali, E., Li, C., Güell, A., Wu, F., Kandiyoti, R., Bridgwater, R. (1994). Effect of reactor configuration on the yields and structures of pine-wood derived pyrolysis liquids: A comparison between ablative and wire-mesh pyrolysis, Biomass and Bioenergy 7(1-6): 155-167.

Phanphanich, M., Mani, S. (2010). Impact of torrefaction on the grindability and fuel characteristics of forest biomass. Bioresource Technology 102: 1246–1253.

Pimental, D. (2003). Ethanol fuels: Energy balance, economics, and environmental impacts are negative. Natural Resources Research 12(2): 127-134.

Pimental, D., Patzek. W. (2005). Ethanol production using corn, switchgrass, and wood; Biodiesel production using soybean and sunflower. Natural Resources Research 14(1): 65-76.

Pleanjai, S.,Gheewala, S.H. (2009). Full chain energy analysis of biodiesel production from palm oil in Thailand. Applied Energy 86: S209-214.

Poultry – Production and Value, 2008 Summary; U.S. Department of Agriculture, U.S. National Agricultural Statistics Service. May 2009.

Pütün, A. (2002). Biomass to bio-oil via fast pyrolysis of cotton straw and stalk, Energy Sources 24: 275-285.

Radich, A. (1998). Biodiesel Performance, Costs, and Use. Energy Information Administration.

Renaud, M., Grandmaison, J. L., Roy, Ch. & Kaliaguine, S. (1987). Conversion of vacuum pyrolytic oils from populus deltoids over HZSM-5. ACS, Div. Fuel Chem. 32(2): 276-86.

Ruthven, D. (1984). Principles of Adsorption and Adsorption Processes. Wiley: New York.

Scholze, B., Meier, D. (2001). Characterization of the water-insoluble fraction from pyrolysis oil (pyrolytic lignin). Part I. PY-GC/MS, FTIR, and functional groups. J. Anal. Appl. Pyrolysis 60: 41-54.

Schwan, P., Möller, K. (2001). Analysis of the pulse response in a CSTR for diffusion measurement in bi-porous adsorbent pellets. Chemical Engineering Science 56: 2821-2830.

Sena, R., Tambosi, J., Genena, A., Moreira, R., Schröder, H., José, H. (2009). Treatment of meat processing industry wastewater using dissolved air flotation and advanced oxidation processes monitored by GC-MS and LC-MS, Chemical Engineering Journal 152(1): 151-157.

Shapouri, H., Duffield, J., Wang, M. (2002). The Energy Balance of Corn Ethanol: An Update. United States Department of Agriculture, Agricultural Economic Report 813.

Sharma, R., Bakhshi, N. (1991). Upgrading of wood-derived bio-oil over HZSM-5. Bioresource Technology 35: 57-66.

Sharma, R., Bakhshi, N. (1993a). Catalytic conversion of fast pyrolysis oil to hydrocarbons over HZSM-5 in a dual reactor system. Biomass and Bioenergy 5(6): 445-455.

Sharma, R., Bakhshi, N. (1993b). Conversion of non-phenolic fraction of biomass-derived pyrolysis oil to hydrocarbons over HZSM-5 using a dual reactor system. Bioresource Technology 45: 195-203.

Sheu, Y., Anthony, R., Soltes, E. (1988). Fuel Processing Technology 19: 31-50.

Simons, R.M. (1983). In Encyclopedia of Chemical Processing and Design, 19, J.J. McKetta and W.A. Cunningham, Eds.; Marcel Dekker, N.Y., p 381.

Singh, N., Delgass, W., Ribeiro, F., Agrawal, R. (2010). Estimation of liquid fuel yields from biomass. Environ. Sci. Technol 44: 5298-5305.

Smith, J., Garcia-Perez, M., Das, K.C. (2009). Producing fuel and specialty chemicals from the slow pyrolysis of poultry DAF skimmings, J. Anal. Appl. Pyrolysis 86: 115-121.

Stamatov, V., Honnery, D., Soria, J. (2006). Combustion properties of slow pyrolysis bio-oil produced from indigenous Australian species. Renewable Energy 31: 2108–2121.

Swisher, K. (2007). Market Report 2006. Render - The National Magazine of Rendering.

Tamunaidu, P., Bhatia, S. (2007). Catalytic cracking of palm oil for the production of biofuels: optimization studies. Bioresour. Technol. 98: 3593-3601.

Tang, Y., Yu, W., Mo, L., Lou, H., Zheng, X. (2008). One-step hydrogenation-esterification of aldehyde and acid to ester over bifunctional Pt catalysts: A model reaction as novel route for catalytic upgrading of fast pyrolysis bio-oil. Energy Fuels 22(5): 3484-3488.

Twaiq, F., Mohamed, A., Bhatia, S. (2003). Liquid hydrocarbon fuels from palm oil by catalytic cracking over aluminosilicate mesoporous catalysts with various Si/Al ratios. Microporous and Mesoporous Materials 64(1-3): 95-107.

Twaiq, F., Zabidi, N.A.M., Bhatia, S. (1999). Catalytic conversion of palm oil to hydrocarbons: performance of various zeolite catalysts. Ind. Eng. Chem. Res. 38: 3230-3238.

Twaiq, F.A.A., Mohamad, A.R., Bhatia, S. (2004). Performance of composite catalysts in palm oil cracking for the production of liquid fuels and chemicals. Fuel Process. Technol. 85(11): 1283-1300.

Valle, B., Gayubo, A., Atutxa, A., Alonso, A., Bilbao, J. (2007). Integration of thermal and catalytic transformation for upgrading biomass pyrolysis oil, International Journal of Chemical Reactor Engineering 5 (2007): 1-10.

Vitolo, S., Seggiani, M., Frediani, P., Ambrosini, G., Politi, L. (1999). Catalytic Upgrading of Pyrolytic Oils to Fuel over Different Zeolites, Fuel 78: 1147-1159.

Weigert, F., Ragosta, J. (1993). Nickel-on-alumina catalyzed polymethylbenzene dealkylation. J. Molec. Catal. 85: 237-251..

Wiggers, V., Meier, H., Wisniewski, A., Barros, A., Maciel, M. (2009). Biofuels from continuous fast pyrolysis of soybean oil: A pilot plant study. Bioresource Technology 100: 6570-6577.

Wildschut, J., Mahfud, F., Venderbosch, R., Heeres, H. (2009). Hydrotreatment of fast pyrolysis oil using heterogeneous noble-metal catalysts. Ind. Eng. Chem. Res. 48: 10324-10334.

Wildschut, J., Melian-Cabrera, I., Heeres, H. (2010) Catalyst studies on the hydrotreatment of fast pyrolysis oil. Applied Catalysis B: Environmental 99: 298-306.

Williams, P., Nugranad, N. (2000). Comparison of products from the pyrolysis and catalytic pyrolysis of rice husks. Energy 25: 493–513.

Xu, J., Jiang, J., Sun, Y., Chen, J. (2010). Production of hydrocarbon fuels from pyrolysis using a basic catalyst. Bioresource Technology 101: 9803-9806.

Yean-Sang, O., Bhatia, S. (2007). Aluminum-containing SBA-15 as cracking catalyst for the production of biofuel from waste used palm oil. Micropor. Mesopor. Mater. 102: 310-317.

Yee, K.F.,Tan, K.T., Abdullah ,A.Z., Lee, K.T., 2009. Life cycle assessment of palm biodiesel: revealing facts and benefits for sustainability. Applied Energy 86, S189-196.

Yu, S., Tao, J. (2009). Economic, energy and environmental evaluations of biomass-based fuel ethanol projects based on life cycle assessment and simulation. Applied Energy 86: S178-S188.

Zhang, Q., Chang, J., Wang, T., Xu, Y. (2006). Upgrading Bio-oil over Different Solid Catalysts. Energy Fuels 20: 2717-2720.